Reports and Monographs of the International Ocean Colour Coordinating Group

An Affiliated Program of the Scientific Committee on Oceanic Research (SCOR) An Associated Member of the Committee on Earth Observation Satellites (CEOS)

IOCCG Report Number XX, 202X

Benthic reflectance measurements for aquatic applications

Edited by:
Heidi M. Dierssen, Stuart Phinn

Report of an IOCCG working group chaired by Heidi M. Dierssen and based on contributions from (in alphabetical order)

Steve Ackleson	Naval Research Lab, USA
Touria Bajjouk	Ifremer, DYNECO/LEBCO, France
Brian B. Barnes	University of South Florida, USA
Ved Chirayath	University of Miami, USA
Maycira Costa	Spectral Lab, University of Victoria, Canada
Heidi M. Dierssen	University of Connecticut, USA
Arnold Dekker	CSIRO, Australia
Andrea Faltynkova	F&Z Solutions, Norway
George Fournier	DRDC Valcartier Research Centre, Canada
Peter Gege	DLR, Germany
Jamie Goodman	HySpeed Computing LLC., USA
John Hedley	Numerical Optics Ltd., UK
Erin Hestir	University of California, Merced, USA
Eric Hochberg	Bermuda Institute of Ocean Sciences, Bermuda
Geir Johnsen	Norwegian University of Science and Technology, Norway
Wonkook Kim	Pusan National University, Korea
Tiit Kutser	University of Tartu, Estonia
Julien Laliberté	Department of Fisheries and Oceans, Canada
Øyvind Ødegård	Norwegian University of Science and Technology, Norway
Natascha Oppelt	Kiel University, Germany
Gema Casal	Oceanographic Centre of A Coruña (IEO-CSIC), Spain
Stuart Phinn	University of Queensland, Australia
Jaime Pitarch	CNR-ISMAR, Italy
Chris Roelfsema	University of Queensland, Australia
Gillian Rowan	University of Queensland, Australia
Brandon Russell	Labsphere, Inc., USA
Eva Scrivner	University of Connecticut, USA
Asgeir J. Sørensen	Norwegian University of Science and Technology, Norway
Murat Van Ardelan	Norwegian University of Science and Technology, Norway
Ele Vahtmäe	University of Tartu, Estonia
Richard Zimmerman	Old Dominion University, USA

Series Editor: Raisha Lovindeer

Table of Contents

Chapter 1

Introduction

Heidi Dierssen, Stuart Phinn

1.1 What is Benthic Reflectance?

Benthic reflectance is an optical property quantifying how much a bottom boundary reflects and absorbs incident light across the electromagnetic spectrum. A lay-person may consider it a detailed measure of the "colours" of the seafloor if the "eye" was a spectrometer perceiving reflected light divided into hundreds of wavelengths instead of the three broad Red-Green-Blue colours in human vision. Abbreviated here as R_b, benthic reflectance is the bi-hemispherical reflectance defined as the ratio of the spectral-upwelling-plane-irradiance reflected from a substrate surface and the downwelling-plane-irradiance incident on the surface. For this report, benthic reflectance represents how the bottom boundary of a water body (e.g., algae, seagrass, sediment, coral) reflects and absorbs some fraction of impinging light, or irradiance, spectrally from ultraviolet (UV) to shortwave infrared (SWIR) roughly from 350 to 2500 nm.

For many aquatic mapping and monitoring applications, benthic reflectance is restricted to visible wavelengths (400-700 nm) because the water medium is highly absorbing outside this range. Benthic reflectance varies spectrally with the type of material on the bottom and typically has peaks and troughs that relate to pigments and other light absorbing, scattering and fluorescent features of the benthos. Benthic reflectance has been likened to a spectral "fingerprint" (Adams et al. 1977) that can be characteristic of the type of benthic constituent, mixture of different constituents, concentration of pigments, leaf area index, sediment grain size, and ecosystem health.

Reflectance measurements depend on the absorbing and scattering properties of the observed surface, the atmospheric and water optical properties, the object's surroundings, the topography of both the sea surface and the benthos, as well as the incident light and viewing geometry. In the aquatic optics community, reflectance is viewed as an "apparent" optical property, whereby the parameter is largely dependent on the object or medium sampled, but has some dependence on the directional structure of the light field (Mobley 1994). The dependence of benthic reflectance on the light field is quite minimal under most sampling regimes and for many applications, as noted in the various methods for measuring benthic reflectance from using natural illumination of the material in air to artificial lighting underwater. Because reflectance is normalized to the intensity and spectral properties of the illuminating light, reflectance properties are generally similar whether the impinging light is blue-enhanced (sunlight) or red-enhanced (artificial light). This means that your eye may see a benthic feature as a colour that is quite

different from its reflectance properties – just like a white wedding dress may appear blue when lit by blue light. However, many aquatic organisms produce inelastic scattering or fluorescence that can change with the incident light field. Furthermore, subtle changes in benthic reflectance may occur if light absorption properties change with different types of incident light.

The term “bottom boundary” is used in this definition because water bodies have a variety of hard, soft, and canopied bottom structures. No single definition of the bottom boundary applies to all benthic types and measurement techniques. Benthic reflectance can refer to measurements made at the top, within, or at the base of a seagrass or macroalgal canopy. Furthermore, the field of view of the measurement is quite critical to understanding the scale and scope of the measurement and what a single benthic reflectance measurement represents. The field of view can determine whether reflectance applies to a single polyp on a coral head or the entire multi-species coral reef habitat. With imaging technology, the benthic reflectance across an entire image can be made at very high spatial resolutions (< 1 mm pixels) to identify different structures within a single organism, such as the location of light absorbing organelles within a seagrass leaf. Here, we allow for benthic reflectance to be obtained from a variety of spatial scales on the benthos as defined by the user and/or the field of view of the instrumentation. We also note that shadows and other inanimate factors like detritus play a significant role in the benthic reflectance of a natural bottom boundary in aquatic environments.

For most applications in this report, the benthos is treated as a horizontal plane of homogenous material on the bottom boundary. However, as highlighted in Chapter 2 of this report, natural surfaces are typically far more complex and have multifaceted three-dimensional structures that include diverse mixtures of materials and organisms. Additionally, most models presume the bottom is opaque and reflects equally in all directions (i.e., Lambertian) (e.g., Mobley et al. 2003b); however, in reality, light reflects disproportionally in different directions as a function of surface characteristics and the view and illumination angles. The bidirectional reflectance distribution function (BRDF) relates how the irradiance incident from one given direction contributes to the reflected radiance in another direction (Schaepman-Strub et al. 2006). Very few measurements have been made of the BRDF of aquatic benthic surfaces (e.g., Joyce and Phinn 2002) due to challenges in making such measurements underwater with varying waves, currents and light conditions. Measurements of benthic reflectance can include caustics due to wave focusing at the sea surface and “hot spot” or “retroreflection” effects when sampling at angles similar to or at right angles to the illumination direction (e.g., Hedley and Enriquez, 2010). Benthic reflectance from sediment is additionally complex because it includes rays that are absorbed and multiply-scattered from the inner surfaces of differently-sized grains beneath the boundary layer (Fournier et al. 2018).

Despite all of these challenges, a recent review of optically shallow remote sensing by Kutser et al. (2020) concluded that optical properties of major bottom types are similar in tropical and temperate as well as freshwater and oceanic environments. Specifically, characteristic features in reflectance spectra of major aquatic flora, such as green or brown macroalgae, have consistent spectral shapes across diverse

habitats and are related to variations in pigments that occur in the major groups (e.g., chlorophyll-a, fucoxanthin, phycoerythrin, peridinin, etc.; Hedley and Mumby, 2002). However, this does not account for differences in solar-induced fluorescent properties, a form of elastic scattering that can create peaks in benthic reflectance depending on the light history and physiology of the organism. This is particularly notable for tropical corals that have a variety of green fluorescent proteins that can produce distinct reflectance peaks throughout the blue to green parts of the spectrum (Chapter 7). Even with such variability, modeling and sensitivity analyses based on field and laboratory measurements of reflectance spectra reveal that spectral separation of benthic types based on hyperspectral reflectance is possible (Lubin et al. 2001; Hochberg and Atkinson 2003; Hedley et al. 2012). A study using hyperspectral PRISM imagery, for example, provided >90% classification accuracy at differentiating bottom types (Garcia et al. 2018).

1.2 Historical Perspective

Remote sensing of optically shallow water developed before libraries of systematically collected and archived benthic spectral reflectance measurements were available for different benthic constituents. To illustrate this paucity of data, Lyzenga (1978) used terrestrial proxies in their study mapping water depth and bottom features stating: “In the absence of reliable reflectance measurements for actual bottom materials, the reflectances of beach sand, dark soil (representing mud), and wheat leaves (representing aquatic vegetation) were used for this calculation”. Early measurements of benthic reflectance were often done in the laboratory or measured in air shortly after collection. As highlighted in Chapter 4, this is still a commonly used method of measuring benthic reflectance.

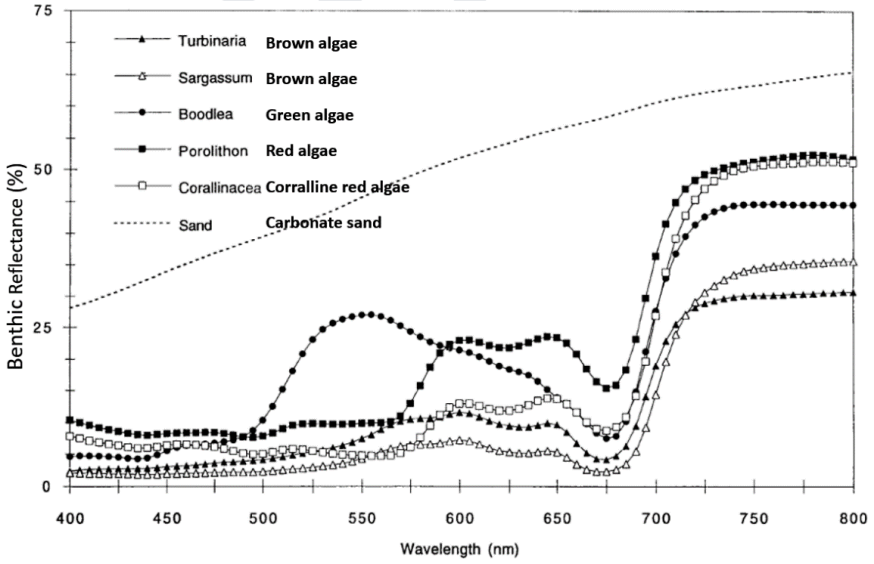

Figure 1.1 Early measurements of high quality benthic reflectance of macroalgae and sand recorded in the literature (modified from Maritorena et al. 1994)

Some of the first laboratory reflectance measurements of macrophytes and satellite imagery including “bottom effects” were summarized in Adams et al. 1977. They note that the *“type of bottom (dark mud, light sand, or green weeds), also will give a different characteristic modification to signals from each of the water types. The*

depth to bottom also affects the strength of the signal and its spectral distribution." and that, fortunately, "*the fingerprint from the sand bottom is different than those from algae, humic material, or red clay, etc. The computer analyzing satellite data can be trained to recognize sand bottom conditions.*" It is quite poignant that these statements were made nearly 50 years ago before machine learning!

As part of model development for optically shallow water, Maritorena et al. (1994) used an underwater spectroradiometer to quantify downwelling and upwelling irradiances in lagoons near Moorea. They stated that their setup could not be used for benthic reflectance due to instrument shadowing. Hence, they collected macroalgae and sand samples and took careful spectral measurements with an integrating sphere in the laboratory. These might be some of the first high quality benthic reflectance measurements in the literature (Figure 1.1).

The field of remote sensing often characterizes spectra in terms of "endmembers" that represent the "pure signature" of a single feature or object of interest. The benthic reflectance endmembers originally distributed with the radiative transfer software Hydrolight (Mobley 1994 and now Numerical Optics https://www.numopt.com/hydrolight.html) have perhaps been the most widely used aquatic spectra for research purposes to date. Spectra for sediment, seagrass, and corals were largely collected as part of a vast field effort at Lee Stocking Island, Bahamas (May/June 1999 and May 2000) known as the Coastal Benthic Optical Properties (CoBOP) program. These spectra have been incorporated in radiative transfer runs with different water depths, water column optical properties, and combinations of benthic types (e.g., Mobley et al. 2005). In current versions of the software, benthic types have been expanded and the spectra have been extrapolated to UV and NIR wavelengths (Figure 1.2)

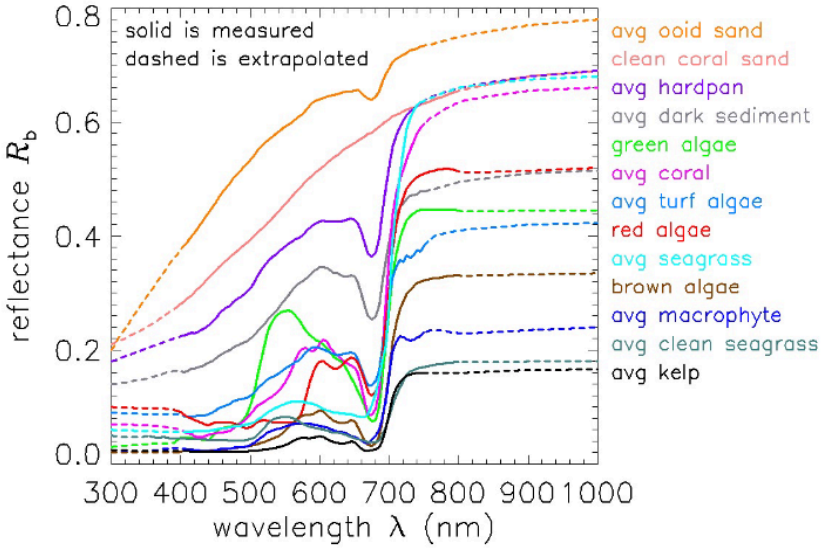

Figure 1.2 Benthic reflectance endmembers provided with the current Hydrolight radiative transfer code. Solid lines are measured; dashed lines are subjective extrapolations. Adapted from Hedley and Mobley (2021).

Chapter 7 provides an overview of the types of spectra to be expected for the major groups of sub- and inter-tidal benthic habitats around the earth including sediment,

corals, minerals and rubble, submerged aquatic vegetation, macroalgae, detritus/debris, shadows; and others. While not exhaustive, this compilation can provide a reference for users to evaluate how a typical spectrum may look for a given habitat. As noted, while many features are consistent within a group, single "average" endmembers may not adequately represent the diversity of spectra related to any benthic type. The variability in sediment types, for example, is vast, going from bright white carbonate sediment to dark clay muds with varying amounts of algal film (Dierssen 2010). Reducing this variability to a single or few distinct sediment endmembers can be challenging for many applications. Hence, the use of ensemble or probabilistic methods involving spectral libraries with many replicates of the same types of benthic endmembers is becoming more common (e.g., Garcia et al. 2019; Dierssen et al. 2015).

1.3 How to measure Benthic Reflectance

As detailed in Kutser et al. (2020), the emergence of hyperspectral sensors led to the rise of research groups around the world developing field sensors and collecting data from tropical to temperate coastal and inland waters. Presently, there are a limited number of commercial/off-the-shelf instruments and a very wide variety of techniques for making benthic reflectance measurements. No recommendations for the best practices to reduce uncertainties in the measurement have been agreed upon by the community. This report brought together experts for the first time who have conducted these *ad hoc* measurements to share experience, guidance, and potential pitfalls. A step-by-step manual of best practices is not included here, but such efforts would be useful in the future to aid in the advancement of the field. Chapters 3 and 4 provide an overview of the types of platforms, instruments and measurement techniques that have been commonly used for a variety of benthic habitats. As noted, different habitats can require different types of methods. Some have used sensors with closed path, internal lighting and others with open path relying on natural sunlight (Kutser et al. 2020). In addition to diver-operated spectrometers, methods include those where a benthic substrate is brought up from the water and measurements are taken in air. Some discussion is included as to the limitations in terms of which substrate can be assessed and how to account for differences between samples measured in air and in water. The use of a new radiative transfer model relating spectral reflectance signatures measured in air to the underwater environment also warrants consideration in methodology (Fournier et al. 2018).

Figure 1.3 Divers in Kaneohe Bay, Hawaii 2022 measuring the benthic reflectance of coral reefs using a hand-built diver-operated spectrometer from Dierssen COLORS Lab at the University of Connecticut. Photo credit: Heidi Dierssen

A recent benthic reflectance database compiled for Australian waters included spectra collected from 1994 to 2016 as part of the Australian National Spectral Database (Dekker 2021 and www.dea.ga.gov.au/products/national-spectral-database). The report notes that underwater measurements of benthic reflectance contained higher uncertainty and more artifacts compared to laboratory measurements due to low light levels, particularly in blue and red wavelengths, variable light levels due to waves creating caustics, and changing distance from target. Making careful underwater measurements requires optimal environmental conditions and instrumentation. Diver-operated spectrometers are hand-built units with bespoke underwater housings that are generally best-optimized for two divers working in tandem to set the sensor properties (e.g., integration times, averaging), point to targets of interest, and record the measurements and metadata (Figure 1.3).

Some methods for measuring benthic reflectance underwater use a calibration plaque/panel and others take simultaneous upwelling and downwelling radiance/irradiance measurements. Chapter 4 highlights which approaches are appropriate for different types of substrates and conditions. Calibration plaques, such as Spectralon®, perform differently in a water media compared to air and few studies have characterized and incorporated these differences in their measurements (Russell et al. 2023). Some methods suggest blocking of the direct beam underwater to prevent fluctuations due to wave focusing and hot spot effects. Orientation of the measurement can also be optimized for specific angles to minimize glint. Certain environmental conditions limit the use of sunlight such as when the sea surface is too wavy and incident light fluctuates with the passing of each wave, or when the measurements are too deep for adequate penetration of certain wavelengths of light. Challenges exist in diagnosing the overall uncertainty in the measurement at each wavelength.

Assessing the three-dimensional structure of the substrate and incident lighting conditions (e.g., the amount of direct versus diffuse light) at the time of measurement may provide important information in assessing the variability and uncertainty in benthic reflectance. Recent modeling work shows that the three-dimensionality

influences the benthic reflectance from shadowing in a manner that is related to the rugosity of the benthic structure (Hedley et al. 2018).

1.4 Why measure Benthic Reflectance?

Benthic reflectance is an essential parameter used in remote sensing of optically shallow waters and for mapping and monitoring the extent and biophysical properties of the benthos. Optically shallow water is defined as a region of a water body where the bottom boundary has a measurable influence on the water-leaving reflectance and is dependent on the bathymetry and the optical properties of both the water column and the benthos. Understanding the variability in benthic reflectance across different habitats is an important aspect in assessing the limitations and capabilities of benthic remote sensing. Chapter 8 presents a high level overview of mapping benthic habitats using remote sensing imagery..

Benthic reflectance also finds relevant applications in Ecology (Chapter 9), Global Change (Chapter 10), and Deep sea mining, archeology, and marine litter (Chapter 11). For ecological purposes, for example, understanding the variability of benthic reflectance within a group can provide additional physiological characteristics about the health of an organism including the amount of pigment (Hochberg et al. 2025), concentration of symbionts, and the presence of epiphytes. Benthic reflectance measurements *in situ* can be a valuable method to assess symbiont concentration in corals (Russell et al. 2016) and ultimately evaluating the health of the organism in response to global changes. The use of non-destructive methods like underwater spectrometry can play a larger role in aquatic ecological studies.

Benthic reflectance is also useful for deep sea applications including finding locations for and assessing impacts of deep-sea mining of the seafloor. The use of underwater imaging on robotic instrumentation for mapping deep sea benthos has progressed in the last few decades with the advance of underwater autonomous vehicles, dynamic positioning, and lighting (Sørensen et al. 2020). Measuring benthic reflectance can help identify different types of mineralogy useful for finding mining sites. In addition, benthic reflectance measurements can aid in assessing habitat destruction due to mining operations, as well as quantifying sediment plumes related to mining operations. Similarly, benthic reflectance can also be used to assess the composition of underwater archeological sites of interest.

Finally, benthic reflectance relates to a variety of citizen science projects that use hands-on sampling from the public to advance outreach and monitoring efforts of various aquatic habitats. One such effort is the Australian CoralWatch program (https://coralwatch.org), which engages and trains users on simple tools to collect scientific data on coral bleaching. Changes of one or two degrees in sea temperature can cause corals to bleach. The Coral Health Chart is an easy-to-use tool to quantify changes in coral colour associated with coral bleaching on a coral reef. While “colour” is related to human perception, the selections on the chart can be mapped to a corresponding estimate of benthic reflectance (e.g., Figure 1.4) that has applications to remote sensing and mapping efforts. Such assessments, moreover, are critical for evaluating how these organisms cope with temperature shifts and can

be a factor in their susceptibility to diseases and changes to growth rates and reproduction.

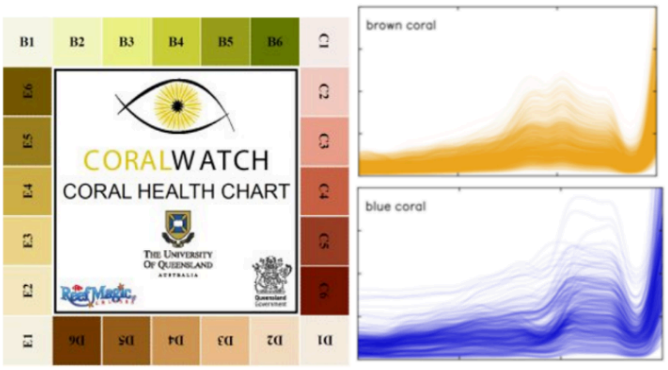

Figure 1.4 Example of the citizen science CoralWatch project involving documentation of coral health together with spectral reflectance examples of brown and blue coral.

Chapter 2

Overview of Theory

George Fournier, Peter Gege, and John Hedley

2.1 Physics of Bottom Reflectance

A model for the physical basis underlying the reflectance of substances is a key tool that can help in the interpretation and understanding of both the measurement methods used and their results. In this section, we will try to convey the basic theoretical framework required to develop a physical understanding of bottom observations and the implications of this model for both the measurement techniques and the interpretation of the results. To achieve this we will combine elements from the fields of spectroscopy and light scattering. A basic familiarity with the concepts used in these fields will help the reader better understand the material of this section. Note that the intervening water column, although inherent to *in situ* measurements, is treated separately.

2.1.1 Mathematical foundation

Measurements of reflectance can be generalized into one of three principal categories according to the angular characteristics of the detector and the illumination source with respect to the surface being measured (Schaepman-Strub et al. 2006; the following section is adapted from Goodman 2004 with permission):

- Directional-directional, or bi-directional, reflectance, which describes how much light is reflected from a particular illumination direction into a particular viewing direction.
- Hemispherical-directional reflectance, which describes how much light is reflected from all downward illumination directions into a particular viewing direction.
- Hemispherical-hemispherical, or bi-hemispherical, reflectance, which describes how much light is reflected from all downward illumination directions into all upward viewing directions.

The mathematical foundation for each of these measurements is illustrated here using a horizontal plane as a representative measurement surface (Figure 2.1). Light travelling downward onto this surface is denoted with a subscript d, where downwelling radiance is designated as L_d and downwelling irradiance as E_d. Correspondingly, light reflected upward from this surface is denoted with a subscript u, where upwelling radiance is designated as L_u and upwelling irradiance as E_u. The direction of the light source illuminating the surface is defined by (θ_s, φ_s) and the direction of the detector viewing the surface by (θ_v, φ_v). Additionally, measurements are a function of wavelength, λ.

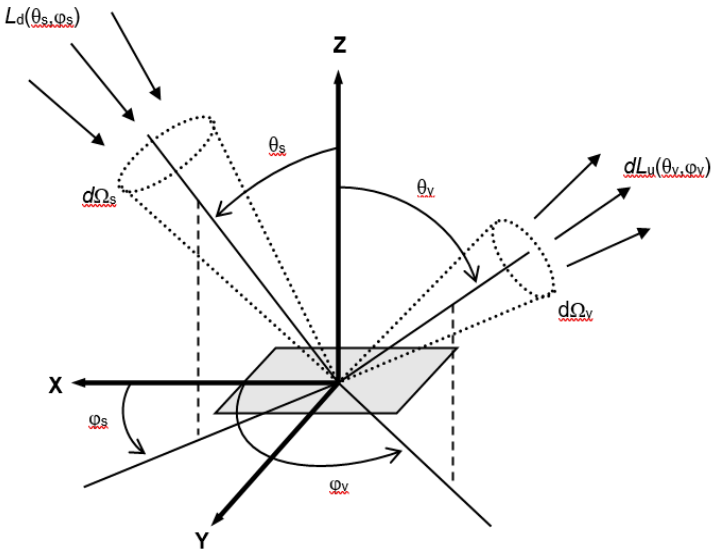

Figure 2.1 Coordinate system, geometry and variables used for defining measurements of reflectance. Figure reproduced from Goodman (2004) with permission.

The fundamental parameter specifying the angular dependency of reflectance is the Bidirectional Reflectance Distribution Function, $BRDF\left(sr^{-1}\right)$, which is defined the ratio of the angular distribution of upwelling radiance, $dL_u\left(\theta_v, \varphi_v; \theta_s, \varphi_s; \lambda\right)$ to downwelling irradiance at a certain illumination direction, $dE_d\left(\theta_s, \varphi_s; \lambda\right)$ (Nicodemus et al. 1977):

$$BRDF\left(\theta_v, \varphi_v; \theta_s, \varphi_s; \lambda\right) = \frac{dL_u\left(\theta_v,\varphi_v;\theta_s,\varphi_s;\lambda\right)}{dE_d\left(\theta_s,\varphi_s;\lambda\right)} \tag{2.1}$$

The differentials indicate that both light field parameters are defined for infinitesimal small solid angles, hence they cannot be measured directly. An approximate determination of the $BRDF$ of a surface requires use of a gonioreflectometer to measure the light from multiple combinations of viewing and illumination directions (Sandmeier 2000).

More commonly, however, bi-directional reflectance properties are measured in terms of the Bidirectional Reflectance Factor, $BRF(unitless)$, which defines the ratio of upwelling radiance, $L_u\left(\theta_v, \varphi_v; \theta_s; \lambda\right)$, for a particular viewing direction, to upwelling radiance from a diffuse reference panel, $L_u{}^P\left(\theta_v, \varphi_v; \lambda\right)$, measured using the same viewing, illumination and environmental conditions as the surface measurement:

$$BRF\left(\theta_v, \varphi_v; \theta_s, \varphi_s; \lambda\right) = \frac{L_u\left(\theta_v,\varphi_v;\theta_s;\lambda\right)}{L_u{}^P\left(\theta_s,\varphi_s;\lambda\right)} K\left(\theta_v, \varphi_v; \theta_s, \varphi_s; \lambda\right) \tag{2.2}$$

where the correction factor, $K\left(\theta_v, \varphi_v; \theta_s, \varphi_s; \lambda\right)$, is used to equate measurement of the reference panel to that of a perfectly diffuse surface (Voss and Zhang, 2006).

Hemispherical-directional reflectance defines the ratio of upwelling radiance, $L_u\left(\theta_v, \varphi_v; \lambda\right)$, for a particular viewing direction, to downwelling plane irradiance, $E_d(\lambda)$, as measured using a cosine collector across the entire hemisphere:

$$r_{rs}\left(\theta_v, \varphi_v; \lambda\right) = \frac{L_u\left(\theta_v, \varphi_v; \lambda\right)}{E_d(\lambda)}. \tag{2.3}$$

L_u is the sum of two components: water leaving radiance (L_w) and radiance reflected at the water surface. The ratio of $L_w(\lambda)$ to $E_d(\lambda)$ is commonly reported as remote sensing reflectance, $R_{rs}\left(sr^{-1}\right)$, in aquatic optics:

$$R_{rs}\left(\theta_v, \varphi_v; \lambda\right) = \frac{L_w\left(\theta_v, \varphi_v; \lambda\right)}{E_d(\lambda)}. \tag{2.4}$$

Bi-hemispherical reflectance, $R(unitless)$, defines the ratio of upwelling plane irradiance, $E_u(\lambda)$, to downwelling plane irradiance, $E_d(\lambda)$, where light is measured using a cosine collector across the entire hemisphere in both corresponding directions:

$$R(\lambda) = \frac{E_u(\lambda)}{E_d(\lambda)} \tag{2.5}$$

While a horizontal plane is useful for introducing the mathematics of reflectance, natural surfaces are typically far more complex, encompassing multifaceted three-dimensional structures with a mixture of materials and/or species. Furthermore, light reflects disproportionally in different directions as a function of both surface characteristics and view and illumination angles. As such, it is important to understand that most reflectance measurements are in fact a generalized representation of an inherently complex parameter, particularly in the natural environment.

2.1.2 Microscopic description of reflectance

The intensity and angular patterns of reflection which we have described above are dependent on the interaction of light with the microscopic structure of the reflecting materials both organic and inorganic. Analysing the relationships between the bulk reflection coefficients and the properties of these microscopic structures can lead us to more general expressions that can be applied more widely to different environmental conditions. They also reveal how information about the physiological and physical state of a material can be derived from measuring its spectral reflectance.

Figure 2.2 shows a schematic of the microstructure elements relevant to scattering and absorption for both minerals (crystal grains) and vegetation (cells). The incident light rays are reflected and transmitted at the first surface. The rays transmitted through the first surface are subsequently both reflected back from the inner surfaces of the grains and absorbed in the bulk of the grain volume. The rays that penetrate deeper are multiply-scattered before coming back to the surface. These multiply-scattered photons result in a near Lambertian (uniform) scattering. Note that this scattering and absorption pattern is almost identical with the well known process of scattering from particles in the water column with one exception. For sediment, there is no diffraction effect (i.e., curvature of the light rays passing around the particle due to the wave nature of light) because of the close packing of the scattering and absorbing grains. The remaining reflection and refraction components of scattering of the grains in the solid aggregates are identical to those of the individual isolated inorganic and organic particles. This suggests that we can use some of the well known results of the studies of water column remote sensing reflectance and apply them to the estimation of reflectance of bulk organic and inorganic materials simply scaling them appropriately to account for the close packing arrangement and the resulting absence of the diffusion component from the scattering function.

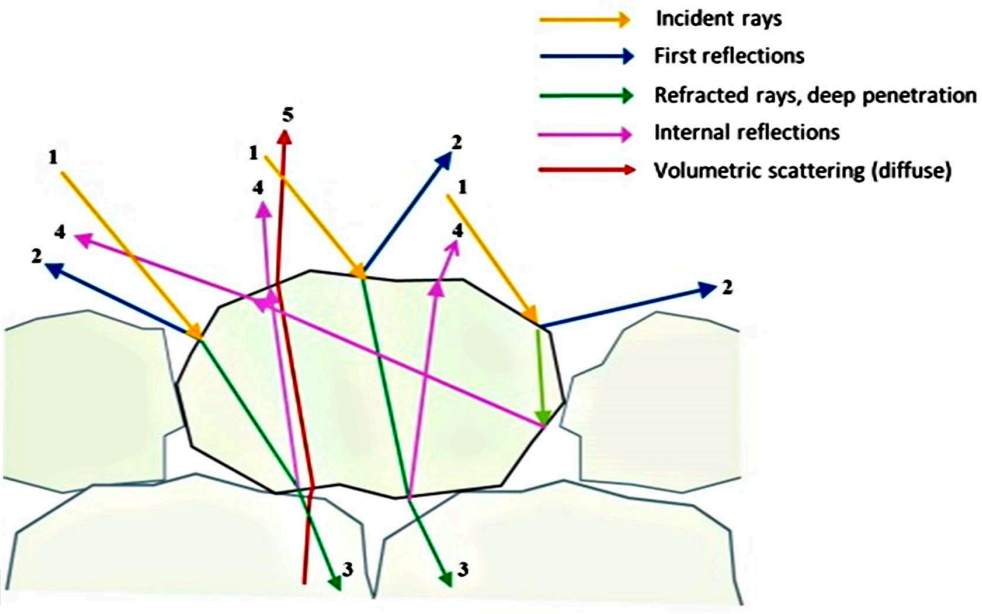

Figure 2.2 Schematic of the microstructure elements relevant to scattering and absorption for both minerals (grains) and vegetation (cells). The incident light rays (1) are reflected (2) and transmitted at the first surface (3). The rays transmitted through the first surface are subsequently both reflected back from the inner surfaces of the grains (4) and absorbed. The rays that penetrate deeper (5) are multiply scattered before coming back to the surface and have a near Lambertian (uniform) scattering distribution. Modified from Fournier et al. (2018).

2.1.2.1 Theory of irradiance reflectance from a scattering and absorbing medium

Broadly speaking, there are two general approaches to solving for the light exiting back out of the surface of a uniformly illuminated extended body after having been

diffused by multiple scattering and absorption. A well known instance of this problem, familiar to all oceanographers, is the irradiance reflection from sunlight illuminating the ocean. The first approach is based on the two stream model. It has the virtue of often producing reasonably accurate results that are essentially analytic and have the potential of describing simply the behaviour of the solutions that can then be used as basic elements for understanding more complex cases (Bohren, 1987). This model is most useful in the case of a very thick or deep medium where there is no return or exit from a bounding or bottom surface. The second approach is to use the full general scattering solution that can be obtained numerically either by a number of Monte-Carlo codes or a mathematical formulation known as invariant imbedding (C-disort, Hydro light; Mobley et al.1993). Albert and Mobley (2003) used the Hydrolight program to analyze the irradiance and radiance reflections from over 85,000 water columns with a wide range of absorption and scattering parameters and for a complete set of illumination and viewing angles. They derived a set of simple formulas that closely fit the full ensemble of their numerical results. They also obtained formulas for bottoms located at arbitrary depths and with various irradiance reflection values. These formulas for finite reflectance from finite depth media will be of particular use to us when analysing the effect of thin translucent materials such as algae and seagrass and the resulting problems in measuring their reflectance values.

In the former studies, two non dimensional parameters stand out as being key variables, the mean cosine of the scattering phase function and the backscattering albedo. Substances with the same mean cosine and the same backscattering albedo in the same physical disposition (illumination/viewing angles and depth) will have identical radiance and irradiance reflectance.

The mean cosine of the scattering distribution is defined as:

$$g(\lambda) = 2\pi \int_0^{\pi} p(\theta, \lambda) \cos\ \theta\ \sin\ \theta\, d\theta \qquad (2.6)$$

Where the phase function $p(\theta, \lambda)$ is scattering at a wavelength λ in a given direction θ and the cosine is taken between the scattering and the illumination direction in the plane containing both vectors. The formula uses the standard assumption that the scattering is independent of the rotation angle φ about the illumination direction, which is reasonable if we assume an ensemble of randomly oriented particles. This mean cosine is a measure of the amount of forward peaking of the scattering function with $g = 0$ being a uniform isotropic distribution and $g \approx 1$ being the case where the scattered photons are bunched in a very small cone around the illumination direction. In this second case it means that when looking along the direction of the light impinging on a surface, a medium with $g \approx 1$, even if only slightly absorbing, appears black since almost all the light is absorbed before it can resurface.

The backscattering albedo is defined as:

$$x(\lambda) = \frac{b_b(\lambda)}{a(\lambda)+b_b(\lambda)} \tag{2.7}$$

$a(\lambda)$ is the absorption coefficient and $b_b(\lambda)$ is backscattering coefficient which defines the fraction of the scattered light that is reflected in the backward hemisphere. The backscattering coefficient is given by:

$$b_b(\lambda) = 2\pi \int_{\frac{\pi}{2}}^{\pi} p(\theta,\lambda)\, b(\lambda)\, sin\,\theta\, d\theta \tag{2.8}$$

Both have units of inverse lengths. The problem we will address later is how to estimate the backscattering coefficient from knowledge of the microstructure of organic and inorganic materials

The two stream model simplifies the analysis of the penetration of an extended uniform source of radiation into a diffusing medium and its subsequent reflection by considering only the total upward and downward fluxes and their cross-interaction. These cross-interactions represent the transfer through diffusion from the downwelling radiation flux to the upwelling flux and the corresponding back transfer from the upwelling to the downwelling flux. The accuracy of the model depends directly on the accuracy of the evaluation of these transfer terms. The mean cosine $g(\lambda)$ is obviously a key parameter in the evaluation of the magnitude of these transfer terms. If the scattering distribution is highly forward peaked the initial transfer terms will be smaller at shallow depths. Conversely these terms will grow larger as the phase function approaches the isotropic limit where they will reach their maximum values.

Using the two stream model, Aas (1987) found a simple way to express the irradiance reflectance R_∞ as a function of the backscatter albedo and an approximation of the mean cosine. He derived a simple formula for the irradiance reflectance from a bottomless ocean illuminated by the sun at zenith and assuming constant absorption and scattering coefficients as a function of depth.

$$R_\infty = \frac{\left(1+f^2\right)-\sqrt{\left(1+f^2\right)^2-4f^2x^2}}{2\,f^2x}, \tag{2.9}$$

f is a parameter closely related but not equal to the mean cosine. Note that it is possible to estimate the backscatter albedo of a material given a measured irradiance reflectance, and therefore its absorption to backscattering ratio, by simply inverting the formula above.

$$x = \frac{\left(1+f^2\right)R_\infty}{1+f^2R_\infty^2}, \tag{2.10}$$

A best fit to the formulas for R_∞ derived by Albert and Mobley (2003) from the results of their detailed model gives a value of $f = 0.79$ (Fournier et al. 2018). With this

value, the results of Aas (1987) are virtually indistinguishable from those of Albert and Mobley (2003). For reference the results are shown in Figure 2.3A.

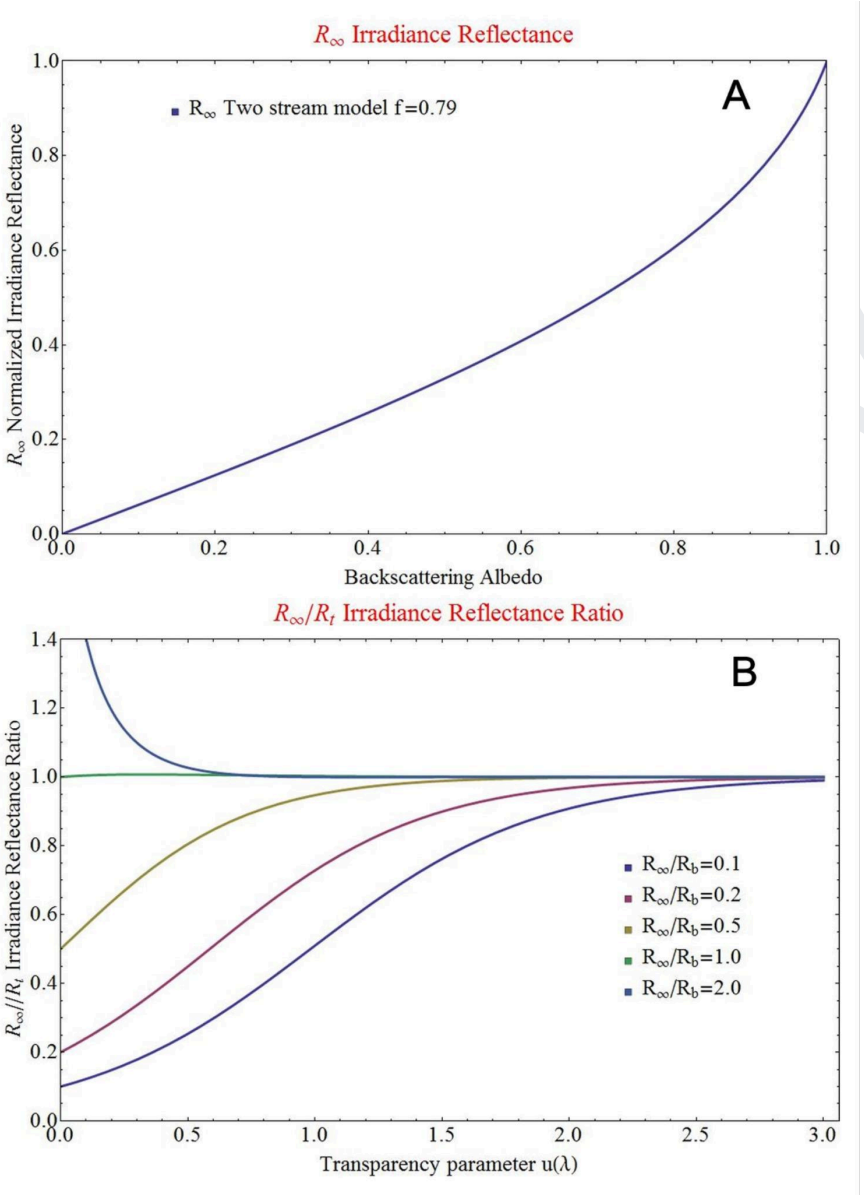

Figure 2.3 A) Irradiance reflectance for an infinite depth medium as a function of the backscattering albedo. The plot is based on the two stream model results of Aas (1987) combined with the Hydro light solutions of Albert and Mobley (2003) B) ratio of the cover irradiance reflectance to the total irradiance reflectance as a function of the transparency parameter for different values of the ratio of cover reflectance to bottom reflectance. Modified from Fournier et al. (2018).

2.1.2.2 Translucent material overlaid over a bottom substrate

Using their exact model, Albert and Mobley were further able to come up with approximate solutions for the case of finite depth z_b over a bottom that has its own irradiance reflectance R_b. These formulas allow us to model the important case of a

translucent organic material of reflectance R_∞ and thickness z_b deposited over a substrate of reflectance R_b.

$$R_t = R_\infty\left[1 - A_1 e^{-\gamma_0(\lambda)u(\lambda)}\right] + R_b A_2 e^{-\delta_0(\lambda)\,u(\lambda)}, \tag{2.11}$$

$$\delta_0(\lambda) = \left[\kappa_0 + (1 + x(\lambda))^{\kappa_{1w}}\left(1 + \kappa_{2w}\right)\right] \tag{2.12}$$

$$\gamma_0(\lambda) = \left[\kappa_0 + (1 + x(\lambda))^{\kappa_{1b}}\left(1 + \kappa_{2b}\right)\right] \tag{2.13}$$

$$u(\lambda) = \left(\frac{b_b(\lambda) z_b}{x(\lambda)}\right) \tag{2.14}$$

Table 2.1 gives the coefficients of Equations 2.11 to 2.14.

Table 2.1 Coefficients of the Albert and Mobley (2003) model for the finite medium depth case adjusted to correctly account for the limiting cases.

Coefficient	R_t
A_1	1.0000
κ_0	1.0546
κ_{1W}	1.9991
κ_{2W}	0.2995
A_2	1.0000
κ_{1b}	1.2441
κ_{2b}	0.5182

The term $u(\lambda)$ acts as a transparency parameter. As the thickness of the overlay z_b increases, the transparency decreases and the reflectance becomes close to that of the translucent overlay material, R_∞. As the thickness of the overlay z_b becomes small, its influence becomes negligible and the reflectance approaches the reflectance of the underlying substrate R_b. This behavior has important implications both in the measurement of the reference signatures for the irradiance reflectance of underwater vegetation and in the estimation of the fractional area coverage of that vegetation. The thickness of the organic overlay and its transparency must be measured. The model above also shows that the usual approach of linearly combining the separate reflectance signatures of the mineral substrate and the organic cover according to the weights of their relative areas only works in the limit where the cover is thick enough. For thin organic covers there is an exponential transfer of signature from substrate to cover which is a strong function of wavelength through the backscattering albedo of the translucent overlay $x(\lambda)$. Figure 2.3B shows the behaviour of the ratio of the overlay irradiance reflectance to the total irradiance

reflectance $\frac{R_\infty}{R_t}$ as a function of the transparency parameter and for different values of the ratio of overlay cover reflectance to bottom reflectance $\frac{R_\infty}{R_b}$. It clearly shows the transfer from the case of thin cover $\frac{R_\infty}{R_t} = \frac{R}{R_b}$ to the case of thick cover $\frac{R_\infty}{R_t} = 1$.

2.1.2.3 Estimation of the backscattering coefficient

To obtain estimates of R_∞ and R_t we now need to determine $b_b(\lambda)$. All the materials of interest to us absorb little per grain or cell and the light ray will encounter many inner surfaces before being scattered back out. In our evaluation of $b_b(\lambda)$ we will treat the reflection from the first surface boundary as similar to that of the inner deeper boundaries. The simplest model we can use for the backscattering from the surfaces is that of reflection from rough surface elements with random orientation. The backscattering cross-section for the reflection from a randomly oriented set of rough diffusers is given by (Fournier et al. 2018):

$$\sigma_b(\lambda) = \frac{5}{6}\,\sigma_g\,\omega_t(n) \tag{2.15}$$

σ_g is the geometric cross-section of an individual scattering structure and $\omega_t(n)$ is the Fresnel reflectance integrated over a set of randomly oriented surfaces of relative index of refraction n that together compose the boundaries of those structures. The total backscattering coefficient of the ensemble of the scattering elements with a number density N is by definition:

$$b_b(\lambda) = \frac{5}{6}\,\omega_t(n)\,N\,\sigma_g\,, \tag{2.16}$$

Assuming that the number density of the scattering structures N is such that the sum of their geometric cross-sections is equal to the area of the material normal to the impinging light, i.e. the structures are in close packing as in any inorganic or organic solid, we obtain the following formula for the backscattering coefficient of the material.

$$b_b(\lambda) = \frac{5}{6}\frac{\omega_t(n)}{\langle d\rangle}\,, \tag{2.17}$$

Where $\langle d\rangle$ is the mean diameter of the scattering structures. The formulas for $\omega_t(n)$ can be found in Fournier et al. 2018 and are given in Table 2.2 below for calcite and quartz which compose the majority of inorganic crystal grains found in the aquatic environment and cellulose which is the dominant organic cell and cell substructure wall material. The index of refraction of cell walls has been measured by Baranoski (2006). The values of $\omega_t(n)$ are given assuming that the gaps between the grains are either air filled $\left(n_w = 1.0\right)$ or water filled $\left(n_w = 1.333\right)$. Also shown are the resultant backscattering coefficients computed assuming mean grains sizes of 5 micron in diameter.

Table 2.2 Evaluation of the backscattering coefficients in m^{-1} of inorganic and organic materials for $5\ \mu m$ mean grain size

Material	$\omega_t(n)$	$\omega_t\left(\frac{n}{n_w}\right)$	$b_b(d = 5\mu m)$ $[m^{-1}]$	$b_{bw}(d = 5\mu m)$ $[m^{-1}]$
Calcite	0.1067	0.0445	17,794	7,409
Quartz	0.0990	0.0371	16,500	6,183
Cell walls	0.0789	0.0160	13,144	2,658

2.1.2.4 Evaluating weathering effects

When the gaps between the microstructure grains are water filled, the relative index of refraction at the boundaries is smaller and the resulting reflection and backscattering coefficients are considerably reduced. Since the absorption coefficient internal to the grains is unchanged in both cases, the corresponding backscattering albedo will be reduced and the irradiance reflectance will also be smaller (Fig 2.3) A common example of this phenomenon which we have all experienced is the fact that wet sand always appears darker than the same sand when dry. This has significant implications for when one is using irradiance reflectance signatures taken in air and attempts to extrapolate them to the case where the substances are immersed. In particular, if the inorganic substances have been immersed for a long time, water will have seeped between the grains composing their surface and several layers below that surface. This form of weathering will over time significantly reduce the irradiance reflectance of the inorganic materials. The reflectance will lie at a value somewhere between the dry and wet gap cases with the long term exposure asymptotic state approaching the water filled gap case.

The situation is different for organic materials such as algae or seagrass as their cells are basically composed of cellulose walls in water. The air gap index would correspond to the completely desiccated case which is rarely the state in which the reflectance of these substances is measured. For organic substances the increase or reduction in mean size $\langle d \rangle$ of the cells as a function of the health of the cell and saturation by the sea water environment is much more relevant to the estimation of their backscattering coefficient.

2.1.2.5 Analysis of inorganic material absorption

To complete our analysis we need to account for the absorption of materials. For pure minerals this absorption comes from the broadened far wing of the lowest energy electronic transitions in the deep UV and thus generally exhibits a smooth inverse power reduction as a function of increasing wavelength. Materials are however generally composed of aggregates of grains of different crystal types which modify the shape and rate of reduction of the overall absorption as the wavelength increases. A proportion of these crystalline grains also include colour center defects in their structures which give rise to further significant modulations that are superimposed on the smoothly varying background signatures.

The usual method for obtaining the absorption spectrum of mineral compounds is to measure the transmission loss through a sample of known thickness made from mineral powder that has been pressed and sintered. This is a time consuming process which requires great care to obtain sufficiently low backscatter. Using our model for reflectance opens up the alternative possibility of obtaining the relative absorption spectra in the visible and near-infrared region by simply measuring their irradiance reflectance. Given the irradiance reflectance R_∞ we first obtain the backscattering albedo x from the inverse relationship. Using the definition of the backscattering albedo and the formula we derived for $b_b(\lambda)$ we obtain the following expression for the absorption spectrum.

$$\langle d \rangle \, a(\lambda) = \frac{5}{6} \, \omega_t(n) \frac{(1-x)}{x} \tag{2.18}$$

Except for the scale factor of the mean crystalline grain size $\langle d \rangle$ we can now directly obtain the absorption spectrum for any substance for which we have measured an irradiance reflectance. In principle the detailed absorption shape could be further analysed to obtain an estimate of the details of the nature and proportions of the different crystals of the material of interest. It's interesting to note that for rocks that are near the shoreline this technique can easily detect the telltale signature of residual chlorophyll from surface embedded organic material. It's also possible to obtain an absolute value of absorption by visually measuring the grain size using thin slices of the materials, a standard geological analysis technique (petrographic thin section).

2.1.2.6 Analysis of organic material absorption

Absorption in vegetation is controlled by a combination of organic pigments contained in their cellular structure. Given the relative abundance of these pigments it is possible to reconstruct the complete absorption spectrum of any plant. Conversely it is also possible to extract the composition of the pigments by fitting the individual component spectra to the measured absorption spectrum of the vegetation (Lohrenz et al. 2003). In most cases the dominant component in the maritime environment is the absorption of the chlorophyll-a in the cells of the plants. This absorption takes place in the chloroplasts which are small disk-like vesicles floating freely inside the cells of the plants and that contain almost the entirety of the chlorophyll-a.

As the concentration of chlorophyll-a and/or the size of the chloroplasts increases, the absorption through the cell increases and the chloroplasts absorb more of the light until in the limit of large concentrations they become dark spots masking all the light their surface intercepts at a given wavelength. This absorption saturation effect was extensively studied by Morel and Bricaud (1981) who called it the package effect. This is the factor that dominates the variability seen in the absorption spectrum of different types of vegetation, even when they share single chlorophyll-a primary pigment (Fournier et al. 2018). The spectral variation of chlorophyll-a

absorption as a function of concentration increase can be adequately modeled by the following equation.

$$\frac{a_v^*(\lambda)}{a_o^*(\lambda)} = \left(\frac{1}{a_o^*(\lambda)\, 2\, \rho_{cp} \tau_{cp}}\right)\left(1 - e^{-a_o^*(\lambda) 2\, \rho_{cp} \tau_{cp}}\right) \tag{2.19}$$

$a_v^*(\lambda)$ is the specific mass absorption coefficient of chlorophyll-a in units of $m^2\ g^{-1}$. Multiplying this factor by the mass density of the chlorophyll in g/ m^3 gives $a(\lambda)$ the actual absorption coefficient in inverse meters. $a_o^*(\lambda)$ is the specific mass absorption coefficient of chlorophyll-a in the limit of low concentration (Bricaud et al. 1998). ρ_{cp} is the chlorophyll-a mass density inside the chloroplast in g m^{-3} and τ_{cp} is the thickness of the chloroplast disk in meters. The main implication of the discussion above is that we expect to be able to model the spectral shape of the absorption spectrum of chlorophyll-a with a single fitting parameter $\rho_{cp}\tau_{cp}$. Conversely it now becomes possible to infer the health status of vegetation from a measurement of the spectrum of irradiance reflectance, i.e. the plant's spectral reflectance signature. A more extensive discussion of the detailed techniques to achieve this and their constraints and limitations can be found in Fournier et al. (2018).

2.2 Radiative Transfer in Optically Shallow Water

The propagation of light from the benthos and through an intervening water column must be considered when making measurements of benthic reflectance. In general, the paths of light are very complicated. The basic equation describing all interaction processes with matter is the *radiative transfer equation*, RTE (Jerlov, 1976; Bukata et al. 1995; Kirk 2011; Gege 2017; Mobley et al. 2023). A simplified version of the RTE that ignores polarization is used here to explain the fundamental environmental parameters and measurement quantities and their relationships. This section briefly summarizes the aspects most relevant to this report. However, the reader is referred to the references above for more detailed information relevant to remote sensing of optically shallow water.

Liquid water absorbs electromagnetic radiation very strongly at almost all wavelengths. For pure water, the distance after which 90 % of incident radiation is absorbed exceeds 1 m only from 277 to 714 nm (Hale and Querry, 1973). The ubiquitous organic compounds absorb short-wave radiation very effectively, so that light penetration in the ultraviolet range is further greatly reduced even in very clear waters. Consequently, only the spectral range from about 300 to 715 nm is relevant for biologic processes such as photosynthesis and vision (Figure 2.4), even in clear and shallow water. This is the spectral region of light visible to humans, extended a bit towards the ultraviolet.

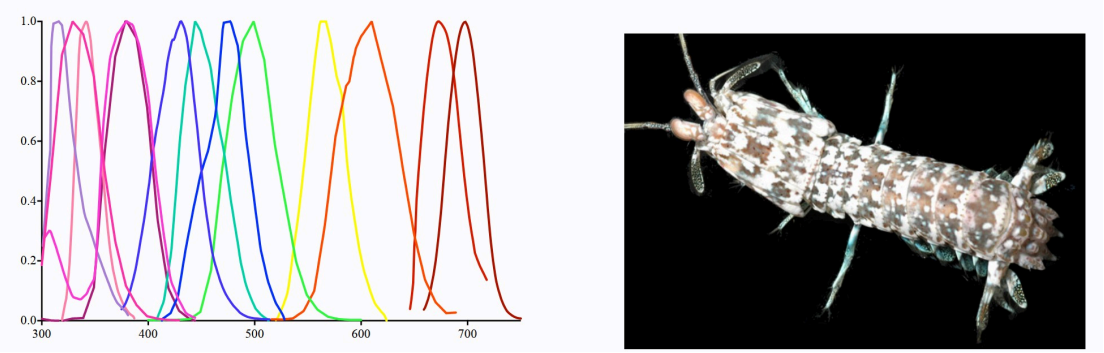

Figure 2.4 A complex optical sensor for benthic environments is the eye of mantis shrimps (right) from the Order Stomatopoda. The spectral sensitivity of the 12 photoreceptors used for colour vision (left) covers the range in which electromagnetic radiation can penetrate more than 1 m into the water. The number of these photoreceptors, and hence their absolute sensitivity, is adjusted to the environment in which the animal lives; they inhabit depths between 0 and 1500 m. Their eyes also can detect linear and even circular polarization. As each eye can be moved independently, the field of view is very large. Pictures from Thoen (2014).

Light is expressed in the RTE by two parameters: radiance L and wavelength λ. As noted above, radiance is defined as the radiant flux ϕ impinging from the direction (θ, φ) inside a small solid angle $d\Omega$ on a small area dA:

$$L(\lambda, \theta, \varphi) = \frac{d^2\phi(\lambda,\theta,\varphi)}{dA\, d\Omega}. \quad (2.20)$$

The radiant flux is the energy ε of N photons per unit of time, t:

$$\phi(\lambda) = \frac{N\varepsilon(\lambda)}{t}. \quad (2.21)$$

Because the energy of a photon depends on wavelength, ϕ and L are λ-dependent.

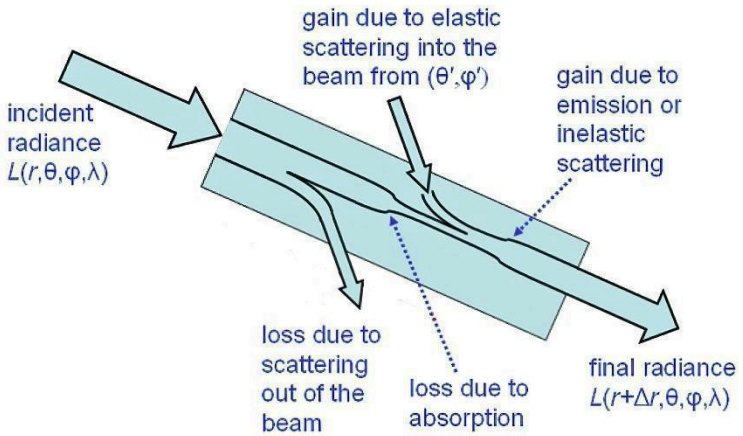

Figure 2.5 Illustration of the processes that change the radiance of a light beam travelling in a medium. Adopted from Mobley et al. (2023).

The RTE expresses the change of radiance, dL, of a light beam of wavelength λ travelling a small distance dz in a medium at depth z in the direction (θ, φ) in terms of losses by attenuation (coefficient c) and gains by elastic scattering (radiance L_s^*) and inelastic scattering (radiance L_{in}^*) (Figure 2.5):

$$cos\theta \frac{dL(\lambda,z,\theta,\varphi)}{dz} = -\, c(\lambda, z)L(\lambda, z, \theta, \varphi) + L_s^*(\lambda, z, \theta, \varphi) + L_{in}^*(\lambda, z, \theta, \varphi). \qquad (2.22)$$

The processes leading to L_s^* and L_{in}^* act as light sources along the light beam. Elastic scattering by water molecules and by dissolved and suspended constituents produces the radiance L_s^*:

$$L_s^*(\lambda, z, \theta, \varphi) = \int_0^{2\pi} \int_0^{\pi} \beta(\lambda; \theta, \varphi; \theta', \varphi')L(\lambda, z, \theta', \varphi')sin\theta' d\theta' d\varphi'. \qquad (2.23)$$

The function $\beta(\lambda; \theta, \varphi; \theta', \varphi')$ specifies the probability that radiance is scattered from initial directions (θ', φ') to the direction (θ, φ) without change in wavelength. It is called *volume scattering function*, VSF, and has units of $m^{-1}\, sr^{-1}$.

Trans-spectral processes like Raman scattering and fluorescence, and emission processes like bioluminescence, are summarized in the radiance term L_{in}^* representing inelastic scattering. As noted in Chapter 7, some benthos have unique pigments that fluoresce differently from water column phytoplankton, including the green fluorescence proteins found in tropical coral reefs ecosystems. The corresponding VSF $\beta_{in}(\lambda, \lambda'; \theta, \varphi; \theta', \varphi')$ parameterizes both probabilities for a change of wavelength from λ' to λ and for a change of direction from (θ', φ') to (θ, φ). L_{in}^* is given by

$$L_{in}^*(\lambda, z, \theta, \varphi) = \int_0^{2\pi} \int_0^{\pi} \int_0^{\infty} \beta_{in}(\lambda, \lambda'; \theta, \varphi; \theta', \varphi')L(\lambda', z, \theta', \varphi')sin\theta' d\lambda' d\theta' d\varphi'. \qquad (2.24)$$

In shallow water, reflectance from benthic substrates, including benthic fluorescence and bioluminescence, are an additional and very important source of radiance:

$$L_r^*(\lambda, z, \theta, \varphi) = \int_0^{2\pi} \int_0^{\pi} f_r(\lambda; \theta, \varphi; \theta', \varphi')L(\lambda, z, \theta', \varphi')sin\theta' d\theta' d\varphi'. \qquad (2.25)$$

The function $f_r(\lambda; \theta, \varphi; \theta', \varphi')$ is the counterpart to $\beta(\lambda; \theta, \varphi; \theta', \varphi')$ for reflection at a solid surface. It specifies the probability that radiance is reflected from initial directions (θ', φ') to the direction (θ, φ) without change in wavelength. As noted

above, the BRDF parameterizes the reflection from a surface while a VSF describes scattering along a path, the units are different, i.e. sr^{-1} and $m^{-1}\,sr^{-1}$, respectively.

2.3 Apparent optical properties

Preisendorfer (1961) has coined the terms inherent optical property (IOP) and apparent optical property (AOP) to distinguish between material parameters which are independent (IOP) and dependent (AOP) on the illumination and observation geometries. The material parameters in the RTE are IOPs, while most parameters relevant to studies of the benthos are AOPs (e.g., R_B,, K_d). The IOPs of a mixture of components are additive and depend linearly on the concentrations, which is in general not the case for AOPs. The AOPs are bulk material properties which can be measured under natural illumination conditions in the field. They are defined in terms of ratios or depth derivatives of radiometric measurement parameters, since these are much less dependent on the light field than the radiometric quantities themselves.

Light extinction by a water body is characterized by a number of attenuation coefficients, defined as the rates of change with depth of radiometric quantities. The *diffuse attenuation coefficient of irradiance* is defined as the depth derivative of irradiance:

$$K(\lambda) = -\frac{1}{E(\lambda)}\frac{dE(\lambda)}{dz}, \tag{2.26}$$

and the *diffuse attenuation coefficient of radiance* is analogously given by the depth derivative of radiance:

$$k(\lambda;\theta,\varphi) = -\frac{1}{L(\lambda;\theta,\varphi)}\frac{dL(\lambda;\theta,\varphi)}{dz}. \tag{2.27}$$

Both K and k have units of m^{-1}. Common variants of K are K_d and K_u, in which E (Eq. (2.7)) is specified for horizontally oriented plane surfaces illuminated from downwelling and upwelling directions, respectively. Similarly, common variants of k are k_d and k_u with L (Eq. (2.1)) being measured in zenith ($\theta = 0$) and nadir ($\theta = \pi$) direction, respectively. Attenuation coefficients are determined by measuring irradiance or radiance in different depths and computing their depth derivatives.

For reflection at the bottom, the exact relationship between the radiance reflected at the bottom, the incident light field and the optical properties of the bottom is given by Eq. (2.6). In all practical applications, neither the light field under water nor the BRDF of the substrate are accurately known. Bottom reflectance is, therefore, usually approximated either by an AOP that depends on λ, θ and the sun zenith angle θ_{sun}, or by an AOP that completely ignores all angular dependencies. Benthic reflectance is defined as the ratio of upwelling to downwelling plane irradiance at the depth of the benthos (B):

$$R_B(\lambda) = \frac{E_u(B,\lambda)}{E_d(B,\lambda)} . \qquad (2.28)$$

R_B is the bi-hemispherical reflectance (BHR) or albedo (Nicodemus et al. 1977; Schaepman-Strub et al. 2006). If all angular dependencies of light reflectance can be neglected, the substrate is a so-called Lambertian reflector.

2.4 Effects of three-dimensional structure

In general, bottom types are not flat surfaces. Even the flattest sandy substrates have undulations and a granular microstructure, vegetation canopies have a vertical structure underlain by a substrate, and coral reefs exhibit complex three-dimensional structures across scales from millimeters to many meters. This three-dimensional structure complicates the notion of "benthic reflectance" in the following ways:

- There is variable orientation of surfaces with respect to the incident light and view directions, for example, consider the top and sides of a dome shaped coral.
- Shadows − some parts of the benthic structure occlude other parts of the structure from incident light, the effect depends on the spectral and directional nature of the incident light.
- Vertical height differences mean that within a remote sensing pixel (for example) there may be a variable contribution of overlying water to the "bottom reflectance".
- All of the above are dependent on the direction of illumination and the view direction onto the benthic structures.

Consequently, the following concepts are important theoretical and practical considerations in measurement and modelling of benthic reflectance.

2.4.1 Spatial scale

The spatial scale of interest is the key parameter to guide best practice. For example, the reflectance of a large dome shaped coral taken close to the surface is not the benthic reflectance of that same structure at remote sensing scales (e.g., several metres). Even in an area of 100% cover of such corals, image pixels at scales larger than the coral will encompass the sides of the corals, which are illuminated differently than the top. Shadows are also evident where the structure occludes the incident light (Hedley, 2008). In addition, the light reflected from the regions between the corals passes through more water than that reflected from the tops of the corals.

The issue is minimised if benthic reflectances are measured at scales that fully encompass the three-dimensional structure, because the measurement 'averages out' any structural effects. This can be achieved either by individual measurements having a sufficiently large field of view (Leiper et al. 2011), or, by averaging multiple measurements that are distributed spatially. In general, care must be taken when the spatial scale of measurement is smaller than that at which the canopy structure can be considered homogenous.

2.4.2 BRDF effects

An important concept is that almost all surfaces potentially exhibit a 'hot spot' or 'retroreflection' effect in the BRDF: the reflectance is higher when the view and illumination directions are the same or close. In this illumination-view geometry shadows are at a minimum, as the view 'looks into' the structure in the same way it is illuminated. This is true even for ostensibly flat sandy bottoms because it occurs at the scale of the grains (Mobley et al. 2003a). However, for vegetation canopies the effect may be more profound, especially if the underlying substrate is bright (Figure 2.6a-c). Best practice is simply to be aware of the potential of the hotspot effect and avoid it where possible, it can occur both in benthic measurements and in remote sensing data, if the solar illumination and sensor view are aligned. Other BRDF features are in general less important, specular reflection is typically minimal in natural underwater surfaces (Mobley et al. 2003a) and features close to horizontal directions are less relevant (Hedley and Enríquez, 2010). In practice, aquatic applications rarely employ full BRDFs but predominantly assume Lambertian (diffuse) bottom reflectance. Mobley et al. (2003a) found this approximation generally leads to errors of less than 10% in modelled water-leaving radiances.

2.4.3 Spectral mixing

The benthic composition is often heterogeneous at scales smaller than those relevant to remote sensing applications. To handle this, it is frequently assumed that mixed pixel reflectance can be treated as the reflectances of individual benthic types and substrates summed, scaled in proportion to their areal cover within the pixel. This concept, referred to as 'linear mixing' originated in the context of minerals (Adams et al. 1986). Benthic structural complexity complicates the situation and while relatively few aquatic studies have been done, data frequently does not conform to a linear mixing model (Hedley et al. 2004). Multiple scattering between the overlying water column and benthos may also lead to a non-linear contribution from the benthic reflectance, but the effect is likely to be small.

2.4.4 Canopy modelling

One approach to understand the influence of benthic structure on reflectance is via canopy modelling (Ackleson and Klemas 1986; Hedley 2008; Zhou et al. 2015; Zimmerman 2003a,b). This enables an inherently small-scale measurement, such as the reflectance of a coral surface, or the reflectance and transmission of a seagrass leaf, to be scaled up to canopy scale. For example, coral surface reflectance can be mapped over a dome shaped structure and the model can estimate the large-scale reflectance over the structure (Hedley 2008). Note the converse issue arises for inputs for such models; the reflectance of "a coral" is not the same as the *coral surface* reflectance, and vice-versa, except if the coral is a completely flat surface (Figure 2.6d-e). Canopy models can be used to establish approximate relationships, for example, shading in coral structures has been shown to be reasonably captured by scaling the surface reflectance, effectively introducing a black reflectance component (Figure 2.3.1, Hedley et al. 2018).

(a) Fisheye view over modelled canopy

(b) Modelled BRDF over dense seagrass canopy

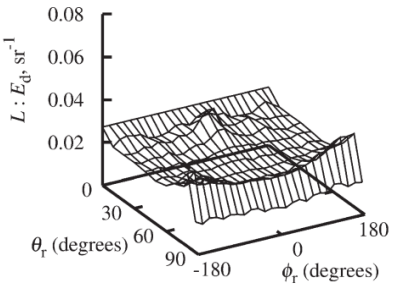

(c) Modelled BRDF over sparse seagrass canopy

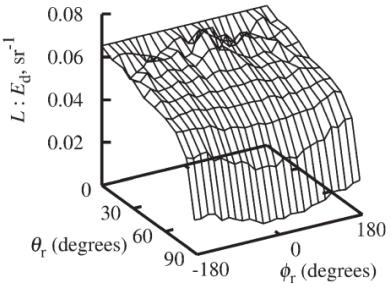

(d) Modelled coral on sand substrate illustrating shadows

(e) Reflectance including shadows in (d) is approximately coral surface reflectance · 0.76

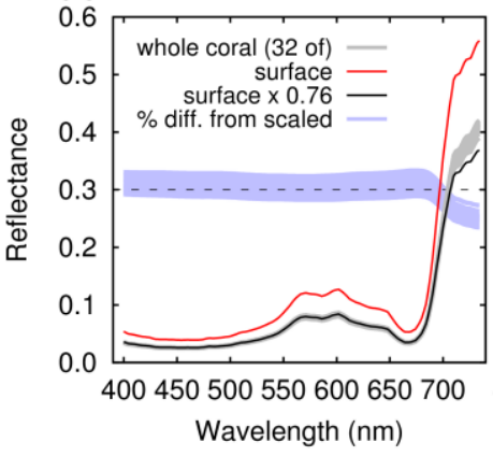

Figure 2.6 Effects of three dimensional structure on reflectance. (a) At certain view angles over a canopy shadows are minimal and more substrate is visible. (b,c) Retroreflection peak in modelled seagrass BRDFs for illumination at 20 zenith angle. (d,e) Relationship between coral reflectance, coral surface reflectance and shadows (Hedley and Enríquez 2010; Hedley et al. 2018).

Chapter 3

Instrumentation and Measurement Techniques

Richard C. Zimmerman, Heidi Dierssen, Tiit Kutser, Peter Gege, Natascha Oppelt, Brandon Russell, Arnold Dekker, Julien Laliberté, Geir Johnsen, Gema Casal, Jaime Pitarch

The reflectance properties of an object can be measured using a variety of instruments and approaches depending on the nature of the object, the spatial scale of interest, and the intent of the investigator. This chapter provides information on sensing instruments and a range of sampling approaches that have been used to measure reflectance of targets ranging in size from a few μm^2 to several m^2 in scale. These approaches have been conducted using natural and artificial illumination transmitted through air and natural water that contain a range of optically active materials. The inclusion of a method here does not imply it is a “preferred” method or “best practice” that has been vetted by the larger community. Rather, we include a wide variety of techniques that have been used for a diverse suite of benthic targets. No single approach fits every type of benthic habitat and all approaches have both strengths and weaknesses, as well as varying degrees of uncertainty, for different applications. Moreover, future advances in instrument technology and theory may lead to new methods not discussed here (see Chapter 11).

Reproducible measurements of object reflectance can be made only in the laboratory under carefully controlled illumination conditions. For example, bright field microscopes fitted with optical spectrometers can measure the albedo of individual cells, sand grains and other extremely small objects at a spatial scale of 5 µm or less under diffuse illumination. Integrating spheres can be used with scanning spectrophotometers to measure the spectral albedo of a few cm^2 of relatively flat surfaces of seagrass leaves, algal thalli and other objects small enough to be placed in the reflectance window.

Laboratory measurements are useful to make different objects comparable under repeatable controlled conditions, but this may not represent the true reflectance within an underwater habitat. For example, reflectance based on pieces of individual leaves, thalli, or coral polyps do not necessarily represent the reflectance of complex 3-dimensional organisms suspended in a fluid medium. Reflectance measured in the field may better incorporate the 3-dimensional geometry of the target but issues of illumination can become more challenging.

Field measurements using natural illumination are dependent upon the illumination geometry, in particular on the sun-zenith angle and cloud conditions, and water column optical properties. Beyond a point measurement, imaging spectrometers in the field and laboratory provide an image with reflectance values spatially varying across a sample. Detectors can have differing spectral resolution and fields of view placed at a range of distances and viewing angles from the target that can be

illuminated with natural light or various sources of artificial light. Here, we highlight methods to quantify benthic reflectance: 1) In-air; 2) In-water: Proximal to target (cm-scale); 3) In-water: Distal to target (m-scale). As the distance between target and sensor grows, it becomes increasingly difficult to get an accurate measurement without interference from the absorbing and scattering properties of the water column (Maritorena et al. 1994). For purposes of this report, we feel that measurements much greater than 2 m from the substrate are considered modeled estimates of benthic reflectance rather than measurements. Additionally, we discuss the necessity to properly collect metadata with each measurement. Some additional information on sampling different types of habitats can also be found in Chapter 7.

3.1 In-air Measurements

A common method to measure the reflectance of a target is to collect it from the benthos and make the measurement in air. Such measurements avoid the need to correct for light attenuation and scattering by the water column. They also allow measurements to be extended well into the UV and infrared where water is highly absorbing. However, removing samples from the water may introduce measurement artifacts resulting from desiccation, high light exposure and disruption of the natural orientation between the target material and the illumination field. If the sample is left damp, the measurement can suffer from considerable glint from the illumination source that would not be present underwater. If the sample has a thin layer of water above, such as for a sediment core, the reflectance measurements may require corrections for the air-water interface and changes in the index of refraction. As with all measurements, the user is responsible for ensuring that the reflectance measurement technique is appropriate for the scientific goals of the study.

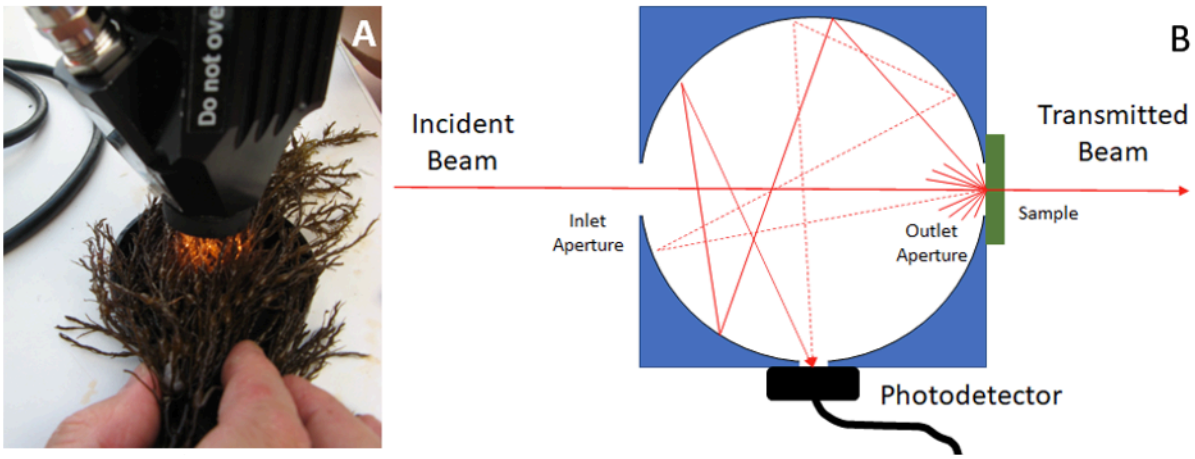

Figure 3.1 Laboratory measurements can involve various techniques including A) Controlled light conditions with ASD FieldSpec FR spectroradiometer including a high intensity contact probe housed with a 100 W halogen lamp B) use of integrating spheres. Photo credit: A) G. Casal

Benchtop spectrophotometers and fiberoptic spectrometers can be utilized to deliver reproducible reflectance measurements of objects placed in the outlet aperture (or reflectance window) of an integrating sphere that captures all the light reflected from the sample (Figure 3.1). The target area is illuminated by a narrow incident beam passing through the sphere without scattering in the absence of a target placed over

the apertures. The incident beam can be monochromatic light in the case of a scanning spectrophotometer that uses a single photodiode or photomultiplier tube photodetector, or white light in the case of a CCD array photodetector. The sphere is lined with diffuse, highly reflective white material such as Spectralon® or tightly packed barium sulfate. The instrument is baselined using a ~100% reflectance target (e.g., Spectralon® or barium sulfate) plaque placed in the outlet aperture of the sphere. The reflectance plaque is then replaced with a sample of interest for measuring reflectance. Care must be taken to ensure that the wet sample completely obscures the outlet aperture but is not held against the sphere so long as to dry out. The method can provide reflectance estimates for small samples of a few cm^2 for isotropic illumination and has been commonly used for algal thalli or seagrass leaves (e.g., Cummings and Zimmerman, 2003; Léger-Daigle et al. 2022).

Integrating spheres (Figure 3.1B) provide reproducible estimates of reflectance independent of object shape and orientation at very small spatial scales from both Lambertian and non-Lambertian surfaces because they capture all the light reflected from the target. They can also be used to measure the reflectance and absorption of epiphyte layers growing on intact leaves, and their impacts on combined reflectance of the leaf-epiphyte assemblage (Drake et al. 2003).

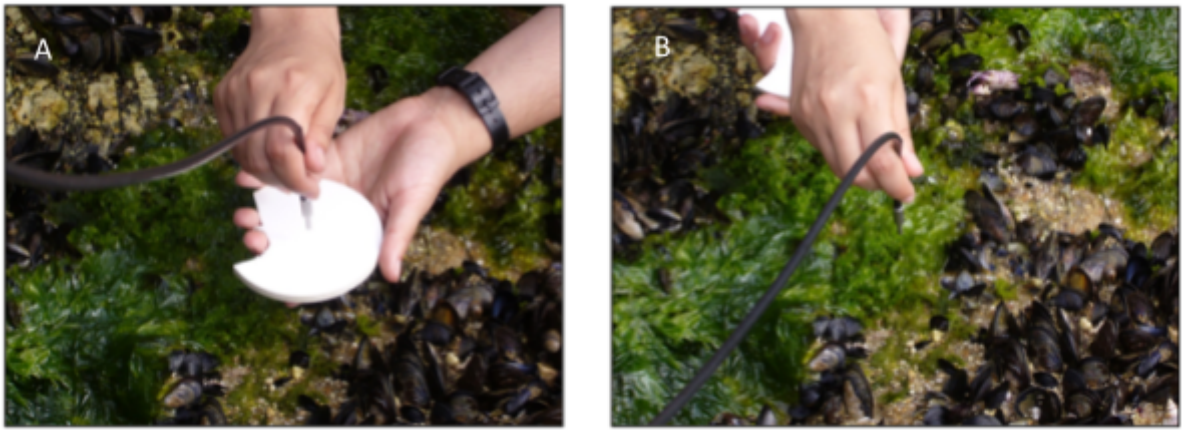

Figure 3.2 Example of using a hand-held fiber optic probe in air to measure intertidal organisms A) over a white plaque to estimate downwelling irradiance and B) over a target of interest. Probe set at a nadir viewing angle in this example with diffuse light. Photo credit: G. Casal

Spectral reflectance can also be measured in the field or laboratory using portable fiberoptic systems without an integrating sphere (Figure 3.1A, Figure 3.2). This may be particularly advantageous for large and irregularly shaped objects that do not fit easily into the reflectance window of an integrating sphere. Illumination may be provided by natural sunlight or artificial light sources. The sample must be arranged to fill the entire field of view of the detector to avoid mixed signals. Samples should be placed on a dark black substrate to minimize the secondary reflection of light off the substrate and transmitted back through the sample to the sensor. Regardless of illumination source, the instrument is calibrated against a reference plaque, usually white or gray, of known spectral reflectance immediately prior to measuring the reflectance of each sample (Chapter 4.1). Care must be taken to ensure that (i) both the reference plaque and the sample are uniformly illuminated at the same intensity

and minimizing glint angles, (ii) the field of view of the radiometer is filled completely by the reference plaque or sample, and (iii) the reflectance of the neutral density black substrate used beneath the sample is sufficiently low (R < 0.05) so as not to contaminate the measurement with stray reflected light.

One of the most accessible benthic habitats is the intertidal zone which contains mudflats and emergent vegetation. In such cases, a variety of measurement techniques have been used to collect time-dependent variability in the reflectance of mud flat algal biofilms, for example (Figure 3.3). Sensors should be oriented to avoid shading of the target and receiving direct sun glint. Reference irradiance sensors may, when possible, be located at an elevated position, to avoid ambient interference. The distance to the target is less important because atmospheric contributions to the detected signal are minimal at only a few feet. In terms of data sampling, a sequence of measurements for each sensor, followed by temporal uniformity check, and posterior data reduction, is advisable.

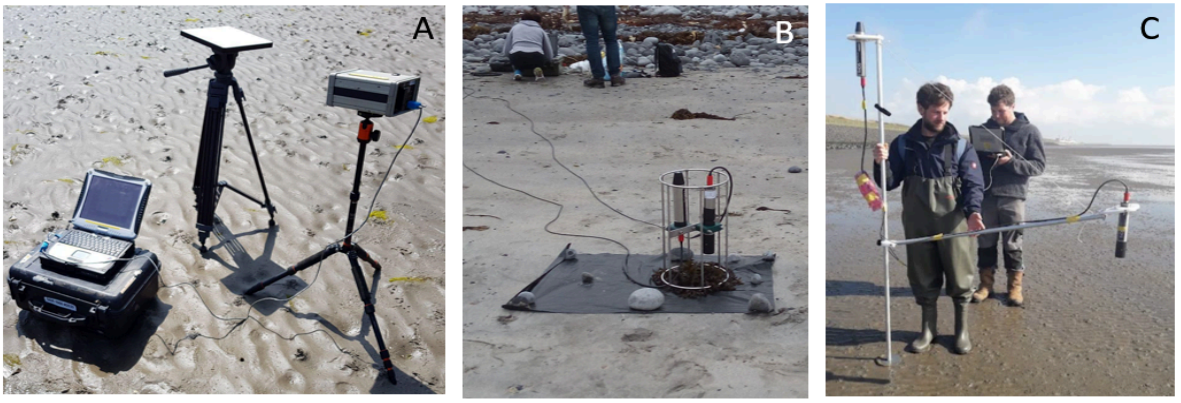

Figure 3.3 Various systems devised to measure reflectances of mud flats and associated organisms that include A) a single spectrometer (GER1500) with a plaque measurement using a tripod for maintaining horizontal orientation; B-C) two calibrated sensors (TriOS RAMSES) measuring upwelling radiance and downwelling irradiance simultaneously. Photo credit: A,B) G. Casal, C) J. Pitarch

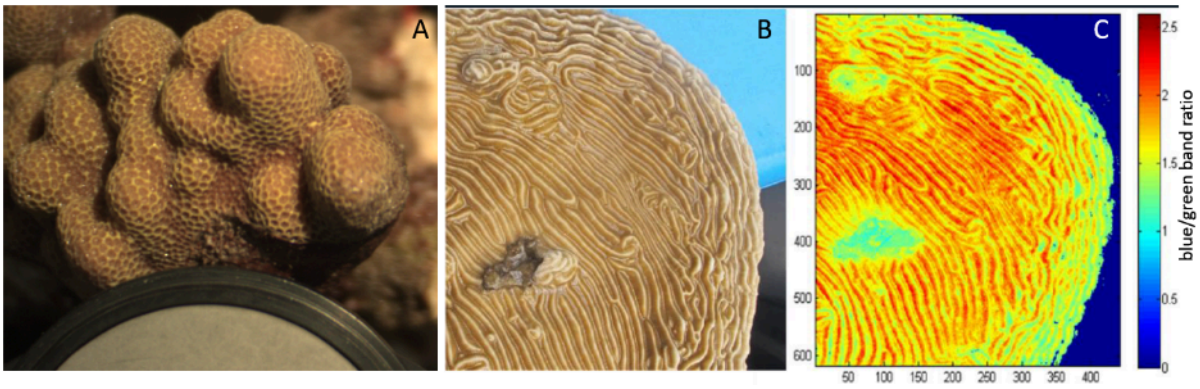

Figure 3.4 Examples of imaging spectrometers used in air to measure coral benthic reflectance A) incorporating a gray plaque in the imagery; B-C) High resolution imagery provides estimates of where pigments are located in the coral head using standard blue to green reflectance ratios. Photo credit: H. Dierssen, B. Russell.

Imaging spectrometers can add important spatial information to the reflectance measurement. Rather than providing a single reflectance spectrum averaged over

the field of view of a particular target, imaging systems provide an array of potentially unique spectra for each pixel in the image. However, the determination of reflectance values from such imagery depends on the ability to quantify the light intensity falling on each pixel from the source of illumination. Although this may be determined easily for flat surfaces under ambient solar illumination, it may be more challenging to determine the illumination for each pixel with artificial light and/or irregular surfaces. Imaging spectrometers have been used in both the field and laboratory to study reflectance of different targets spatially. For example, the HySpex airborne hyperspectral imager has been used with a special bench to move the pushbroom camera in a uniform direction to develop an image. This approach was used to measure a variety of benthic targets in the lab using artificial lighting (Vahtmäe et al. 2017). Commercial imagers like the 710 Hyperspectral Imager (Surface Optics Corporation) internally sample across a target to develop an image (520 x 696 pixels) across visible and NIR wavelengths. Such imagers have been used in the field to sample benthic reflectance of pelagic *Sargassum fluitans* (Russell et al. 2015) and coral fragments (Russell et al. 2016). For example, the imager was able to acquire 10,000 pixels per cm^2 of coral sample to evaluate changes spatially and develop a robust average and standard deviation per sample (Russell et al. 2016) (e.g., Figure 3.4) Letnes et al. (2019) conducted laboratory experiments with an imaging spectrometer to assess how changes in benthic reflectance could inform the responses of cold water corals to oil spills.

The more isotropic (i.e., Lambertian) the target, the less it will depend on the view angle and the illumination direction. Examples for relatively isotropic reflectors are sediment surfaces, the rough side of flat leaves and algal thalli (Mobley et al. 2003b, Voss et al. 2003). The reflectance of non-Lambertian surfaces will be affected by the directions of the incident illumination and reflected radiances. These angular dependencies are specified by the bidirectional reflectance distribution function (BRDF). Determining the BRDF requires a large number of measurements at various illumination and viewing angles. Voss et al. (2000) describe an instrument to measure the BRDF of flat surfaces in the laboratory and *in situ*.

The uniformity of the target surface determines the working distance between the target and the sensor. At extremely small scales, the spectral reflectance of living (cells and subcellular components) and non-living materials (crystalline objects, glass, polymers, ores, ceramics, etc.) can be obtained using reflected light microscopy by placing a spectrometer in the optical viewing path of the microscope. In this case, the working distance will be determined by the focal length of the microscope's objective lens. As with the macroscopic benchtop instruments mentioned above, the reflectance measurement can be calibrated using a reference slide placed prior to measuring the sample reflectance.

At the macroscopic scale of apparently homogeneous, diffuse reflecting surfaces such as sediments, plant leaves or algal thalli, the working distance between the target and the sensor can be as close as practical without casting a shadow on the target. As the target becomes increasingly heterogeneous (e.g., a 3-dimensional coral head or 3-dimensional vegetation canopy), the field of view of the detector must increase to integrate that heterogeneity into the reflectance measurement

accurately. Because such heterogeneous materials are not likely to be Lambertian reflectors, measurements should be made at multiple angles to estimate the BRDF. However, this represents a considerable measurement / instrumentation challenge for 3-dimensional objects since the determination of BRDF with instruments such as that described by Voss et al. (2000) requires precise knowledge of sample height at each illumination/measurement angle.

For all methods mentioned above, caution must be taken to avoid glint when sampling damp objects in air. Wet seagrass leaves, macroalgal thalli, and sediment cores may create significant glint (Vahtmäe et al. 2017). To minimize water reflections, some sample preparations can involve gently centrifuging the samples with a salad spinner (Perry et al. 2018) or drying the study objects with paper tissue before sampling to remove standing water. Care must be taken such that the optical properties are not changed by removing epiphytes, detritus and other material that may influence the reflectance properties. Both preparation of the study objects and the light geometry during the sampling must be taken into account when sampling in air.

3.2 In-water Measurements – Proximal to Target (cm-scale)

Instruments and procedures for measuring benthic reflectance underwater, in many respects, are conceptually similar to the laboratory measurements described above. In-water measurements makes it possible to gather benthic reflectance from features in their natural environment, and does not require taking benthic features out of the water that require potential permits and changes their natural surroundings. However, the current lack of commercially available systems ready for underwater use has necessitated practitioners to assemble their own units of varying complexity, using commercially available miniature spectrometers. This section outlines the “proximal” approach to obtaining benthic reflectance when the sensor probe is at or within a few centimeters from the target. These types of measurements can be conducted in experimental tanks of material where a probe is placed above or underwater. Commonly they are conducted underwater by divers using hand-held units (Figure 3.5). In such cases, divers can manually set integration times and make individual measurements of specified substrates. These methods are restricted to relatively shallow waters where divers can operate, or to experimental tanks.

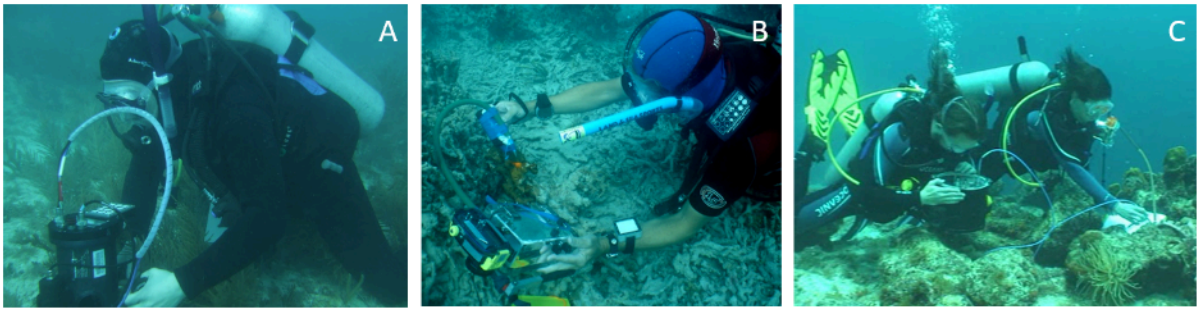

Figure 3.5 Hand-held underwater spectroradiometer systems with fiber optic probes A) once commercially-available Night-sea unit with artificial illumination in a closed path system; Photo credit: H. Dierssen B) single diver unit with artificial illumination and a fibre optic cable; Photo credit: C. Roelfsema. C) two divers operating a handheld system with ambient solar illumination. Photo credit: Jeff Godfrey (UConn).

Making high quality reflectance measurements underwater with ambient illumination can be challenging in turbid or deep water where incident blue and red wavelengths have been absorbed by the overlying water column. In clear shallow waters, surface waves can produce caustics that rapidly focus/defocus the incident light beam in ways that may bias the reflectance measurement. Further, strong currents and wave-induced surge can affect the diver's ability to maintain proper orientation over the substrate while the measurement is being made. Using external illumination sources can mitigate some of these issues, but significant challenges exist in providing sufficient illumination across the full visible spectrum, providing even illumination across both the sample and calibration plaque, and avoiding glint.

The simplest underwater systems involve a single spectrometer placed in a waterproof housing and connected to a fiberoptic probe that collects radiance from a defined angular field of view (Figure 3.5; Joyce et al. 2002; Gilerson et al. 2013). These systems have the added advantage in that they can also be used out of the water, following the procedures outlined in Section 3.1, above. As with the laboratory instruments, these field spectrometers can employ natural or artificial illumination and can be deployed by a single operator below water. Each measurement must be carefully recorded with a reflectance standard at the same depth and orientation as the target. Using one spectrometer with a plaque avoids the need for absolute radiometric calibration of the instrument. Furthermore, because the target and the reference standard are measured by the same sensor in the same environment, there is no need to determine the immersion coefficient (Smith 1969) for these systems. However, wavelength registration of the field instrument must be calibrated and corrected for any temperature effects that alter the grating-CCD alignment in the spectrometer.

Many different protocols are possible for sampling with a plaque underwater. A possible approach is as follows where each measurement may be an instrument-derived average of several measurements. The integration times can be long underwater under natural illumination and it is imperative to complete the sampling sequence as quickly as possible so light conditions do not change:

1. Optimize the instrument to local light conditions
2. Make 1 to 2 measurement of the plaque shading direct beam
3. Make 8 to 10 measurements of the target from different angles around target maintaining shading, distance, and orientation to the target
4. Make 1 to 2 measurements of the plaque shading direct beam
5. Make 1 to 2 measurements with a probe covered for dark current
6. Record spectrometer sample numbers, depth, and target type on a data sheet
7. Photograph the target
8. Photograph the data sheet to record the sample number of the target
9. Positioning method (Chapter 4.7)

The use of submerged reference plaques can be avoided completely by employing a suite of radiometrically calibrated sensors to simultaneously measure downwelling and upwelling light fields (Figure 3.6). However, all radiometers in the system must be intercalibrated in order to prevent error in the final derived reflectance from differential response by each instrument. In particular, commercial radiometers have high uncertainty in the cosine corrections for planar irradiance. Zimmerman (2003b) developed a diver-operated system for measuring benthic reflectances using the HOBI Labs HydroRad 3-channel spectrometer for measuring the spectral albedo of benthic targets illuminated by natural sunlight (Figure 3.6A). This instrument measures reflectance directly from the two plane irradiance sensors at the end of the horizontal wand placed over the target of interest. The wand height is manually adjustable, allowing the sensors to be placed within a few cm of the target without casting a shadow on its surface, thereby minimizing the in-water path traversed by the reflected light. The adjustable wand also permits the measurement of reflected and absorbed light within vertically oriented vegetation canopies. Additional radiometers can also be added to such systems to measure additional optical parameters of interest such as the spectral diffuse attenuation coefficient for downwelling irradiance by the water column [$K_d(\lambda)$] and the average cosine of the submarine light field (Zimmerman 2003b, Figure 3.6B).

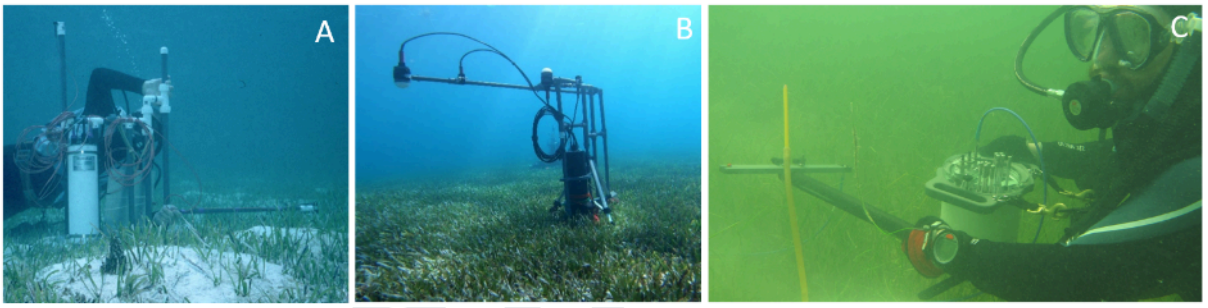

Figure 3.6 A) Underwater diver-operated instruments using an adjustable wand at the height of a canopy to measure upwelling irradiance and flipped for downwelling irradiance (Zimmerman 2003b). B) the same instrument with scalar irradiance collectors to evaluate water column optical properties; and C) a hand-held wand to simultaneously measure both upwelling and downwelling irradiance at the top of a canopy.

This type of measurement is ideal for canopy-level measurements but requires water column, and potentially shading, corrections when used over hard substrates. However, reflectance over a canopy can vary due to morphology of the organism (e.g., leaf, blade), canopy height & orientation, waves, currents, epiphytic growth, and shadows cast by ambient light. Moreover, the bottom substratum can be detectable in variable amounts through the canopy. This makes interpretation of a canopy endmember challenging for intercomparison considering the spectrum represents an unknown mixture of many components. More metadata may be necessary for widely interpreting such spectra (Section 3.4).

3.3 In-water Measurements – Distal to Target (m-scale)

The above methods are primarily used for shallow water systems where sufficient light penetrates to the seafloor and in the realm where a diver can identify the benthic target of interest. However, benthic reflectance in the mesophotic and deep

ocean is also of interest to map habitats like mesophotic coral ecosystems, cold coral reefs, hydrothermal vents, as well as to study archeology, mineralogy (Chapter 10). Targets can be challenging to bring up from depth for in-air measurements and hence these measurements are often conducted underwater at depth where there is little ambient light. New technology has allowed for hyperspectral imaging spectrometry to be used to estimate deep sea benthic reflectance from tethered or autonomous underwater vehicles (Sørensen et al. 2020). We refer to this approach as “distal” to target because the sensor packages are larger and there will be significant amounts of water between the target and the sensor. Generally, sampling distances for these applications are less than 2 m from the target (Johnsen et al. 2013). We note that there is a limit to making measurements close to target without artificial illumination to avoid shadow of the submerged system.

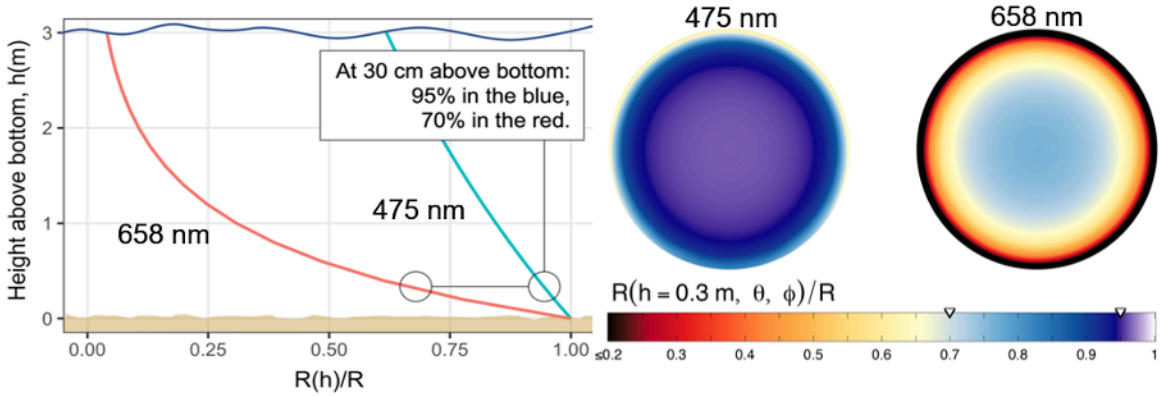

Figure 3.7 Simulations showing the impact of light attenuation at a blue (475 nm) and red (658 nm) wavelength on measurements of benthic reflectance at some height above the target. The panels on the right show the data at 30 cm above benthos and how viewing angle also impacts the water column corrections at these wavelengths. Nadir is the center of the circular plot and the horizon is at the edge of the circles, with the viewing angle increasing in proportion to the distance from the center.

As measurements are made further away from the target, incorporating the directional light field from the intervening water column increases the difficulty to adequately correct for the water column. For example, Figure 3.7 shows how the signal from the benthos is attenuated with distance from the target. In this simulation, the reflectance is 95% in blue at nadir angles and 70% in the red at a distance of 0.3 m from the benthos.

Mobile platforms including Remotely Operated Vehicles (ROVs), Autonomous Underwater Vehicle (AUVs), and gliders have been used to map deep sea features, but deriving accurate benthic reflectance depends on the skill and accuracy of the positioning system, precision of sensor-target distance measures, and knowledge of optical properties of the aquatic medium and the light source (Sørensen et al. 2020, Martinsen and Johnsen 2025). Sensor range and spatial and spectral resolution vary with the technology and corresponding configurations, and greatly depend on how the platform navigates in relation to the feature or process to be measured and risk of collision. If no reflectance standard is available and/or the survey altitude varies significantly during the hyperspectral image acquisition, benthic reflectance can be estimated using a calibrated light source, real-time distance between the detector

and the benthos, and an estimate of spectral light attenuation (Mogstad et al. 2022). Another approach is to derive “relative” benthic reflectance such that the spectral shapes are fairly well conserved, but the magnitude is not well constrained. This approach can be achieved by selecting a benthic feature in the imagery with a flat or monotonic spectral shape, such as sediment, and using that as a type of calibration “plaque” to normalize the imagery. Relative benthic reflectance can be used to differentiate narrow-band spectral features that can map seafloor habitats.

Hyperspectral imagers have been implemented on underwater vehicles *in situ* for mapping a variety of seafloor habitats from deep-water corals to red calcareous algae and anthropogenic changes like deposited drill cuttings on the seafloor (Johnsen et al. 2016; Foglini et al. 2019; Cochrane et al. 2019; Mogstad et al. 2022). However, few of these studies have attempted to derive accurate measurements in terms of both spectral shape and magnitude of benthic reflectance from the imagery across the visible spectrum. Mogstad (2021) provides some benthic reflectance measurements derived from underwater hyperspectral imagery (Figure 3.8).

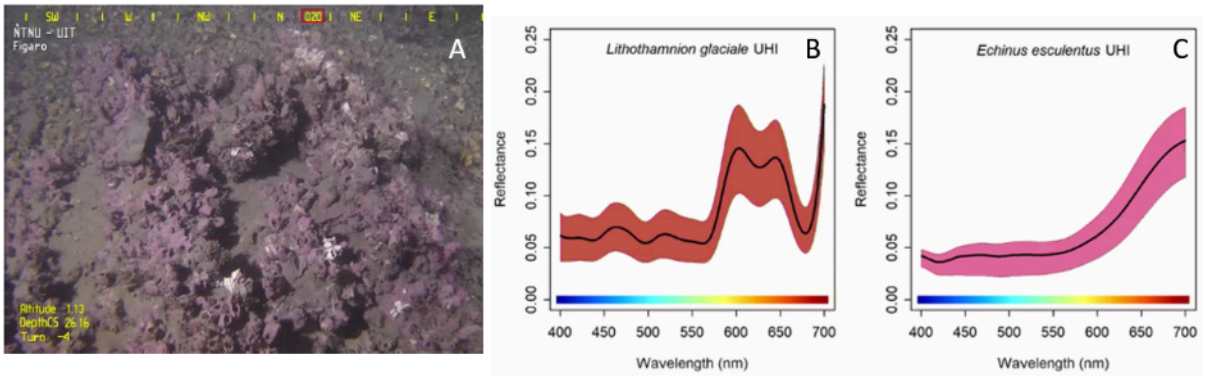

Figure 3.8 A) Underwater hyperspectral imagery with artificial illumination used to map deep sea benthos; B) Benthic reflectance of red encrusting algae with standard deviation; and C) common sea urchin with standard deviation (Mogstad and Johnsen 2017).

3.4 Recording Field Metadata

Metadata are crucial for field measurements as they provide essential context, ensuring data are both interpretable and reliable. They encompass information about the time, location, and conditions under which data were collected, as well as the methodologies and instruments used. This comprehensive background allows researchers to assess the quality and comparability of the data and facilitates accurate analyses of trends over time. Moreover, metadata supports data integration from diverse sources, enabling wide usage of the data by researchers, modellers and decision makers. Without detailed metadata, benthic reflectance measurements lose much of their scientific value and applicability. At the start of any field campaign, it is important to synchronize all of the various computer and instrument clocks (including GPS and cameras) so that exact match-ups can be made between various co-located measurements.

Collecting metadata during underwater surveys presents several unique challenges, primarily due to the complex and dynamic nature of marine environments and the

ability to record information while underwater. The fact that Global Positioning System (GPS) does not work underwater complicates locating any target on the seafloor precisely (Chapter 4.7). The remote and inaccessible locations where surveys are conducted further complicate real-time monitoring and verification of metadata. Human factors, such as challenges in keeping track of diverse instrument sources (photographs, sample numbers, sample order, bottom depth, etc…) and the potential need for multiple divers to record and sample simultaneously, also play a role in the variability and completeness of metadata collection. These challenges necessitate robust protocols and innovative technologies to ensure comprehensive and accurate metadata acquisition in data collection.

The simplest metadata identifies organisms at a very broad taxonomic level such as sediment, algae, seagrass and coral. However identifying organisms down to the species level provides more scientific information that adds significant value to the data. Classifying the organism using the World Register of Marine Species (WoRMS) database is extremely helpful, as these categories are globally recognized (WoRMS Editorial Board, 2016). For example, different coral species can form a range of shapes, including branching, massive, plate-like, and encrusting forms. Branching corals, such as staghorn corals, feature tree-like structures that enhance their ability to capture sunlight and nutrients. Massive corals, like brain corals, grow in large, dome-shaped colonies that are highly resistant to wave action. Plate-like corals spread out horizontally, optimizing light absorption in deeper waters. Encrusting corals grow as thin layers over substrates, providing stability in turbulent conditions. As described in Chapter 2.3, understanding the morphology of the species of coral and the three-dimensional morphology is important for interpreting benthic reflectance (Hedley et al. 2018).

In general, it is recommended to take a picture of each benthic target to associate with the reflectance measurement. Often a subsequent picture of the data sheet can be recorded to ensure the target picture corresponds to the spectrometer sample number. Pictures can aid in later taxonomic identification of the target and provide information on the health, setting, and other features. In addition, recording the sea surface conditions, such as estimating wave height, can be important for understanding the variability in determining the depth of the target. Recording the cloud conditions with a photo or standard categories (dividing the sky into eighths) and noting whether the solar disk is obscured by clouds provides a context for the diffuse and direct illumination underwater and potentially shadowing of targets.

For profiling systems, cameras can be mounted to mimic the field of view of the radiometric sensors. For instance, an upward looking camera can enable a better understanding of the environment by:

1. capturing potential patches of floating algae at the surface,
2. identifying bubbles near the surface or caused by the divers,
3. inform on frequency of surface waves,
4. confirm strong in-water scattering by the blurring of above water elements such as clouds, or even detect a stratification caused by the intrusion of a freshwater plume that would result in a discontinuity of the refractive index of the water column.

A downward looking camera allows one to:

1. identify miscellaneous objects at the bottom that would otherwise have been hard to identify using only the reflectance spectrum or unknown to the diver (e.g., mussel clusters),
2. identify the way in which constituents of the bottom are spatially arranged, which is impossible to achieve through a notebook. This is useful to inform on the anisotropy of bottom reflectance.
3. study the effect of wave focusing on the bottom since the acquisition with video is generally fast (~30 images/s),
4. confirm the presence of sediments in the water column, including resuspension, either occurring naturally or caused by the investigator.

Together, cameras provide much information for the screening of the data while doing post-processing. In addition, it is also an intuitive educational tool for the public, illustrating the marine world in a more sensible fashion than spectrums generated by radiometric quantities.

From a methodological perspective, it is also important to record the type of sensor, the calibration (if needed), the plaque calibration (if needed), distance from target, the IFOV, the illumination source, the type of measurement (dark, plaque, target), type of target, and make detailed accounts of the sampling and environmental notes. Following from the work from Dekker (2021) who compiled a database of over 2500 endmembers collected in Australian waters, we have included a metadata template that includes what we deem the essential minimum information and additional information that can be useful for users (see Supplemental Materials: Metadata Template).

Chapter 4

Methodological Considerations

Heidi Dierssen, Brandon Russell, Richard C. Zimmerman, Tiit Kutser, Peter Gege, Eric Hochberg, Arnold Dekker, John Hedley, Gema Casal

In this chapter, we go beyond the sampling approaches provided in Chapter 3 and highlight methodological considerations about plaques, detectors, illumination sources, targets, and positioning that a practitioner should be aware of when embarking on making high quality benthic reflectance measurements. The experts assembled here have been making benthic reflectance measurements over many years and share some of the background knowledge required to make high quality measurements, as well as tips on what to do and what not to do. Many factors related to the instrument influence the reliability and interpretation of spectral reflectance measurements such as the characteristics of the system including the Instantaneous Field Of View (IFOV), spectral resolution and sampling, radiometric sensitivity, spectral and radiometric stability as a function of light intensity, temperature of the spectrometer, transmissivity through optical fibre cables, integration times, and other influences. Most of these factors should be weighed by a practitioner when making decisions about which equipment to buy/build and how to avoid some known pitfalls. More than one field campaign has been “ruined” by not knowing the detector IFOV and being too far from the calibration plaque. More than one field campaign has been “saved” by taking a dark current manually, by physically covering the detector, rather than relying on the dark correction internal to the instrument. A thorough understanding of a given instrument’s performance characteristics allows the user to optimize their technique to the goals and environmental conditions of a given measurement event.

4.1 Plaque Considerations

Challenges are involved in using a calibration plaque both for measurements in air and in water. Because air is extremely transparent across the electromagnetic spectrum for most of the distances considered here (cm to a few m), the in-air distance from the target to the sensor becomes relatively unimportant. However, in-air measurements conducted under extreme aerosol events, such as thick marine fog or wildfire smoke, may impact the measurement and create larger uncertainty in derived parameters. In contrast to measurements in air, methods using an underwater plaque all require some correction or special technique to account for the water column light attenuation. Even a few centimeters from a target is enough to change the measurement underwater, particularly at highly absorbing wavelengths (blue in turbid coastal waters and red in all waters). In addition, immersion of plaques in water can change their reflectance properties significantly. Most measurements to date do not account for this.

Even when using a plaque in air, several techniques can be followed to maximize the accuracy. Castagna et al. (2019) provide some recommendations based on uncertainty estimates of using the plaque for field measurements, many of which can be applied with some modification to underwater measurements. These include:

- Plaque reflectivity should be carefully selected to be around the highest expected benthic reflectance within the wavelengths of interest;
- Plaque should be exactly horizontal when making measurements using ambient sunlight;
- Viewing angles should be optimized at 40° for white plaque and at nadir for a gray plaque, both at a 90° relative azimuth to the Sun to reduce operator shadow and secondary reflection;
- Plaque diameter should be at least three times larger than the sensor field-of-view footprint for a given view angle and distance;
- Plaque placement should be selected to minimize scattering from surrounding structures;
- Operator should wear dark clothing. If holding, the plaque should be at the height of the upper chest or neck, ~40 cm from the body, with sensor at distances >20 cm from the plaque;
- Measurements should be performed under stable illumination and for natural illumination ideally with solar zenith angles from 20 to 60º.

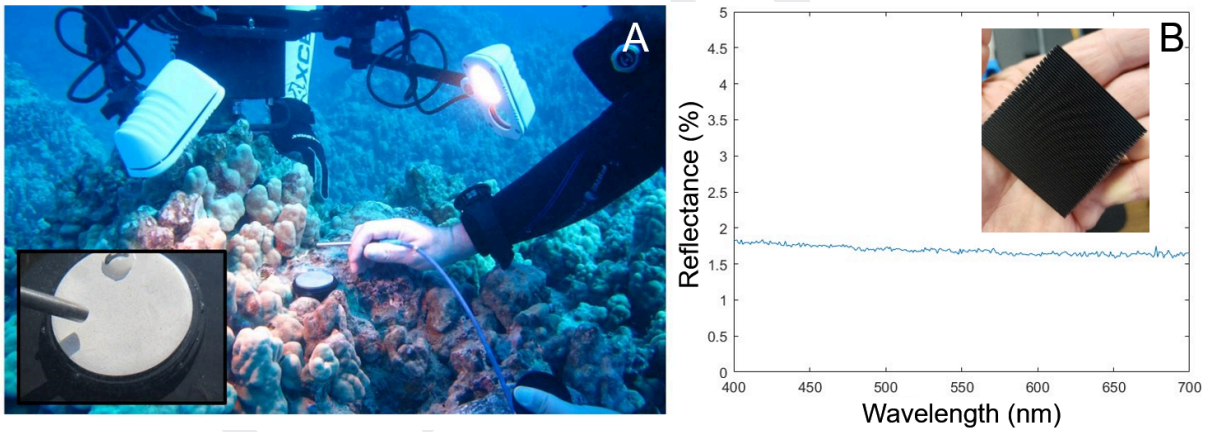

Figure 4.1 A) Divers using augmented illumination and placing a gray standard (20%) at the same depth and orientation as the sample. Inset shows a surface bubble that must be removed from the plaque (adapted from Russell and Dierssen 2023). B) Spectral reflectance of a beam-dump style black target (<2% across visible) fabricated from black polylactic acid (PLA) using a 3-D printer. Inset photo provides an example of the target.

The use of a submerged reflectance standard also requires careful consideration. Generally gray plaques of <50% nominal reflectance are optimal for underwater use because measurements >700 nm are generally not feasible and it is important that the integration time used for the plaque measurement be similar to that used to measure the target (Figure 4.1A) (also see Sec. 4.3). Additionally, the accuracy of the measurement depends on the turbidity of the water. If the radiance contribution from the surrounding water column is too high at any wavelength, then the approach cannot be used to generate accurate reflectance values. In theory, the water column contribution can be measured by conducting an additional measurement over a

perfectly black target (0% reflectance). However, the in-air reflectivity of many black targets consisting of flat sheets is 3-5%, which may cause the light attenuation by the water column to be under-estimated. Further, the performance of these materials may change when immersed in water, introducing more uncertainty in the measurement. A simple black target with <2% reflectance can be made using a 3-D printer following the design of optical beam block commonly used in laser laboratories that employ vertical fins to more effectively trap photons within the target (Figure 4.1B). The plastic materials typically used in 3-D printing are not hydroscopic and their mechanical/optical properties are not affected by immersion.

In turbid water, even small differences in the distance between the probe and the reference plaque and the probe and the target can introduce considerable error (Figure 4.2). An additional consideration occurs whenever the illumination field in part of the spectrum is too low to produce a reliable reflectance measurement. This can be particularly problematic for reflectance measurements in the red part of the spectrum using natural light at great depths in clear, oligotrophic waters, and in both red and blue portions of the spectrum in green coastal waters. Supplemental target illumination can be employed to enhance the signal in some spectral regions (Section 4.5), but the spectrum of the source must be considered and its distance and orientation to both reference plaque and target must be equal.

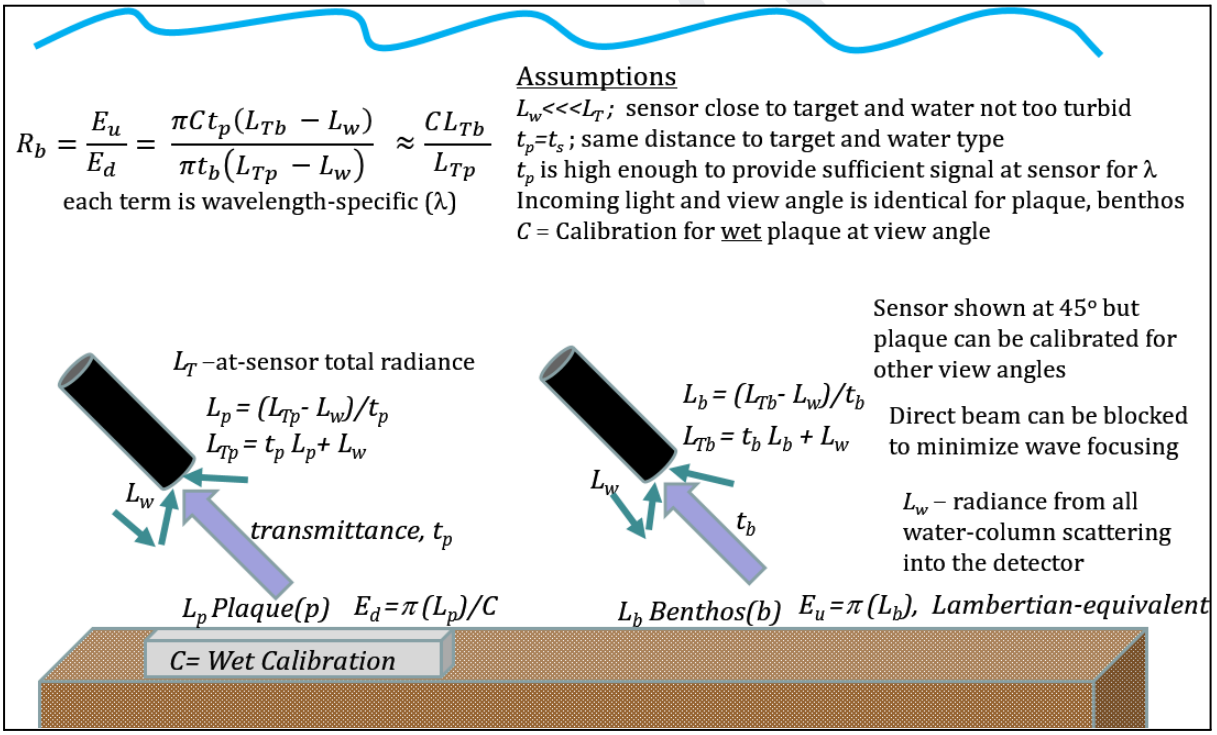

Figure 4.2 Schematic of the assumptions involved in using a plaque measurement underwater.

The diffuse reflectance standard Spectralon®, a compressed form of powdered polytetrafluoroethylene (PTFE), is often used because of its near-Lambertian behavior at near-normal illuminations. The manufacturer provides a NIST traceable reflectance spectrum with each calibrated reference standard. However, this spectrum is valid only at the measurement geometry specified and for a pristine

panel. Even when used in air, factors such as solar illumination angle (azimuth and elevation), probe measurement angle, direct/diffuse irradiance ratio, and degradation of the standard itself with use, may lead to differences of several percent absolute reflectance from the manufacturer's specification at a given wavelength (Soffer et al. 2019). Spectralon® is lipophilic and is subject to contamination by hydrocarbons such as skin oils, hydrocarbon fumes, and biological debris in the marine environment. The surface of the material is soft and porous and can easily be deformed or damaged by contact. Care should be taken to prevent contamination or damage by using protective covers when the standard is not in use. Light damage or soiling can be removed by gentle hand sanding of the surface with a random motion under running purified water. However, the reflectance of the standard should be recharacterized (such as by reference to a pristine standard) after such reconditioning (Russell and Dierssen 2023).

When submerged, however, the reflectance behavior of Spectralon® becomes decidedly peaked (non-lambertian) with respect to viewing and illumination angles (Zhang and Voss 2006). Target reflectances calculated with air-calibrated values are 10%–60% lower than those estimated with submerged plaque calibrations (Russell and Dierssen 2023). Accurate measurements of the plane downwelling irradiance require the Spectralon® plaque to be viewed at 45°. Viewing the submerged reference plaque at near-normal viewing angles (<40°) may cause the target reflectance to be underestimated as much as 15% and viewing the submerged reference plaque at strongly oblique angles (>50°) may overestimate the target reflectance as much as 20% (Russell and Dierssen 2023). Underwater calibration of the plaque is recommended following the procedure outlined in Russell and Dierssen (2023). Further, the hydrophobic nature of Spectralon® causes bubbles to form on its surface underwater. Any small bubbles that form on the surface of the plaque underwater should be gently removed before sampling, taking care not to contaminate the plaque surface with skin oil or other hydrophobic material.

4.2 Wavelength Considerations

There are a number of commercial spectrometers available for use in the laboratory and in the field. Some of the spectrometers are designed specifically for underwater applications, while others are designed for in-air applications. Some in-air spectrometers have been fit with custom underwater housing to sample underwater. Since they differ significantly in spectral range and resolution, size, weatherproofing, construction and price, which instrument is best suited depends on the application. An important application that has driven the development of robust and well-calibrated field spectrometers is the validation of ocean colour satellite-borne data.

Field spectrometers useful for benthic applications cover either the spectral range from 350 nm to approximately 850 nm or from 350 to 2500 nm (Table 4.1). Bench-top laboratory spectrometers extend these ranges down to approximately 200 nm. Table 1 is intended to give an overview of the typical spectral parameters, but not to assess their quality or usability for benthic applications. There are many more instruments on the market including systems consisting of multiple spectrometers, and for some of the listed spectrometers different variants are available. The spectral

range of radiometers covering the visible to near infrared can be realized with relatively cheap silicon detectors operated at room temperature, while wavelengths beyond 1000 nm require additional and cooled detectors, e.g., made of InGaAs, which makes the device complex and expensive.

Table 4.1 Typical spectral parameters of field spectrometers.

Manufacturer	Model	Spectral range [nm]	Sampling interval [nm]	Spectral resolution [nm]
Submersible				
Eelume	Ecotone Underwater Hyperspectral Imager	400-720	variable	2.2-5.5
In Situ Marine Optics	uSPEC	380-870	1.8	8-10
Seabird	HyperOCR	320-1050	3.3	10
TriOS	RAMSES	320-1050	3.3	10
In air or underwater housing				
Analytical Spectral Devices (ASD)	FieldSpec 4 Hi-Res	350-2500	1.1-1.4	3-8
Broadcom	Qwave	350-880	0.15	0.6
Ocean Optics	STS-VIS	350-800	0.5	1.5
Spectral Evolution	SR-3500	350-2500	1.2-3.8	3-8
Spectra Vista	HR-1024i	350-2500	1.5-3.8	3.3-9.5
Surface Optics	710 Hyperspectral Camera	400-1000	2.3	2.3

Because water absorbs light very strongly below 300 nm and above 720 nm, the first group of submersible instruments are well suited for measuring the submerged benthos under natural illumination conditions. Wavelengths above 850 nm, allow useful benthic measurements under water only if a lamp provides sufficient light, and above water only in very shallow water of a few centimetres depth and for bare surfaces. Some systems come with lamps and are designed for deep sea applications (e.g., Eelume).

Remote sensing can acquire benthic information only in the range from approximately 350 to 850 nm, depending on water depth, sun elevation, turbidity and the albedo of the substrate. If the water is deeper than around 1 m, the upper

spectral limit is near 720 nm. Many spectra in databases were obtained from underwater measurements and are therefore restricted to the range from 350 to 720 nm. It would be desirable to extend the databases to at least 850 nm so that remote sensing in very shallow water can make use of the additional information available above 720 nm.

Most field spectrometers are constructed such that the light collected by a lens is focused on a slit, and the passing light is dispersed by a grating or a prism across a linear array of detectors. In this way each detector element receives light from a narrow field of view and a limited wavelength interval. The dispersion of the wavelengths in the focal plane depends on the groove pattern of the grating or the refractive index of the prism, and the spectral resolution on the slit width. Size and spacing of the detector elements determine the wavelengths received by each element. The difference of the center wavelengths of two adjacent detector elements is called *sampling interval*.

The intensity which a detector element receives light from different wavelengths decreases towards the ends of the spectral interval. The function describing the wavelength dependency of the signal of a detector element is called *spectral response function*, SRF. For narrow slits, the SRF can be approximated by a Gaussian function, while wider slits add a rectangular component to the SRF. The SRF's full width at half maximum is called *spectral resolution*.

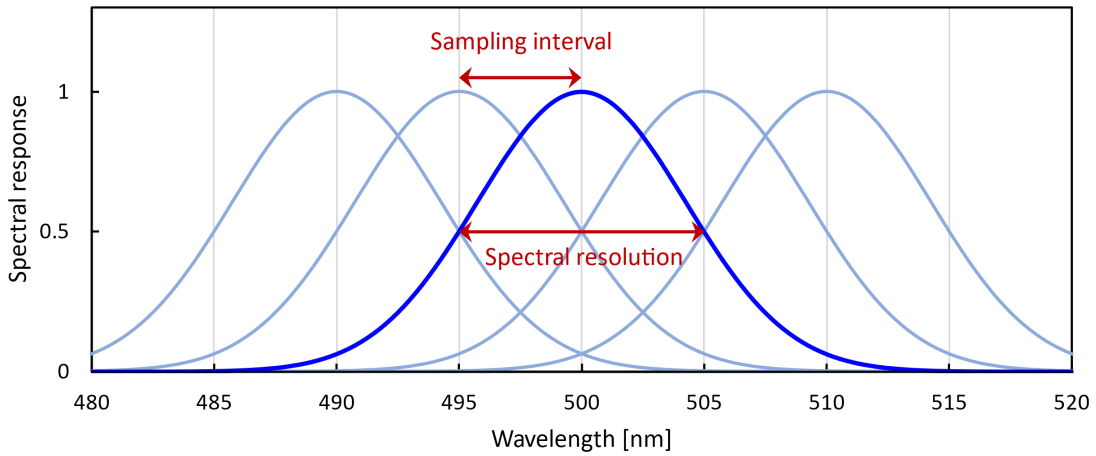

Figure 4.3 Illustration of spectral sampling using a detector array. Each curve represents the spectral response of a single detector element. The distance between adjacent detector elements is the sampling interval; the full width at half maximum (FWHM) is the spectral resolution. In this example the spectral resolution is 2 times the sampling interval, corresponding to the Nyquist requirement. Smaller sampling intervals lead to an oversampling, larger sampling intervals to an undersampling.

Figure 4.3 illustrates the wavelength dependent sampling of light by adjacent detector elements. According to the Nyquist theorem from information theory, a signal must be sampled at more than twice the highest frequency component of the signal to collect all information. For practical applications, that means that the ratio of spectral resolution to sampling interval must exceed 2. This ratio is between 2.1 and 10 for the spectrometers of Table 1. Such gapless sampling of light over a wide spectral range defines a "hyperspectral" sensor. In contrast, multi-spectral sensors,

as are commonly used on satellites, undersample the spectrum, i.e. the ratio is below 2 and there can be large wavelength gaps between adjacent spectral bands.

The downwelling solar irradiance spectrum (including both direct solar and diffuse skylight) has many strong but narrow absorption bands from the sun and the atmosphere (Fraunhofer lines) with bandwidths in the nm- and sub-nm range. Consequently, the spectral details of a radiance or irradiance measurement under natural illumination conditions depend on the center wavelengths and spectral resolutions of the sensor's detector elements. The higher the spectral resolution, the more pronounced are the intensity differences between adjacent detectors at the wavelengths of the Fraunhofer lines. These spectral gradients can lead to strong artifacts in reflectance spectra if the upwelling radiance and the downwelling irradiance are recorded with two instruments that have not been properly calibrated with respect to wavelength registration and radiometric intensity. If there is any doubt about instrument calibration, it may be advantageous to use the same instrument for both measurements, in particular for measurements with high spectral resolution since uncertainties in radiometric calibration will cancel when the reflectance is calculated from the ratio of two measurements performed with the same instrument.

While manufacturers do provide spectral calibrations with most of their instruments, it is also recommended that users check the accuracy of these calibrations with known spectral features. Relatively inexpensive pure gas spectrum tubes (<$500 US) offered by a number of scientific vendors (e.g., Vernier Science Education) can provide easy-to-use wavelength calibration standards for those requiring extremely high precision. The atmospheric oxygen A absorption band centered at 770 nm also provides a quick reference point for spectral calibration in the field. Other narrowband solar lines (Coddington et al. 2023) can also be checked with a measurement of downwelling solar illumination. Fluorescent lighting also provides spectral peaks due to different elements (mercury, terbium, europium) that can be used to verify spectral calibration of detectors in the laboratory. When using such non-standard calibration sources, one highly calibrated sensor should provide the calibration standard for comparison to other detectors.

4.3 Radiometric Considerations

Of all of the aspects, setting the integration time underwater may be the most important for obtaining a reliable spectrum. In a nod to Einstein (who borrowed the concept from Occam), we note that obtaining a reliable spectral measurement requires integration times to be as short as possible, but not shorter than necessary. For underwater applications, which are inherently photon-limited, the inverse may be more applicable. Integration times need to be as long as possible to get a good signal at wavelengths subject to low light intensity (e.g., blue and red) and avoid saturation at wavelengths with higher light (e.g., green). Under-exposures caused by short integration times result from collecting an insufficient number of photons for the signal to rise above the inherent "dark" noise of the detector. Over-exposures caused by long integration times run the risk of saturating the detector and distorting the spectrum. As with photographs, long integration times make the recorded spectrum vulnerable to target and/or detector motion that may also distort, or 'smear,' the spectrum across unintended targets.

Thus, obtaining an optimum signal requires the user to have a clear understanding of their spectrometer system's dynamic range, including the effect of integration times on dark current values, digitization limits, aperture diameters to ensure that the sensitivity of the instrument fits the light environment in which it will be used. For a single acquisition, adjustable integration times allow a point spectrometer capable of 14-bit digitization to cover a dynamic range of about 40 dB (16,000:1). The upper and lower limits of that range are controlled by the aperture diameter, a feature that is not typically adjustable during use. Consequently, care must be taken to match the aperture diameter to the operating light environment to ensure proper exposure within the integration time limits of the system.

Imaging systems can increase the dynamic range even further using adjustable *f*-stop lenses. A photographic lens with an aperture range from *f*/2 to *f*/22 can increase the dynamic range of the system to about 65 dB (3.07×10^6:1) but that is still considerably less than the dynamic range afforded by the retina and pupil of the human eye, which is typically reported to be about 125 dB (3.2×10^{12}:1). Although the use of low *f*-stops increases the sensitivity to low light, it also reduces the depth of field, requiring more precise focus adjustments to prevent image blurring that could smear the reflectance spectra across different targets in the image.

Field spectrometers use a linear array of detectors to measure the intensity of light at different wavelengths. The detectors are made of semiconductors that utilize the photoelectric effect to create free electrons by absorption of photons. An analog-to-digital converter (ADC) digitizes the voltage into a digital signal S. To avoid negative input voltages for the ADC, a positive offset voltage is applied, leading to an electronic offset signal S_0. Besides light, temperature also generates electrons in the detector, leading to a thermal signal S_t. Since S_0 originates from the ADC and S_t from the detector, S_0 is identical for all detector elements, but S_t is not. The digital signal measured by detector element number i is the sum of these three components:

$$S_i^{'} = S_0 + S_{t,i} + S_i. \qquad (4.1)$$

The sum $S_{d,i} = S_0 + S_{t,i}$ is called dark current signal because it is the signal obtained at darkness. As S_0, $S_{t,i}$ and S_i depend on temperature, the dark current signal should be recorded together with each measurement to determine the light-induced signals S_i as accurately as possible.

The ADC of most current spectrometers has a dynamic range of 16 bit, i.e. it can distinguish 2^{16} = 65,536 values of $S_i^{'}$. The dark current signal $S_{d,i}$ reduces this nominal dynamic range for the light-induced signal.

The effective dynamic range is limited by the detector noise which can be quantified in terms of the standard deviation of the light-induced signal (σ_S) at constant light

intensity. Field spectrometers allow one to distinguish typically between 1500 (Broadcom Qwave) and 4600 (Ocean Optics STS-VIS) intensity values of S. The ratio is called *signal-to-noise ratio* (SNR; Equation 4.2).

$$SNR = \frac{S}{\sigma_S} \tag{4.2}$$

The SNR at maximum signal specifies the maximum number of intensity values induced by light that can be distinguished by a measurement.

In order to minimize the measurement noise, the integration time should be chosen such that the dynamic range of the instrument can be utilized as far as possible. Care must be taken to avoid saturation because detector elements in saturation provide no usable data. To account for possible intensity fluctuations and to avoid non-linear effects near saturation, a maximum signal of ~80 % of the saturation signal is a good choice, i.e. around 50,000 DN for a 16 bit ADC.

If the same instrument is used for measuring the target and the downwelling irradiance by means of a plaque with known reflectance, the reflectance of the plaque should either be similar to the maximum reflectance of the target, or the integration times of the two measurements should be optimized independently. Caution is warranted if it takes time to optimize the instrument, as the light field could change significantly between measurements of plaque and target (Figure 4.2).

Since downwelling irradiance, reflectance and radiometric response are wavelength dependent, usually only a few detector elements measure the maximum signal, while the majority of detector elements provide a lower signal and thus lower SNR. Depending on the illumination and target, this can lead to large noise in some spectral regions. It is recommended to record in general a series of subsequent measurements because the average spectra have less noise than individual measurements. Measurement series have the further advantage that environmental conditions leading to random outliers, for example variable sun glint, can make a measurement still usable by removing the erroneous spectra.

4.4 Geometric Considerations

The instantaneous field of view (IFOV) of field spectrometers is usually symmetrical around its optical axis and identical for all wavelengths. A standard fiber optic probe typically has an IFOV of 25 ° and will have a nominal FOV of diameter footprint of 0.8 cm when probe is 3 cm from target at a viewing angle of 45º. Most spectrometers can be fitted with a “foreoptic” lens that reduces the IFOV to a specified angle. For above surface water-leaving reflectance measurements, for example, an 8.5º foreoptic is often used to reduce the sample footprint on the water and in the sky (Mobley 1999), but smaller IFOVs (e.g., 1.5º) can also be employed (Zibordi et al. 2010).

It is tempting to presume that the IFOV measures and weights photons equally across the surface that is being viewed. However, significant spatial asymmetries have been observed for many spectrometers, particularly those belonging to the

second group listed in Table 4.1 (Mac Arthur et al. 2012). Specifically, the size and alignment of the viewing optics and technology adopted to transfer light from the foreoptic to individual spectrometers may cause significant nonuniformity of spectral response across the area of measurement. This means that certain parts of the sampling area are preferentially and unequally sampled compared to other parts of the sampling area for different detectors (VNIR, SWIR etc…). The uneven IFOV is caused by the randomly distributed optical fibres used in each of the three detectors. This introduces uncertainty when targets are heterogeneous and different reflecting surfaces are present in varying proportions within the field of view. The directional response function (DRF) should be measured for a given instrument for certain applications, particularly when considering the full spectrum from visible to SWIR (Figure 4.4). Making multiple measurements while moving the foreoptic across a target can also mitigate this issue. This may not be a large issue for many benthic underwater applications, but could be an issue in mudflats and other targets that are more emergent.

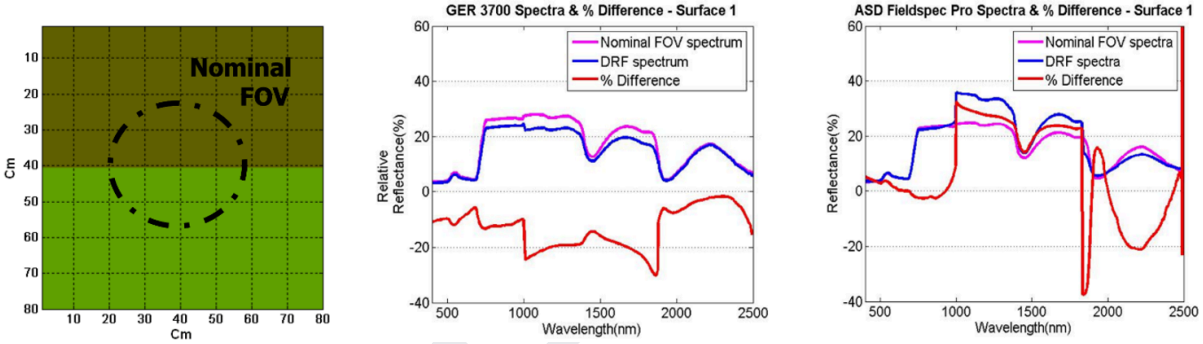

Figure 4.4 An example of the how differences in the spatial dark response function (DRF) across the IFOV of two different detectors produces uncertainty in the reflectance spectrum. (Mac Arthur et al. 2013)

4.5 Illumination Considerations

An ideal light source would have bright, stable output that evenly illuminates the target and reference. Sunlight under clear sky conditions is an excellent light source for most spectroscopic applications in air with high output from UV to SWIR wavelengths. There are some known spectral gaps where the atmosphere is opaque and very little light is transmitted to Earth's surface (e.g., ~1400 nm and 1900 nm, Figure 4.5). Due to differences in spectral intervals of detectors, atmospheric gases can also create artificial dips or troughs in reflectance measurements at certain regions like 770 nm (oxygen A) and 940 nm (water vapor) (Fogarty et al. 2018). Since water is highly absorbing at these NIR and SWIR wavelengths, these features are not very relevant to most in-water studies but would be relevant to mud flats and other shallow benthic targets.

Conducting measurements under variable cloud conditions creates additional challenges. Clouds influence the light field on time scales of seconds to minutes and can influence above water and underwater measurements. Under "uniform" cloud conditions that are consistent over the course of a sampling sequence, the

measurement uncertainty can be low enough for high quality data. However, measurements should be timed to avoid transitions between direct sunlight and cloud shading. If a cloud transition occurs during sampling, this should be noted in the metadata and the measurement should be postponed until the light field stabilizes. Another approach would be to record downwelling irradiance continuously at some fixed location (e.g., above water) at the study site and use the time-stamped observations to correct the *in situ* measures for variations in solar illumination.

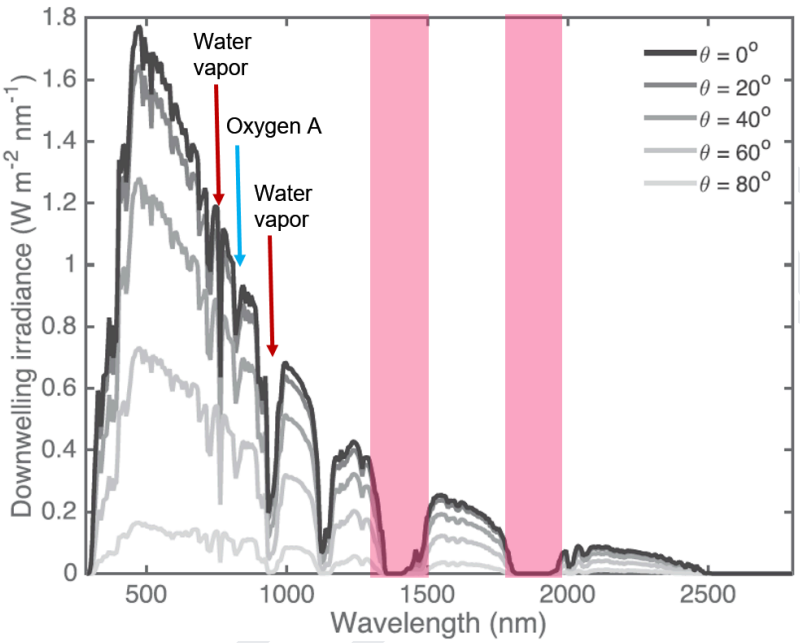

Figure 4.5 Examples of solar irradiance from 300-2500 nm at different solar zenith angles (0-80º). Note the reduction in photons in NIR and SWIR and low signals at low zenith angles. Specific absorption features are highlighted for water vapor (red) and oxygen A (blue). Modified from Fogarty et al. (2018)

When sampling underwater, the penetration of sunlight across visible to NIR wavelengths is dependent on the water depth and optical properties of the water column. Large waves create fluctuations in the water depth overlying the benthic target, which causes significant differences in the light field reaching the benthos. More studies are needed to determine the uncertainty caused by light fluctuations caused by waves with different heights at different water depths. Owing to the exponential attenuation of light in water, however, the impact of differential attenuation is greater near the water surface. Additionally, waves on the water surface also focus light on time scales of tens of milliseconds (Mobley 1994). The focusing effect can cause bright flashes (caustics) on underwater targets. A spectrometer pointed at a coral, for example, might inadvertently capture a wave flash. Thus, if natural daylight is the illumination source, multiple measurements should be obtained to minimize the uncertainty and data processing should be conducted accordingly (Chapter 5) since this influences the data non-normally (Gernez et al. 2011). Or, the user can block the direct beam in a consistent way for all measurements leaving only the diffuse light field to reduce the impact of wave focusing/defocusing.

The impacts of a fluctuating ambient light field can be greatly reduced, and even eliminated, through use of artificial illumination. Dive lamps/torches are useful for handheld applications underwater by scuba divers. Halogen lamps typically have spectrally smooth output that is low at blue wavelengths and increases through the red and NIR. Consumer-grade white LEDs typically emit a combination of a narrow blue band (near 450 nm) and a broad green-red band (500–600+ nm). These LEDs do not usually emit at either UV or NIR wavelengths. As LED technology advances, new ways to create both a more spectrally flat output and include output in the UV/NIR ranges are emerging. Underwater LED ring lamps (Figure 4.6) are being tested as an exciting new option for artificial illumination.

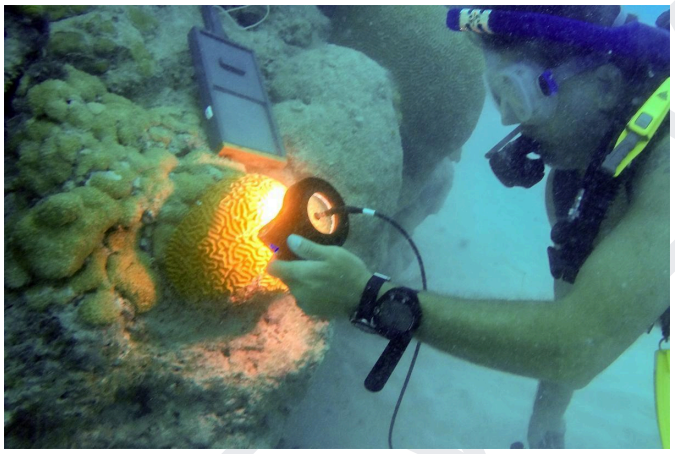

Figure 4.6 Underwater LED ring lamp used for measurements of coral reflectance. The fiber optic probe is centered in the LED ring. The bright light source evenly illuminates the target and minimizes the impacts of changes in the ambient light field. A Spectralon® reference (calibrated 10% reflectance) is placed adjacent to the coral target and measured at the same distance and orientation. Photo credit: E. Hochberg

4.6 Target Considerations

Benthic substrates can range from sediments, such as rock or sand, to living organisms such as seagrasses, macroalgae or corals. This diversity of substrates leads to a wide range of protocols for sample preparation, which can also differ among researchers as no standardised approach is broadly established. In addition to the type of target, the goal of the measurement and whether it will be used for applications such as remote sensing or physiology will also influence the sample preparation (e.g., epiphytes vs clean leaves).

Handling of benthic material is challenging when conducting measurements in air. Material can be stored in a dark ice chest onboard a vessel, but it is recommended that ambient water is included with the sample if possible. Cooling of a sample can also shock living material that is collected from warm waters and may impact their optical properties. Putting samples in a ziplock bag in a shaded dark bucket may also be appropriate. Generally, it is recommended that samples are measured immediately upon collection to avoid degradation of epiphytes, pigments, and symbionts.

Many leaves and fronds are transparent to a degree. If a measurement is made on different backgrounds, then part of the signal in the spectral measurement may come from the background through the leaf or frond. Alternatively, leaves or fronds can be stacked over each other till they are optically thick - giving a pure end-member spectrum (Fyfe, 2003). However, this pure endmember spectrum is not representative of the leaves *in situ* where they will have all the effects of a canopy underwater.

When measuring leaves or fronds lying flat, sun glint and sky glint from the wet layer on the surface of the leaves or fronds may occur depending on the illumination conditions (also the water layer on the leaves may change composition and thickness as the drying process starts). Another aspect to take into account is the change in colour by the desiccation that can happen during low tide or when the samples are transported to a different place. For example, macroalgae such as *Ascophyllum nodosum* can change from a dark green colour to yellow depending on the desiccation degree.

By measuring indoors in laboratory conditions some of these effects can be suppressed or controlled (e.g., by having a stable light source) although then a source of uncertainty is the change in the samples between times of sampling and measurement and dessication; these effects can be reduced by storing and transporting samples in the dark at temperature just above 0°C. This latter method has the advantage that personnel without spectral measurement expertise and with knowledge of the different bottom features, such as coastal management agency staff, could take care of the sample collection.

Different parts of the leaves will have slightly different cell structure, physiology, and colour (e.g., tops of *Posidonia* leaves are dark green whereas the bottom are bright yellow to light green). For remote sensing applications, a spectral signal is normally measured from the leaf tops. Additionally, epiphytic growth on leaf surfaces contains pigments and cell skeleton material that will change the spectral reflectance. If epiphytes occur, one protocol is to make spectral measurements of leaves with and without epiphytes to determine the effect of epiphytes. Notes on type and density of epiphyte growth on samples should be made when taking spectral measurements, or epiphytes samples stored for later genomic analysis.

When representative samples from benthic substrates are collected to be measured outside the water, several steps can be taken to ensure that the desired endmember is obtained and the metadata accurately represents the treatment of the sample. Some of these steps used to treat a sample can be described as follows:

- Rinse and clean: Rinsing and cleaning the sample may be part of the protocol prior to making measurements, as the sample may contain unwanted material or become contaminated during sample collection. Samples should be measured immediately after rinsing to avoid any desiccation process.
- Dry: The presence of water in the sample could affect the reflectance measurements. Therefore, if a significant amount of water remains after

rinsing, it should be removed. The sample can be drained or dried with absorbent paper. Exposing the sample to direct sunlight or heat should be avoided, as this could impact their optical properties.

- Centrifuge: To remove excess water, samples can also be centrifuged in suitable containers, which should be able to hold the samples securely. They should be centrifuged at low speed (e.g., a salad spinner used in Perry et al. 2018) to avoid excessive stress that could damage the samples.
- Scrape: Depending on the objective of the study scraping may be necessary to ensure the removal of fouling, epiphytes, or other material. Scraping should be done with caution avoiding any damage to the sample. After scraping the sample should be rinsed with clean water to eliminate any remaining debris or particles dislodged during the scraping process. If any excess water remains after this step, it should be removed by drying or centrifuging.
- Layer: Staking the leaves in distinct layers helps to achieve "pure endmembers", isolating the optical signals contributed by individual layers. This process reduces variations caused by factors like pigmentation, cell structure or morphology, but may not be representative of the target *in situ*.
- Sort for age class: If the sample contains living organisms, they should be sorted by age classes. Reflectance values may change as the organisms (e.g., macroalgae, seagrasses) progress through different developmental stages. This process involves identifying and separating different age groups of organisms (e.g., juveniles, adults) which requires expertise to determine their life cycle stage.
- Document/photograph sample. Phenotypic traits can also be influenced by biological factors, including genetics, environmental conditions, and health status. These factors may vary according to species and ecological conditions. For this reason, it is advisable to document traits in the metadata such as colour, size or any other unique characteristics and photograph the target if possible.

4.7 Positioning Considerations

Investing in an accurate and reliable GPS handheld device with a powerful antenna is worthwhile for finding the exact position of your field samples. In air, such measurements are quite routine. However, locating underwater targets is extremely challenging because GPS does not work underwater. A diver has no way of recording their exact position when making a measurement or collecting a field sample underwater. Many techniques have been used to estimate the sample position underwater. A diver can:

1. raise and lower a lift bag with a GPS at each sample and the GPS will record a position when it reaches the surface. Strong currents should be avoided
2. swim with a buoy and GPS that stays at the surface and is kept vertical at the location of interest
3. deploy a buoy at each benthic location and the position can be later determined from a surface vessel or diver ensuring that the buoy is as vertical as possible

4. a swimmer or individual on a personal watercraft (e.g., paddleboard) can record locations as the divers sample along the seafloor. A time stamp can be used to synchronize the measurements and ensure no shadowing occurs.

Other options include setting up a fixed transect with a measuring tape fixed along the seafloor where samples are taken at regular intervals. In that case, only the first and last locations must be recorded and the length of the measuring tape. Station locations can then be inferred using geometry. Note, because light refracts underwater, underwater positions determined from sea surface observations are not accurate at off-nadir angles. Also, it is imperative that the GPS units and instruments are all working with the same time reference.

Chapter 5

Overview of Processing and Documentation

Eric J. Hochberg, Heidi M. Dierssen, Richard C. Zimmerman, Arnold Dekker

Data processing is usually not an automated process. As recommended for any field sampling, individuals should download all of their data after sampling, take a picture of datasheets, and save a backup of all data to hard drives. Especially at the start of a field campaign, we highly recommend plotting and working up some of the data to a first order to ensure that the instrumentation and sampling protocol are working well enough to obtain reasonable data in the field. The more processing scripts that are written before the field season, the easier this process may be for a tired field-weary investigator. Adjustments can be made day-by-day to achieve high quality reflectance data, such as using longer integration times, changing the sample number, adjusting illumination, shading the direct beam, etc. This chapter presents some of the data processing and quality assurance/control techniques that can be useful when processing data to a draft or final form. A user should also read Chapter 7 carefully for their target of interest and be familiar with what an expected reflectance spectrum should look like for their target.

5.1 Plot Instrument Data

Before processing data, it is useful to plot the individual data streams to evaluate the environmental variability and conduct initial assessments of the measured signal from all sensors and targets. Some example plots of data collected in tanks with a probe held near the target underwater (Figure 5.1) were collected following this protocol:

1. Probe covered with dark material for Dark Current (DC) (1900 spectra)
2. Probe over white Spectralon® (1200 spectra)
3. Probe over target (2800 spectra)

Plot the digital counts from each type of target by wavelength to evaluate the variability within each type given the IFOV of the instrument (Figure 5.1A). The samples on the Spectralon® plaque should have the least variability given the assumption that the light field is constant between subsequent measurements. It is clear that DC has low absolute noise. The Spectralon® and coral are fairly stable, but they exhibit much greater absolute noise. Much of the noise is due to wave flashes, which are apparent as ms-scale spikes. This illustrates a major potential pitfall when using natural daylight for illumination in reflectance measurements. The coral data also show some 2–3 s excursions from the overall trend, most apparent around 13 s and 20 s. These are due to actual variations across the coral colony

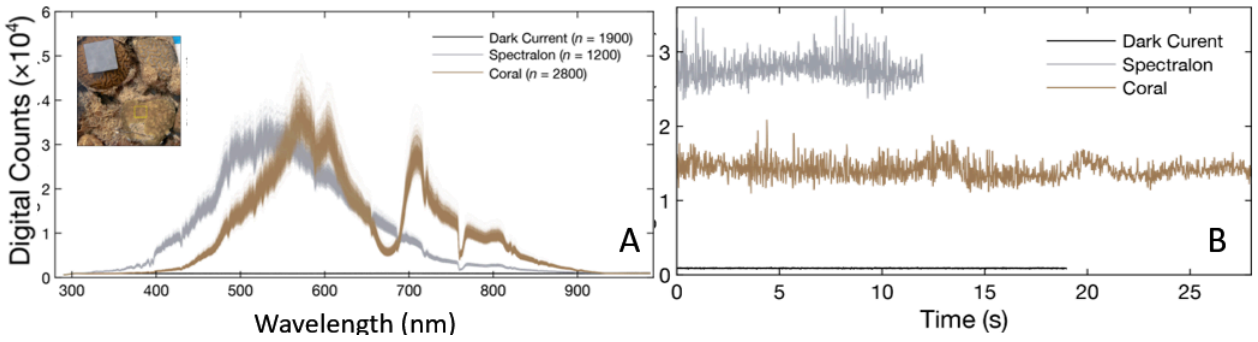

Figure 5.1 Example reflectance data set for coral referenced to a 10% (gray) Spectralon® plaque. A) Individual spectra in digital counts for dark current, Spectralon®, and coral. B) Data plotted over time for a single wavelength. Variability due to wave focusing and de-focusing can be observed in the measurements made over time.

5.2 Apply Dark Current Correction

As discussed in section 4.3, any photosensitive device has a background electrical dark current (DC) that is present even when no photons are entering the device. DC may vary with wavelength, and it does vary with sensor temperature and integration time (Burkart et al. 2013). DC is subject to temporal shot noise, but it can have a stable time-averaged mean value. The effect of DC is to add a (typically) small but positive value to the measured flux. Calculation of R_B requires subtraction of DC from the recorded apparent fluxes.

Some spectrometer systems include a mechanical shutter that enables direct quantification of DC in the field at the time of data collection. Subsequent recorded spectra are automatically compensated for DC. Such mechanical shutters can malfunction and hence manufacturers have come up with alternative mechanisms for determining the DC. For example, an “electronic dark” correction (is used where first few spectral pixels are blocked internally, and their values are assumed to represent all dark values across the entire spectrum. Even if the instrument does compensate automatically for a dark, it is still useful to take an occasional underwater dark measurement blocking the probe.

There are a few different approaches to DC correction. The first is to obtain a full DC spectrum by blocking the input optics, then subtract the result from other measurements. The second is to subtract the “electrical” DC from each measurement. This is automated in many commercial spectrometer systems when optimizing the integration times. The final approach is to perform no DC correction at all. The results of all three approaches are illustrated in Figure 5.2. Where DC is small relative to the signal (e.g., 450 to 650 nm), dark corrections have little impact on the final calculated R_B. However, where DC is larger relative to the signal in UV and NIR wavelengths for example, compensation has a much greater impact on R_B. Note that the “electrical” DC correction does not fully mitigate the impact. It is recommended that full DC correction be incorporated into all measurements of R_B.

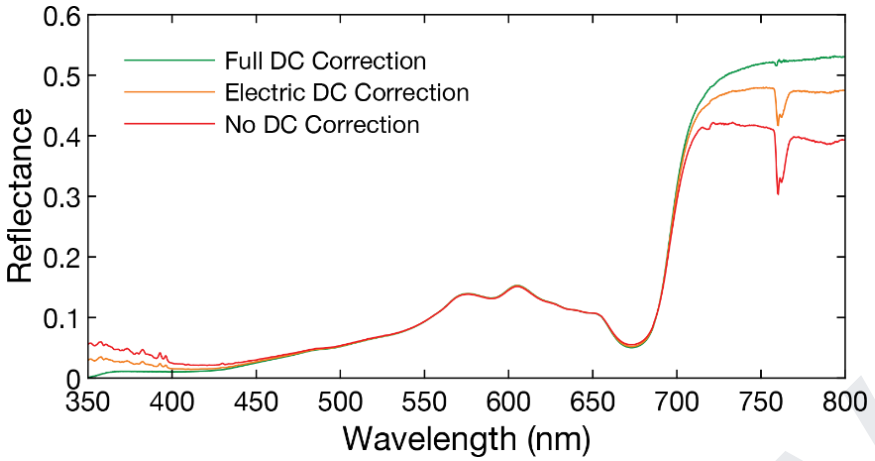

Figure 5.2 Impacts of different Dark Current (DC) corrections on calculated benthic reflectance of a coral specimen. Incomplete (and potentially inadequate) DC correction imparts artifacts in the final spectrum. The effects can be minimal at wavelengths where DC is small relative to the incident and reflected fluxes.

5.3 Evaluate Noise

Noise is inescapable in spectroscopy; at a fundamental level, it results from the particulate nature of light and matter (Ball 2006). Shot noise is the stochastic electronic signal arising from the discrete nature of charge carriers and photons. It manifests as a current fluctuation due to the temporal randomness of individual particle arrivals at the detector, generating a non-thermal noise floor that scales with the square root of the signal intensity. Thermal noise is the stochastic electronic signal arising from the thermal motion of charge carriers within a detection system. It manifests as a voltage fluctuation that sets a fundamental limit on measurement sensitivity and signal-to-noise ratio by imposing a continuous, broadband noise floor across the acquired spectrum. These factors are generally characterized as noise within the sensor. Environmental noise is much more complex and arises from the interaction of the system and its surroundings. Such noise can be produced by a variety of factors including variations due to atmospheric and oceanic properties. Both sensor and environmental noise can create both random and spectrally-correlated noise in the samples (e.g., Garcia et al. 2014).

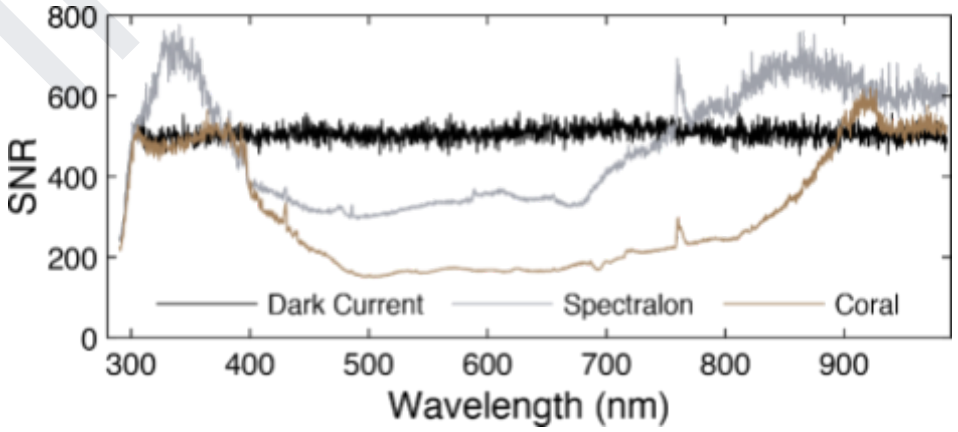

Figure 5.3 Signal-to-noise ratio (SNR) calculated for the three measurement types: Dark current (DC), Spectralon®, and coral. SNR is calculated as the signal mean ($\bar{x}$) squared divided by the signal standard deviation (s) squared or $\bar{x}^2/s^2$.

The signal-to-noise ratio (SNR) is the ratio of signal power to noise power, sometimes calculated as the signal mean ($\bar{x}$) divided by the signal standard deviation (s), or more often as $\bar{x}^2/s^2$. A high SNR (>100) is desirable, but a minimum SNR of 3 is required to identify the presence of a signal (Ball 2006). In the example illustrated by Figure 5.3, the dark current showed a nearly constant SNR of around 500 (calculated as $\bar{x}^2/s^2$) across the entire spectral range of the instrument. The Spectralon® plaque and coral had spectrally variable SNR, with lowest values between 500 nm and 700 nm. Coral SNR reached a minimum of ~150 near 505 nm. These spectrally variable SNRs arise due to the convolved influences of spectrometer sensitivity and environmental variability. Thus, only the dark current data truly approximate sensor SNR.

5.4 Spectral Resampling

A quick way to evaluate the wavelength registration is to evaluate a few of the specific atmospheric gas absorption bands from an environmental measurement of a plaque. An obvious feature is the absorption at 760 nm due to Oxygen A (see Figure 5.1A). Ensuring that this feature is located properly for all individual spectrometers can be valuable for gaining confidence in the measurement. More than one commercial spectrometer has had a poor wavelength registration for their instrument and this should be evaluated by the user directly. A spectral offset, which requires multiple registration wavelengths, may be required to align the spectra properly.

If more than one spectrometer is used, the output from different sensors must be resampled to the same wavelengths before calculating reflectance. In addition, spectrometers measure spectra at irregular wavelength intervals, and these data are resampled to monotonically increasing, equidistant wavelengths for many subsequent applications. A wavelength increment of 1 nm is typically suitable (e.g., 400 nm, 401 nm, 402 nm…), but that value can be changed as necessary to suit the scientific question and spectral resolution of the spectrometer system. However, the resampling interval should not be much smaller than that measured by the spectrometer system. Providing the raw data in the documentation may be desirable for many users.

5.5 Apply Plaque Calibration

Discussion of plaque usage is presented in Chapter 4.1. The reflectance value should be corrected for the calibration of the plaque across all wavelengths and using the underwater calibration factors if appropriate (Russell and Dierssen 2023). The measured flux is divided by the calibration (as shown in Figure 4.1). In the current example, the reference target had a calibrated reflectance of ~10%. This was specifically chosen to approximate the same brightness as coral and algae targets, so that the same optimal spectrometer settings (i.e., integration time) could be used for both reference and target. Often, calibration values are provided at only select wavelengths; a full spectrum can be obtained via interpolation. While the spectral

shape is largely preserved, using a dry calibration for a plaque that is underwater will result in significant differences in the derived benthic reflectance (Figure 5.4)

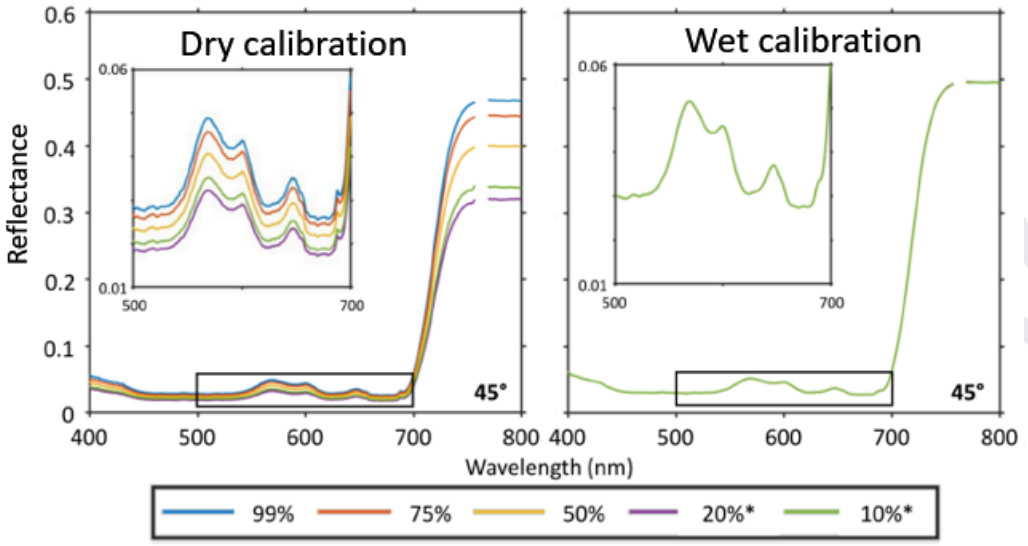

Figure 5.4 Reflectance of rockweed *Fucus sp*. calculated using dry reflectance factors (left columns) and with the calibrated submerged standard data (right columns) for viewing angles 5 and 45°. Adapted from Russell and Dierssen (2023).

5.6 Calculate Benthic Reflectance

Once all of the above factors are taken into account, the reflectance is simply the ratio of the upwelling irradiance (= measured target radiance x π) divided by the downwelling irradiance (= measured plaque radiance/plaque reflectance x π) . In this example, the assumptions would be similar to those shown in Figure 4.1. Namely, that the sensor is close enough to the target and the water is not too turbid to require corrections for scattered light from the water column. The distance, orientation, and light field are identical between target and plaque measurements. The target is presumed to be Lambertian and reflect light equally at all angles similarly to the one measured at the viewing angle.

5.7 Additional Processing

5.7.1 Spectral Smoothing

The best approach to reducing noise is to collect many spectra and take the average. In this case, there is no deformation or distortion of the R_B spectrum. However, if it is not feasible to accumulate many spectra, then digital smoothing can be a practical alternative. The most simple approach is a 3- or 5-point moving average. The aim is to reduce noise while minimizing changes to the shape of the R_B spectrum. A slightly more advanced approach is Savitsky-Golay (SG) filtering, which

can be used for both smoothing and differentiation. A SG filter is a set of coefficients that is applied to the spectrum via convolution. SG filters can operate across different window sizes and produce derivatives of any order, with zero-order being the smoothing filter. Talsky (1994) recommends a 3- or 5-point window for smoothing. The smoothing operation, whether moving average or SG, can be repeated multiple times, as needed (Figure 5.5).

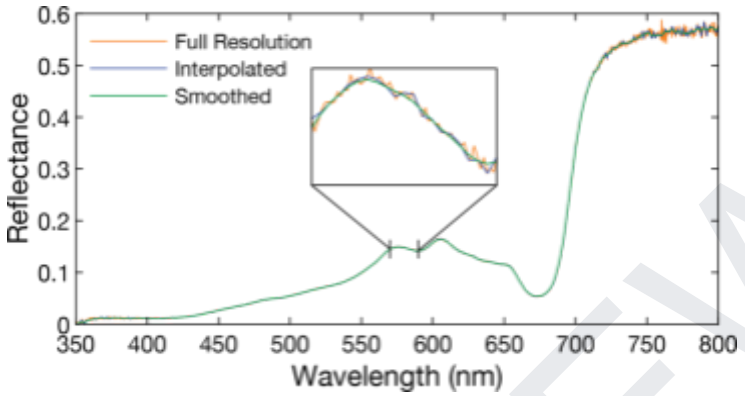

Figure 5.5 Full-resolution spectra with non-uniformly spaced wavelengths must be interpolated to equidistant wavelengths prior to smoothing. Here, simple linear interpolation is used, with a 1-nm increment. Then, a 3-point (i.e., 3-nm) SG filter is applied twice to the resampled spectrum. Inset shows wavelength range 570–590 nm.

5.7.2 Truncating Data

Data may need to be truncated or discarded when the uncertainty is too high and reflectance values become too noisy or unrealistic. This usually occurs in the spectral regions where the light field is inadequate and the SNR is too low, most often in the UV and blue (350-440 nm) and the red and near infrared (670-800 nm). Some post-processing metrics that can be used include identifying when reflectance becomes too high or too low (below 0 and above 1) or results in unusual spectral shapes for the type of benthos. An example of a typical sediment spectrum is shown in Figure 5.6A with examples of unusual spectral shapes produced when SNR is not adequate (Fig 5.6B-D). Flagging bad benthic data is challenging because sometimes a particular spectrum is not noisy but peaks where it should not (e.g., Figure 5.6D)

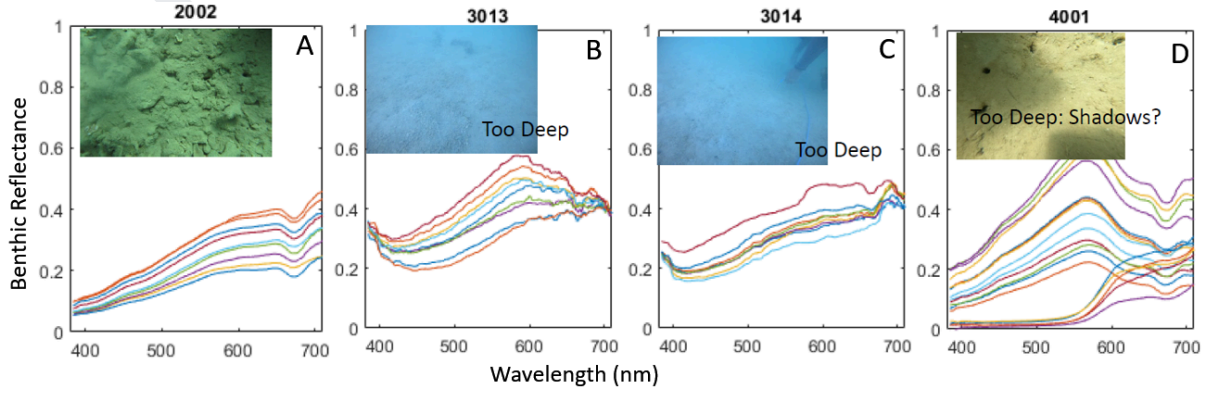

Figure 5.6 Benthic reflectance measured over different sediments at different depths using ambient light. A) typical sediment spectra; B-D) examples of spectra with high uncertainty due to low light (too deep) or shadowing.

5.7.3 Derivatives

Spectral derivatives are useful to highlight features of interest while at the same time eliminating unwanted background (Figure 5.7). Examples of spectral derivatives for analysis of R_B include Andréfouët et al. (2003b) and Hochberg et al. (2003a). For higher derivatives, Talsky (1994) notes that better results are obtained by repeat differentiation with a first-order filter than by a single differentiation with a higher-order filter. For example, if the fourth-derivative ($d^4R/d\lambda^4$) is desired, it is best to sequentially calculate the first ($dR/d\lambda$), second ($d^2R/d\lambda^2$), and third ($d^3R/d\lambda^3$) derivatives, then finally $d^4R/d\lambda^4$. The 2nd and 4th derivatives are commonly used because the peaks and troughs match the wavelengths corresponding to peaks and troughs in the spectrum. The 4th derivative is sometimes preferred as a visual tool because it provides peaks (positive anomalies) corresponding to peaks in the spectrum and vice-versa.

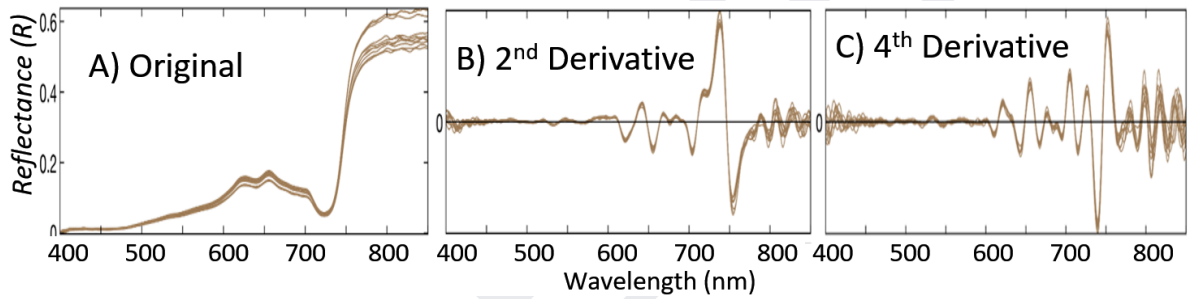

Figure 5.7 Derivative analysis reveals subtle peaks and troughs in the spectrum. The 2nd and 4th derivatives are the most common because the peaks and troughs match the wavelengths corresponding to peaks and troughs in the original spectrum.

5.7.4 Normalization

Another useful processing step is to normalize R_B. This may be desirable when, for example, uncertainties arise due to variable illumination or use of an uncalibrated reference target. Normalization of R_B removes differences in magnitude/brightness between spectra and highlights spectral shape. Two common approaches include dividing R_B by its value at a reference wavelength and dividing R_B by its vector length (L2 norm). Figure 5.8 illustrates the two approaches using coral and algae spectra (10 each) from the library of Hochberg et al. (2003b).

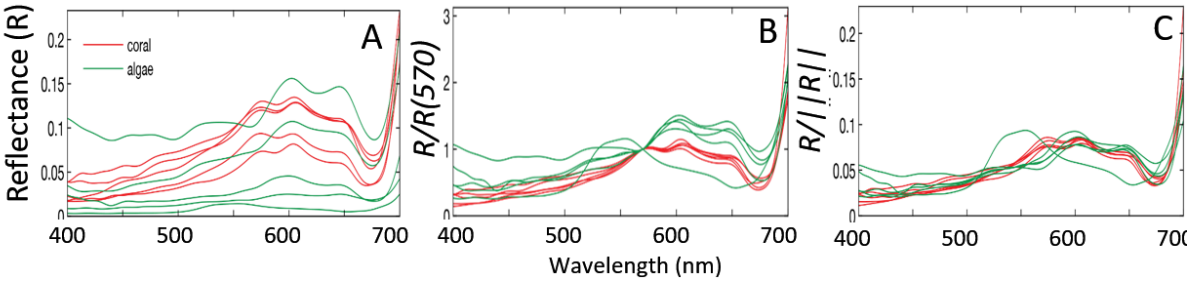

Figure 5.8 Normalizing to highlight spectral shape. A) 10 coral and 10 algae spectra. B) The same spectra divided by their values at 570 nm. C) The same spectra divided by their vector lengths (L2 norms).

5.8 Documentation

Spectral databases, also referred to as “spectral libraries” or “spectral information systems” (Hueni 2020; Di Franco et al. 2022), attempt to solve the technical challenge of the long-term archiving, organization and management of field spectral data, such that they serve as the basis for data sharing and re-use of the data held within them (via APIs or web portals). Example spectral databases include SPECCHIO (https://specchio.ch), EcoSIS (https://ecosis.org) and ECOSTRESS (https://speclib.jpl.nasa.gov/download). Key modes of interaction include the **ingestion** and structured storage of the data and associated contextual metadata via use of an input schema, and the **harvesting** of data through tools allowing the search and ‘browsability’ (Di Franco et al. 2022). Flexibility in data handling and use, and intuitiveness in operation are critical elements to the successful implementation of spectral database concepts. Additional functionality may include the ability to augment metadata entries (Hueni et al. 2020). They may also hold associated data (or links to associated data) including shapefiles of sample locations as photos specific to the data acquisition as well as documentation outlining methods of collection or sample analysis.

Of note, spectral databases generally score low on metadata completeness and metadata quality (Rasaiah 2015), thus hindering data discoverability, interoperability and the assessment of spectra for reuse. As discussed in Chapter 3.4, extensive metadata should be collected during a field campaign to capture the different conditions encountered during sampling. However, additional metadata is also required post-collection to document methods, sensor and plaque calibrations, and post-processing of the data (see Supplemental Materials: Metadata Template). Key documentation items should include:

- Field records of samples taken, and the conditions encountered during the measurement process.
- Documentation of sensors, methods, and post-processing information including subsequent laboratory analyses, spectral resampling, and other post-processing information.
- Additional files including spectral calibrations, photographs, and other relevant information.

A recent study compiled historic benthic reflectance spectra in a coherent database from all over Australian waters covering West Australia, South Australia, Victoria, New South Wales, and Queensland from 1994 to the present (Dekker 2021). As noted in that study, there was a large variation in how the measurements were done due to weather conditions, accessibility, and the varied platforms, sensors, equipment, and methods discussed here in Chapter 3. Over 2500 spectra and metadata from 1994 to 2016 were consolidated with an estimated economic value of approximately 2,000 AUD per spectrum and a total value of ~5 million AUD (Dekker 2021). The reader is referred to that report for detailed information on efforts to standardize the measurements, fill in missing metadata, and construct a consistent database to be used as an important resource for the community.

While many publically available database services are available for submission of data, the following are commonly used for archiving spectral data: Spectral Information System (SPECCHIO), NASA SeaWiFS Bio-optical Archive and Storage System (SeaBASS), and the Ecological Spectral Information System (EcoSIS).

Chapter 6

Spatial Scale of Variability

Steve Ackleson, Tiit Kutser, Ele Vahtmäe

The importance of scale and variability in space and time is a key issue in ecological modeling and central to understanding disturbance and recovery dynamics in benthic environments (Ellis and Schneider, 2008 and references therein). The ocean benthic environment is spatially complex and comprised of spectrally dissimilar features with length scale ranging from micrometers to tens of meters. Spatial complexity starts already from microscale. For example, Figure 6.1 illustrates spectral variability within a single polype of *Fungia granulosa.*

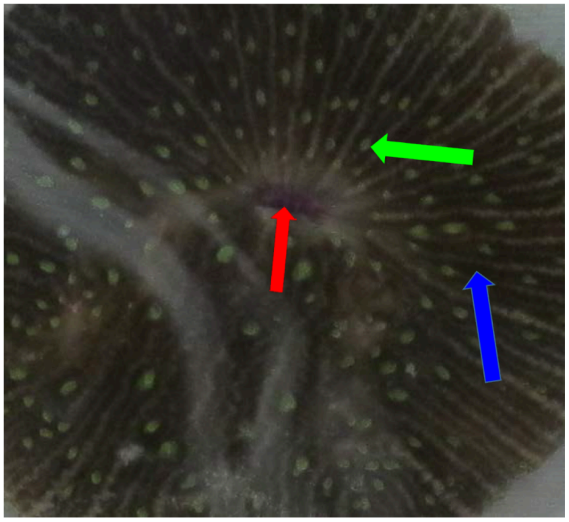

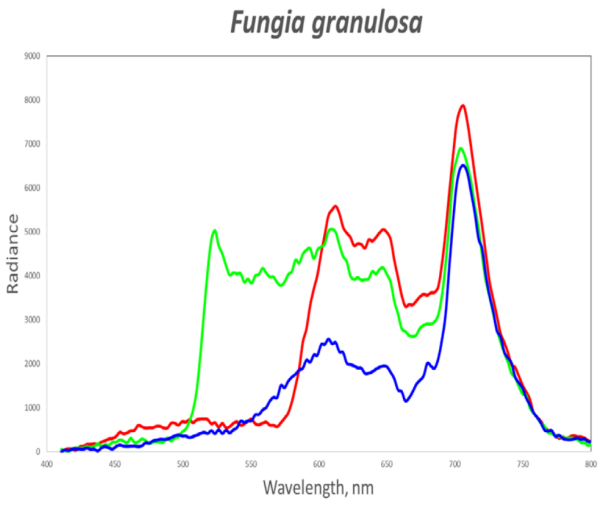

Figure 6.1. Reflectance spectra of a coral polype of *Fungia granulosa* sampled with HySpex imaging spectrometer in a lab aquarium with 0.09 mm spatial resolution. Arrows indicate the locations from where the respective pixels were taken. Reflectance is cut from 700 nm onwards by filter of the light sours in order to prevent overheating of live samples.

Collecting imagery with such microscale resolution allows the study of processes taking place in live corals, algae, or other organisms. For example, Vahtmäe et al. (2017) used microscale imaging spectroscopy to study the distribution of Chl-a in macroalgae grown in different nutrient and temperature conditions. Figure 6.2 illustrates the distribution of Chl-a in two blades of brown algae *Fucus vesiculosus*, grown in mesocosms in different conditions.

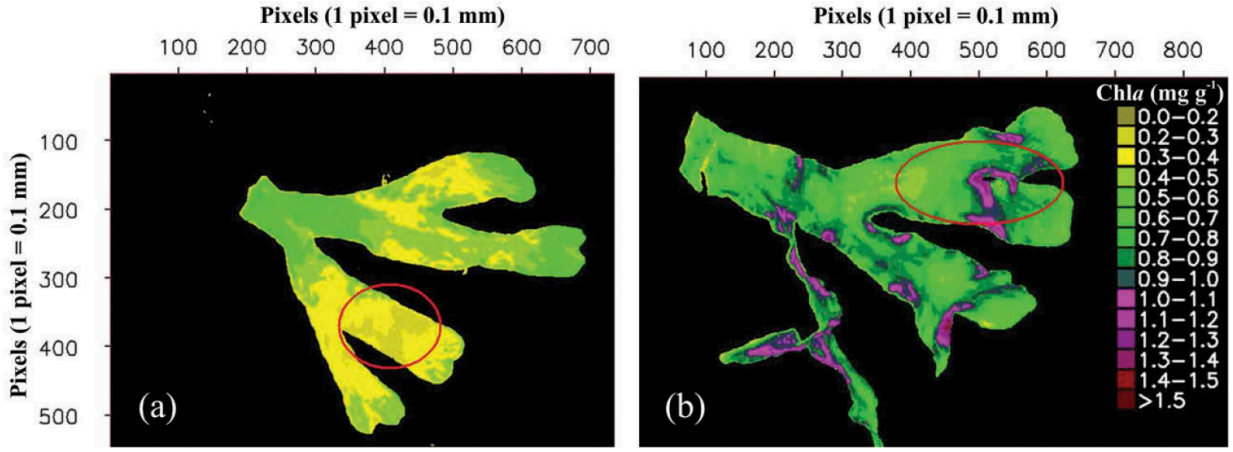

Figure 6.2 Spatial variability of Chl-a in two blades of *Fucus vesiculosus* grown in different light and nutrient conditions (figure from Vahtmäe et al. 2017).

Spatial variability in reflectance is clearly evident even in a seemingly homogeneous environment like sandy bottom. Each grain of sand hosts communities of sediment microbes and associated biofilms (Shaffer and Onuf, 1985; Stephens et al. 2003; Chapman et al. 2010; Besterman et al. 2021). Thickness and composition of the microfilm around each sand grain determines its optical properties. Moreover, there are different materials among sand grains and there may be mats of microalgae growing on the sand surface. All of those are continuously modified by erosion caused by tidal or wave movements. Thus the seemingly homogenous sandy bottom may have highly variable (in space and time) optical properties. It follows, therefore, that benthic reflectance is influenced by the measurement scale and represents the combined effects of spectrally dissimilar components occurring at spatial scales smaller than the measurement scale. The integrated reflectance of a coral species, for example, will represent the combined reflectance of all small-scale structures comprising the coral, e.g., polyps, zooxanthellae (the symbiotic coral algae), boundary regions between polyps, and any sediment deposited on the coral surface. It is seen in Figure 6.1 that the variability even within a coral polyp is very high and the integrated reflectance will also depend on the field of view of the instrument used to collect the reflectance spectra. If in the course of a reflectance measurement the

sample is illuminated oblique to the observation angle, as is often the case, the reflected light integrated across the field of view of the radiometer will likely also include shadowed areas resulting from the microtopography of the coral surface (Hedley et al. 2018). Measurements collected over seemingly uncolonized and homogeneous sediment will include the effects of spatially variable grain size, sand ripples, and small-scale patchiness in the concentration of sediment microorganisms on the directional reflectance function (Nelson et al. 1999; Zhang, et al. 2003; Ramey et al. 2009). Reflectance from seagrass meadows offer additional scaling problems associated with changing canopy morphology in response to forcing by waves and tidal currents (Hedley et al. 2016b). Consequently, any measurement of ρ_b will include a degree of uncertainty of unknown magnitude associated with sub-sample scale variability.

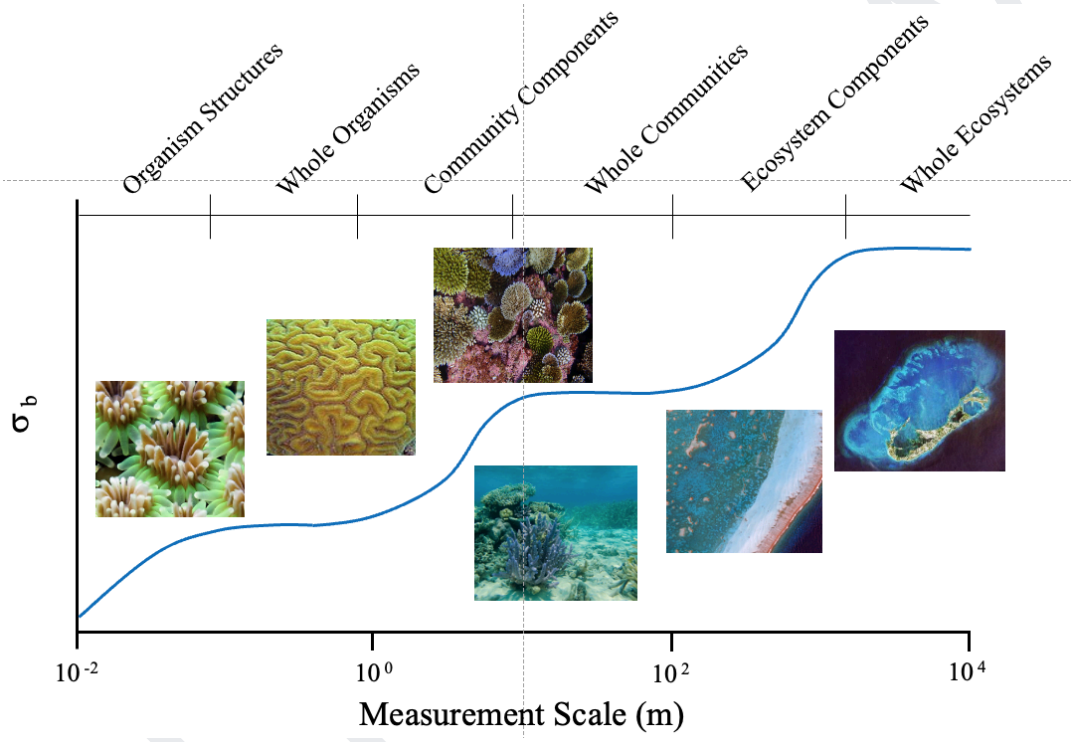

Figure 6.3 Illustration of how sub-measurement scale variability in benthic reflectance changes with measurement scale.

Using the example of a coral reef, we can illustrate how sub-sample variability is expected to impact benthic reflectance measured at different scales (Figure 6.1). At the coral polyp scale, e.g., 1 cm^2, sub-sample variability (σ_b) is likely most dominated by the distribution of chlorophyll within the individual coral polyps. As the measurement scale increases to 1 m^2, e.g., using a non-proximal radiometer positioned within the water column, sub-sample variability increases as the reflectance starts to include small-scale features, such as crevasses in the surface of the coral colony, polyp variability across the coral surface, and perhaps mixtures of several types of reef organisms. As the measurement scale continues to increase, the curve may develop an inflection point leading to a plateau describing nearly constant spatial variability, a condition perhaps best described as homogeneously heterogenous, representing a continuous mix of reef organisms. Continuing along

the curve one might encounter other scales of increasing σ_b and plateaus as the measurement scale, e.g., imaged by remote sensing systems of different ground resolution, includes multiple patch reefs, areas dominated by algae or seagrass, and tidal channels of uncolonized sand.

For optical mapping and monitoring purposes it is often desirable to identify key benthic cover types within an environment, often referred to as spectral endmembers. Endmembers are assumed to dominate the observed variability in bottom reflectance and to be optically stable throughout the area of interest, i.e., statistically constant regardless of measurement location. Since the contribution of endmembers to integrated reflectance scales with the fractional area cover within the measurement field of view, endmember reflectance may be combined linearly to describe the measured integrated reflectance regardless of scale. Consider, for example, a simplistic shallow water environment consisting only of two bottom types, bright sand and vegetation. The reflectance of each *pure* bottom type, perhaps measured *in situ* at a few locations, represents the associated spectral endmember. Armed with this knowledge, benthic reflectance measured anywhere within the environment may be described as a linear combination of the two endmembers. The endmember approach has been used frequently to map bottom cover, such as specific coral species, benthic algae, seagrass, calcareous and siliceous sediments, and mud (Hochberg et al. 2003b; Wicaksono et al. 2019).

However, endmembers are only useful to the extent that they accurately represent the features of interest across a useful range in measurement scale. They are tightly coupled with ecological length scales and are most effectively applied to common scales of benthic variability. For example, proximal measurements of coral reflectance made at the polyp scale may be quite useful for *in situ* monitoring of coral health, such as coral bleaching. However, endmembers derived from small-scale proximal measurements may not accurately represent the integrated reflectance of the entire coral colony that includes microtopographic effects, sediment deposition, or other organisms not represented as an endmember. Similarly, proximal measurements of seagrass leaf reflectance may be useful for monitoring the growth of epiphytic organisms, but may not adequately represent the effects of other canopy structures, the sediment substrate, and changes in canopy structure resulting from forcing by waves and currents on meadow reflectance made at larger length scales.

Another source of uncertainty associated with non-proximal and remote sensing determinations of benthic reflectance is small-scale changes in bathymetry (Zwada et al. 2010; Lecours et al. 2015; Hedley et al. 2018). That is, changes in bottom depth that occur within the spatial footprint of a radiometric measurement. Previously, we referred to shadowing that can occur with oblique illumination of an irregular surface, but larger vertical changes are present, attenuation due to increased pathlength through the intervening water can impact corrections for water column attenuation and introduce uncertainty to endmember estimations. Note, however, that with diver-based proximal measurements effects of irregular bathymetry can be easily avoided.

Chapter 7

Benthic Reflectance by Bottom Type

Stuart Phinn, Chris Roelfsema, Heidi Dierssen, Eric Hochberg, Geir Johnsen, Richard Zimmerman, Erin Hestir, Tiit Kutser, Arnold Dekker, John Hedley, Natascha Oppelt, Jaime Pitarch, Gillian Rowan, Maycira Costa.

This chapter provides examples of spectral reflectance measurements for a range of subtidal and intertidal benthic habitats around the Earth. The measurements are grouped by substrate and benthos types into:

- sediment;
- corals;
- minerals and rubble;
- submerged aquatic vegetation;
- macroalgae;
- microalgae on mudflats;
- detritus and debris;
- shadows; and
- others.

The measurement scales used follow from Chapter 6, and will focus on: organism; canopy; and aqua-scape/sea-scape scales, primarily from *in situ* point-based measurements, with some imaging spectrometer measurements.

We have attempted to cover as many relevant global bottom types as possible, but can only provide information from those with completed surveys. This led to an impressive list, considering the lack of coordinated and funded work in this area. As a result, however, the range of benthic environments and benthos/substrate types included is not exhaustive. For each bottom type we define the feature(s) that are measured, then briefly identify the biological, physical, and chemical properties that control their spectral absorption, transmission and scattering.

Different bottom types co-occur with each other at various spatial scales, which is relevant for attempting to differentiate bottom types via spectral signatures. The co-occurances highlight the ecologically relevant combinations that need to be considered. For instance as seagrass predominantly grows on soft substrate it is not common to occur next to hard coral that requires hard substrate for growth. A matrix representing the co-occurant relationships between various bottom types is available (Figure 7.1) that was generated from qualitative bottom composition data and/or field experience for submerged habitats for various coral reef and/or seagrass habitats from Fiji, Australia, Solomon Islands, Indonesia, Bahamas, and Belize.

		Brown Hard Coral	Blue Hard Coral	Soft Coral	Algae Brown	Algae Green	Algae Red	Turf Algae	Crustose Coraline Algae	Seagrass	Detritus	Sand BMA	Sand Carbonate	Sand Teriginous	Rubble
Coral	Brown Hard Coral		H	H	M	L	L	L	H	VL	VL	VL	L	VL	L
	Blue Hard Coral			H	M	L	L	L	H	VL	VL	VL	L	VL	L
	Soft Coral				M	L	L	L	H	VL	VL	VL	L	VL	L
Algae	Algae Brown					H	H	M	M	L	L	L	L	M	M
	Algae Green						M	L	M	M	L	M	L	M	M
	Algae Red							L	M	M	L	L	L	M	M
	Turf Algae								H	VL	L	VL	VL	L	H
	Crustose Coraline Algae									VL	L	VL	VL	L	H
Seagrass	Seagrass										M	H	H	H	VL
	Detritus											M	L	L	L
Sand	Sand BMA												H	M	L
	Sand Carbonate													VL	L
	Sand Teriginous														L
Rubble	Rubble														

H=High chance; M = Medium chance; L= Low chance; VL = Very low chance

Figure 7.1 Matrix of co-occurrant relationships derived for the various common bottom types qualitatively determined by expert-based synthesis of various benthic datasets throughout Fiji, Belize, Bahamas, Indonesia, Australia and Solomon Islands.

7.1 Sediments

Sediments are one of the most common optically shallow benthic habitats and are often found with other endmembers like seagrass and corals. Sediment is defined here as unconsolidated inorganic grains or particles which are interspersed with water molecules, and living and detrital organic matter. Sediment types are primarily differentiated by their dominant particle diameter, using the Wentworth or ISO scales, from clay (0.98 – 3.9 μm), silt (3.9 – 62.5 μm), sand (0.062 – 2 mm) to gravel (2 – 64 mm). Larger types of sediment are referred to as pebbles, rocks/rubble, and boulders. The primary controls on spectral absorption, transmission and scattering of electromagnetic energy by sediments include:

- mineralogy of the sediment particles;
- particle form and size distribution;
- amount of organic material on and around sediment particles; and
- water content (and in-water constituents) within interstitial spaces.

For minerogenic material, the absorption comes from the broadened far wing of electronic transitions in the deep UV and the backscattering from reflections of the interface between the crystalline grains of the material (Fournier et al. 2018). Sediment absorption can vary such that sediments with more iron tend to absorb more blue light compared to those composed of calcite derived from living material. Backscattering is dependent on the structural elements of sediments in terms of particle orientation and the surface interface roughness. While such data is scarce,

Fournier et al. (2018) successfully modeled benthic reflectance presuming the sediment interfaces were rough with randomly oriented particles.

Sediment colours vary from bright “white” carbonate sediment to green-hued sediment with algal film to very dark brown muds. The benthic reflectance at 555 nm, for example, can range from over 60% for very clean carbonate sediments to less than 5% for dark muds. Without accounting for algal contributions, the spectral shapes tend to go from nearly spectrally flat for dark muds to monotonically increasing from blue to red wavelengths depending on the sediment composition.

Sediment reflectance has been measured both *in situ* by divers with spectrometers (from cores in laboratories with integrating spheres) and from drone, airborne, and satellite sensors. Several of the different dive spectrometer systems used for this work are described in Chapter 3 and measurements have been made both with ambient sunlight and with closed path sensors using active light sources. Since sediment is flatter than most other benthic habitats, both closed and open path systems are possible. Shading of the direct solar beam can be advantageous in shallow water scenarios where there is considerable wave-induced caustics that create variability in the ambient light field.

For measurements made in air, many challenges make this an “approximate” or even “relative” measurement. A major issue in this type of sampling is accurately preserving the sediment microlayer, particle orientation, and pore water. A carefully obtained sediment core, preferably collected by divers, with intact sediment surface and water above the interface is, therefore, preferred over random grab samples. The user must determine how much water to leave on the sample as residual that keeps the pore spaces filled and minimizes the layer of water above the sediment. Dry or disturbed sediment can provide a useful relative measure of the sediment composition, but may not be an accurate measure of the sediment found at the sea bed. The light source and sensor orientation must be carefully designed to minimize sun glint reflected off of the wet sediment surface. Having a diffuse light source (either the sun or artificial) that illuminates the sediment evenly can be important.

Finally, sediment reflectance measurements made in air are challenging because the spectra are normalized to downwelling light in air which is not necessarily representative of the light hitting the sediment through a water interface on the sample. A measurement of the reflected light must then consider the attenuation of light through a microlayer of water and changes to the directionality of the light due to the angle of refraction changes between air and water. More research is needed to characterize the uncertainty associated with making measurements of downwelling irradiance in air and upwelling measurements in air over a wet uneven sediment surface. Measurements of the BRDF of different types of sediment surfaces *in situ* would also be warranted to develop the most accurate methods for estimating benthic reflectance of the sediment.

Most sediment in optically shallow water has benthic microalgae that influence the reflectance (Roelfsema et al. 2003; Borrego-Acevedo et al. 2014). Benthic microalgae or microphytobenthos are microscopic algae (diatoms, dinoflagellates

and cyanobacteria) that have a variety of different pigment compositions. They could be found within the top centimeter of sediment, sometimes forming a mat-like layer on top, and can photosynthesize several centimeters deep. As shown below, the amount of benthic algae on sediment is highly variable over space and time and the use of a single generic “sediment” endmember is generally not feasible for most remote sensing applications. Since many benthic algae are diatomaceous, they have very similar absorption properties to water column phytoplankton. Hence, separating the reflectance properties associated with water column phytoplankton absorption from benthic algal absorption can be extremely challenging for remote sensing applications. This means that retrieval algorithms can attribute absorption from benthic sediment to that occurring in the water column, and vice versa.

The types of different sediment habitats are vast across inland, estuarine, coastal, and open ocean habitats. Below we provide an overview of reflectance properties from a few major types including intertidal mud flats, submerged carbonate sediment, and submerged mud.

7.1.1 Intertidal mudflats

Mudflats, also known as tidal or inter-tidal flats, are coastal wetlands composed of silts, clays and organic matter, deposited by tides or rivers. that generally have no emergent vegetation. Mudflats play an important role in coastal defence, dissipating wave energy, and have high biological productivity, from benthic microalgae leading to abundant invertebrates (worms, clams and other shellfish) that provide food for populations of migrant and wintering birds and other wildlife. A defining feature is that they are completely covered by water at high tide and exposed to air at low tide. In many estuaries, photosynthesis primarily takes place during emersion periods because the water is too turbid for sufficient light to penetrate to the benthos during immersion periods.

The sampling logistics are rather complex. Mudflats may be reached from land, or from the sea, as in Figure 7.2 A). In this latter case, a rubber boat can be intentionally stranded during lowering tide, and the field campaign is conducted until water rises again and the boat is freed. Some types of mud are soft to traverse, and may even sink underfoot, making the sampling strenuous for untrained individuals. Surveys are made with a group of people performing radiometry, followed by another group that takes samples to be analyzed in the laboratory. Benthic microalgae migrate vertically during a tidal cycle, which imposes stark temporal constraints when radiometry is about to be compared to data resulting from sample analysis or to satellite images. We recommend recording precise time stamps of any benthic measurements of mud flats to be able to link the spectrum to properties of the benthos, the tidal cycle and the time of emergence.

Radiometry on mudflats is generally performed at low tide while standing directly on the substrate and using spectrometers designed for in-air measurements. A radiance sensor pointing at the sediment constitutes the signal, which is normalized by the downwelling irradiance (Figure 7.2 B)) or using a single sensor mounted on a tripod making sequential measurements of a standardized plaque and sediment.

Figure 7.2 A) Drone image of a sampling group at the Heringsplaat, Netherlands. The group arrived on a rubber boat that was stationed on the mud. B) Sampling gear for measuring downwelling irradiance and upwelling radiance over the mud flat. Photo source: J. Pitarch

Examples of the benthic reflectance of mud flats are provided in Figure 7.3 from field measurements made on the mudflats of the Eems Dollard in 2018 and 2019. Reflectance shows a large range of variability corresponding to changes in algal pigment. The Chl-a absorption feature at 665 nm is noticeably larger for the darker mud with lower reflectance compared to the mud with higher reflectance. The darker mud also has higher absorption in the blue (400 - 500 nm) consistent with more absorption by Chl-a and other accessory pigments. Reflectance increases into the near infrared with values ranging from 8 to 15% at 900 nm.

The variability of benthic reflectance of mudflats across a continuum suggests the development of tailored algorithms to retrieve biophysical variables. Specifically, the Chl-a absorption trough at 665 nm has shown correlation to in situ measurements of Chl-a, measured in terms of surface concentration ($mg\,m^{-2}$). This allows obtaining quantitative estimates that may in turn be used to estimate primary production. High-resolution sensors, such as Sentinel-2, possess the minimal set of bands needed to apply such algorithms, allowing global mapping of these important ecosystems (Jacobs et al. 2021).

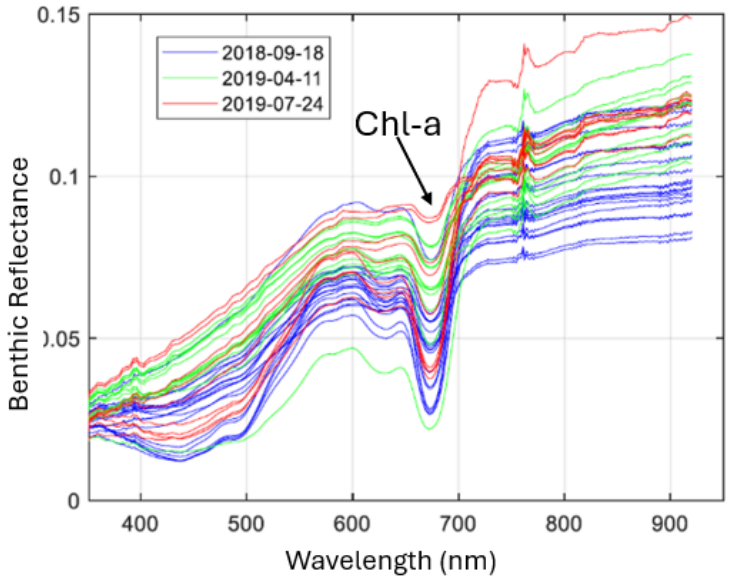

Figure 7.3: Reflectance spectra collected during the three campaigns at the Heringsplaat, Netherlands (modified from Jacobs et al. 2021).

7.1.2 Submerged carbonate sediment

Carbonate systems are a major component of the shallow water habitats across the subtropical to tropical world ocean and are considered an important component of the marine carbon cycle (Laugié et al. 2019). Shelves, banks, lagoons, and coral reef tracts of carbonate sediment are formed in shallow, warm waters either from direct precipitation of calcium carbonate from seawater or by biological organisms that form secretions and skeletal material (e.g., corals, foraminifera, algae, etc.). Carbonate sediment has diverse particle sizes, shapes and textures and can be bound together by encrusting organisms or found as loose sediment subject to resuspension and transport by currents. Various carbonate classifications have been proposed on the basis of grain characteristics and environmental factors such as the tectonic setting, hydrodynamics, salinity, temperature, biota and nutrients (Figure 7.4, Laugie et al. 2019).

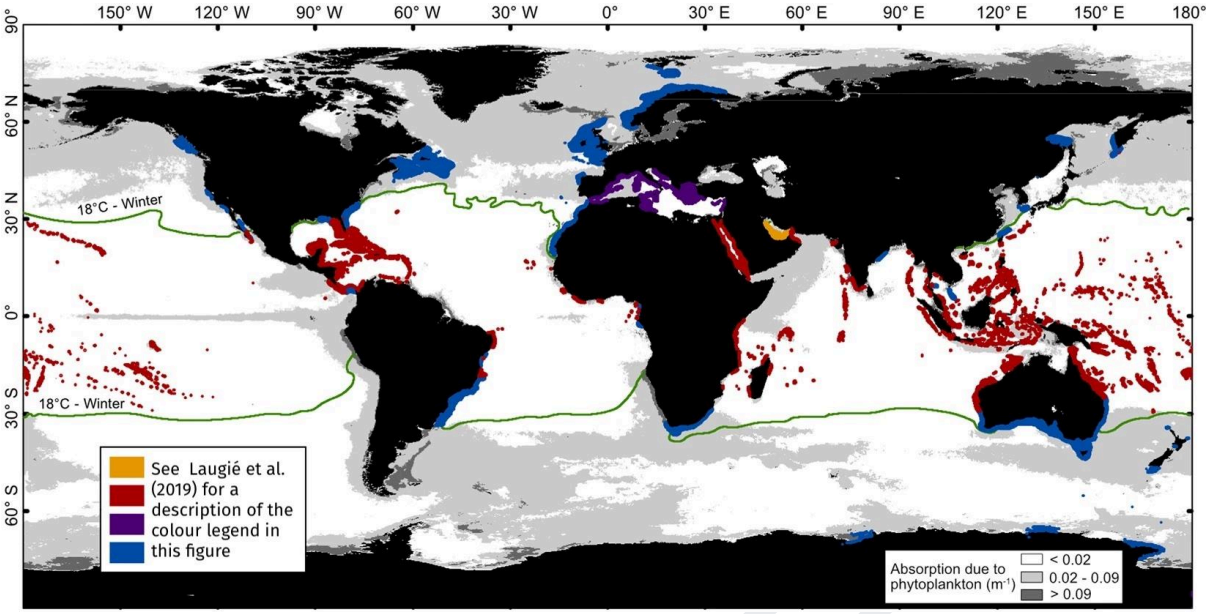

Figure 7.4. Distribution of carbonate sediments across the world ocean as adapted from Laugié et al. (2019). The gray background shows average absorption by phytoplankton in the water column used in the classification scheme. Creative Commons CC BY license.

Benthic reflectance is variable across carbonate sediment platforms. In the Bahamas Banks, for example, Dierssen et al. (2009, 2010) found that the benthic reflectance varied from whiter carbonate sediment in the Andros and Exumas regions to dark green “grapestone” sediment that could mimic seagrass from multi-spectral satellite imagery (Garcia et al. 2020; Figure 7.5). Forming in low-energy subtidal areas, the grapestone sediment is an aggregate of carbonate particles bound together by algae or micritic cement with an appearance resembling a bunch of grapes. Hence, even within this one category of sediment, the spectral range can be quite large in benthic reflectance and variable with different amounts of algal contributions and pigment absorption features.

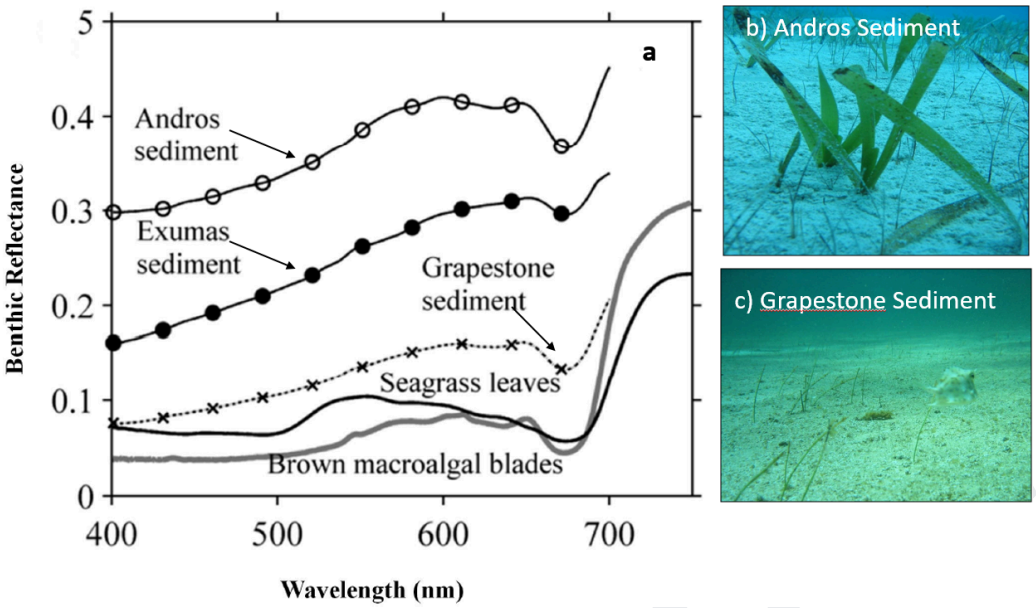

Figure 7.5 a) Benthic reflectance measured over different carbonate sediment types in the Bahamas Bank from whiter sediment to dark green grapestone sediment with similar magnitude reflectance to seagrass leaves and macroalgal blades. Underwater pictures of b) Andros sediment; c) grapestone sediment (photos by L. Bodensteiner). Modified from Dierssen et al. (2010).

7.1.3 Submerged mud sediments

Sandy bottoms are more common in shallower coastal areas, while mud sediments are found in lakes, estuaries, lagoons and the vast deep-sea environment of the world's ocean. Mud sediment is considered mixtures of small clay and/or silt particles below 0.06 mm diameter and is often rich in organic matter. Mud can be coloured tan, brown, red, or black, depending on the organic content. Black muds occur in areas where organic material accumulates faster than it is consumed. Such conditions can occur when bottom waters get oxygen-depleted and/or regions receive considerable influx of organic debris, including leaves and pollen.

Here, we provide an example of some of the darkest sediments common to estuaries. Elkhorn Slough on the central California coast U.S.A. consists of a subtidal channel, tidal creeks, intertidal mudflats, and salt marshes with an average depth of 3 meters. The sediments are highly organic and those located closer to the tidal channel have a high content of clay, while cores closer to salt marshes have a high content of peat. In Elkhorn Slough, sediment benthic reflectance was quantified using the DiveSpec underwater spectrometer with measurements normalized to a Spectralon® plaque set on the substrate (Dierssen et al. 2019). The reflectance ranged from 3% to 7% across the visible spectrum (Figure 7.6). Sediment spectra increased monotonically from 400 to 700 nm and showed only a slight dip at the chlorophyll-a absorption band at ~660 nm indicating low amounts of associated algae or biofilm. Sediment within the eelgrass bed was 11% darker than sediment outside the bed likely due to enhanced organic detritus and other absorbing matter trapped within the eelgrass meadow.

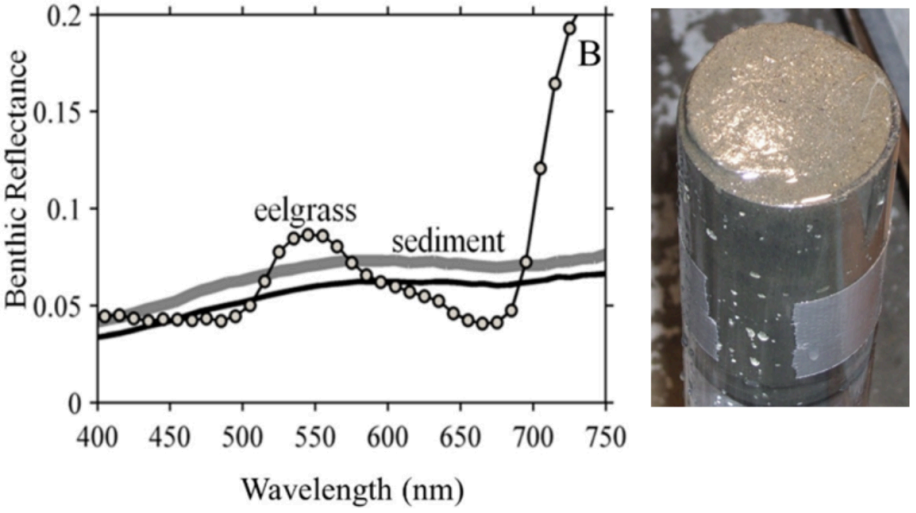

Figure 7.6 Benthic reflectance from Elkhorn Slough, central California, of sediment measured by divers both within (solid black line) and outside the eelgrass beds (solid grey line) compared to eelgrass leaf reflectance measured in the laboratory (dotted line). Modified from Dierssen et al. (2019).

7.1.4 Benthic microalgal films and mats

Algal films and mats are biofilms composed of microalgae that grow on various surfaces in aquatic and inter-tidal environments. Algal films typically refer to thin, nearly invisible layers of algae on surfaces, while algal mats are thicker, more cohesive structures. These features are found in a range of environments, including on benthic sediments, amongst other submerged aquatic vegetation, and commonly in in-frequently inundated areas shoreline/estuarine/saltmarsh/wetlands next to inter-tidal areas, through to other environments with highly episodic rainfall events and impervious sub-surface layers, e.g., deserts and Antarctic/Arctic locations (Murphy et al. 2005; Hubas et al. 2011; Klemas 2012; Salvatore et al. 2020; Montes-Herrera et al. 2024). They also occur within coral reef lagoons, reef-flats, and reef crest areas under certain conditions (Andrefouet et al. 2003a, c). In some cases, if surface algal-blooms occur in sheltered coastal environments, and encounter conditions favourable to large-scale blooms without disturbance, they develop into consolidated mats (Rousset et al. 2018). These algal communities play important roles in aquatic ecosystems, affecting nutrient cycling and serving as food sources for other organisms.

The spectral reflectance, transmission and absorption properties of algal films and mats, primarily in the visible and near-infrared wavelengths are influenced by a combination of biological, physical, and chemical factors. These properties interact to determine the overall spectral reflectance characteristics of algal films and mats:

- Absorption is primarily controlled by pigment composition and concentration, with chlorophyll-a showing strong absorption peaks around 430 nm and 662 nm.

- Transmittance is influenced by the thickness of the film/mat, cell density, and overall absorption.
- Reflectance is a result of both absorption and scattering processes, with peaks often observed in the green region (around 550 nm) due to lower absorption by chlorophyll.

Specific controlling properties are included in Table 7.1

Table 7.1 Properties within a microbial mat that will influence the optical properties including absorption and scattering

Biological	Physical	Chemical
Pigment composition: -chlorophylls, carotenoids, phycobiliproteins	Thickness of the algal film or mat	Water content
Cell size and shape	Density of algal cells	Mineral content
Community composition	Surface texture or roughness	Dissolved organic matter content
Nutrient status	Underlying substrate characteristics	Extracellular polymeric substances (EPS)
Growth phase	Vertical structure and layering within mat	Gas bubbles from photosynthesis

Examples of spectral reflectance signatures of purple sulphur bacteria mats are included in Figure 7.7.

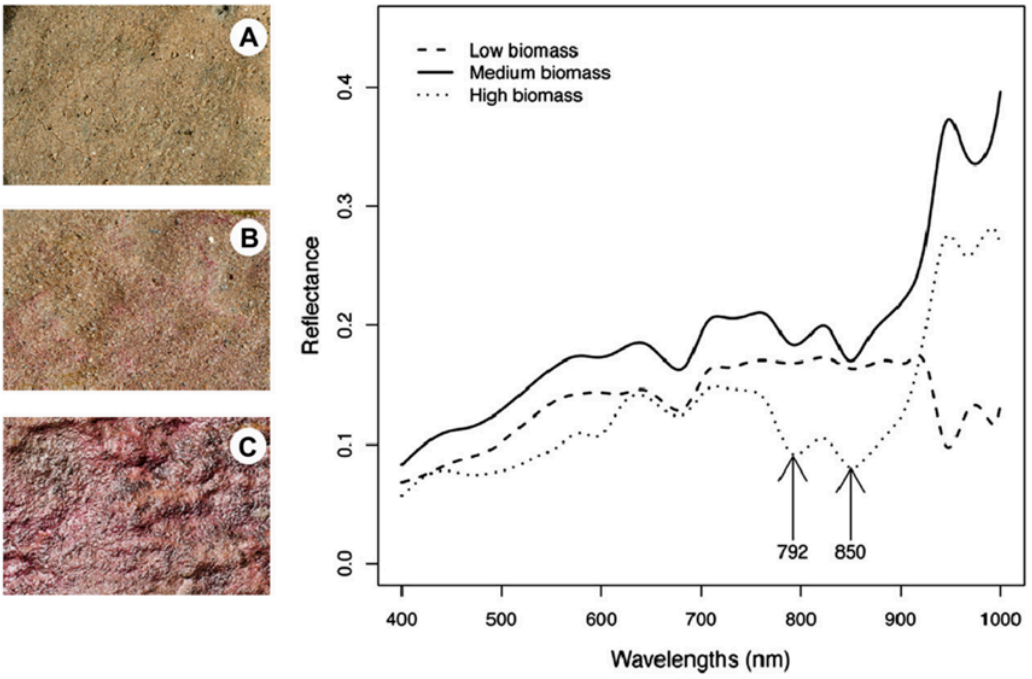

Figure 7.7 Left panel: Pictures of sediment from Roscoff Aber Bay showing A) low; B) medium and C) high biomass of purple sulfur bacteria. Right panel: Spectral

reflectance in sites with low (dashed line), medium (solid line), and high (dotted line) biomass. The arrows point to the bacteriochlorophyll-a absorption peaks.

7.2 Corals

7.2.1 Shallow Sea Corals

Coral reef benthic ecosystems are collections of distinctive communities, which are distinguished by their characteristic assemblages of organisms and substrates (Stoddart 1969). A benthic community's structure is defined by its component set of organisms and substrates: benthic functional types (BFTs). Several reef communities may share bottom-types in common, but the BFTs' proportional contributions vary both between and within communities. Reef community structure exhibits tremendous spatial heterogeneity over scales of centimeters to hundreds of meters and, in contrast to phytoplankton and macrophyte communities, is inherently stable on time scales of months to years (Buddemeier and Smith 1999).

Table 7.2 illustrates a functional classification scheme for coral reef BFTs as they relate to both reef ecology and spectral reflectance. The fundamental, predominant bottom-types are coral, various algae, and sediments dominated by carbonate sand (Kinsey 1985).

Table 7.2. Classification scheme for functional coral reef benthic functional types.

algae	turf algae
	crustose coralline algae
	macroalgae, brown
	macroalgae, green
	macroalgae, red
coral	blue
	brown
sediment	carbonate sand/mud
	terrigenous mud
other	seagrass
	octocoral

There are three basic forms of reef algae: turf algae, crustose calcareous algae, and fleshy macroalgae (Berner 1990). Crustose calcareous algae are important reef calcifiers (Kinsey 1985), cementing the products of disintegration of various other calcifying reef organisms, thus creating a harder skin for the reef (Berner 1990). Turf algae and fleshy macroalgae are a major source of fixed carbon to reef primary consumers (Klumpp and McKinnon 1989). Because of their importances to different reef processes, these three algal types form sub-classes within the broader algae class.

While crustose calcareous algae are mainly rhodophytes (order Corallinales), algal turfs are often a mixture of chlorophytes, phaeophytes, rhodophytes, and cyanobacteria (Berner 1990) that can mix on spatial scales of <1 cm, well beyond

the spatial abilities of today's remote sensors (smallest footprint ~2 m). However, discounting their epiphytic communities, fleshy macroalgae—mainly chlorophytes, phaeophytes, and rhodophytes—exist at a spatial scale (0.1's - 10's of m) that may be resolvable by remote sensing. The different fleshy macroalgae taxa are preferred forage material for different reef consumers (Glynn 1990). Furthermore, chlorophytes, phaeophytes, and rhodophytes possess different photosynthetic accessory pigments (Kirk 2011) and thus often exhibit their characteristic colours of green, brown and red, respectively. These groups may be individually important to energy flow through the reef system, and they can be discriminated based on their optical reflectance spectra.

Seagrass is an essential habitat in the life histories of many reef species and can cover extensive back-reef and lagoonal areas (Enríquez et al. 2002).

Carbonate sand is by far the predominant BFT by area for most shallow reefs, and sand provides an important resource and habitat (Conger et al. 2009). Finer-grained carbonate muds occur in deeper lagoonal areas with slower water flow (Kench 2011). The spread and deposition of terrigenous sediments can be deleterious to reefs near high islands (Watanabe et al. 1993).

With respect to hard corals, examination of multiple data sets has revealed two basic modes of coral spectral reflectance: one mode is associated with corals that are visually (to humans) brown, red, orange, yellow, or green. The other mode is associated with corals that appear purple, blue, pink, or gray. These patterns of association occur across taxonomic lines and in all oceans. A mode of "green" corals with spectra peaking at 500-530 nm have also been described (Kutser and Jupp 2006), but peaks in these wavelengths are often related to green fluorescent proteins (see below). Soft corals or octocorals can occupy substantial reef areas and may compete with scleractinian corals for space (Fabricius 1997; Ben-Yosef and Benayahu 1999; Bastidas et al. 2001).

Reflectance Spectra Characteristics

There are spectral features that are common to all benthic types (Figure 7.8). Low values at blue and green wavelengths are largely the result of absorption by photosynthetic and photoprotective compounds (Bidigare et al. 1990; Dove et al. 1995; Salih et al. 2000; Kirk 2011). Higher values at red wavelengths indicate relative lack of absorption. Chlorophyll absorption is readily apparent near 675 nm, and the effect of strong near-infrared reflectance is apparent at 700 nm. Except for carbonate sand, all BFTs have low average reflectance, generally falling in the range 0 - 0.3, and all have either peaks or shoulders near 600 and 650 nm. Finally, all BFTs exhibit wide variations in the magnitude of reflectance, while generally maintaining their same relative shapes.

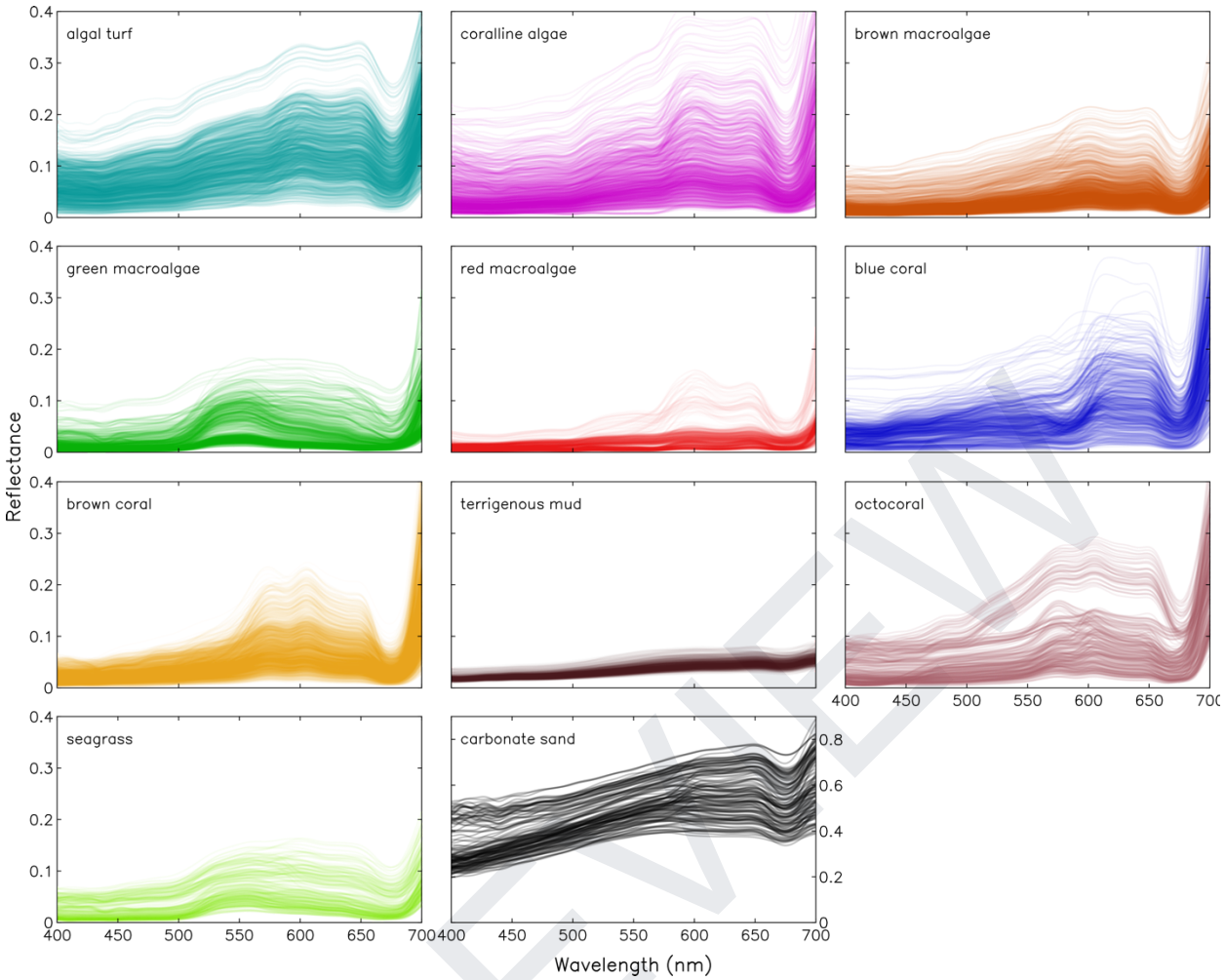

Figure 7.8: Spectral reflectance at visible wavelengths for coral reef benthic functional types. Spectra were collected during 1999–2002 on Atlantic and Indo-Pacific reefs. See Hochberg et al. (2003b, 2004). Note different reflectance scale for carbonate sand.

An important point is that the shapes of BFT reflectance spectra are conservative worldwide (Hochberg et al. 2003b). This consistency results from each BFT having its own suite of pigments that is conservative throughout the world, and it is spectral absorption by these pigments that ultimately determines the shape of spectral reflectance.

7.2.1.1 Brown Hard Corals

Coral spectral reflectance is dominated by pigments in the endosymbiotic zooxanthellae, which are photosynthetic dinoflagellates (Hochberg et al. 2003b). These pigments produce a triple-peaked pattern characterized by depressed reflectance between 400 and 550 nm and by positive reflectance features (i.e., local maxima or shoulders) near 575, 600, and 650 nm (Figure 7.9). This is the basic shape of spectral reflectance for corals that visually appear brown, red, orange, yellow, or green. This form has been labeled the ‘‘brown coral’’ mode (Hochberg et al. 2004). The 575 nm feature, in particular, is due to an absorption minimum between peridinin and chlorophyll *a*. Because peridinin is diagnostic of dinoflagellates, and because corals are the predominant BFT to harbour zooxanthellae, the 575 nm feature is an effective diagnostic of corals. Unfortunately,

because coral reflectance is driven by zooxanthellae pigments, it is not possible to spectrally discriminate between most species (Hochberg et al. 2004). Moreover, corals of the same species (e.g. plate coral *Acropora hyacinthus*, and several others) may be brown, blue or green (Kutser and Jupp 2006).

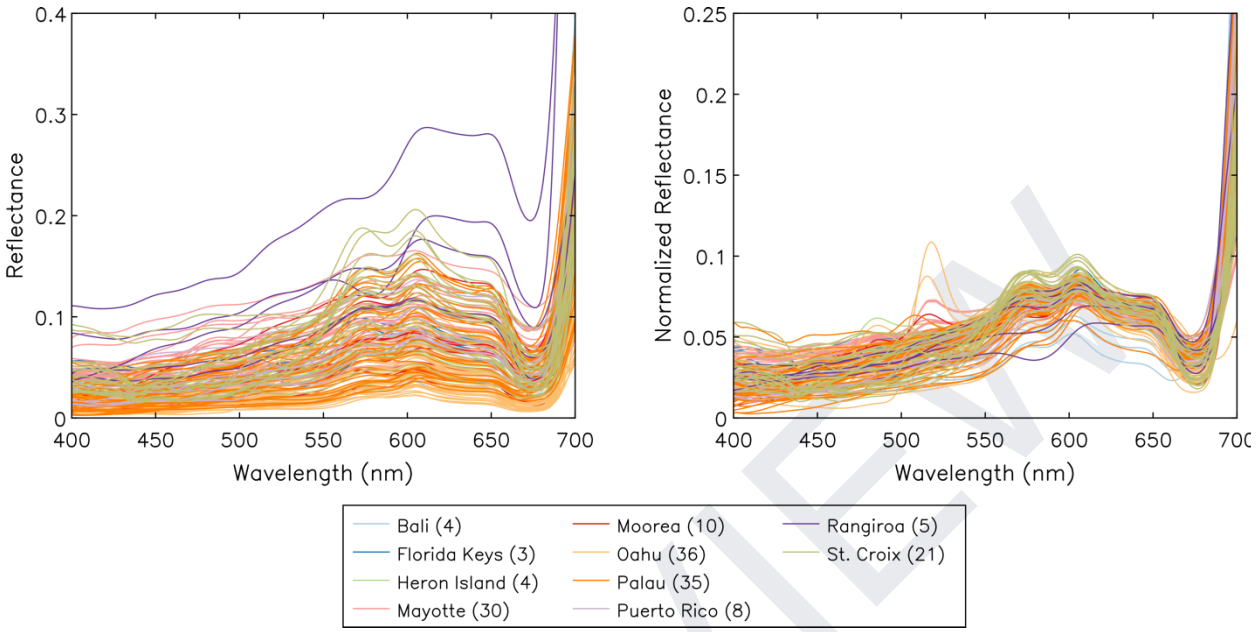

Figure 7.9 Spectral reflectance of brown-mode corals from Atlantic and Indo-Pacific reefs. These corals visually appear brown, red, orange, yellow, or green. Values in parentheses indicate the number of spectra for the given locale.

Coral-host pigments modulate the basic spectral shape, especially for green corals that obtain their colouration via fluorescence, typically between 495 and 520 nm (Figure 7.10). Green fluorescent proteins (GFPs) absorb and fluoresce light at shorter and longer wavelengths, respectively, contributing to striking, human-perceived colourations (Dove et al. 2001; Mazel et al. 2003).

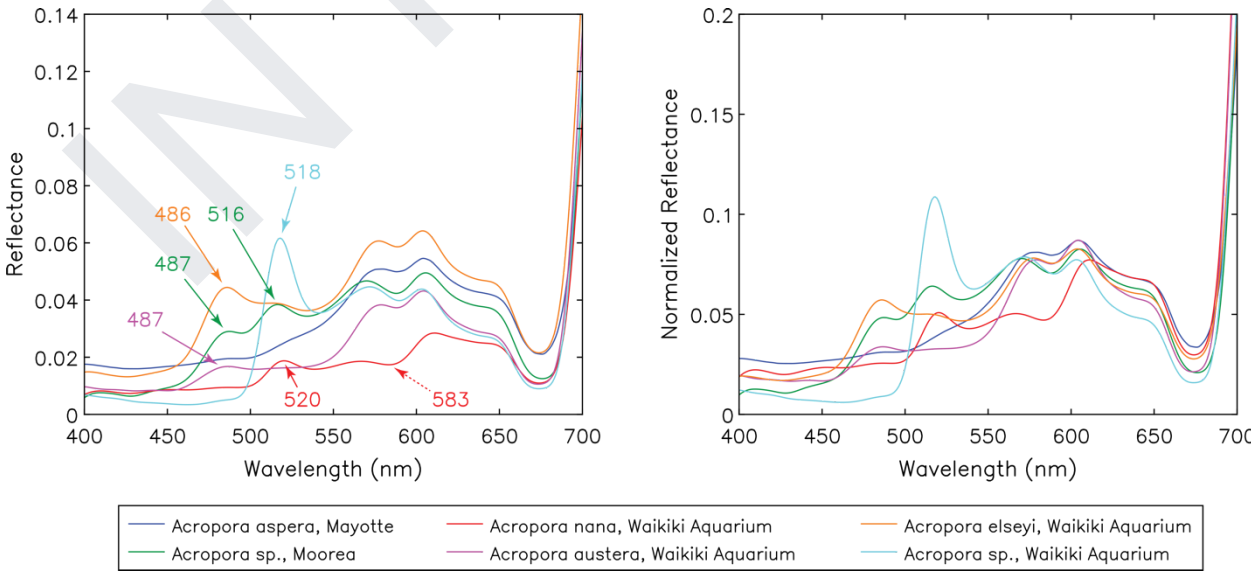

Figure 7.10 Spectral reflectance of *Acropora sp*. corals illustrating fluorescence at green wavelengths. Numbers and solid arrows indicate locations of fluorescence. Dashed arrow indicates absorption feature in place of reflectance peak typically near 575 nm; this is an example of blue-mode reflectance.

7.2.1.2 Blue Hard Corals

Blue-mode coral spectral reflectance is exhibited by those corals visually appearing purple, blue, pink, or gray. In this mode, the 575 nm feature diagnostic of brown corals is generally absent, leaving a plateau-like shape between 600 and 650 nm (Figure 7.11). In some colonies it appears that the 575 nm feature has shifted to shorter wavelengths, while in other colonies there is a strong absorption feature in the region 560–570 nm. The absorption in this region is likely due to a non-fluorescing GFP (Dove et al. 1995; Lukyanov et al. 2000).

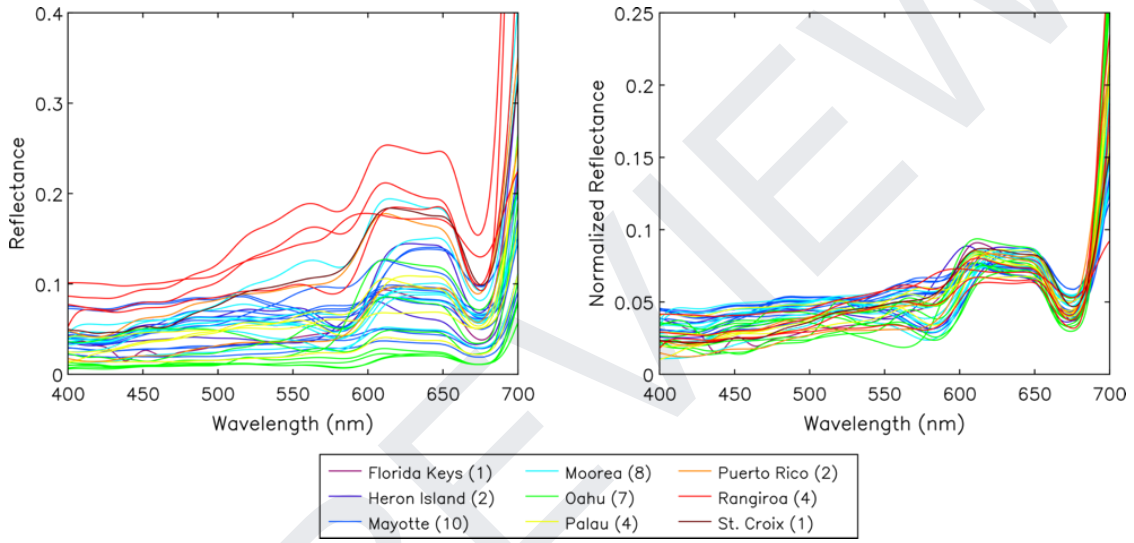

Figure 7.11 Spectral reflectance of blue-mode corals from Atlantic and Indo-Pacific reefs. These corals visually appear purple, blue, pink, or gray. Values in parentheses indicate the number of spectra for the given locale.

Expression of blue mode coral reflectance is neither ubiquitous nor constant. Some coral species only exhibit brown mode reflectance. Among those that exhibit blue mode reflectance, the effect is variable (Figure 7.12). This suggests variable expression of the responsible coral-host pigment in relation to the density of zooxanthellae pigments.

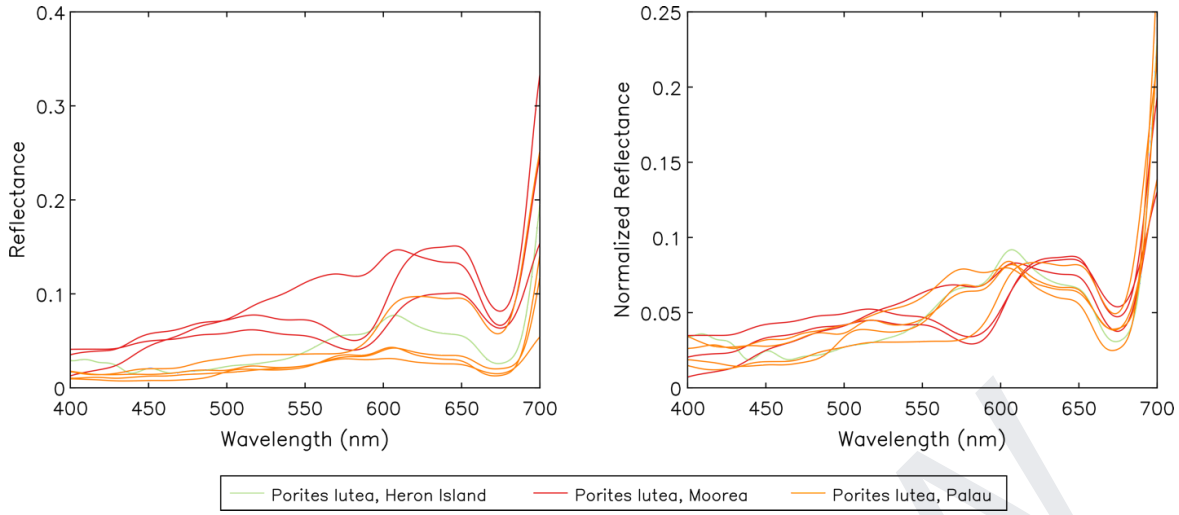

Figure 7.12 Spectral reflectance of *Porites lutea* from three Indo-Pacific coral reefs. These spectra vary between brown mode and blue mode, even within a single locale (both Mo‘ore‘a and Palau). The intensity of absorption near 580 nm suggests variable expression of the pigment underlying blue mode reflectance.

7.2.1.3 Soft Corals or Octocoral

Some octocorals possess the same zooxanthellae that occur in scleractinian corals, and thus their spectral reflectance resembles that of brown coral (Figure 7.13). From the remote sensing perspective, this similarity confounds discrimination between the two BFTs (Hochberg et al. 2003b). This is a problematic issue for areas where octocorals and scleractinian corals co-dominate the seascape.

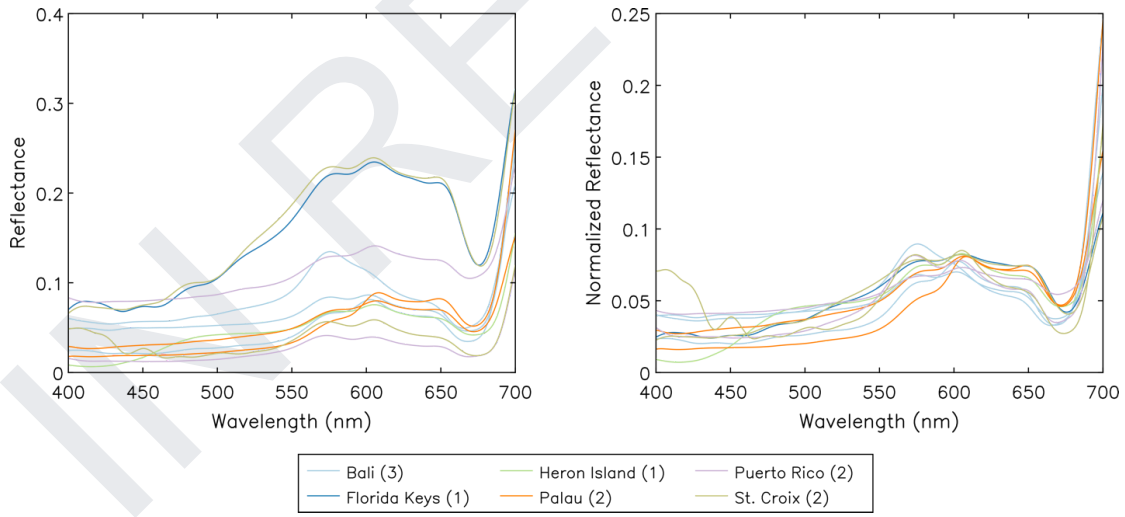

Figure 7.13 Spectral reflectance of octocorals from Atlantic and Indo-Pacific reefs. Values in parentheses indicate the number of spectra for the given locale.

7.2.1.4 Coral Morphologies (Branching, Massive, Plate, etc)

Hard corals exhibit a range of morphologies, both within and between coral species. Common morphologies are: branching, massive, plate, corymbose, encrusting, foliose (Ortiz et al. 2014; Done 1982). Coral morphology types each have certain functional roles on coral reefs regardless of their colour (Ortiz et al. 2014). A majority of the spectral reflectance measurements published and discussed previously, are based on measurements from a relatively small area on the surface of each coral.

These often do not include a range of measurements representative of different coral morphologic forms, shading effects of the coral itself, the neighbouring coral shapes, or other bottom structures and types (Joyce et al. 2002; Miller et al. 2016). Coral reflectance signatures also vary significantly in response to different viewing and illumination geometries (Hedley 2008; Joyce et al. 2002). This becomes further complicated when multiple benthic features combine, e.g., a mixture of corals (Leiper et al. 2011; Miller et al. 2016). Coral morphologies on their own have not yet been differentiated based on benthic reflectance signatures, hence current mapping of coral reef compositions depends on a combination of different environmental variables (Roelfsema et al. 2018; Hamylton 2017).

7.2.2 Deep sea coral

Deep and cold water Scleractinian corals found at 100 to 500 m depths are dominated by the reef building *Desmophyllum pertusum* (*Lophelia pertusa*). This species thrives in well oxygenated waters; regions with strong currents with zooplankton (food); stable salinities of >34 ppt; and water temperatures at 7-7.5^{o}C (Sakshaug and Sneli 2000; Mortensen et al. 2001; Elde et al. 2012; Liefmann et al. 2018). Deep water coral habitats have been well studied in fjord systems, but deep corals in other parts of the global ocean have been under sampled, and little laboratory work has been conducted *in vivo* and *in vitro* on coral habitat species ecology and physiology.

Examples of deep water corals, dominated by the *Desmophyllum pertusum* were taken from a total survey area of 6 km^2 (Mogstad et al. 2022) The area contained more than 70 deep water stone corals (Scleractinian) reefs from the Tautra reef system in Trondheims Fjord, Norway, from 40-100 m depth (Løvås et al. 2022; Mogstad et al. 2022). The total survey area was carried out by means of a vessel equipped with a multi beam echo-sounder (Vessel-MBE), an AUV equipped with Synthetic Aperture Sonar (AUV-SAS) providing 4 cm spatial resolution, followed by a ROV based Underwater Hyperspectral Imaging (UHI) providing 1 cm spatial resolution (ROV-UHI), (Figure 7.14, Mogstad et al. 2022).

Orange and white colour morphs occur in *D. pertusum* related to the carotenoid composition. For the orange colour morphs, the carotenoids astaxanthin (major) and canthaxanthin (minor), both bonded to specific proteins, are responsible for the overall colouration and spectral absorbance/reflectance characteristics (Elde et al.

2012; .

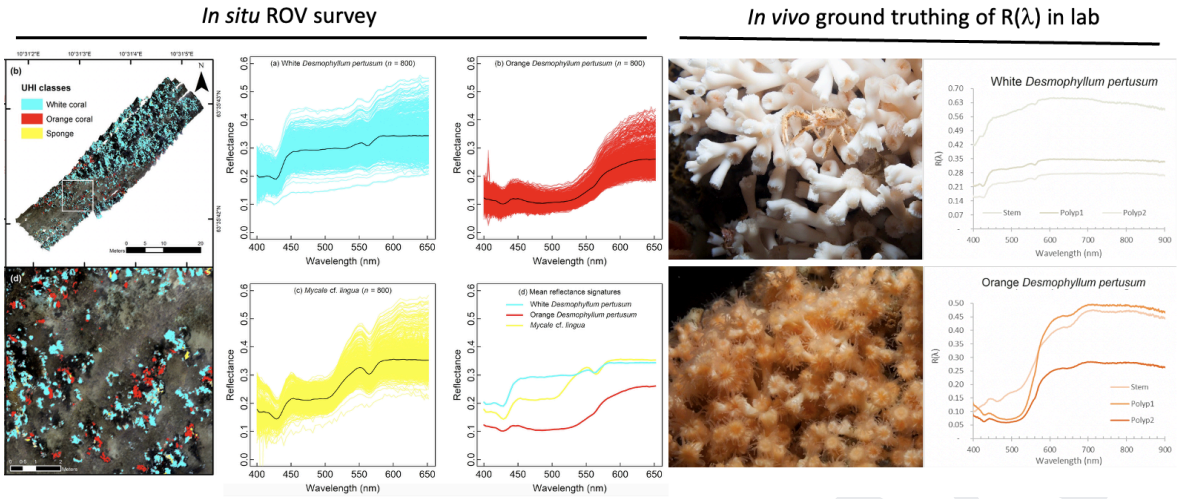

Figure 7.14. Examples of Remotely operated vehicle (ROV) carrying an underwater hyperspectral imager (UHI) to map 787 m^2 of deep and cold water reef building coral species, dominated by white (marked blue) and orange (marked red) color morphs of *Desmophyllum pertusum* providing. These reefs are typically found at 100-500 meters depth along Norwegian coast.This species is also a habitat for the sponge *Mycale* cf. *lingua* (marked yellow). *In situ* ROV survey from Mogstad et al. 2022. Ground truthing of spectral reflectance of living deep water specimens in laboratory for supervised classification purposes of ROV-UHI surveys. Note differences in R(λ) intensity and shape at different parts of the corals, by using spectrometer and fiber optics. Data from Andersson 2017, by permission.

Geodia barretti is one of the most common and largest species of sponges along the Norwegian Sea and southern Barents Sea. The blue sponge *Hymedesmia paupertas* is often found on vertical walls and reflectance is species-specific due to the presence of lactarazulene absorbing heavily in the UV and red region of the visible spectrum giving the species a bright blue colour (for characterization of pigments, see Pettersen et al. 2013). The magnitude of reflectance varies for different parts of the organisms, as observed by using spectrometers and fiber optics (Figure 7.15; Andersson 2017).

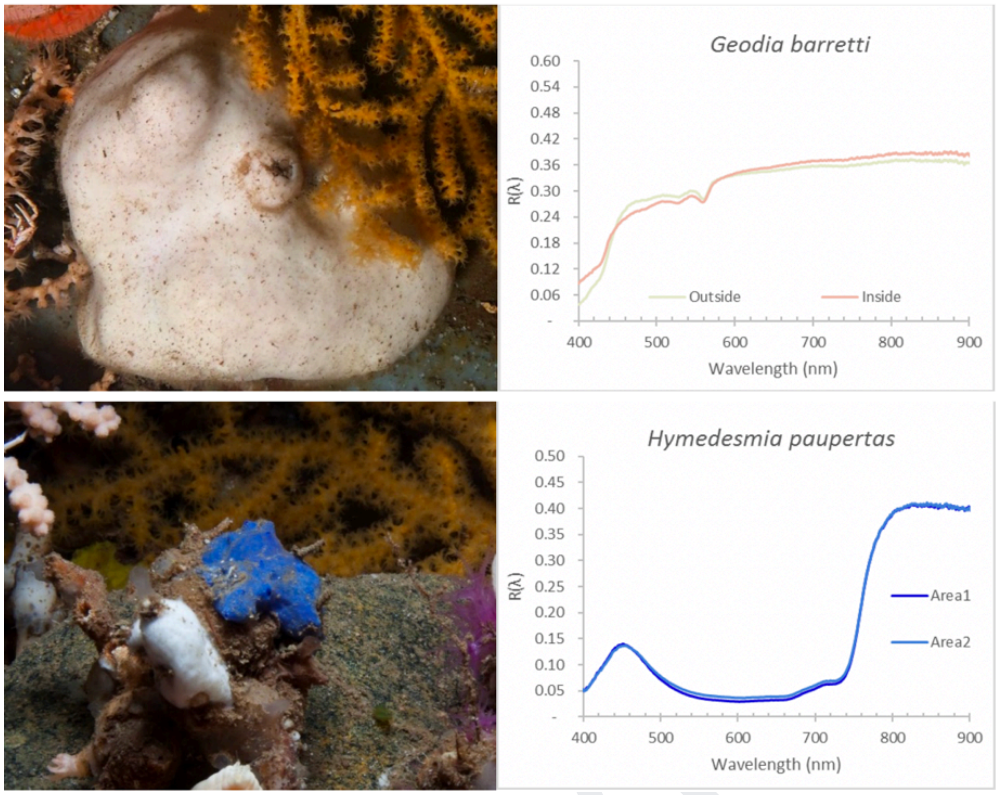

Figure 7.15 Pictures and reflectance spectra from two species of sponges, *Geodia barretti* (top) and *Hymedesmia paupertas* (bottom) found along the Norwegian Sea and southern Barents Sea. Modified from Andersson 2017 with permission.

7.3 Deep Sea Minerals and Rubble

The seafloor geochemistry comprises different bottom habitats, substrates and minerals. Two important perspectives of concern include: 1) ocean acidification and 2) sea floor exploration and utilization of “seafloor Massive Sulfides” (SMS). Figure 7.16 provides an example of how a remotely operated vehicle (ROV) equipped with an Underwater Hyperspectral Imager (UHI) can provide details from 4200 m depth regarding biogeochemical information (Figure 7.16; Dumke et al. 2018b).

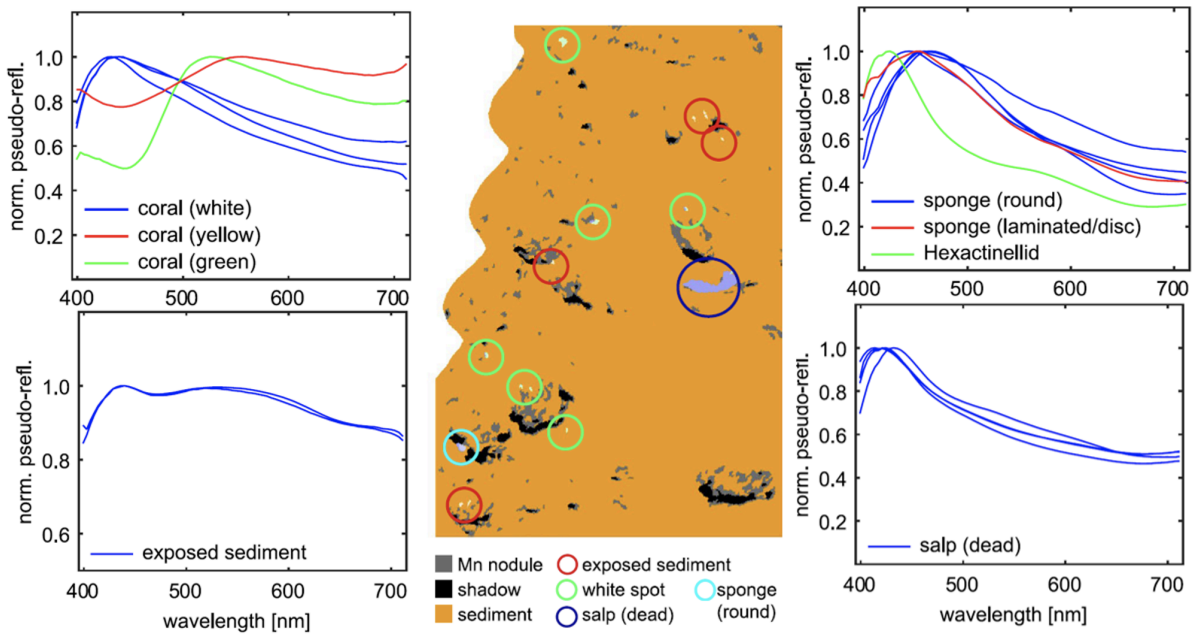

Figure 7.16 Classification of biology and mineral composition at 4200 m depth using a ROV equipped with an underwater hyperspectral imager (UHI), and corresponding relative spectral benthic reflectance of different organisms. Adapted from Dumke et al. 2018b.

7.4 Seagrass

The term used for rooted aquatic plants that grow completely under water is submerged aquatic vegetation (SAV). Occurring in both marine and freshwater ecosystems, these plants can form canopies that provide physical structure serving as habitat for many commercially important species. Significant advances have been made in remote sensing of these ecosystems due to their importance in carbon dynamics. SAVs have also been threatened due to declining water quality, coastal development activities, and disease. Below, we describe benthic reflectance for seagrass and freshwater vascular plants.

Seagrasses are rooted flowering marine plants that support complex food webs by virtue of both their physical structure and primary production. Often called “ecosystem engineers”, they provide shelter and food to an incredibly diverse community, from tiny invertebrates, to large fish, crabs, turtles, marine mammals and birds. The plants improve water quality by filtering suspended sediments and nutrients from coastal waters and they prevent coastal erosion by stabilizing sediments and acting to dampen wave action. Seagrasses also serve as the basis of an important detrital food chain gathering organic matter in the sediments and contributing to long-lived stored “blue carbon”. The high capacity of seagrass meadows to store carbon results from their high primary productivity and capacity to trap water-column particles in the soil, as well as the low decomposition rates in the oxygen-poor soils. Seagrass ecosystems occur widely across the world ocean from the colder subpolar fjords of northern Norway, to the salty warm Mediterranean Sea, to the carbonate sediment banks of the Indo-Pacific. There are approximately 72 different seagrass species that belong to four major groups (examples in Figure 7.17).

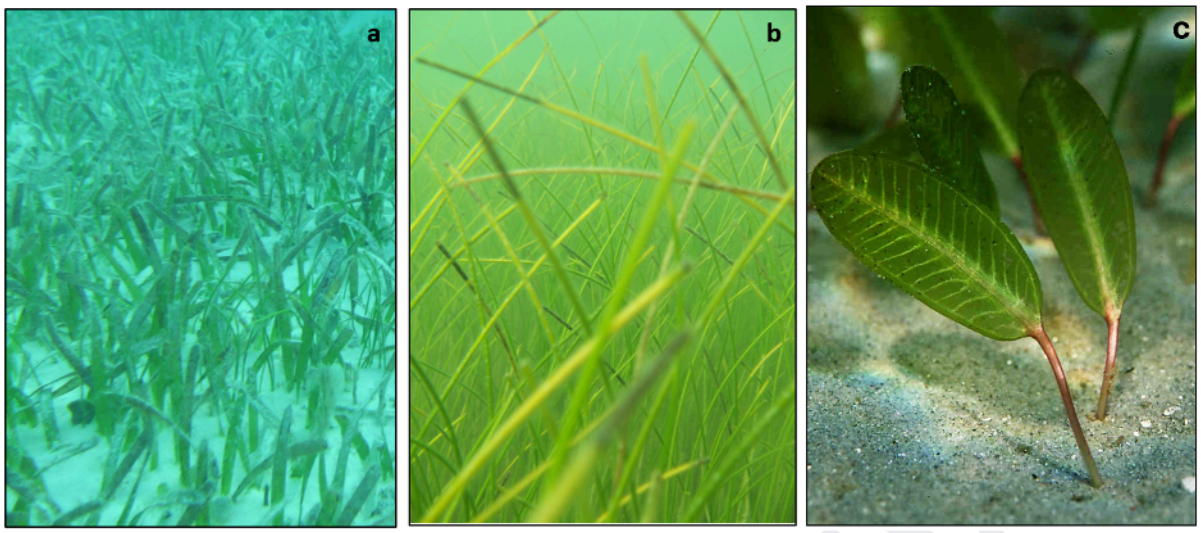

Figure 7.17 a) strap-like *Thalassia testudinum* (turtlegrass) found on the carbonate sediment bank oceanside in the Florida Keys, USA; b) cylindrical *Syringodium filiforme* (manateegrass) meadow bayside in the Florida Keys, USA; c) leaf-like *Halophila ovalis* from Australian waters. Photo credit: a-b) H. Dierssen, c) C. Roelfsema).

Benthic reflectance of seagrass has been conducted at both the leaf and canopy level for the most common seagrass species. Representing a seagrass meadow with a single leaf spectrum can be problematic, especially for some of the longer denser canopies where there are shadows and detrital matter that contribute to the reflectance (Figure 7.18). Representing seagrass meadows as a flat laminar green leaf leads to errors in optical closure studies and can result in an overestimate of water column particulate backscattering in remote sensing studies (Fogarty et al 2019, Hedley et al. 2016b, Dierssen et al. 2019).

Despite differently shaped leaves, the visible benthic reflectance is found to be quite similar, for instance, between *Zostera marina* (eel grass), *Thalassia testudinum* (turtle grass) and *Syringodium filiforme* (manatee grass) (Figure 7.18; Stoughton 2009). Measurements are particularly challenging to make for thin cylindrical leaves like *S. filiforme* where the leaves must be aggregated tightly together during measurement. Even at the canopy level, *T. testudinium* and *S. filiforme* are too spectrally similar to be discriminated purely on spectral grounds (Hedley et al. 2017). Seagrass leaf spectra also have a considerable red edge of reflectance common to vegetation, peaking in the near infrared (700-1400 nm) and short wave infrared (1400 – 2800 nm; Fogarty et al. 2019; Figure 7.18).

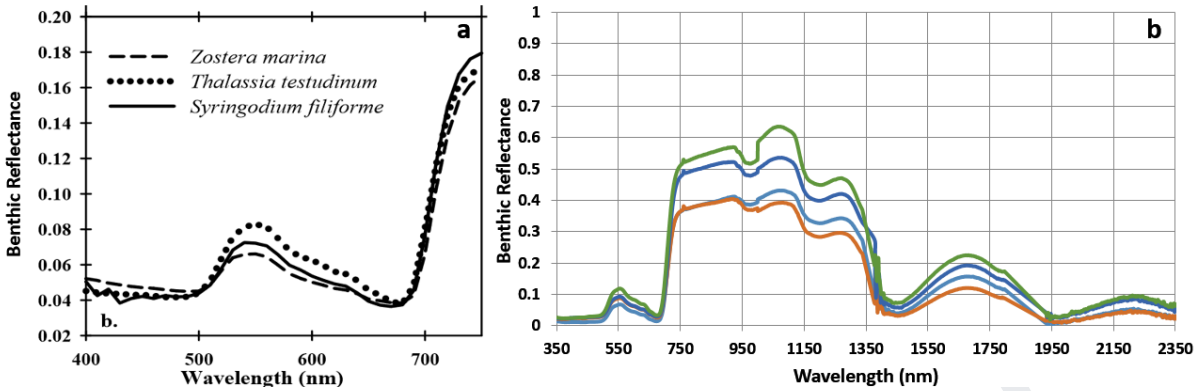

Figure 7.18 a) average leaf reflectance from three common species of seagrass (Stoughton 2009); b) leaf reflectance replicates from *Zostera marina* in Long Island Sound, CT from visible to short wave infrared (modified from Fogarty et al. 2018)

At the canopy-level, many considerations must be taken into account to measure or model reflectance, including the time-dependent canopy changes due to water currents, and the amount of sediment visible through the canopy. Leaves bend in the direction of currents and flap back and forth with waves. Other factors contributing to canopy-level reflectance include the morphology of seagrass leaves, shoot density, height of the canopy, bending of the canopy under flow, water column optical properties, underlying sediment spectral properties, epiphytes and detrital matter obscuring the leaves, shading within the canopy, and to some extent the solar zenith angle (Hedley and Enríquez, 2010; Zimmerman 2003a,b). While leaf reflectance is commonly done with measurements in air, canopy-level measurements require measurements made at the top of the canopy usually with diver-operated spectrometers. Ancillary measurements including canopy height, sediment reflectance inside and outside the seagrass bed and water column optical properties are valuable for interpretation of the measurements.

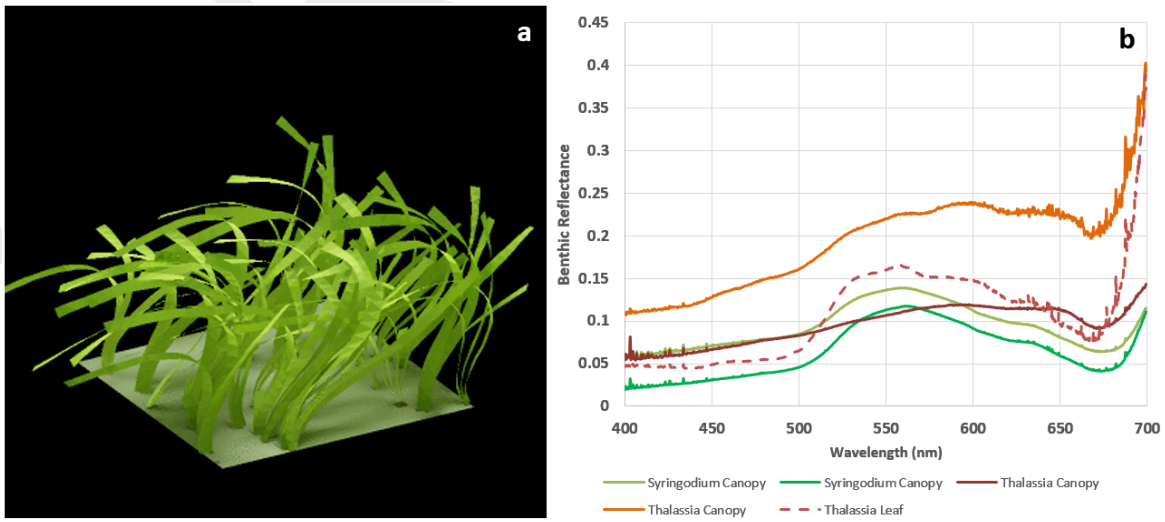

Figure 7.19 a) Three-dimensional radiative transfer model used to model the relationship between flow and canopy architecture (Hedley et al. 2016b). b) Measurements of canopy-level reflectance in Florida Bay of moderately dense *Thalassia testudinum* and dense *Syringodium filiforme* (Gilerson et al. 2013).

The canopy-level measurements in Figure 7.19 demonstrate that a dense canopy of long dense *S. filiforme* can appear similar to leaf reflectances, but that the canopy-level *T. testudinum* was higher in magnitude with a flatter spectral shape due to contributions from the underlying sediment reflectance. Most field measurements are localized at a finer scale than required for many applications. One method to estimate canopy-level benthic reflectance at a larger pixel-level was described by Gilerson et al. (2010). In that study, RGB photographs were taken of the area directly beneath a surface deployed sensor. The images were processed using empirical band ratios to differentiate individual target types (e.g., sand, *Thalassia* leaves). Percent cover of each constituent was calculated as the the pixel count per RGB image for the site and the areal-averaged benthic reflectance was computed as the mean of all target spectra weighted by the fractional percentage cover.

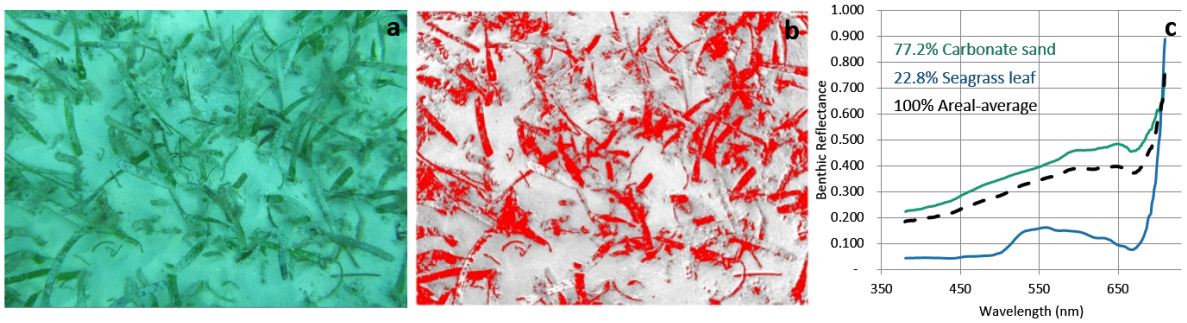

Figure 7.20 a) Estimating pixel-level benthic reflectance of a seagrass meadow from a) an RGB image of a seagrass habitat; b) image classification of targets of interest; c) estimate of benthic reflectance combining a percentage of sediment and seagrass leaf reflectances. (Method from Dierssen COLORS lab published in Gilerson et al. 2010).

As outlined in previous Chapters, radiative transfer of seagrass canopies is well established to assess how light penetrates the canopy and to model canopy-level benthic reflectance (Figure 7.19). Zimmerman (2003b) parameterized a two-flow model of the plane irradiance distribution through a seagrass canopy submerged in an optically active water column with several allometric functions describing canopy architecture. He noted that better knowledge of leaf orientation could reduce uncertainties in the model. Hedley and Enríquez (2010) constructed three-dimensional models of canopies with leaf orientation related to current flow (Figure 7.19) and noted that canopy BRDF's were not Lambertian, but exhibited features related to canopy architecture. The strongest nonisotropic reflectance was associated with denser, longer-leaved, canopies which could impact near-surface radiance measurements greater than 10%. Subsequent modeling of canopy reflectance revealed that the spectral reflectance of a seagrass meadow becomes nearly saturated at dense concentrations of eelgrass corresponding to a leaf area index around 3 (Hedley et al. 2016b, 2017).

7.5 Algae

7.5.1 Macroalgae

Macroalgae is a multicellular class of algae that possess plant-like structural features that allow them to grow to fairly large sizes. This section provides an overview of the benthic reflectance across broad types of benthic macroalgae, grouped by colour: brown, green and red. Kelp is separated from other brown algae because of its unique size and morphology. Generally, reflectance spectra of broad macroalgae groups (brown, green, red) are consistent in their spectral shape around the world independent of the type of the water (e.g., lakes, brackish waters, or oceanic waters) or major climatic zone (Kutser et al. 2020). Evidence suggests that the spectral shape of reflectance is also stable during the phenological cycle for some macroalgae. Spectral shapes can vary with age and level of decay of the blades. Even during the polar night in Svalbard, however, macroalgae grow and are healthy after several months of constant darkness.

All macroalgae have high reflectance in the NIR part of the spectrum (>700 nm), exactly like terrestrial plants. Many of the figures below present reflectance only across visible wavelengths, truncating the NIR values, because water is highly absorbing beyond 700 nm and this part of the signal is challenging to measure *in situ* or use for remote sensing applications.

7.5.1.1 Brown algae (Phaeophyta)

The term kelp herein refers to the canopy-forming brown algae of the Order Laminariales. Well established kelp populations form submerged forests that can grow up to 50-60 m in height, often in dense stands, and provides three-dimensional structure to coastal habitats (Figure 7.21; Abbott and Hollenberg, 1976). Kelp often have pneumatocysts, specialized air-filled structures that help float the blades, the morphologies of which differ across species. They are known to occur in the temperate to sub-polar waters of all continents except Antarctica, and are found in intertidal areas to depths of up to 70 m (Graham et al. 2007). Giant kelp reproduction is limited to waters between 11-19°C, and growth is reduced in higher water temperatures (>16°C) by induced low nutrient availability (Graham et al. 2007). Kelp forest have been declining globally under the combined effects of climate change and anthropogenic drivers such as ocean warming and heatwaves (Trégarot et al., 2024) Drastic reductions in canopy extent have also been observed in kelp populations after marine heat wave events (e.g., Cavanaugh et al. 2019; Tait et al. 2021; Schroeder et al. 2020). Growth rate and survival are both affected by current and wave action, though in opposing directions, resulting in a hump-shaped relationship between kelp extent and wave-action (Mora-Soto et al. 2021). Herbivory, particularly by benthic invertebrates, is a direct control on kelp populations, and acute herbivory stress has the potential to cause rapid and persistent ecological shifts from kelp forests to barrens.

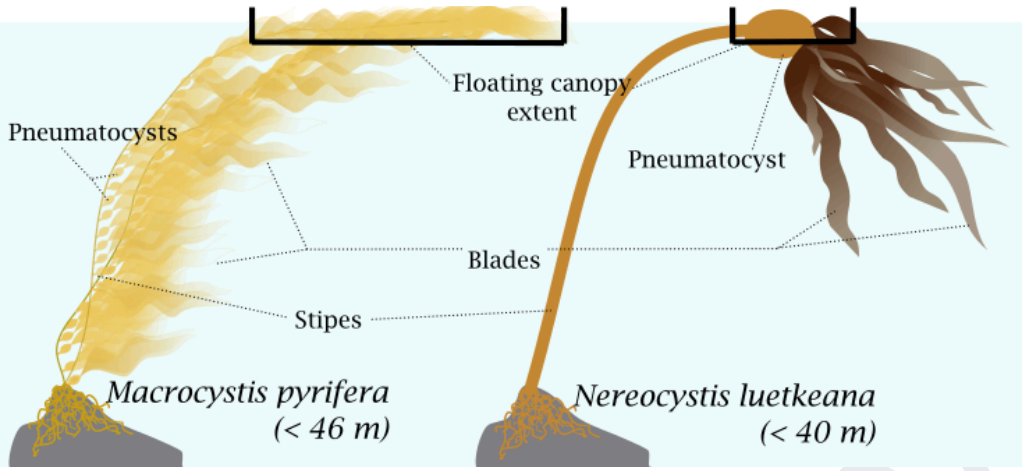

Figure 7.21 Illustration of the vertical structure of *Macrosystis pyrifera* (common name Giant kelp) and *Nereocystis leutkeana* (common name Bull kelp). Note that the extent of the floating canopy at the water's surface depends on species' morphologies and can differ according to physical conditions (e.g., tidal height, current, etc.).

The primary controls on spectral absorption, transmission and scattering of electromagnetic energy by kelp can be considered at two scales:

- **At the scale of individual blades:** Spectral reflectance is governed by photosynthetic pigments in visible wavelengths and by water content, blade form/structure and cellular structure in longer wavelengths. The type and concentrations of pigments present determine the shape of kelp's reflectance curve in visible wavelengths (400-700 nm), while blade form/structure and cellular structure determine the shape and magnitude of reflectance in infrared wavelengths (700 – 1500 nm). As with other brown algae, the three principal pigments in kelp are chlorophyll-a, chlorophyll-c, and fucoxanthin, each bound in pigment-protein complexes (Barrett and Anderson, 1980). The combined absorption by these pigments produce major reflectance peaks at 600 and 650 nm, and a less pronounced peak at 580 nm (Schroeder et al. 2019; Olmedo-Masat et al. 2020). As with vascular plants and other algae, kelp's transmission and scattering are primarily dependent on cellular structure, which differs across morphological features. Multiple refractions and reflections occur as light travels between cell walls, (extra-)cellular matrices, and gas cavities, and increase in number with tissue complexity (Knipling 1970). More complex structures like pneumatocysts are, therefore, more reflective than simpler structures like blades (Olmedo-Masat et al. 2020; Timmer et al. 2022). Transmission is inversely dependent on cellular structure, occurring most in simple structures with few cell layers, like blades. Additionally, solar-induced chlorophyll fluorescence (SICF) peak centred at 761 nm has been identified for floating Bull kelp (Timmer et al. 2022). Note that blade-level spectral responses vary according to the light environment and can differ significantly between canopy and basal samples (Colombo-Pallotta et al. 2006).
- **At the scale of kelp forest canopies:** the above-water reflectance depends on the fraction of the measurement footprint covered by floating kelp material, the optical characteristics of the surrounding and/or overlaying water column, and contributions from the physical environment (Schroeder et al. 2019). If a pixel's

footprint is partially covered by kelp, the surrounding water column will, and benthic material may, contribute to the measured signal. Shallowly submerged kelp may be discernible in imagery depending on the submersion depth, water clarity, and available spectral bands. Even in the case of dense floating kelp canopy carpeting an image pixel, the spectral response may contain contributions from a thin layer of water coating the leaves and producing glint (Bell et al. 2015).

Detailed descriptions of the spectral regions where each of these properties controls spectral absorption, transmission, and scattering, along with the biological, chemical, and physical mechanisms responsible for these are described by Barrett and Anderson (1980) and Knipling (1970). Examples of kelp blades' spectral reflectance signatures are included in Figure 7.22.

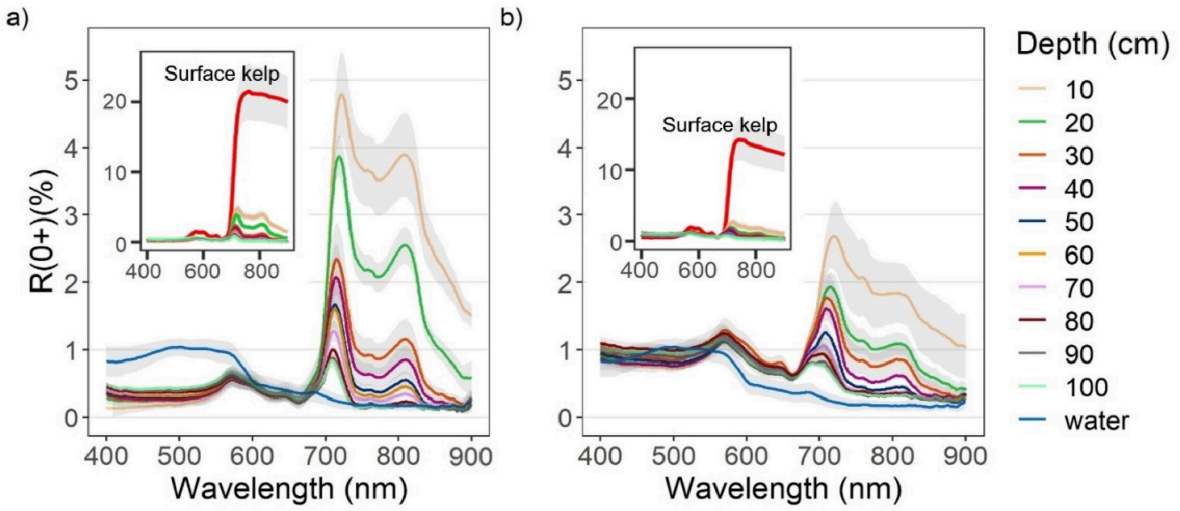

Figure 7.22 Controlled field measurements: Reflectance values (R0+) between 400–900 nm (mean +/- sd) of water with (**a**) Nereocystis bulbs, and (**b**) Nereocystis blades, at incremental depths below water surface. The inset plots contain spectra of bulbs and blades on the surface compared to the same spectra of submerged bulb and blades as in the main plots, for the purpose of showing the difference in magnitude. (Timmer et al. 2022)

Olmedo-Masat et al. (2020), Schroeder et al. (2019) and Timmer et al. (2022) have examined the reflectance properties of kelp. Examples of spectral reflectance signatures collected at the height of 1 m above the water's surface of a *Nereocystis leutkeana* forest canopy off the coast of British Columbia, Canada, are included in Figure 7.23 (Schroeder et al. 2019). The spectrum of dense forest (>50% of the measurement footprint) displays three local reflectance maxima in the visible region (580, 600, and 650 nm) caused by kelp photosynthetic pigments. The very high NIR reflectance mirrors that typical of terrestrial vegetation. The signal magnitude is drastically reduced for sparse forests (<50% of the measurement footprint) as water contributed more to the recorded signal and had very low reflectance across the spectrum. The water column overlaying submerged kelp can further reduce the strength of the apparent kelp reflectance.

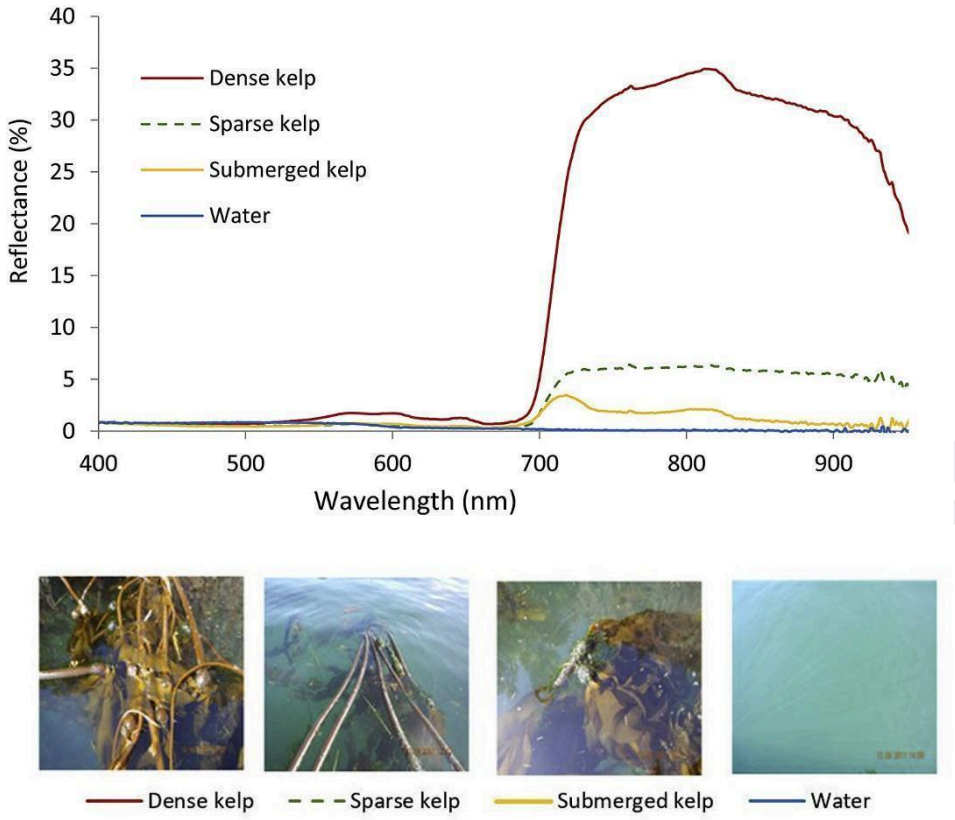

Figure 7.23 *In situ* spectral reflectance measurements of *Nereocystis luetkeana* kelp forest canopy off the coast of British Columbia, Canada, using a Fieldspec Pro sensor held ~1 m above the surface and averaged within each class (n=10). Submerged kelp was at an estimated depth of 20 cm or less. Dense and sparse refer to kelp coverage greater than or less than 50% of the measurement footprint, respectively. Figure from Schroeder et al. 2019, available under CC BY-NC-ND https://creativecommons.org/licenses/by-nc-nd/4.0/.

Characteristic features in reflectance spectra of other brown macroalgae are peaks at 600-610 nm and at 650 nm, as well as a shoulder around 570 nm. Note that these spectral features are also characteristic to kelp and common yellowish-brownish corals (Holden and LeDrew 1999; Kutser et al. 2000, 2006; Hochberg and Atkinson 2003; Hochberg et al. 2003b, 2004; Kutser and Jupp 2006; Vahtmäe et al. 2006), which contain zooxanthellae that are ultimately brown algae.

Vahtmäe et al. (2017) made mesocosm experiments with different species of macroalgae measuring their reflectance in May, August and October. Figure 7.24 shows that the characteristic features of brown macroalgae stay consistent through the growing season. It was possible to estimate chlorophyll-a+b content through the growing season in the brown macroalgae using different band ratio algorithms (r^2=0.88, $p<0.001$). Thus, the reflectance spectra contain information about the phenology of the macroalgae. However, the typical features in reflectance are consistent all year round.

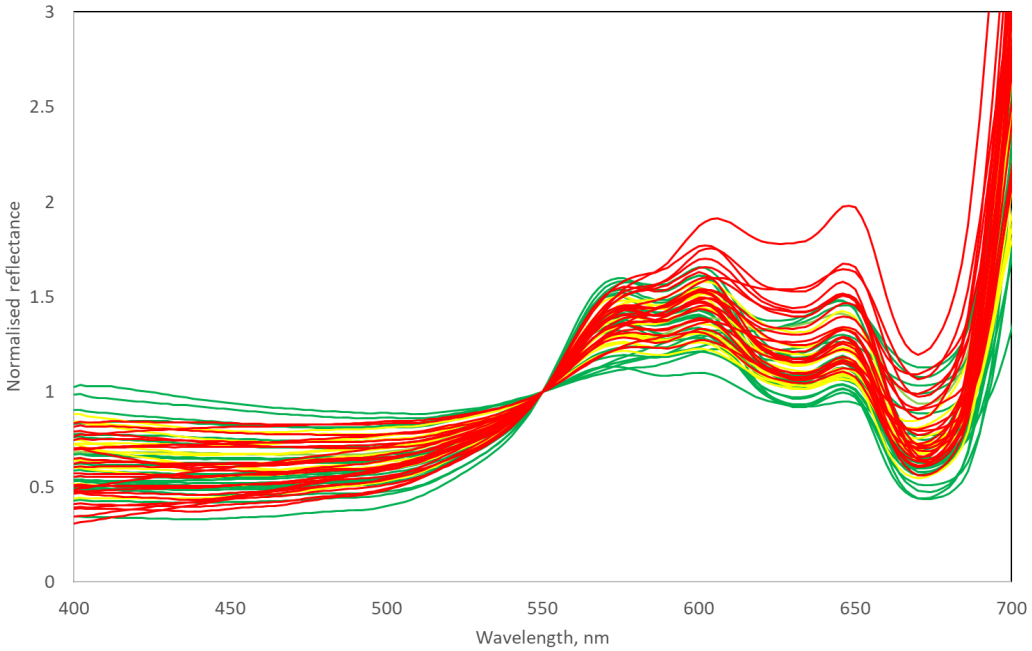

Figure 7.24 Reflectance spectra of brown macroalgae *Fucus vesiculosus* normalised to 550 nm, and measured in mesocosms in May (green), August (yellow) and October (red). Vahtmäe et al. (2017).

7.5.1.2 Green algae (Chlorophyta)

Green macroalgae, seagrasses and other vascular plants appear to have very similar reflectance spectra. Their reflectance is relatively low in the blue part of the spectrum, with a broad maximum from green (550 nm) to red (650 nm; Figure 7.25).

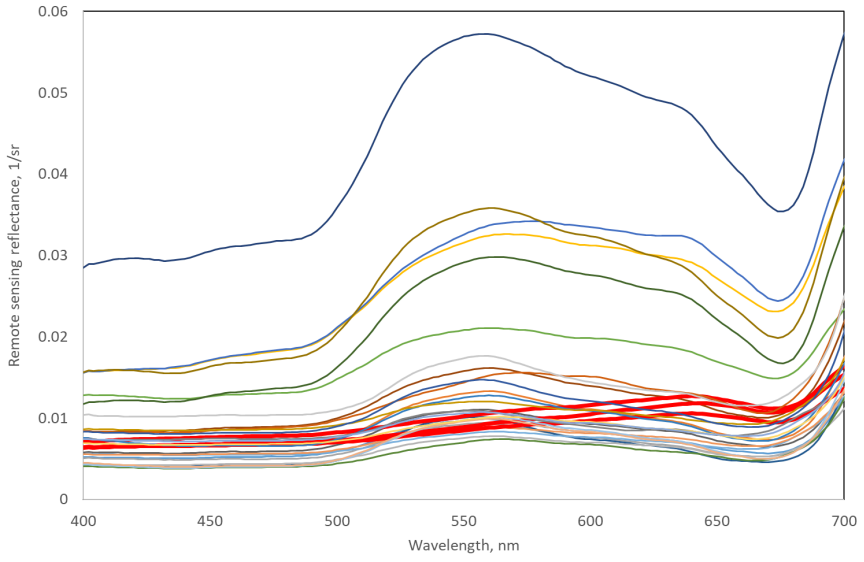

Figure 7.25 Remote sensing reflectance spectra of green macroalgae *Cladophora glomerata* in the beginning of growing season (May) and towards the end of their growing cycle (August). Bold red spectra are of specimen that had already started to decay.

7.5.1.3 Red algae (Rhodophyta)

Red leafy macroalgae have characteristic double peaks in their reflectance spectra at 600 nm and 650 nm. Nearly identical are reflectance spectra of dead coral and coral rubble, indicating that long-dead coral may be covered with red algae. Similar reflectance spectra were measured in the case of cyanobacteria (*Lyngbya)* covering corals and seagrasses (Figure 7.26). Red algae appear to have very consistent reflectance spectra. For example, commercially harvested unattached forms of *Furcellaria lumbricalis* appeared almost black under normal conditions, but may be greenish-grey under conditions of stress (e.g., too much light in shallower water). The shape of the reflectance spectra remained the same, and only the intensity (reflectance values) differed.

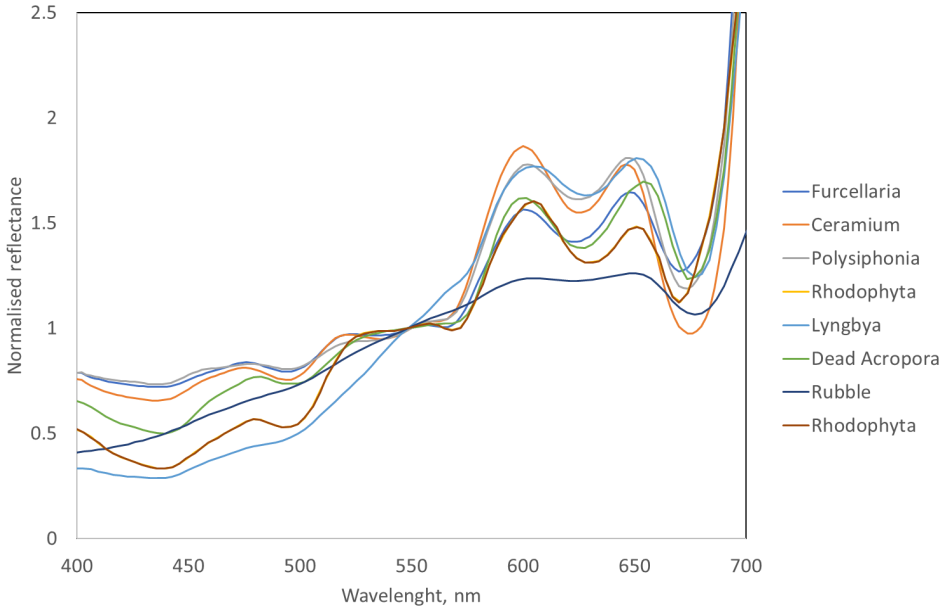

Figure 7.26 Reflectance spectra of red leafy algae and benthic cyanobacteria collected in the Baltic Sea (Furcellaria, Ceramium, Polysiphonia, Rhodophyta) and in the Great Barrier Reef (cyanobacteria (*Lyngbya*), Rhodophyta) as well as dead Acropora coral and rubble covered with red algae turf sampled in the GBR. Reflectances normalised to 550 nm.

Red coralline algae (calcifying Rhodophytes in the order Corallinales) contain the main accessory pigment, lutein. These algae are often pink or red, but they can also exhibit shades of purple, blue, gray-green, or brown. Coralline algae have spectral reflectances that vary widely depending on pigment density relative to their internal calcite deposits, but spectral shapes are very consistently identifiable as red algae (Figure 7.28).

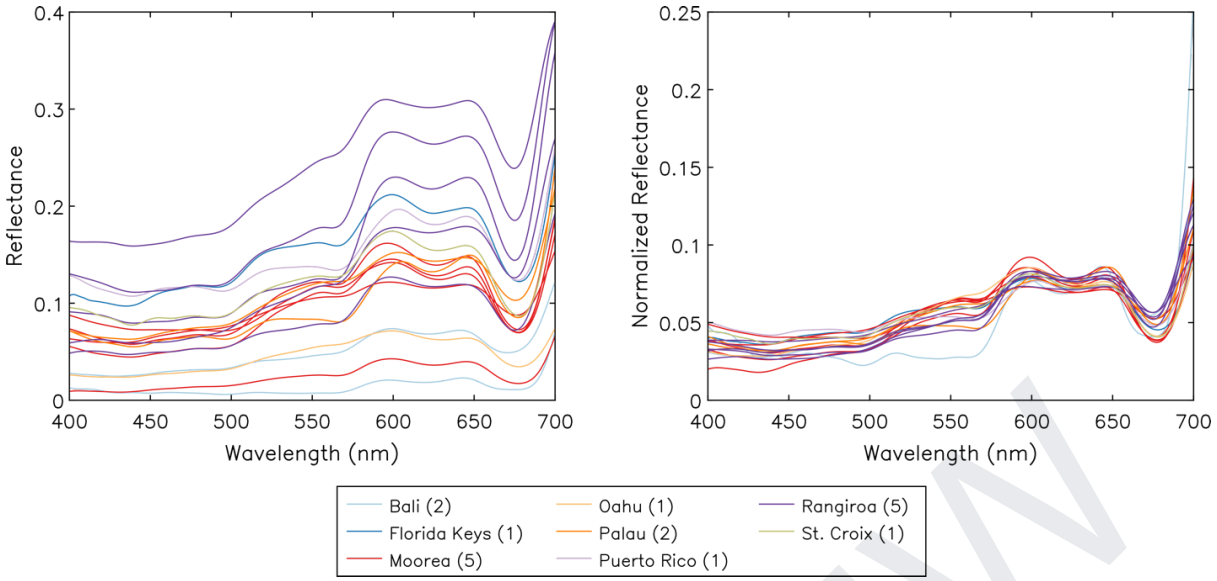

Figure 7.28 Spectral reflectance of coralline algae from Atlantic and Indo-Pacific reefs. Values in parentheses indicate the number of spectra for the given locale.

7.5.2 Algal Turfs

Algal turfs are described as a mixture of brown, green and/or red algae that is not much higher than a couple of centimeters high. Turfs can be dense or sparse, overgrowing hard substrate. They exhibit widely variable reflectance, both in magnitude and shape, owing to their near-infinite composite mixtures. Many species present in turfs are small filamentous algae and cropped bases of macroalgae (Fong and Paul 2011; Littler and Littler 2011). The example spectra shown in Figure 7.27 appear dominated by rhodophytes, with contributions by phaeophytes. The spectra represent convolutions of algal thalli and their underlying substrates.

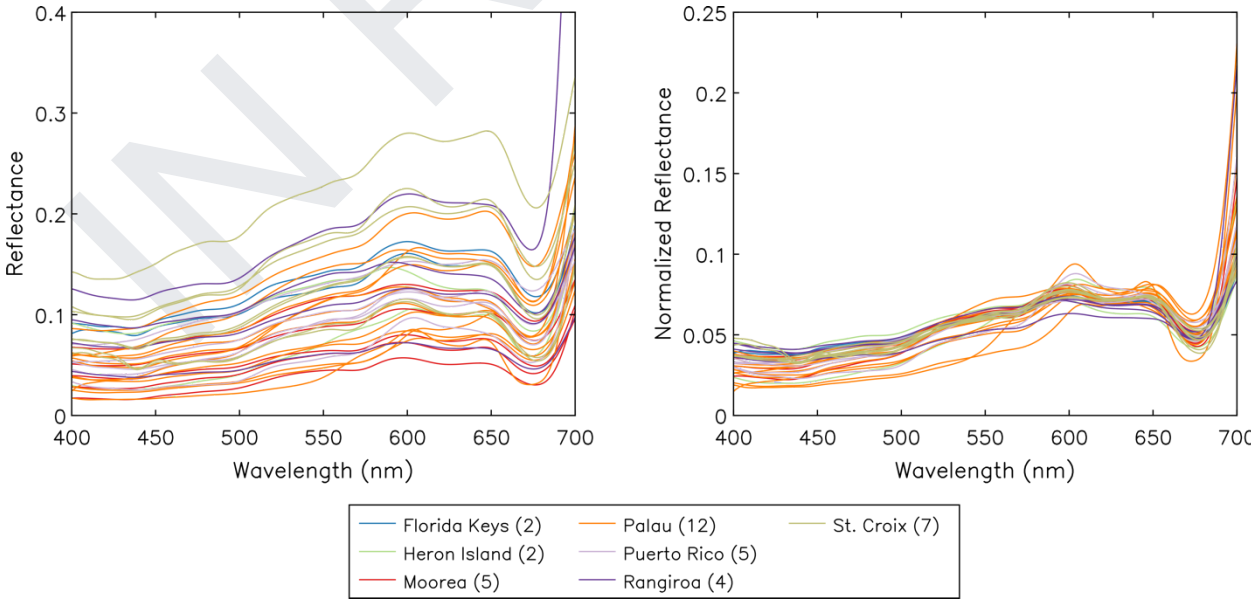

Figure 7.27 Spectral reflectance of algal turfs from Atlantic and Indo-Pacific reefs. Values in parentheses indicate the number of spectra for the given locale. Source Hochberg et al.

7.6 Detritus and debris

In this context detritus and debris are the remains of plants and algae that occur anywhere in the benthic matrix, or washed up on shore. Debris is a generic term for destroyed material, and in the context of this report, is used in combination with the material from which it originates (e.g., seagrass debris or macroalgal debris). In aquatic environments, debris and detritus can also come from other organic sources such as waterlogged wood (from natural sources in the catchment or from wood used by humans etc.). The colour in general is dark brown to black although in certain cases it may be purple to pink (in the case of decaying Rhodophyta) or light green to yellow (in the case of e.g., Ulva) etc. There is a fine line between senescing plants and dead plants, and here we limit ourselves to dead plants and their derived material.

The primary controls on spectral absorption, transmission and scattering of electromagnetic energy by detritus and debris is their usual dark colour that will lower benthic reflectance significantly, depending on the relative ratio of dead to living material, and the substrate colour itself. There are exceptions of decay that is lighter than the living organism (e.g., coral bleaching) that will lead to higher benthic reflectance.

A significant number of publications on the spectral reflectance of benthos and substratum ignore the presence of detritus and debris, which may lead to erroneous inversion or classification results or affect the shallow water bathymetry estimates (as e.g., a darker reflectance may trick the algorithm into estimating a deeper water column, etc.). In areas where the bottom is uneven, detritus and debris often accumulates in the depressions. This may lead to either an overestimation of water column depth estimates, or an incorrect classification of e.g., a seagrass or macroalgae species, or placing these species at a greater depth than they occur. As the spectra signature is in general very dark, this spectral effect also interferes with, or may be mistaken for, shading of seagrass, macroalgal or other benthic cover material.

Raising awareness of these spectral reflectance effects is perhaps the most important aspect of the section. In any aquatic benthic environment, it is likely that the spectral signatures of the detritus and debris will be different based on their composition, and level of degradation of the (mainly plant) material. As an illustration take e.g., giant kelp washing up on shore degrading into an almost black (or sun bleached) colour and then being washed back into the water, subsequently ending up as large dead fronds in depressions in the substratum versus very fine detritus that is so fine that it resuspends easily.

7.7 Melt ponds

The observed reflectance of melt ponds can vary over a wide range (e.g., Perovich 1996; Nicolaus et al. 2010; Polashenski et al. 2012; Gege et al. 2019). In general,

melt pond bottoms are unvegetated. Their reflectance properties are mainly influenced by the underlying ice and the presence of water. The absolute reflectance is primarily influenced by the thickness of the ice layer beneath the pond, as the dark hue of the ocean is more or less visible. Ponds in thicker, multi-year sea ice appear light blue or turquoise in colour, while on thinner, seasonal ice they tend to be darker. Besides the thickness of the ice, the amount of air bubbles and brine mainly influence the inherent optical properties of the sea ice and therefore the absolute reflectance of melt ponds (Malinka et al. 2018).

The shape of pond reflectance spectra, however, seem to be similar for all melt ponds and independent from their geographic location. All melt ponds show a higher reflectance in the VIS and almost no reflectance in the NIR; the former is due to the properties of the sea ice, the latter is due to the strong absorption by water in the NIR (Figures 7.29 and 7.30).

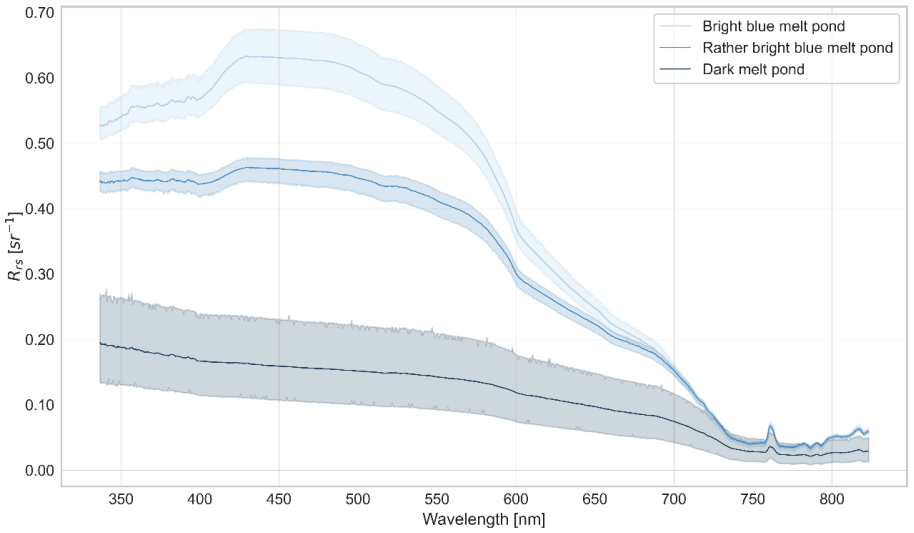

Figure 7.29 Melt pond bottom reflectance in Arctic sea ice (Northern Fram strait) as measured during Polarstern cruise PS106 (Gege et al. 2019).

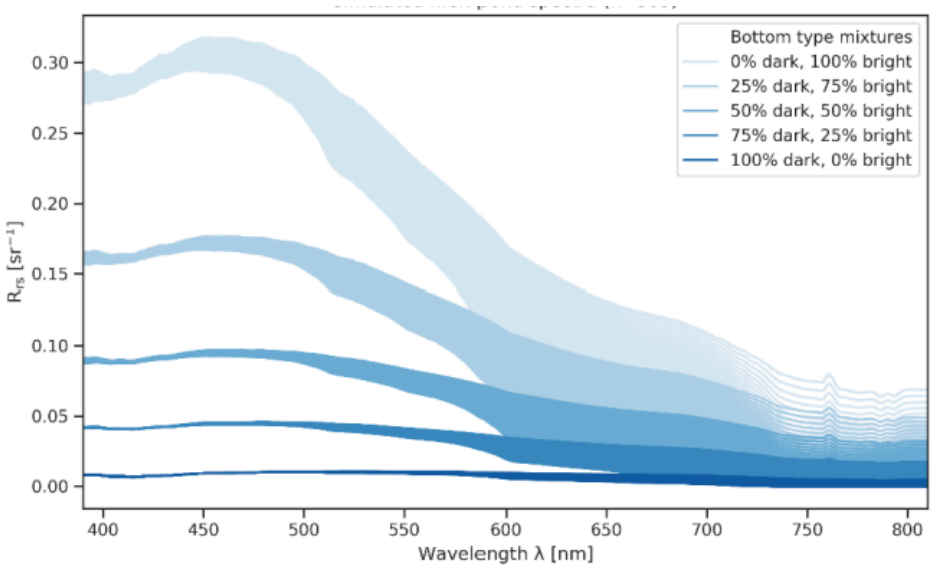

Figure 7.30 Range of melt pond bottom reflectance spectra as simulated with WASI-2D; each pond type was simulated with for different pond depths ranging from 0 to 100cm in intervals of 1cm (modified from König and Oppelt 2019)

Chapter 8

Remote Sensing of Benthic Habitats in Optically Shallow Water

Natascha Oppelt, Brian B. Barnes, Heidi Dierssen, Tiit Kutser, Arnold Dekker, Gema Casal, Peter Gege, Jaime Goodman, Jaime Pitarch, Eva Scrivner, Touria Bajjouk

---

Remote sensing of benthic reflectance allows derivation of benthic habitat distribution and characteristics in optically shallow bodies of water. Benthic habitats often cover large areas (e.g., 10's – 1000's km^2) and provide important ecological, management, economic, and cultural benefits (Cavanaugh et al. 2010). Their distribution serves as a key indicator of the ecological health and water quality in coastal environments, as well as responses to major disturbances (e.g., Figure 7 in Dierssen et al. 2021). For example, seagrasses and benthic macroalgae are essential for many organisms offering habitats, mating, and nursery grounds, feeding areas and refuges for several species. They can further play a vital role in stabilizing sediments and protecting the coastal zone from erosion and storm impacts. Additionally, the coastal area is a dynamic interface where matter exchanges between the land and water. As a part of this area, benthic vegetation such as macroalgae, seagrass beds or coral reefs are essential as processors of land-based fluxes, ranging from nutrients to pollutants (Hestir and Dronova, 2023; Kutser et al. 2020). The potential of coastal vegetation for long-term carbon sequestration, the so-called blue carbon, is subject to active research worldwide (e.g., Duarte, 2017; Park et al. 2024; Yao et al. 2025).

Typically, remote sensing quantifies the extent of the benthos, including details about the type of benthos, and, in some cases, extending to identifying dominant taxa (e.g., seagrass and macroalgae) (Casal et al., 2011a; Casal et al, 2012). Although other biophysical properties of the benthos can be estimated, including measures of horizontal and vertical structure, biomass, and physiology, they are not covered in this work. To date, no space-based sensing system combines the necessary spectral, spatial, radiometric, and temporal resolutions ideal for remote assessment and monitoring of aquatic ecosystems (e.g., Muller-Karger et al. 2018; CEOS, 2018, Hestir and Dronova, 2023). Nevertheless, technology has advanced dramatically over the last decade with the advent of space-based sensors with better spectral and radiometric capabilities for aquatic applications. Remote sensing is becoming an increasingly important tool for conservation, management, and research of critical benthic ecosystems (e.g., Bell et al. 2023). By providing detailed information about the distribution and characteristics of benthic habitats and organisms, remote sensing-based mapping can help guide conservation and management efforts (e.g., Schütt et al. 2025), as well as advance our understanding of these complex ecosystems.

The aim of this chapter is to provide an overview of remote sensing-based mapping of benthic shallow water habitats. Sections include definitions of optically shallow

and optically deep water, benthic endmember libraries, atmospheric correction and related image corrections, image- and physics-based approaches used for benthic classification, and challenges inherent to benthic mapping. A separate report is warranted to detail the many methods for mapping the extent and biophysical properties of the benthos from image processing, optimization, validation, and uncertainty propagation for optically shallow water remote sensing, building on previous works examining seagrass (Phinn et al. 2018), coral reefs (Goodman et al. 2013), comparing remote sensing inversion methods (Dekker et al. 2011) and summarising achievements of shallow water remote sensing in coastal and inland waters during the last 50 years (Kutser et al. 2020).

8.1 Defining optically shallow water

In the most general sense, optically shallow waters are those where the bottom is observable from above the water surface. The bottom substrate provides a measurable signal at the water surface and is part of the "water-leaving reflectance" (also called remote sensing reflectance) measured by an *in situ*, airborne or space-borne sensor (Dekker et al. 2011; Maffione, 2000), as highlighted in Fig 8.1. In contrast, optically deep waters do not have a measurable substratum reflectance signal at the water surface. The maximum depth of optically shallow water is defined by the depth of penetration (DOB) of light in the water column i.e. the depth to which light photons can reach and then travel back to the water surface to be detected by remote sensing sensors. The DOB is first of all defined by the optical properties of water molecules, but depends also on other water constituents like CDOM, phytoplankton and other particulate material in water. In the red part of spectrum, where most of the variability between benthic habitats occurs, the DOB is in the range between 9.5 m (at 600 nm) to 3.5 (at 700 nm) in the case of clear oceanic waters (Kutser et al. 2003; 2020). In the blue part of the spectrum (at 420 nm) DOB can reach up to 110 m. Other water constituents absorb and scatter light predominantly in the blue part of the spectrum. Therefore, in moderately complex waters the DOB is significantly reduced at shorter wavelengths and very little reduction occurs at longer wavelengths. On the other hand, in locations with extremely turbid (rich in particulate material) or extremely absorbing (rich in CDOM) waters and weakly reflective benthos (e.g., muddy lakes) water may be optically deep even if the depth is 20-30 cm. Because many nearshore waters are exposed to tidal variability, a specific location can vary from optically shallow to optically deep as water depth and clarity changes throughout the course of a day. Additionally, the water-leaving reflectance in artificial mesocosms is considered optically shallow due to influence from the bottom and sides of the tank (even if painted black), unless the water is extremely turbid (due to a combination of backscattering and absorption).

Distinguishing between optically deep and optically shallow conditions is challenging, and unfortunately, no model has been developed that accurately differentiates optically shallow and optically deep waters consistently across different environments and sensors. However, in Brando et al. (2009), a physics-based algorithm approach is described and applied in a coastal bay environment where it is possible to distinguish between optically deep, quasi-optically deep (when there is a diffuse signal from the benthos) and optically shallow waters in a hyperspectral

airborne remote sensing image. The essence of the method is to determine an optically deep water spectrum and then to assess whether any image spectra deviates between 1 to 5 Noise Equivalent Reflectance differences (quasi-optically deep) or more than 5 Noise Equivalent Reflectance differences (optically shallow). Knowledge of the Noise Equivalent Reflectance difference (Wettle et al. 2004) is essential for this method, as well as assumptions regarding the consistency of IOPs between shallow and deep pixels.

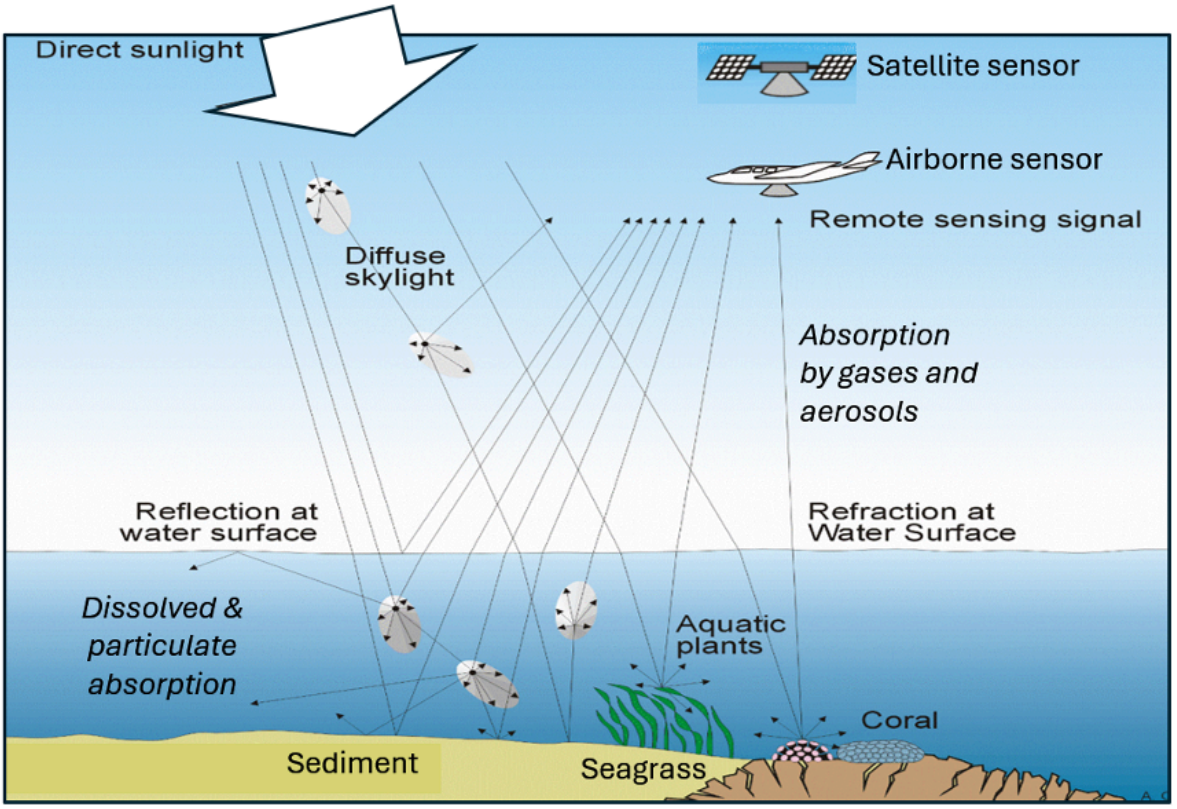

Figure 8.1 Graphic illustration of remote sensing of optically shallow waters where the signal is absorbed and reflected from various benthic substrates including sediment, seagrass and coral (adapted from CEOS 2018).

In satellite remote sensing applications, depth thresholds are often implemented to assign categories. For example, McKinna and Werdell (2018) classify pixels with depth less than 5 m to be optically shallow and greater than 40 m to be optically deep, respectively, while making a model-based determination for remaining pixels with intermediate depths (5-40 m). Such designations do not work in all locations, but are designed to work well in the Great Barrier Reef lagoon and coral waters. Other approaches use ad-hoc image-based methods and/or reflectance or bathymetry thresholds (Casal et al., 2011a; Hill et al. 2014). For example, the Allen Coral Atlas uses a normalized difference index with green and near infrared bands to delineate oceanic pixels (Lyons et al. 2024).

Optically shallow water can theoretically extend to geometric depths of over 100 m in clear waters over bright carbonate sediment sand (Kutser et al. 2020), especially for blue/green wavelengths where light penetrates furthest (i.e., a “transparent window” Lee et al. 2015). A few studies have successfully retrieved benthic properties of

different features at such great depths. However, at such depths it is possible only to detect presence/absence of certain benthic types (e.g., seagrass on bright sandy bottom). Spectral differences between different benthic groups (e.g coral, red algae, green algae/seagrasses) occur at longer wavelengths where absorption of light by water molecules can dominate the spectrum (Kutser et al. 2003; Casal et al., 2013). For the Estonian coasts of the Baltic Sea, Vahtmäe et al. (2020) found detectability limits differed by up to 4.5 m based on the type of bottom boundary. Kuhwald et al. (2022) reported a detection limit of 5 m in the Western Baltic. In these turbid waters, detection limits were 7.5 m for sand substrates, 5.0 m for brighter benthic submerged vegetation, and only 3.0 m for brown macroalgae. It has to be noted that these maximum depths are for presence/absence detection and not for mapping different benthic habitat species or genus separately. Similar results were obtained in the optically complex waters of the Galician coast (NW of Spain) where green and brown macroalgae could be differentiated from deep water up to 6 m while this depth decreases up to 5 m in the case of red macroalgae (Casal et al., 2013). In this case sandy bottoms shower differences in comparison with deep waters up to 13 m depth (Casal et al., 2013).

Typically, optically shallow waters have higher reflectance than optically deep waters across all wavelengths depending on the bathymetry, bottom reflectance and water column properties (Figure 8.2A,B). As waters become increasingly shallow, the scattered light from the benthos contributes ever larger amounts to the water-leaving reflectance and reflectance increases proportionally. Submerged aquatic vegetation, such as eelgrass, absorb blue and red light for photosynthesis and the resulting water-leaving reflectance is highly peaked in green wavelengths (Figure 8.2A) compared to sand (Figure 8.2B).

On rare occasions, benthic substrates can be so highly absorbing (dark) that water-leaving reflectance can have a lower magnitude than optically deep conditions for certain wavebands (e.g., Figure 8.2C). This is still considered optically shallow water. Maffione (2000) suggests that, as long as the benthos has any measurable impact on observed spectral colour, it is considered optically shallow. This is true even for a “black” benthos that, despite not reflecting any light, would still have a measurable impact on observable reflectance at the water surface. Example habitats that exhibit these properties may include fibrous macroalgae that have complex structures that can serve as a “light trap” and subtidal mussel beds that are non-photosynthetic and nearly black in colour.

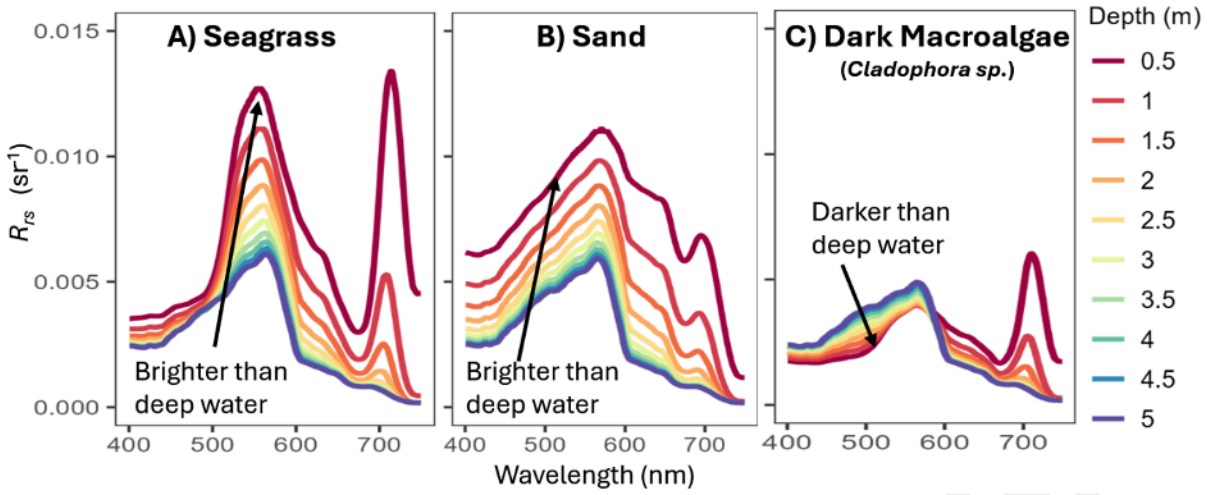

Figure 8.2 Simulated remote sensing reflectance (Rrs) spectra using Hydrolight radiative transfer software for (A) eelgrass, a long-leafed seagrass species, (B) sandy sediment and (C) a dark macroalgae *Cladophora sp*. A fairly turbid water column characteristic of temperate marsh systems was used as input to the model. Black arrows indicate increasing geometric depth.

8.2 Benthic endmembers

Classification of bottom types, whether per-pixel or object-based segmentation, is often based on a spectral library of "endmembers" defined as representative reflectance spectra associated with specific types of benthos or bottom boundaries. The term "bottom boundary" encompasses the variety of hard, soft, and canopied bottom structures that uniquely absorb and scatter light. In principle, benthic reflectance depends on the absorbing and scattering properties of the observed benthic surface, the atmospheric and water optical properties, the topography of both the water surface and the benthos, as well as the incident light and viewing geometry. However, the dependence of benthic reflectance on many of these factors is quite minimal under most sampling regimes and robust remote sensing retrievals have been made using standardized benthic endmembers that broadly represent different types of bottoms (e.g., Phinn et al. 2018; Goodman et al. 2013; Kutser et al. 2020).

In many studies, benthic endmembers do not distinctly consider differences between species or morphologies within a given bottom type (e.g., tropical coral reefs). Studies have shown that broad benthic types (green, red and brown macroalgae) have characteristic reflectance shapes independent of the climate zone or type of waterbody (from lakes to open ocean waters) (Kutser et al. 2020). The shape of coral spectral reflectance is mostly determined by the suite of photosynthetic pigments in zooxanthellae (Hochberg et al. 2003). The base pattern ("brown mode") has low reflectance at wavelengths shorter than 500 nm, then gradually rising to three peaks/shoulders near 572 nm, 605 nm, and 653 nm. However, other reflectance patterns are possible with active narrow-band fluorescence and through

expression of non-fluorescing coral-host pigments (i.e., “blue mode”) (Hochberg et al. 2004; Kutser and Jupp, 2006).

Significant changes to the benthic optical properties occur temporally from shadows related to the directionality of the light, hot spots or caustics caused by wave focusing on shallow benthos, and currents that can bend leaves in canopies and change sedimentation and detrital distributions. For example, a horizontal seagrass leaf may be used to represent a seagrass bed, but a three-dimensional seagrass canopy typically has much lower reflectance depending on density, length, epiphytes, and detrital matter while canopy leaves could be moving due to local currents (Hedley et al. 2017). Sediment generally scatters light more broadly across all visible wavelengths and the spectra tend to be flatter in shape (Figure 8.2B), but sediment reflectance may vary with sediment colour, size, mineral composition, and amount of surface benthic microalgae (Chapter 7). As a result, considerable uncertainty in benthic mapping is caused by variations in bottom sediment colour (Armstrong, 1993; Dierssen et al. 2010).

Ideally, the bidirectional reflectance distribution function (BRDF) would be used to characterize the angular dependence of the reflectance of the benthic material, which can be related to surface roughness or structure. While the BRDF can be highly variable for natural objects and surfaces due to the large variability of their surface microstructure, most remote sensing models presume a Lambertian reflecting benthos and use spectral irradiance reflectance, also referred to as the albedo or bi-hemispherical reflectance (Nicodemus et al. 1977). Modeling studies have shown that the uncertainties associated with BRDF features of the benthos are generally less than 10% in most passive aquatic remote sensing applications because of the absorption and scattering processes of the water medium and air-sea interface (Mobley et al. 2003b). However, in certain shallow benthic types, such as dense long-leaved seagrass canopies and open branching corals, such effects can be greater than 10% (Hedley and Enriquez, 2010; Joyce and Phinn, 2010).

Natural surfaces are rarely homogeneous and are comprised of mixtures of bottom types. For example, in the case of corals, significant differences in colour occur even at sub-centimeter scale (See Figure 6.1 in Chapter 6). A remote sensing measurement of a pixel therefore frequently averages over a number of spectrally different manifestations of a substrate or over different substrate types. The irradiance reflectance of a mixture of substrates is typically modeled as a weighted sum of the albedos of the individual components as in Equation 8.1:

$$R_B(\lambda) = \sum f_n a_n(\lambda). \qquad (8.1)$$

where $a_n(\lambda)$ denotes the albedo of substrate number n at wavelength λ from a database, and f_n is the product of the areal fraction of the substrate within an image pixel and its relative amplitude compared to the albedo in the database. The relative amplitude can differ from 1 due to the natural variability of the substrate type’s albedo and due to BRDF effects. If $a_n(\lambda)$ from the database perfectly represents the

actual albedo for each of the n substrates represented in a pixel, then Σf_n = 1. In real conditions, however, Σf_n generally deviates significantly from 1.

The average benthic reflectance over a pixel or region can be challenging to determine at various taxonomic and spatial scales. For example, many different organisms found in a coral reef ecosystem are quite distinct spectrally with unique peaks and troughs across the visible spectrum (Figure 8.3A). Such is the case for benthic reflectance measured *in situ* over the massive stony coral *Diploria* sp., Gorgonian soft corals, the brown seaweed *Dictyota* sp., various types of sponges and sandy sediment (Gilerson et al. 2013). Fyfe (2003) analyzed the spectral distinctness of *Zostera capricorni*, *Posidonia australis*, and *Halophila ovalis* and found they were theoretically discriminable under ideal conditions. Even though the individual endmembers can be quite distinct, they often represent only a small surface area percentage of the remote sensing signal. In this case, the average benthic reflectance determined from photographs of the benthos is spectrally similar to sand in spectral shape and soft coral in magnitude (Figure 8.3A, black line). As noted in earlier chapters, many species within the same taxonomic class, such as red macroalgae, have very similar spectral shapes (Figure 8.3B) and would be challenging to differentiate down to the genus or species level. On the other hand, corals can be differentiated into green, blue and brown types (Kutser and Jupp, 2006).

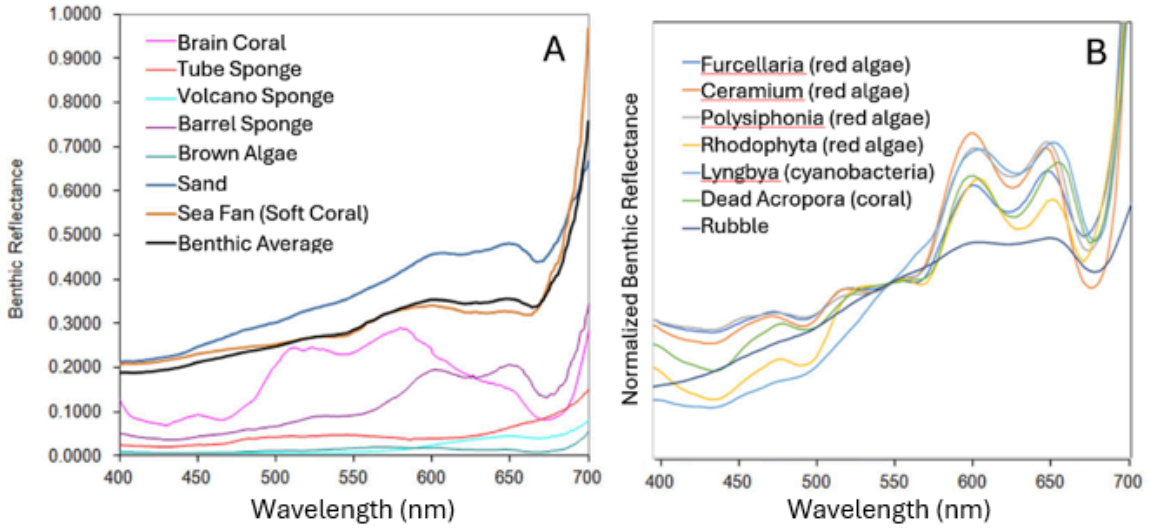

Figure 8.3 A) Benthic reflectance spectra across the visible spectrum obtained within a coral reef ecosystem in the Greater Florida Keys in January 2011 (modified from Dierssen 2013). B) Normalized benthic reflectance of red algae and cyanobacteria collected in the Baltic Sea and the Great Barrier Reef. Spectra are normalised to values at 550 nm modified from Kutser et al. (2020).

For remote sensing applications, benthic training or validation data can be determined by combining data from sensors that monitor at different spatial resolutions. For example, Kuhwald et al. (2022) combined field video data (Figure 8.4A) with airborne aerial photographs (Figure 8.4B) to develop training data across broad classes (i.e., dense seagrass, seagrass dominated, sediment dominated, bare sediment) at the 10 m x 10 m resolution required for Sentinel-2 imagery (8.4C).

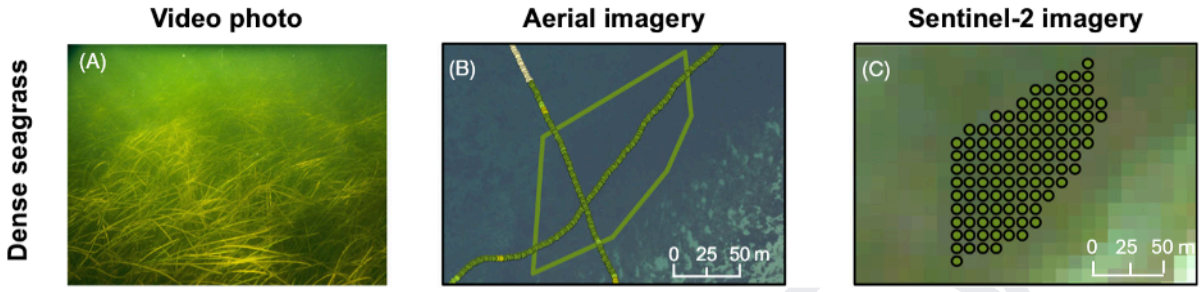

Figure 8.4 Examples of developing training and validation benthic classification data for remote sensing applications using different scales of imagery (from Kuhwald et al. 2022).

8.3 Atmospheric and Other Corrections

One of the most challenging aspects to remote sensing over optically shallow water is called "atmospheric and air-water interface correction," whereby the influences of the atmosphere, water surface, and other environmental factors are removed. An airborne or satellite sensor measures directional radiance coming from the combined water-atmospheric system. As shown in Figure 8.1, corrections must account for the attenuation of the water-leaving radiance through an absorbing and scattering atmosphere, as well as removal of skylight scattered into the sensor field of view, direct and diffuse sunlight reflected off the sea surface and reflections from whitecaps, bubbles and any other floating debris (e.g., Frouin et al. 2019; Hieronymi et al. 2023).

In addition, the downwelling irradiance, $E_d(\gamma)$, at the water surface is modeled for each pixel, in order to produce an estimate of water-leaving reflectance. Since aquatic remote sensing from satellites is generally only available under clear skies, modeling of $E_d(\gamma)$, is generally accurate. However, such modeling of the atmosphere provides uncertainty when isolated or thin clouds are present and/or when obtaining aircraft or drone data beneath cloudy skies (Brando et al. 2009).

Atmospheric correction is challenging, especially in inland and coastal conditions with complex atmospheric aerosols, gases and adjacency effects (Frouin et al. 2019). Such challenges are magnified in optically shallow water where there is a measurable signal in the near infrared that makes standard ocean atmospheric correction methods using the "black-pixel" assumption invalid (Gordon and Wang, 1994). Garcia et al. (2020) found that none of the available off-the-shelf atmospheric corrections for multi-spectral imagery were suitable for the relatively clear shallow water of the Bahamas Bank due to (a) violation of the black pixel assumption in the

NIR; (b) the iterative approach at correcting for non-negligible NIR water-leaving radiance; (c) assumptions about backscattering and consistent proportionality of NIR water-leaving reflectance; and (d) the lack of optically shallow training data in machine learning approaches.

Radiative transfer (Look Up Table) approaches that solve for atmospheric contributions, such as ATREM, MODTRAN and ACOLITE, have been applied over optically shallow water for use with hyperspectral imagery (Gao et al. 2000; Brando et al. 2009; Thompson et al. 2015; Vanhellemont, 2020). New models are also being considered that simultaneously solve for the benthos and the atmosphere as a coupled system (Thompson et al. 2018).

An important distinction in atmospheric correction schemes is whether they apply different correction factors to each pixel individually, or assume the atmospheric contribution is uniform across the image, so that each pixel then has the same correction factors applied. The former approach modifies the spectral data per-pixel whereas the latter is effectively a uniform transform of all pixels. This can become relevant when interpreting the result of any particular mapping technique. For many mapping approaches, atmospheric correction is largely bypassed and empirical line height (ELH) corrections are conducted with known validation points to correct for atmospheric influences (Hill et al. 2023). “White” corrections or ELH corrections can also be applied to tune the reflectance values due to under- or overcorrection of atmospheric inversion models (e.g., Dekker et al. 2011; Dierssen et al. 2003).

Other corrections may include spectral smoothing for wavelengths with low signal to noise and tidal corrections when evaluating time series of images over the same locations.

8.4 Classification Approaches

Different classification approaches have been applied in different locations worldwide using a combination of platforms (satellites, aircrafts and UAV) and sensors, multispectral and hyperspectral. The level of detail of the obtained results will depend on the combination of the different spatial and spectral resolutions. Methodological frameworks for benthic habitat mapping include:

1. **Image-based or Empirical Algorithms**, such as the Spectral Angle Mapper (SAM), derivative-based approaches, machine learning classifiers, and object-based image analysis (OBIA), provide tools often based on training data and/or “tuned” to specific images, regions, or environmental conditions.
2. **Physics-based Models** that involve modeling the optical properties of the water column and benthos for the specific environment. These models generally also retrieve bathymetry as a free parameter or require its inclusion as an additional data channel, which is one of the main advantages. Empirical parametrisation formulations are inherent to these methods as well. The two primary modes for physics-based models include:
    - **Forward Models** simulate expected reflectance by modeling the interaction of light with the water surface, water column, and benthic surface. Spectrum matching is then conducted to find the spectra that

most closely resemble the measured reflectances. The modelled spectral libraries can be simulated for either water leaving signal (benthic reflectance + water column effects) and applied on atmospherically corrected remote sensing imagery or for top of atmosphere signal (benthic reflectance + water column + atmosphere) and applied on top of atmosphere imagery. The latter approach has been demonstrated to work better (Kutser et al. 2006).

- **Inversion Models** work in reverse by estimating benthic depths, reflectances, and water column optical properties from observed reflectances. Several of these models simultaneously incorporate the atmospheric components into the inversion or optimization scheme.

3. **Hybrid Models** combine elements of the above to improve performance, reduce uncertainty and reduce computation time.

Image-based methods, categorized as unsupervised, supervised, object-based and/or machine learning (e.g., see Kutser et al. 2020), are frequently used to classify the benthos. The most common supervised technique in remote sensing is to conduct extensive ground-truth of a region and tune an empirical model of a selected image based on sets of training and validation data. While such approaches are common in terrestrial remote sensing, obtaining sufficient field measurement data is costly in time and resources and the spectral changes expected with different water depths and optical water types make this much more challenging for aquatic remote sensing. Since light attenuation depends exponentially on water depth, the water layer introduces a highly nonlinear component to benthic reflectance. Even a water layer of just 10 cm influences the reflectance significantly.

Even in empirical image-based methods, transformations on the spectra to minimize depth-dependence before classifying the benthos are recommended (e.g., Armstrong, 1993). As noted below, many of the analytical models retrieve bathymetry as part of the forward or inverse solution (e.g., Kutser 2006; Dekker et al. 2011; Dörnhöfer et al. 2016). Depth can also be estimated using empirical methods based on the relationship between band ratios or other band transformation and reference data (Stumpf et al. 2003; Lyzenga et al. 2006). For mapping of coral reef habitats in the Allen Coral Atlas, for example, several constants are calibrated for each study site to estimate depth according to the water column attenuation conditions (Lyons et al. 2024). In general, image-based approaches are most successful with considerable site-specific information about bottom types, water column properties, and bathymetry.

For example, an image-based approach using SPOT-4 imagery was applied to map kelp forests up to 10 m depth along the Galician coast (NW Spain), achieving classification accuracies above 70% for broad substrate categories (sand, rock, and seaweed) (Casal et al., 2011b). The image-based approach was also developed to map seagrass habitats across large regions from broadband Sentinel-2 imagery in turbid waters of the Baltic Sea (Kuhwald et al. 2022; Figure 8.5). The use of broadband sensors like Sentinel-2 is best when the benthic classes are well-known *a priori* and spectrally discrete. As noted below, broadband sensors do not have the spectral capabilities to differentiate “green” macrophytes or fractional mixtures with

other macroalgal types. Using empirical relationships to correct for bathymetry and water column attenuation, a machine learning classifier was built based on training data from the region to model broad classes of seagrass and sand-dominated habitats (see Figure 8.4 above).

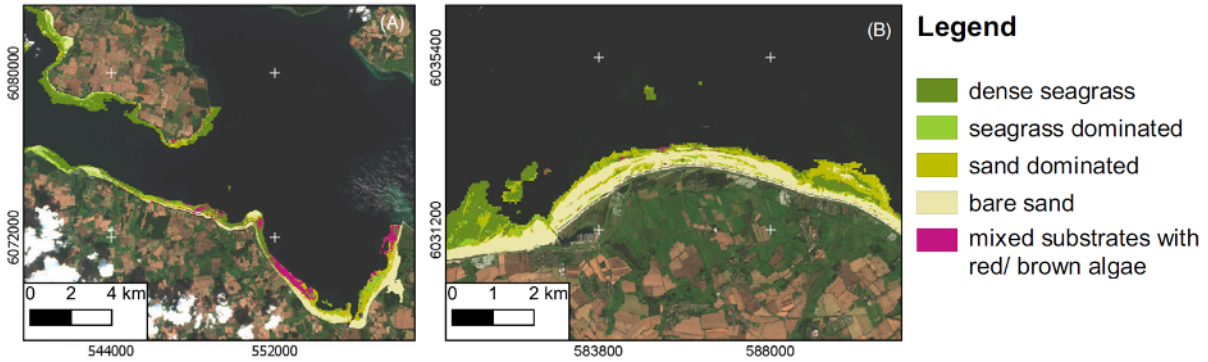

Figure 8.5 Classification results of coastal benthic habitats at the western Baltic coast based on Sentinel-2B in various subareas with extended shallow water areas modified from Kuhwald et al. (2021)

In contrast to image-based approaches, analytical methods use physical models to simulate the concomitant spectral influences of the depth-dependent water column and benthic habitat. Analytical models connect measured quantities with concentrations of different types of material present and their optical properties in the water column. Several analytical models have been developed over the last few decades (e.g., Lee et al. 1998;1999; Albert and Mobley, 2003; Klonowski et al. 2007; Kutser et al. 2006; Brando et al. 2009; Dekker et al. 2011; Giardino et al. 2012). Some are parameterized using inherent optical properties (IOPs) such as absorption and backscattering (Lee et al. 1999) and others on the apparent optical property of downward and upward light attenuation (K_d and K_u) (Philpot, 1987; Maritorena et al. 1994).

Empirical parameterizations are common to all physics-based models in order to reduce the complexity of the problem. For example, the HOPE model (Lee et al. 1998) approximates R_{rs} with five scalar variables: (1) the absorption coefficient of phytoplankton at 440 nm, P; (2) the absorption coefficient of detritus and gelbstoff at 440 nm, G; (3) the backscattering coefficient of suspended particulates at 550 nm, X; (4) water depth, H, and; (5) the bottom albedo at 550 nm, B. Simplifications in the spectral shapes of the IOPs and/or the use of normalized or specific-IOPs (Brando et al. 2009) are needed for such modeling. In addition, a subset of relevant endmembers is commonly employed. Bottom reflectance can either be parameterized as individual endmembers or fractional composition parameterized in terms of Equation 8.1. In some models, Bayesian linear mixtures of large databases of benthic endmembers are included (e.g., Thompson et al. 2017).

Various optimization techniques are used to develop realistic ranges and initial parameterizations for the analytical models (“priors”), to minimize differences between simulated and measured spectra at all available or select “weighted” wavebands, to treat noise in the imagery (Brando et al. 2009), and to avoid biases or

local minima in the solutions. For example, simultaneous retrievals of bathymetry and the fractions of green and brown macroalgae, and sand were obtained using physics-based inverse modeling from airborne imaging spectroscopy (Casal et al. 2012) and from hyperspectral satellite imagery (Kutser et al. 2006). Application of these empirical frameworks have also been demonstrated for heritage multispectral satellite datasets including Landsat (Dekker et al. 2005), MODIS (McKinna et al. 2015) and MERIS (Barnes et al. 2018; Garcia et al. 2020). For these implementations, model parameters (e.g., depth, albedo, spectral shape, etc.) may be highly constrained or fixed in order to accommodate for the reduced spectral resolution.

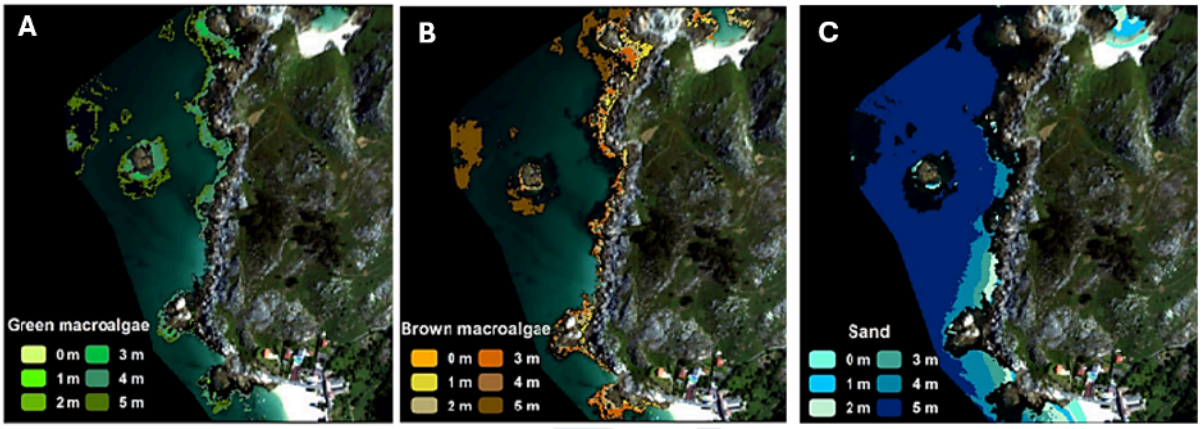

Figure 8.6 Benthic substrates mapped at different depths (up to 5 m) using physics-based classifications from an Airborne Hyperspectral Scanner image showing (A) Green macroalgal distribution, (B) Brown macroalgal distribution, and (C) Sand substrate modified from Casal et al. (2012).

Hybrid approaches that combine a variety of methods in a step-wise decision tree have become increasingly common in optically shallow remote sensing. These approaches can combine both forward and inverse analytical models and machine-learning techniques. Forward radiative transfer modeling can be used to build look-up tables (LUTS); machine learning to simplify and reduce overlaps in LUTS; and inverse modeling to estimate bathymetry, water column properties, and benthic reflectance (e.g., Garcia et al. 2020; Figure 8.7).

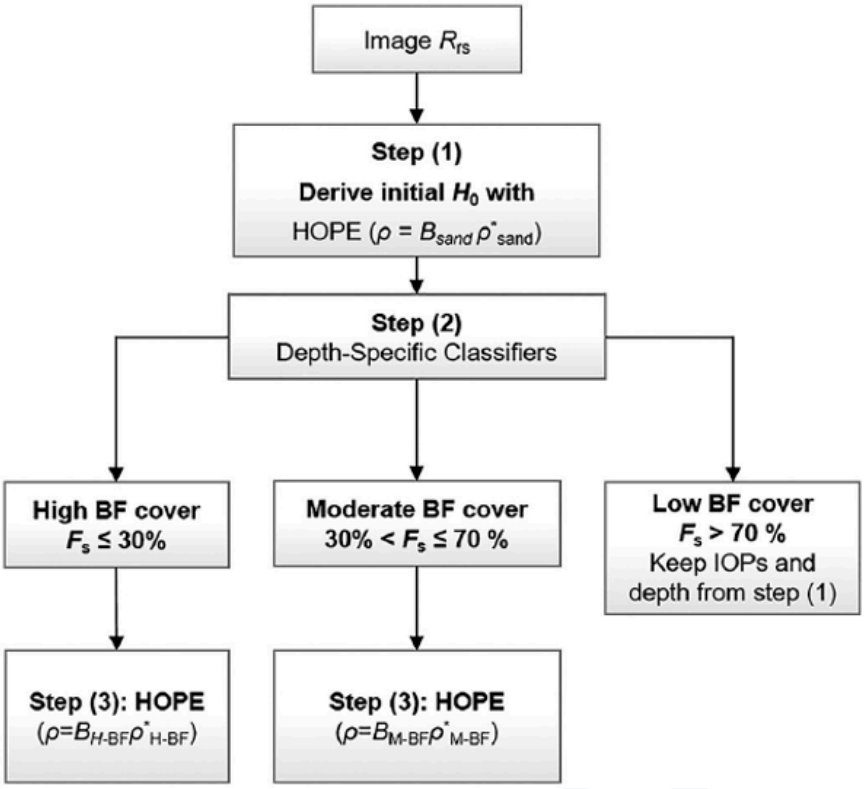

Figure 8.7 Example decision tree of a hybrid approach for estimating fractional coverage of benthic flora (BF) using both forward and inverse analytical modeling and machine learning classifiers. MERIS did not have the spectral capabilities to differentiate between seagrass and grapestone sediment covered with green benthic algae. Adapted from Garcia et al. (2020)

8.5 Challenges and Opportunities in Benthic Remote Sensing

The remote sensing problem may be ill-posed or ambiguous because a given measurement does not contain sufficient information to accurately determine essential environmental parameters. Different sets of optical properties and concentrations can lead to similar spectra which can be indistinguishable in practice (Kutser et al. 2003; 2006). The ambiguity problem increases with the number of environmental variables; hence, it is a big challenge in shallow waters. As shown in Figure 8.8A, under certain conditions, an optically deep water can appear similar to optically shallow water by changing the amount and spectral slope of particulate backscattering in the water column in relation to the amount of suspended particulate matter. Different types of submerged vegetation can appear similarly “green” with very little difference in spectral shape apparent in water-leaving reflectance (Kutser et al. 2020). For example, seagrass *(Posidonia australia)* and the benthic macroalgae *(Chara contraria)* can appear nearly identical for remote sensing purposes (Figure 8.8B). However, increased access to spectral libraries as well as increases in spectral resolution and radiometric sensitivity can counteract these ambiguities.

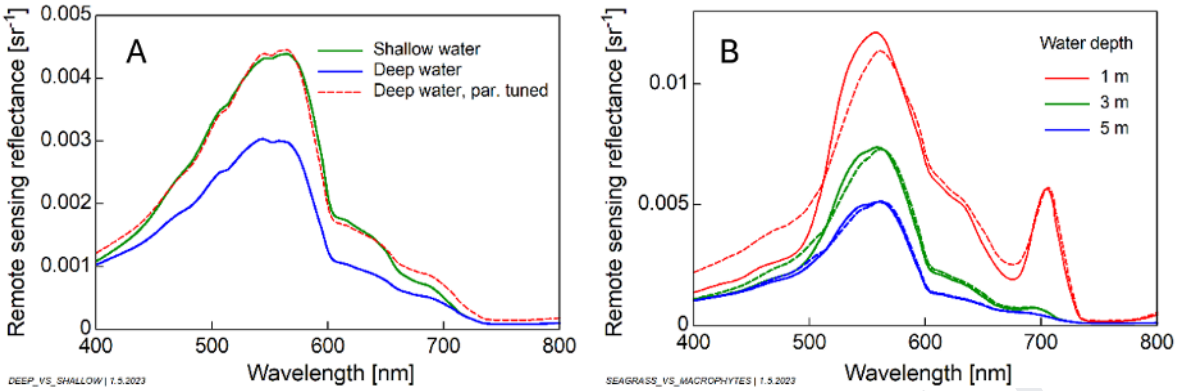

Figure 8.8 Simulations of remote sensing reflectance using different water column and benthic properties. A) The spectrum for deep water (blue line) can appear similar to optically shallow water with a sandy bottom (green line) if additional suspended particulate matter is added to the water column (red dotted line). B) Simulated spectra are nearly identical with depth for seagrass (dotted line) and the macroalgae *(Chara contraria)* commonly known as stonewort.

The only way to address ambiguity is to feed the algorithm with prior information, for example by providing an independent estimation of the water absorption, or by limiting the number of endmembers to a few that are clearly distinguishable and that are known to be present at the area, or by restricting the concentrations of water constituents to ranges realistic for the study site, or by taking the known bathymetry into account. Image-based methods make use of measurements in the area for use as training and validation datasets. Such data can also provide information about the parameter ranges and indirectly about parameter correlations. Physics-based inversion methods and properly-trained machine learning models can use parameter constraints to limit the solution space to realistic values.

Many physics-based remote sensing approaches characterize the water column in optically shallow water using retrievals of chlorophyll from deep offshore pixels. For some habitats, deep water can be a reasonable proxy to quantify the background signal of the water (Kuwald et al. 2022). However, a study of reefs across the Pacific showed that coral reef flora and fauna significantly impact the optical properties of the overlying water column and offshore or ocean waters are consistently lower in absorption and backscattering compared to coral reef waters and for overlying coral reef waters absorption is dominated by coloured dissolved organic matter (CDOM) (Russell et al. 2018) or detrital particles (Dekker et al. 2022). Similarly, water column absorption over seagrass meadows can be dominated by CDOM compared to sandy habitats and optically deep water (McPherson et al. 2011).

Studies carried out at the Great Barrier Reef (Kutser et al. 2003), Hawaiian waters (Hochberg and Atkinson, 2003), the south European Atlantic coast (Casal et al. 2012), Australian estuarine and coral reef waters (Botha et al. 2013) and the Baltic coast (Uhl et al. 2022), reported that bottom separability was not only dependent on substrate type and water depth, but also on the type of sensor used in the classification analyses. Reduced spectral and radiometric characteristics of

observing sensors limit the ability to detect small differences in benthic composition. Broadband sensors have limited ability to differentiate benthic mixtures compared to hyperspectral sensors (Hochberg and Atkinson, 2003). Botha et al. (2013) demonstrated that with increased spectral resolution benthic composition can be determined down to greater depths and with reduced uncertainty. Bush et al. (2017) presented a method that integrates automated recording devices, high-throughput DNA sequencing and advanced ecological modeling to enhance the extraction of information from Earth observation data. The advancement of hyperspectral satellite sensors has made this approach increasingly feasible, allowing for efficient monitoring of the impacts of management practices on benthic biodiversity, as well as its associated functions and services.

In shallow waters, dark bottom types, such as senescent macroalgae *Cladophora sp.*, dark mud sediments, and mussel beds, can lead to large overestimations in bathymetry or even masking as optically deep waters. In intertidal zones, spectral ambiguities may occur due to desiccation during low tide (Uhl et al. 2013) or due natural variations within and between species, even the influence of without water. Using hyperspectral data, the analysis of the derivatives of reflectance spectra showed promise for discriminating intertidal and submerged macroalgae (Uhl et al. 2016). When combined with Light Detection and Ranging (LiDAR) data, hyperspectral images enable a reliable assessment of the spatial distribution of *Sabellaria alveolata* degradation dynamics, serving as an indicator of the ecological status of the largest European “honeycomb worm” biogenic reefs in the Bay of Mont-Saint-Michel, France (Bajjouk et al. 2020).

In conclusion, the field of optically shallow water remote sensing is growing and the opportunities for improvement in technology and methods are vast. The advent of better sensors with higher spatial, temporal, and spectral resolution and better spectral sensitivity, tuned for aquatic applications (such as proposed in CEOS, 2018) will lead to routine mapping of the benthos globally. In tandem, this will require improved methods for obtaining field data for model development and validation, as outlined in this report. The significant increase in the availability of spectral libraries of the benthos and the water column creates opportunities to do massive forward simulations allowing machine learning and AI methods to optimize inversion methods. Merging imagery from a variety of sensors with different passive and active capabilities, including polarization capabilities (Gilerson et al. 2018), and spatial and temporal resolutions will also be necessary to tease out the complexity of changing benthic habitats in optically shallow water. The aim will be to routinely detect subtle changes in the health or condition of benthic habitats to inform management of coastal resources. The decades of critical research in this field have provided solid foundations for this reality.

Chapter 9

Global Change and Benthic Habitats

Natascha Oppelt, Tiit Kutser

Global change encompasses all the major environmental changes occurring on a global scale, including climate change, biodiversity loss, land-use change, and pollution. Global change is a consequence of human activities and their impact on natural ecosystems, leading to significant alterations in the benthos (Birchenough et al. 2015).

Climate change is one of the key drivers for distributional shifts of species by changing environmental conditions and habitat suitability worldwide. Alterations in environmental conditions and habitat suitability lead to shifts in both latitude and altitude ranges for many species (Parmesan and Yohe, 2003; Thuiller, 2004; Hiddink et al. 2015). Altered environmental conditions (e.g., temperature, salinity, hydrodynamics, ocean acidification) can affect species distributions, community structures and diversity patterns (Poloczanska et al. 2016). Besides changing habitat conditions due to a changing climate (i.e. climate change), anthropogenic stressors such as eutrophication, pollution, acidification, overharvesting, invasive neophyte and habitat destruction are well-documented threats to fresh- and seawater benthos, and the goods and services they provide (Birchenough et al, 2015). Therefore, global change describes the consequences of human activities and their impact on natural ecosystems. With continuing global change it has become obvious that the seafloor will not remain untouched, and the future of the benthic communities is one where organisms, species, populations and communities, their ecology, biology and interactions at different life stages will be modified accordingly (Sorte et al. 2010, Sandulli et al. 2021).

Benthic environments offer many opportunities for investigating the biological response and adaptation of organisms to stressful life conditions. Since benthic communities adapted to specific environments, are sessile or have low mobility, are relatively long-lived, and integrate the effects of environmental change and anthropogenic pressure over time. Moreover, macrobenthos of hard and soft substrates are ubiquitous and can thrive in almost any aquatic environment (Sandulli et al. 2021). Benthos, therefore, is useful for long‑term investigations in the context of global and climate change (Birchenough et al. 2015).

Overall, the impact of global change on benthic habitats is complex, with many interacting factors affecting the functioning of benthic species and ecosystems. On a global level, the main physical aspects related to global change affecting submerged aquatic vegetation are the increase in water temperatures, altered hydrodynamics, eutrophication and changing light availability. In coastal and marine environments we also have to consider effects due to ocean acidification, altered salinity, and sea level rise. For a specific area, however, the impact of different factors may vary significantly.

The main effects of global change include 1) changing growth dynamics over time and space, 2) altered hydrodynamics, and 3) distributional shifts, often connected with habitat loss. Global change, however, includes far more impacts including pollution, overfishing, and physical disturbance from human activities such as fishing, dredging and coastal development. These activities can have significant impacts on

benthic vegetation, altering their composition, structure, and function, and leading to long-term changes in ecosystem dynamics (Grall and Chavaud 2002).

9.1 Growth dynamics

Global change affects the growth dynamics of benthic habitats in several ways. Changes in water temperature, for instance, influence growth and reproduction, which has been indicated by mapping and modelling studies for the North Atlantic and the North Sea (e.g., Mieszkowska et al 2006). Growth dynamics of SAV species is strongly connected to their life cycle, and elevated water temperatures can cause some species to reproduce earlier in the year or to grow faster, while others may experience delayed or reduced reproduction and growth (Birchenough et al. 2015). Summer heatwaves with water temperatures above 26°C, however, can lead to tissue necrosis in benthic vegetation such as seagrass and brown macroalgae (Graiff and Karsten 2021).

Increased water temperatures also lead to bleaching and increased mortality of corals (e.g., Fabricius et al. 2005). Additionally, corals and other calcifying organisms are affected by ocean acidification. The ocean has become 30% more acidic since pre-industrial times and is predicted to further increase (Birchenough et al. 2017). The impact on marine benthos is that warmer seawater carries less oxygen and warmer water expands the low-oxygen zones in coastal areas. Ocean acidification further hinders the growth of calcareous benthos since it limits their ability to calcify, thus impacting the ability of coral to form calcareous skeletons This can, in turn, affect their growth and reproductive success (Mollica et al. 2018). With ongoing acidification, it is expected that about 70% of cold water corals worldwide will be affected within the next 100 years (Guinotte et al. 2006).

In addition, global change often involves an increase in nutrient input and eutrophication, which can decrease light availability and oxygen levels. The reduction in light transparency due to eutrophication can affect the species composition and depth distribution of benthic vegetation (Valiela et al. 1997). However, positive and negative effects on growth may differ between seasons and species. Perennial benthic macrophyte production is limited by light availability, leading to shifts from seagrass to ephemeral algae (McClelland & Valiela, 1998). In many shallow coastal ecosystems, eutrophication is considered the most significant pressure affecting the structure of benthic vegetation (Olsson et al. 2015). For instance, a long-term reduction in water transparency in the Baltic Sea (from 1936 to 2017) decreased the favourable sea floor areas for Fucus spp. by 45% (Sahla et al. 2020).

9.2 Hydrodynamics

Benthic vegetation communities are directly and indirectly affected by the physical properties of the water column. Hydrodynamics, such as changes in sedimentation and erosion due to storms or intrusion of saline water, can directly impact the habitat conditions and therefore for the growth and dynamics of benthic vegetation (e.g., Fujii et al. 2008). Furthermore, changing hydrodynamics can indirectly cause oxygen depletion, which is considered one of the most widespread negative influences on

marine and estuarine benthic vegetation due to high bottom water temperature, reduced water circulation, and coastal eutrophication (Halpern et al. 2007). Hypoxic zones are predicted to expand due to global climate change, resulting in a potential loss of biomass or mass mortality (Levin et al. 2009). Larger, long-lived species are expected to disappear first, and the communities shift towards the dominance of smaller, short-lived species (Viitasalo and Bonsdorff 2022). In areas where upwellings bring hypoxic water close to the surface, ocean acidification combined with warming may exacerbate the situation. An experiment simulating an upwelling event showed that hypoxic water caused severe mortality of brown macroalgae (Al-Janabi et al. 2016).

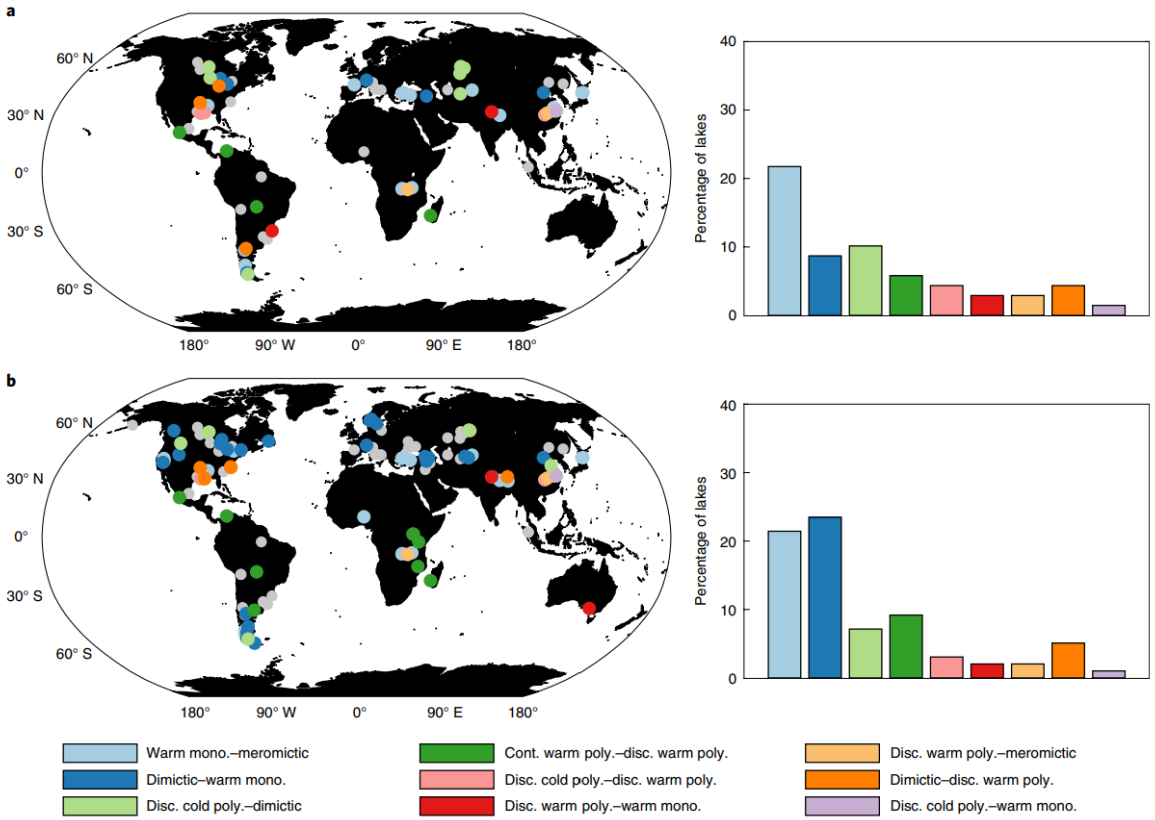

Figure 9.1 Global changes in lake mixing regimes. All changes are for 2080–2100 relative to 1985–2005. a,b, Climate-related changes in lake mixing regimes under RCP 2.6 (a) and RCP 6.0 (b) using a lake model forced with bias-corrected HadGEM2-ES projections. Every lake that experiences a mixing regime alteration is shown in grey in the maps and the most frequent mixing regime alterations (encompassing 80% of the identified mixing regime shifts) are shown with individual colours (see legend). Cont. = continuous; disc. = discontinuous; mono = monomictic; poly = polymictic (Woolway and Merchant 2019)

For lakes, Woolway and Merchant (2019) provided a comprehensive model-based study about changing mixing regimes as a response to climate and global change (Figure 9.1). Although the ecological consequences of these changes already started to appear during the reference period (1985-2005), their projections of future lake mixing regime alterations (2080-2100) suggest a complex pattern of lake responses to climate change. The geographical distribution of alterations in lake mixing do not support simple expectations of regional consistency in lake responses whereby lakes

in a given region will change in a similar manner. Most of the 360 studied lakes, however, are expected to alter their mixing behaviour.

9.3 Distribution shifts and loss of habitat

Distributional shifts are usually a result of a combination of environmental, climatic and anthropogenic factors that act synergistically on the whole ecosystem (Viitasalo and Bondsdorff, 2022). The various factors can lead to changes in the composition and distribution communities, with some species shifting their ranges or disappearing, while others become more dominant. Generally, studies have shown a decrease in biodiversity, especially when vegetation species are highly sensitive to changes in temperature and ocean acidity. This has been observed in shallow-water habitats such as coral reefs, seagrass and macroalgae (Waycott et al. 2009).

Especially documented for lakes and coastal zones in the Northern Hemisphere, atmospheric deposition and surface runoff led to “browning” by increased CDOM concentrations (Neale et al. 2023). Where the inputs of CDOM have increased, transparency to both visible and UV radiation has decreased. The extra energy absorbed by CDOM has enhanced surface warming and led to shallower mixed layers (known as shoaling), especially in smaller lakes (Pilla et al. 2021). However, the decreased transparency outweighs the shoaling effect, so the average UV irradiation and PAR in the surface mixed layer have decreased (Neale et al. 2018).
Together, these results indicate decreasing exposures to UV radiation in the surface mixed layer with increased CDOM. Higher CDOM in lakes and coastal waters also result in less light in the water column, which quite often means that the benthic micro- and macroalgae will be gone as there is no light for photosynthesis. In some places plants take over that can grow quickly from bottom to surface and reach light. Browning seems to occur in many lakes and coastal waters and thus, it is a problem for benthic habitats in many places.

According to species distribution models, certain areas such as the Baltic coast are expected to experience a significant reduction in the distribution of major habitat-forming benthic vegetation due to rising water temperatures and decreased salinity (Hiddink et al. 2015; Meier et al. 2012). Globally, rising water temperatures appear to be the most significant factor, causing a shift in the latitudinal distribution of many species towards cooler marine environments (e.g., Weinert et al. 2021).

In addition to changes in water temperatures and salinity gradients, human activities can also cause physical harm to benthic habitats and promote the spread of invasive species that can outcompete native benthic vegetation. Studies also report that the potential habitat area becomes less or is lost due to a rising sea level and the consequent effects of coastal squeeze (Birchenough et al. 2015).

Research on inland waters revealed that the decline of benthic vegetation is a worldwide issue resulting from both climate change and intensified human activities like land reclamation, eutrophication, and aquaculture (e.g., Sand-Jensen et al. 2000).

9.4 Importance for benthic reflectance measurements

The previous sections demonstrate that attribution of changes in benthic vegetation to global change is challenging because of the multiple synergistic effects between climate and other environmental drivers, such as eutrophication, habitat modification, fishing and introduction of non-indigenous species, which can all exert strong impacts on ecosystems and their dynamics in space and time (Reusch et al. 2018; Stenseth et al. 2020). Consistent measurements of benthic reflectance can be used to assess changes to the benthos over both space and time related to these environmental drivers. As noted in Chapter 8, a major driver for the development of new higher spatial resolution hyperspectral satellite missions, such as CHIME and SBG (Dierssen et al. 2023), is to be able to routinely assess changes in global benthic habitats in areal extent, biodiversity metrics, and in metrics related to ecosystem health (e.g., coral bleaching). As noted in Figure 9.1, many of the Essential Biodiversity Variables for benthic communities have been assessed with remote sensing technology, but generally require new technology (satellite and drones) to be routinely assessed.

Class	Essential Biodiversity Variable (EBV)	Wetlands	Benthic communities	
		Mangrove/ Salt marsh	Macro-phytes & Macroalgae	Coral
Genetic Composition	Population genetic diversity			
Species Populations	Distribution			
	Abundance			
	Size/vertical distribution			
Species Traits	Pigments*			
	Phenology			
Community Composition	Taxonomic diversity*			
Ecosystem Structure	Functional type*			
	Fragmentation/ heterogeneity			
Ecosystem Function	Net primary production			
	Net ecosystem production			

*Select types may be differentiated.

Routine	Demon-strated	Unproven

Figure 9. 1. Current capabilities of remotely sensed data for measuring Essential Biodiversity Variables modified from Dierssen et al. (2021). “Unproven” indicates

that methods have not yet been developed to collect these measurements from remote sensing imagery. “Demonstrated” are methods that have been demonstrated and could potentially be produced with hyperspectral imagery. “Routine” indicates measurements that are produced regularly.

Before planning benthic reflectance measurements, potential changes in benthic vegetation and sediment should be taken into account since new species may emerge, and others may disappear. Changes in phenology may also impede long-term comparisons of benthos reflectance. Under current global change conditions, additional measurements of water temperature, salinity or turbidity should be considered to monitor environmental conditions. These measurements may assist in studying the timing of recurrent life cycle events in benthic systems and how they are influenced by seasonal and interannual variability, which, in turn, would aid in understanding the impacts of climate change on benthic reflectance.

Chapter 10

Deep-sea Applications: Mining, Archeology, and Marine Litter Detection

Geir Johnsen, Øyvind Ødegård, Murat Van Ardelan, Andrea Faltynkova, Asgeir J. Sørensen, Heidi Dierssen

Benthic reflectance can be considered an important variable in exploring deep-sea habitats. Emerging technology, such as hyperspectral imaging with artificial lighting, provides a means to estimate benthic reflectance over swaths of the ocean bottom, as noted in prior chapters. This is different from benthic mapping of optically shallow water with airborne and satellite sensors (see Chapter 8 on Benthic Mapping), as it requires underwater robotic platforms with artificial lights and hyperspectral sensors that can maintain position and sample close to the bottom to obtain swaths of benthic reflectance at high cm-scale spatial resolution (Johnsen et al. 2013, Figure 10.1). For these applications, the term underwater hyperspectral imaging (UHI) is often used. These methods can use the radiance measured by the sensor directly, but this will be impacted by the distance from the targets and the turbidity of the water column. Benthic reflectance can be measured directly from UHI photomosaics per image pixel either with the use of reflectance standards *in situ* or with an analytical approach (Mogstad et al. 2019). By evaluating the spatial differences in benthic reflectance with such technology, the heterogeneity of deep benthic habitats can be assessed (Dumke et al. 2018a). Such results have the potential to be related to a host of natural and anthropogenic factors important for marine ecology, biogeochemistry, litter, bioclastic habitats and resource exploitation.

Natural factors that potentially can be assessed with benthic mapping include relating sediment reflectance to export flux, biogeochemical rates and elemental cycling of carbon, nitrogen and phosphorus. With a few isolated studies related to photodetritus (Dumke et al. 2018b), the use of benthic reflectance obtained in the deep-sea for biogeochemistry is an emerging discipline and not covered here. Another natural factor is the release of semio-chemicals by benthic organisms. Semio-chemicals are functional molecules that organisms use for communication and defense in these highly marginal conditions. Although not yet demonstrated, the use of benthic reflectance to quantify such compounds would have relevance to chemical, pharmaceutical, and agricultural industries (La Barre, 2014).

This chapter focuses on using mobile robotic vehicles carrying Underwater Hyperspectral Imagers (UHI) (to assess human impacts to the deep-sea benthos and habitats. Here, we discuss how benthic reflectance measurements with UHI have been or have the potential to be used in applications related to deep-sea mining, archaeology, assessment of underwater cultural heritage sites, and detection of marine litter and debris on the seafloor.

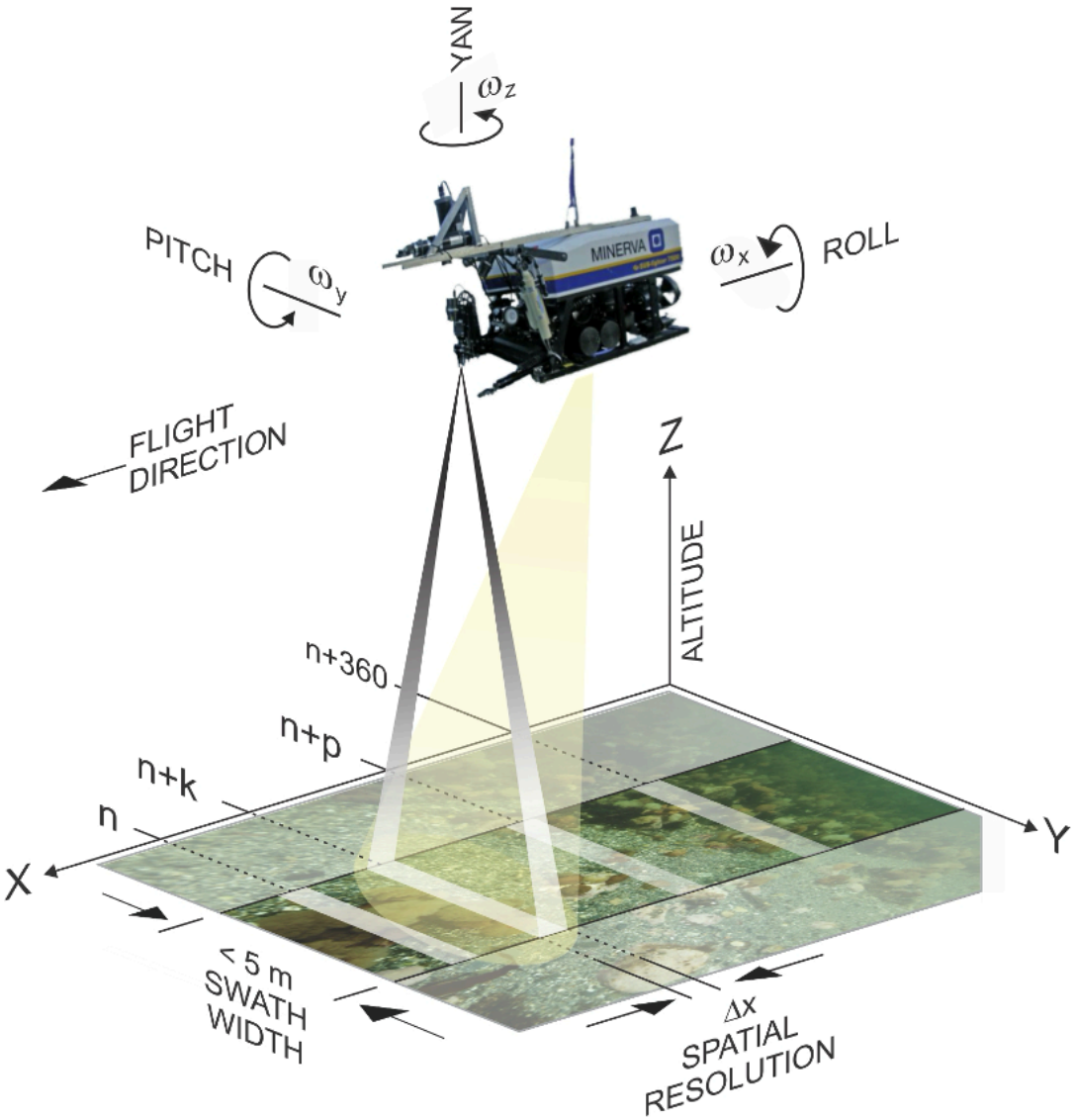

Figure 10.1 Image of an underwater robotic vehicle imaging across a swath along a vertical direction of the seafloor using artificial light while maintaining positioning including pitch, roll, yaw and altitude (Johnsen et al. 2013)

10.1 Deep-Sea Mining (DSM)

Deep-sea mining is an emerging industry driven by the demand for critical minerals. Surface and sub-surface sediment contain various minerals that can have economic and other interests for humanity (Miller et al. 2018; Rahul, 2022). DSM faces significant challenges related to environmental risks, regulatory uncertainties, and economic viability. Benthic monitoring plays an important role in exploration and sustainable exploitation of these minerals including gathering key knowledge on potential extraction sites and adjacent zones (Miller et al. 2018; Rahul, 2022). Here, we briefly outline the types of deep-sea sediments and associated biotic habitats considered for mining operations and the potential use of UHI on different tethered

and untethered underwater vehicles to map benthic habitats relevant to DSM operations (Mogstad et al. 2017; Summers et al. 2022; Johnsen et al. 2013; 2016).

The risks of DSM include a variety of potential negative impacts including destruction of benthic habitats and creation of sediment plumes in the process of separating minerals from sediment (Table 10.1). Ecologically, the impacts may include sedimentation over large areas in time and space, mechanical effects such as burying and clogging, particles in tissue of organisms, toxic effects, altered feeding behavior, retracted or lost polyps by filter feeders, and potentially release of heavy metals (see Liefmann et al. 2018; Ramirez-Llodra et al. 2020; Ellefmo et al. 2024). Further, some deep-sea ecosystems are fragile and slow to recover, potentially leading to species extinction. As outlined in Table 10.1, technology such as UHI has high utility for monitoring many of the expected impacts of DSM on the benthos including assessing changes in marine biodiversity, light pollution, and water column turbidity.

Table 10.1 The use of underwater hyperspectral imaging (UHI) to assess impacts of Deep Sea Mining (DSM)

Impact of DSM	Types of Impacts	Utility of UHI-surveys
Habitat destruction	Decrease in benthic productivity. Loss of biodiversity.	Characterize habitats over time and space. Quantify changes in benthic diversity.
Sediment plumes	Nepheloid layer with high suspended particles. Reduced light penetration. Smothering of marine life Release of heavy metal pollutants.	Assess water column turbidity (spectral Kd) associated with nepheloid layers. Assess changes in benthic sedimentation over time and space.
Noise pollution	Disruption of marine life not adapted to these acoustic frequencies.	None
Light pollution	Disruption of marine life adapted to darker conditions.	Monitor spectral composition and intensity of visible light. Quantify impact on deep sea vision, predator-prey interaction.
Carbon Cycle	Decrease in carbon sequestration. Release of methane.	Relate changes in benthic habitats and microbial mats to carbon cycling. Infrared imaging spectroscopy to quantify methane absorption.

Most of the seafloor substrate surveys have been performed from larger vessels using acoustic methods, such as multi beam echosounders, to survey larger areas. In addition, vessel-based point measurements of sediment sampling (grab and corers) and corresponding underwater video and photography has been used to verify objects of interest at a given site (Buhl-Mortensen et al. 2010; Van Lancker et al. 2012). Side-scan sonars provide acoustic images of the seafloor (acoustic backscatter) and high-resolution seismic data used to quantify sediment thickness and characteristics (Bellec et al. 2014).

A missing piece to this sampling has been *in situ* characterization of the mineralogy. Spectral reflectance provides specific details regarding substrate and mineral composition (Johnsen et al. 2013; Dumke et al. 2018a, b). Incorporating hyperspectral sensors on ROV and AUV systems has high utility to identify and map the seafloor over larger areas. For example, both using HI-in stereo microscopy in laboratory and *in situ* work using UHI have shown promising proof-of-concept to identify, map and monitor high productive areas on seafloor looking at optical fingerprints (i.e., benthic reflectance) of bioclastic matter (see examples in Mogstad et al. 2019). UHI can be used to assess the extent and distribution of sediment blanketing caused by resettled, resuspended material during deep-sea mining. This helps identify key variables to prioritize in models examining plume dispersion and its impact on biogeochemical processes at the sediment–water interface (Ellefmo et al 2024).

Deep-sea benthic microbes play a crucial role in the cycling of carbon, nitrogen, phosphorus, and other essential elements, as well as in the overall functioning of ecosystems. Monitoring microbial mats could serve as a predictive signal of ecological changes triggered by deep-sea mining (DSM) activities. Benthic microbial communities are highly sensitive to changes in particle fluxes. While heterotrophic bacteria decompose organic matter, autotrophic bacteria fix dissolved inorganic carbon at rates comparable to the bacterial assimilation of particulate and dissolved organic matter (Sweetman et al. 2019). DSM-induced sediment resuspension and extreme increases in sedimentation rates (up to 100–1000 times above background) may dramatically alter the aforementioned microbial activity and community composition. These changes could influence redox conditions and potentially lead to the establishment of new biogeochemical regimes at the sediment–water interface (Ellefmo et al. 2024).

10.1.1 Mineral Deposits

Significant interest in DSM is due to the high demand for minerals like cobalt, nickel, and manganese, which are used in electronics and green technologies such as electric vehicles and wind turbines. The greatest unexploited mineral resources are found in the deep seafloor and includes hydrothermal deposits, areas with high density of manganese nodules and cobalt-rich manganese crusts (Glasby 2000). Sediments occurring in different regions of the vast seafloor with depths exceeding 6 km are important for mineral deposits including:

- **Polymetallic nodules**: Deposits containing manganese, nickel, cobalt, and copper, found primarily on abyssal plains at depths of 4 to 6 km.

- **Polymetallic sulfides**: Deposits found near hydrothermal vents in active tectonic areas, rich in copper, gold, lead, silver, and other metals.
- **Cobalt-rich ferromanganese crusts**: Layers of metals that form on seamounts and ocean plateaus at depths ranging from 600 m to 7 km, containing cobalt, nickel, copper, and rare earth elements.

Research has shown that there are distinct differences in optical fingerprints and elemental composition of Mn nodules relative to surrounding substrates. These elemental changes may be discriminated based on their spectral signature with UHI or other spectrophotometric techniques, leading toward automated seafloor identification and mapping of minerals of interest (Johnsen et al. 2013, Dumke et al. 2018a,b).

Oxidation status of metals (e.g., iron and copper) can also be detected and mapped per image pixel from ROV-UHI surveys (Ødegård et al. 2018). UHI detection of manganese nodules, containing enriched concentrations of thallium (TI), copper (Cu), manganese (Mn), cadmium (Cd), nickel (Ni) and molybdenum (Mo) are shown in Johnsen et al. (2013). The hydrothermal deposits, also called Seafloor Massive Sulfide (SMS) deposits, contain copper, lead, zinc, silver and trace metals. In contrast, manganese nodules are polymetallic and usually contain higher concentrations of manganese, nickel, copper, cobalt, iron, silicon and aluminum (Glasby 2000, Johnsen et al. 2013 and references therein).

The amount of mineral deposits for DSM is still relatively unknown across the global ocean. A recent study from the Arctic Mid-Ocean Ridge at 2600 m noted that some regions of interest in the region, such as “Mohn’s Treasure”, has been described as a massive sulfide deposit, but the only evidence of mineralization found during the entire “MarMine" project survey over the area (13 ROV dives) was a few meters of oxidized basalt outcrops comprising minor pyrites and features possibly formed by diffuse discharges (Ludvigsen et al. 2016). Magnetic data collected during a cruise in this region suggested the presence of deposits buried under 15 m of sediments (Lim et al. 2019), which could be challenging for DSM operations to access.

10.1.2 Bioclastic Sediments

Bioclastic sediments in deep-sea environments are primarily composed of the remains of marine organisms, such as shells, corals and other skeletal remains. These skeletal fragments, also known as bioclasts, accumulate particularly in areas of high biological productivity and can be cemented together to form significant deposits like bioclastic limestone. Bioclastic sediment mining involves extracting these materials for various purposes, such as construction, agriculture, or industrial applications. For example, bioclastic limestone is utilized in construction as a source of aggregate for concrete and asphalt, and in agriculture to neutralize soil acidity.

Bioclastic sediments often contain high biomass of “filter feeders” (e.g., deep water stone corals, clams, snails, polychaetes). Marine carbonate sediment can be found both as calcite (rhombohedral crystal structure) and aragonite (orthorhombic crystals) with the same molecular formula, $CaCO_3$, but different crystalline structures. In shallow waters (light zone) aragonite is the dominating carbonate, while calcite

dominates in deep waters (Boggs 2010). Organisms associated with: aragonite include molluscs, gastropods, pteropods, chitons, cephalopods, coccolithophores, stromatolites, corals and annelids. Organisms associated with high magnesian calcite include echinoids, crinoids, benthic foraminifera, coralline red algae and coralline green algae. Organisms associated with low magnesian calcite include planktonic foraminifera and brachiopods.

Eco-physiological responses of cold-water soft corals to anthropogenic sedimentation and resulting changes in suspended particle shape, potentially related to DSM, may affect food uptake negatively. One of the reasons for this is caused by retraction and loss of polyps in the soft coral species *Duva florida* and gorgonian coral *Primnoa resedaeformis* (Liefmann et al. 2018).

UHI can identify and map bioclastic carbonate (fragments from dead organisms) sediments on the seafloor (Boggs 2010; Aarrestad 2014; Nevstad 2022). The presence of bioclastic deposits is indicated by “whiteness” of sediment, iron and organic content (e.g., biofilm, Dierssen et al. 2009; Johnsen et al. 2013; Aarrestad 2014). The largest carbonate areas are found in sub-tropical regions with clear warm waters. In addition, cold water coral habitats are found in cooler environments (usually below 8^{o}C) on continental shelves/slope and on sills in fjords (Hovland and Mortensen 1999; Mogstad et al. 2022). There are several cold-water coral habitats in the North Atlantic, and one of the largest reef structures is found at the Sula Reef in Northern Norway dominated by the stone coral *Lophelia pertusa* (new name *Desmophyllum pertusum*). The hard tissue of the coral consists of aragonite (living specimens on coral heads), while coral block (dead corals with intact skeleton) and rubble (weathered skeleton degraded into small particles) are found at the basis of the reefs (Hovland and Mortensen 1999; Fosså et al. 2005; Roberts et al. 2006; Mogstad et al. 2022). The Norwegian Geological Survey (NGU) reports difficulties in distinguishing bioclastic sediments from bedrock and optical techniques may provide this information (Bellec et al. 2014).

10.2 Marine Archaeology

Marine archaeology is the study of past human culture and history primarily through investigations of cultural heritage deposited on the bottom of the world’s oceans, lakes and river systems. Field methods have developed along with technological advances such as SCUBA-equipment, but also underwater sensors (e.g., side scanning sonar and underwater cameras) deployed on a range of instrument carrying platforms. In deep waters or other areas inaccessible to divers, field work is carried out by using ROVs and AUVs. Remotely operated excavations are inherently difficult even with the advanced robotic technology we have today, and robotic investigations of underwater cultural heritage (UCH) sites are currently limited to non-intrusive inspection and recording of features and objects *in situ.* UHI has a significant potential as a tool for close range remote sensing of UCH. Identification and classification of artefacts and substances/materials is central to analysis and interpretation of UCH sites.

Detection of objects or areas of interest on the seabed can be challenging with remote sensing technology. Acoustic sensors are well suited for registering salient

features that present distinct sonic signatures either as acoustic backscatter images or bathymetric patterns. Sedimentation, growth or disintegration may alter the perceivable morphological characteristics of man-made objects obstructing the possibilities for high confidence classification. Typically, a scientist will categorize possible targets with estimated potential for classification based on experience and expected signatures in acoustic data, and revisit for close range inspection and classification with optical cameras or other relevant sensors (Ødegård et al. 2016). Even at close range the shape and extent of objects or features may be obscured by sediments, growth or corrosion.

By using spectral reflectance measurements of possible targets and referring to spectral libraries or other ground truth data, it can be possible to detect and classify singular or compositions of materials directly associated with particular archaeological artefacts. Hyperspectral images of features on the seabed co-registered and overlayed RGB-image based photomosaics and bathymetric data could hence be used to create georeferenced maps of potential cultural heritage sites, with derived distribution maps at different spatial scales. This could enable analysis either by archaeological visual interpretation (grounded in empirical knowledge of wreck site formation processes) or statistical calculations of probability for presence of underwater cultural heritage without a human in the loop.

To facilitate such methods, efforts to build spectral libraries for typical cultural heritage materials common for historical wreck sites (ceramics, metals, glass, wood etc.) have been made from museum collections measured in the laboratory (e.g., at the Norwegian Technical University). Such libraries are limited to cultural contexts related to historical period, provenance, regional production etc. Thus, a library based on measurements made on medieval Northern European material will not be relevant for e.g., antique shipwrecks in the Mediterranean or colonial materials in America. For hyperspectral imagers to be used for *in situ* identification and classification, a relevant spectral library must be available. Collaborative efforts should be made to create libraries from different cultural contexts, incrementally contributing to a global database that can be openly accessible for science and management.

An example of UHI for marine archeology was conducted at 61 m at a wreck site of a wooden ship. The UHI-based measurement of reflectance could identify and map rust (from iron nails), glass bottles and ceramics (Figure 10.2). Rust and several types of ceramics obtain similar reflectance characteristics and may be hard to discriminate (Ødegård et al. 2018).

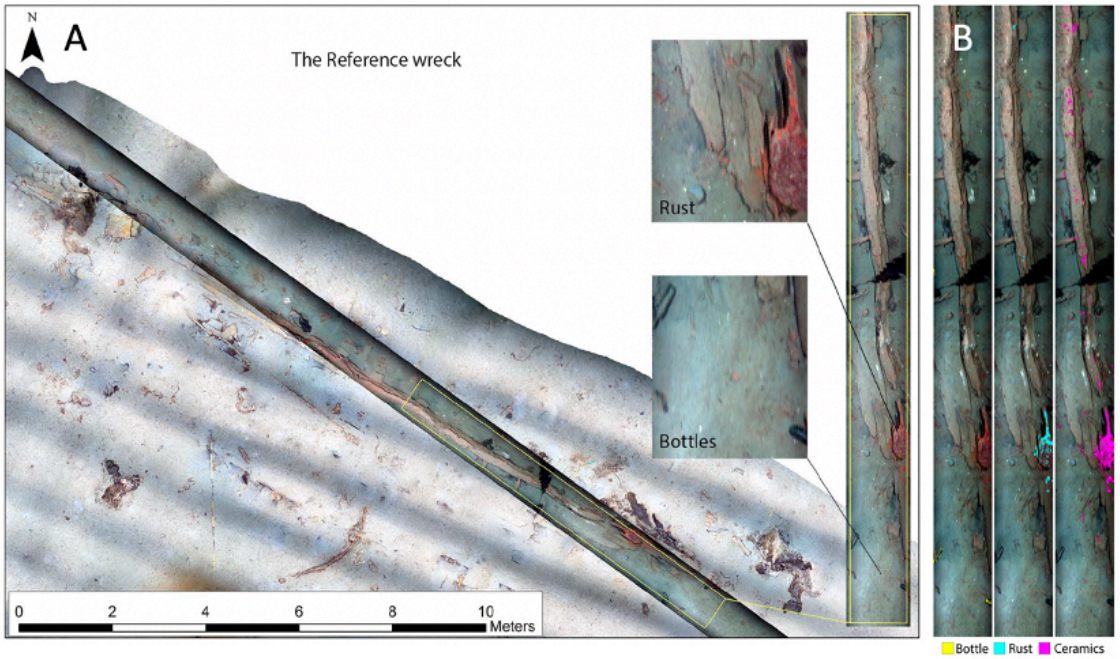

Figure 10.2 (a) ROV-based photomosaic from stereo-camera with corresponding UHI transect line on top. To the right are a section of UHI-transect line (yellow border) showing examples of OOIs containing rust and bottles. (b). UHI identified OOIs, bottles, rust and ceramics based on R(λ) per image pixel. Figures modified from Ødegård et al (2018), CC BY 4.0.

Initial UHI-investigations of historical shipwrecks indicate that certain materials attract different types of biological organisms (Mogstad et al. 2020). Typical examples are tunicates and red coralline algae are found on different types of wood, while copper plates are toxic for most species (seen by little epi growth) (Figure 10.3). Interdisciplinary efforts should be made to determine if classification of different marine organisms could be used as a proxy for mapping the spatial distribution and extent of cultural heritage or other human-made objects and features. Biological organisms are also important factors determining site formation processes, so spectral identification, classification and quantification of different organisms on shipwrecks could potentially be relevant for better understanding events and processes acting on UCH sites over time and be of value for reconstruction and analysis of both heritage objects and the surrounding environmental contexts.

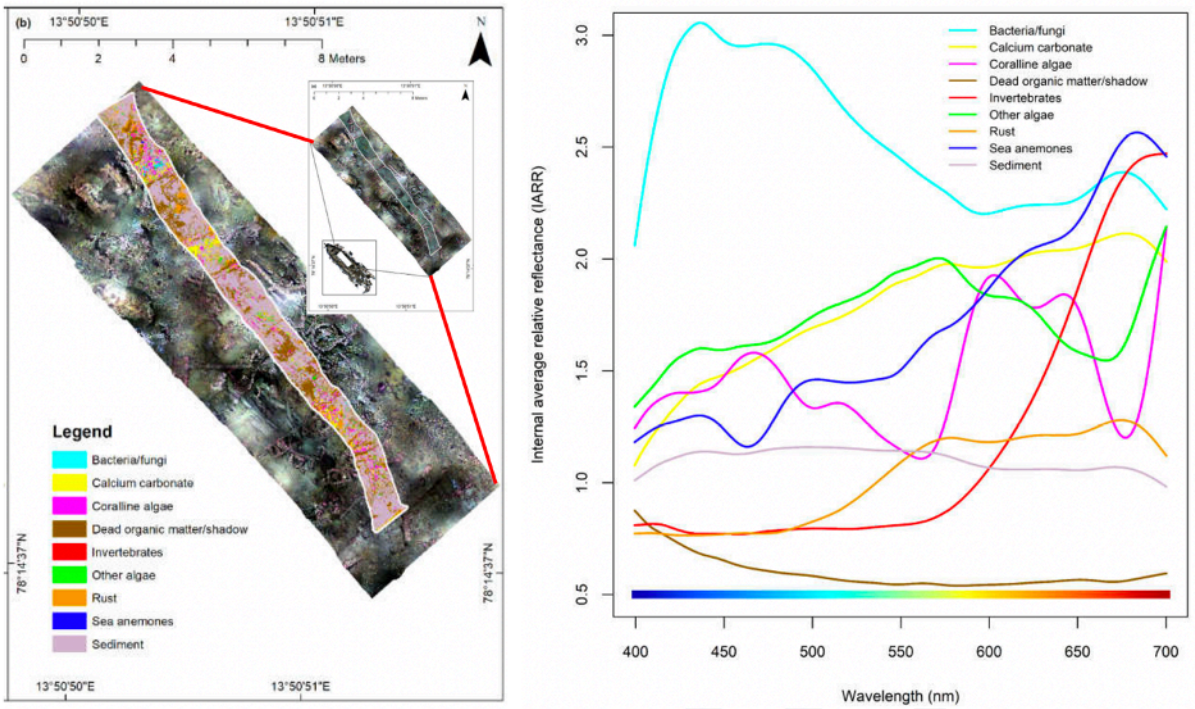

Figure 10.3 (Left) UHI of a whaling factory ship the "Figaro" at Trygghavna, Spitsbergen – the northernmost mapped shipwreck. (Right) Benthic reflectance derived from the UHI of different bottom types. Figure modified from Mogstad et al. (2020), CC BY 4.0.

10.3 Marine Litter and Debris

Marine litter is a growing global concern as it threatens both ecological and human health. Marine litter is defined by the UNEP (United Nations Environmental Program) as "any persistent, manufactured or processed solid material discarded, disposed of or abandoned in the marine and coastal environment". Marine litter is dominated by plastic materials but also includes other materials such as glass, metal, and rubber. Marine litter enters the environment both intentionally through illegal dumping but also unintentionally due to mismanaged or insecure waste processing. Both coastal and inland environments contribute to marine litter, as rivers are a key transport mechanism for litter entering the oceans (Lebreton et al. 2017).

Despite marine litter being a well-documented pollutant, more complex material flows such as release, distribution, transport, and deposition are poorly understood. Pelagic environments have been the primary focus of marine litter research which has led to discoveries of "missing" plastics – estimates suggest that marine litter on the ocean surface is only 1% of the expected stock based on input rates (Cózar et al. 2014; Van Sebille et al. 2015). This has led to a greater focus on the benthic environment as a key compartment for both macro (> 5 mm diameter) and micro (< 5 mm diameter) particles of anthropogenic origin. The benthic environment is now considered an important sink for marine litter which falls out from the surface and water column through a variety of biotic and abiotic processes (Egger et al. 2020).

Estimating the amount of marine litter in the benthic environment presents both practical and analytical challenges. Microplastics can be sampled with traditional sediment sampling methods (e.g., van Veen grab, box corer) and laboratory analysis, but larger debris items are more difficult to sample due to patchiness (Nakajima et al. 2021). Laboratory methods for plastic analysis typically use Fourier transform infrared spectroscopy (FTIR) to identify polymeric materials. FTIR is a mid-IR spectroscopic technique operating in the 2500 – 25 000 nm region of the IR spectrum. Operating in transmission, reflectance and attenuated total reflectance, FTIR is a flexible technique which can be used to create hyperspectral maps of small areas. Due to instrumentation used in FTIR spectrometers (interferometer), this is a time-consuming technique. Efforts to increase sample throughput have led to the exploration of near infrared hyperspectral imaging (NIR-HSI, 1000 – 2500 nm) as a faster analysis method (Faltynkova et al. 2021; Vidal and Pasquini 2021). Spectral features in the NIR region allow for identification of organic compounds (Garaba and Dierssen 2018), which makes polymer identification possible.

Briefly, samples from different environmental compartments can be processed to remove organic material and other interfering matrices. Following this extraction, particles can be imaged using diffuse reflectance mode of acquisition. Spectra from the hyperspectral images are classified using a variety of chemometric approaches (e.g., support vector machine, soft independent model of class analogy, k-nearest neighbour, spectral angle mapper) to simultaneously extract information about the size and shape of polymeric particles, as well as the polymer type.

In situ identification is more challenging, as infrared radiation is rapidly attenuated in the water column. Therefore, visible light is commonly used in benthic environments to detect marine debris. Visualizing and identifying macro-debris on the seafloor can be achieved using ROV or AUV systems equipped with light sources and video capabilities. Both RGB and multi/hyperspectral imaging can be used, however due to the heterogeneity (material, shape, size, colour, surface reflectance properties) of marine debris, spectral information may be of limited use. Using machine learning algorithms for image analysis relying on shape characteristics is a possible strategy for automated detection of marine debris from video and/or VIS hyperspectral imaging.

Other types of marine debris are also deposited on the seafloor. Surplus or outdated stockpiles of munitions from both world wars were typically dumped at sea in the mid 20th century. This practice took place all over the world, from very shallow to deep waters. As metal vessels corrode in seawater, we now see increased awareness from government agencies and other stakeholders of possible seepage from such dumping sites that can have harmful effects on water quality and marine life in affected areas. Detailed knowledge and understanding of such sites and their relevant formation processes are required for environmental mapping and monitoring, and not least the ability to predict potential threats such sites can pose to our oceans in the future. Reflectance data can be very relevant for establishing what geochemical processes are at work, and potentially assessing the degree of deterioration/corrosion and estimating time remaining until action must be taken.

Overall, mapping and monitoring of marine debris, including microplastics, poses a significant challenge both analytically and due to the scale of the marine environment. Decreasing processing time for sample handling or moving towards *in situ* methods could help propel research on fate and transport of marine debris to better understand important mechanisms and establish baselines for environmental monitoring. Interdisciplinary experiments involving archaeology, biogeochemistry and biology/ecology are needed to establish baselines for understanding these processes better.

Chapter 11

Emerging Technologies

Steve Ackleson, Ved Chirayath, Geir Johnsen

Recent advances in optical sensing technology have resulted in new and novel methods of measuring benthic reflectance using non-proximal methods. These include solid state imagers with high spectral resolution and contiguous representation of the entire visible light spectrum, underwater LiDAR capable of recording the full time-resolved return signal from each laser pulse, and above-water water methods that utilize natural wave-focusing to increase signal and resolve smaller benthic features. At the same time, advances in robotic technology and autonomous behavior have yielded new surveying platforms that operate on (Liu et al. 2016) and below (Chai et al. 2020) the water surface. The combination of these new sensors and platforms have yielded environmental data of high quality for less cost and effort, at temporal and spatial scales, and during environmental conditions that exceed what is possible with traditional human-based operations. In addition to new sensing and deployment modalities, real-time data analysis methods based on artificial intelligence are under development that are expected to optimize environmental surveys with multiple, cooperative platforms (Ryan et al. 2010).

11.1 Advanced Sensing

11.1.1 Underwater Hyperspectral Imaging

Hyperspectral imagers, originally developed for laboratory and remote sensing applications, have been integrated into watertight housings, generally referred to as underwater hyperspectral imagers (UHI), and deployed on various surface and sub-surface platforms for conducting benthic surveys (Ødegård et al. 2018; Johnsen et al. 2013; Mogstad et al. 2019 and 2022). . A UHI is essentially a radiometer that divides the collected light into many discrete, contiguous bands spread across the entire visible spectrum and focused onto a detector array. The Ecotone sensor, for example, is a line imager consisting of 1936 pixels spread across a 60^{o} field of view. Light is recorded in 50 – 800 discrete bands with spectral resolution between 2.2 nm and 5.5 nm with the spectral range and specifications dependent on the model (http://www.eelume.com). A hyperspectral image is formed by merging sequential lines of data collected along a survey path.

Unlike a non-imaging radiometer that can be deployed and operated to limit the effects of time-varying solar illumination, an imaging sensor will detect spatial patterns in reflected benthic light due to refraction of downwelling light as it propagates through a wavy sea surface. One method of mitigating uncertainty due to inconsistent illumination is to pair the UHI with a dedicated light source such as a lamp or banks of light emitting diodes. The addition of a dedicated illumination source also enables imaging operations in deeper environments (4200 m depth with ROV-UHI surveys) beyond the limit of solar light penetration (Sture et al. 2019) and

in optically shallow areas during night (Dumke et al. 2018, 2019; Johnsen et al. 2020; Sørensen et al. 2020; Summers et al. 2022).

The altitude of a UHI above the sea floor will impact image spatial resolution and signal intensity due to light attenuation by the intervening water column. Successful UHI benthic surveys, e.g., of coral reef cover have been accomplished with sensor altitudes of < 10 m (optimal range 1 to 3 m distance), depending on water clarity (Dumke et al. 2018; Mogstad and Johnsen 2017; Mogstad et al. 2019; Ødegård et al. 2018). An UHI deployed within the water column, either on an autonomous or remotely controlled platform or towed from a piloted boat is essentially the same as positioning a submerged spectroradiometer and is therefore applicable to the same non-proximal methods for determining benthic reflectance as described in Chapter 5.

11.1.2 Underwater Imaging LiDAR

LiDAR is a method of determining the distance between a laser source and a target by measuring the time of flight between an emitted light pulse and the return light reflected from a target. Since the first demonstration of LiDAR technology in the mid-1960s, applications to environmental problems have expanded enormously and continue to evolve (Kashani et al. 2015). Within aquatic environments, LiDAR has been used to map bathymetry (Guenther et al. 2000; Costa et al. 2009), benthic cover characteristics (Collin et al. 2011; Wilson et al. 2022), water column features (Chen et al. 2021, Zhou et al. 2022) and to locate marine animal species (Dubrovinskaya et al. 2018) using sensors deployed on ships, aircraft, satellites and, most recently, submerged platforms (Huot et al. 2022). In fact, the first commercially available underwater imaging LiDAR has recently been offered by BeamSea Associates, LLC, Loxahatchee, FL, USA (beam-sea.com). The highly focused energy of laser illumination offers a much greater depth of penetration compared with passive approaches which are typically limited to 1.5 Secchi depths. For LiDAR, viable laser returns can routinely be retrieved from up to 2–3 times the Secchi depth (Wang and Philpot, 2007).

Of all water parameters that influence the LiDAR signal water depth is the most easily and accurately determined and, therefore, was one of the first applications developed for aquatic environments (Figure 11.1). Since the speed of light through water is known, bottom depth is proportional to the time difference between the pulse generation and the peak return from the bottom. Neither does the approach depend on peak intensity, but only the detection of a peak associated with the bottom. However, to derive ρ_b it is necessary to accurately measure the magnitude of the return peak and to quantify the losses to the pulse energy within the intervening water column.
The canonical form of the LiDAR equation formulated for a sensor positioned above the water surface is

$$P_r = \frac{P_T \eta \rho_b F_p A_r \cos^2(\theta_a)}{\pi (n_w H + D)^2} e^{-2\, n\, KD \sec(\theta_w)} \qquad (11.1)$$

where P_r is the received power, P_T is the transmitted power, η is the sensor optical efficiency factor, ρ_b is benthic reflectance, F_p represents loss in received power due to insufficient field of view, A_r is the effective area of receiver optics, θ is the nadir transmit angle, n_w is the index of refraction of water relative to air, H is the altitude of the LiDAR above the water surface, D is bottom depth, n is the pulse stretching factor, K is the LiDAR apparent diffuse attenuation coefficient of water, and θ_w is the in-water nadir view angle after refraction at the water surface. Equation 11.1 cannot be solved directly for ρ_b without knowledge of all the other terms involved. Instead, simplifying assumptions such as constant system parameter values and negligible pulse stretching are required to reduce the complexity of the governing equation. A well used reformulation of the LiDAR equation is Equation 11.2:

$$P_r = P_T \rho_b W e^{-2KDsec(\theta_w)} \quad (11.2)$$

where W represents all associated loss terms. Wilson et al. (2022) developed data-driven approaches applied to airborne LiDAR measurements to remove depth and viewing geometry dependencies to yield apparent benthic reflectance, ρ_b'. Correcting the benthic signals for water column attenuation is accomplished with log transforms of the LiDAR signal from homogeneous regions of benthic cover spread across a range in depth and computing absolute reflectance from ρ_b' requires some a priori knowledge of ρ_b.

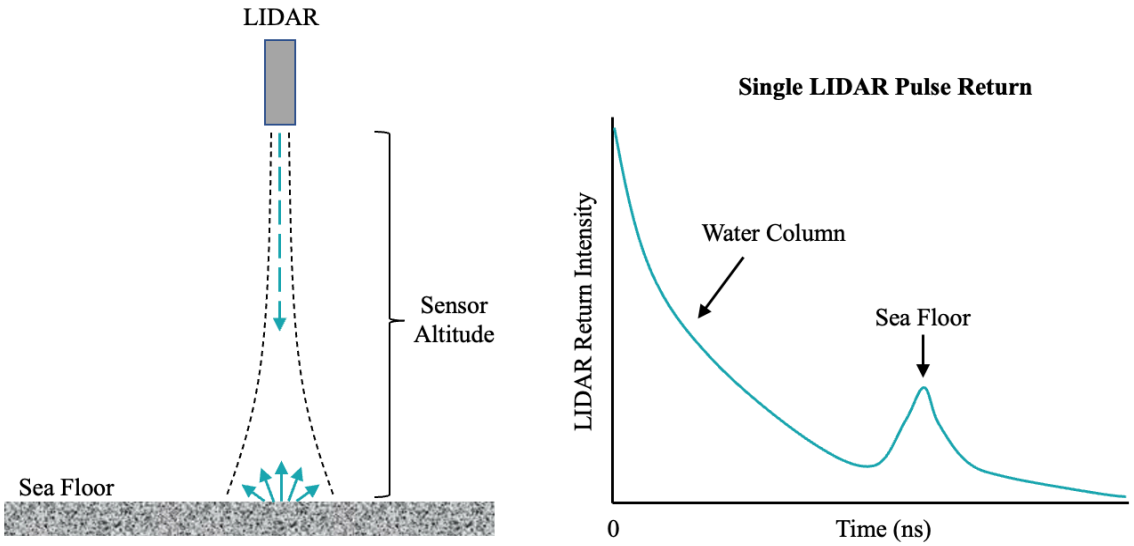

Figure 11.1 Illustrated submersible LiDAR position and orientation relative to the sea floor (left) and time series of the return signal intensity of a single LiDAR pulse (right).

An underwater LiDAR is not affected by uncertainty associated with refraction of the laser pulse through the air-water interface. While the form of the governing LiDAR equation is unchanged, uncertainty in W is reduced since the associated terms are only associated with sensor properties. However, removing the depth dependence of

the benthic signal still requires identifying similar regions of benthic cover at different depths in order to correct the benthic signal for water attenuation. Alternatively, drawing from the non-proximal, *in situ* approach (Chapter 5.5), Equation 11.2 can be solved for K and ρ_b using simultaneous expressions of LiDAR return from judiciously placed bottom targets of known reflectance. Such an approach would remove the uncertainty regarding benthic homogeneity with depth required by the data-driven approach.

Advantages of LiDAR over non-proximal radiometric approaches, especially when using a submerged sensor either towed by a small boat or deployed on an autonomous platform, are that measurements can be made day or night and night surveys will not be affected by caustics within the natural light field. A drawback to currently available LiDAR sensors is that they are monochromatic and centered on the emission wavelength of the laser. However, multispectral LiDAR systems have been developed and tested as experimental prototypes (Briese et al. 2012 & 2013) and pulsed laser sources are rapidly developing towards multispectral (e.g., Held and Schneider von Deimling, 2019) and hyperspectral versions (Chen et al. 2019).

A final point to be made about the LiDAR approach is that modern systems collect data as full wave form returns, i.e., the complete return time series associated with each laser pulse. Wilson et al. (2022) investigated the information content of the shape of the benthic return pulse collected over a coral reef. Simple statistical measures, such as integrated power under the benthic return curve and the standard deviation and skewness of the return signal distribution, have been correlated with high certainty with benthic rugosity and benthic cover type. Letard et al. (2022) showed promising results for mapping shallow benthic habitats by analyzing full waveform returns of a two-band topobathymetric LiDAR system.

11.1.3 Fluid Lensing

NASA has recently developed a novel remote sensing technology called fluid lensing that takes advantage of surface waves to focus downwelling light onto and magnify shallow benthic features (Chirayath & Earle, 2016; Chirayath, 2018; Chirayath & Li, 2019; Chirayath & Instrella, 2019). As light propagates through the air/water interface, the direction of propagation is modified by the change in the refractive index between the air and water (Figure 11.2). If the water surface is wavy, as is almost always the case, facets of waves that are curved convex towards the air will act as a lens to focus transmitted downwelling light at a depth from the surface defined by the focal length of the wave lenslet. If the wave facet is concave, the light will be spread out and defocused. The result will be a pattern of bright and dark illumination projected onto a shallow bottom, commonly seen on the bottom of a swimming pool on a bright, clear day. The bright illumination features are referred to as caustics. This illumination pattern is not static, but changes spatially as the waves propagate along the water surface. Fluid lensing takes advantage of this phenomenon by measuring a time series of imagery and for each image selecting only pixels associated with the caustics. Since the caustics move and change position defined by the surface wave dynamics, a series of segmented images collected over a long enough time period can then be combined to produce a

complete image where each pixel represents a portion of the scene brightly illuminated by a caustic. The advantage of this approach is to greatly increase the signal to noise of light reflected from benthic features. An added benefit of this approach is that each lenslet acts to magnify the benthic features and results in a much sharper merged image. The approach has been shown, using data collected by low-altitude drones, to yield cm-scale, 3D at depths down to ~19m (Chirayath, 2021).

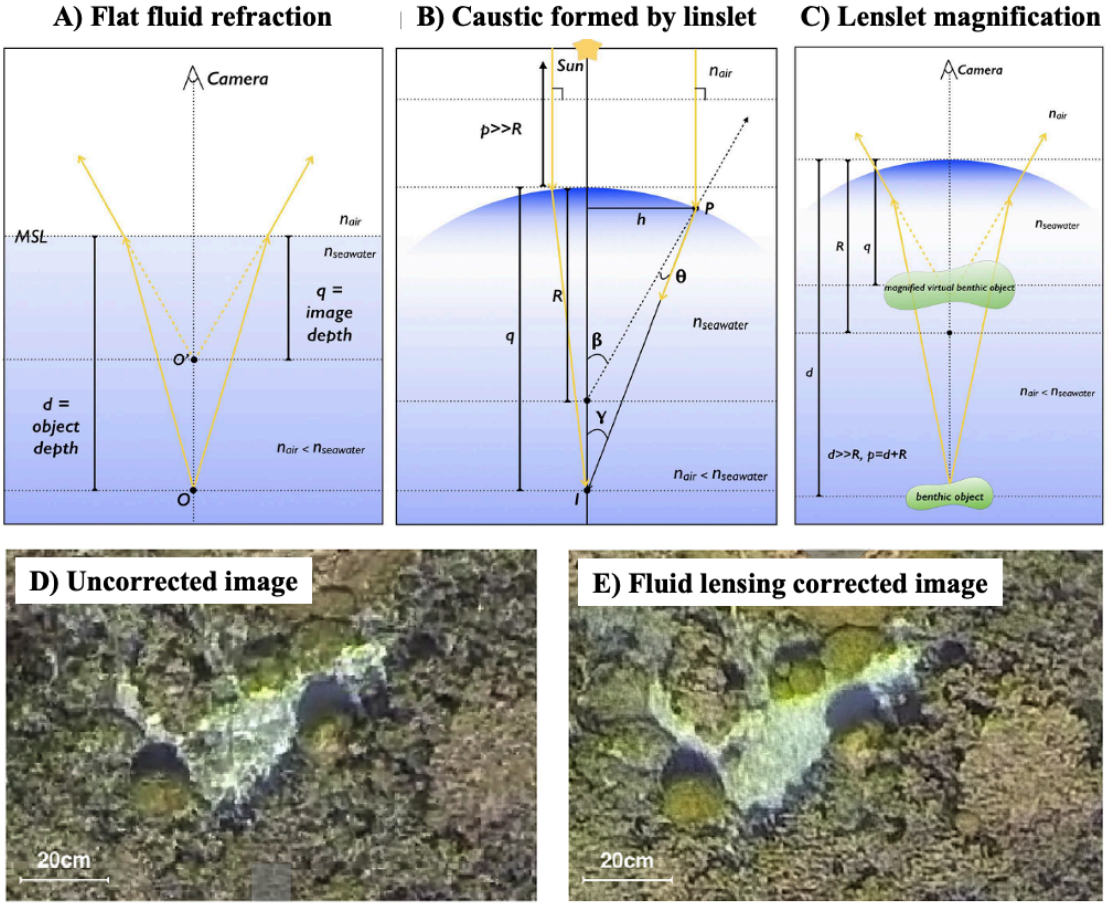

Figure 11.2 Fluid lensing concepts and examples. Light refracted through a flat (A) and wavy water surface forming caustics (B) and magnifying benthic features (C). An image of a shallow water environment uncorrected for wave distortion (D) clearly indicates the presence of caustics projected onto the bottom while the fluid lens corrected image (E) is sharper and free of distortions and caustics.

From a remote sensing perspective, fluid lensing shows great promise for spectrally imaging shallow water aquatic benthic environments at greater depths and with greater fidelity compared with traditional passive approaches. However, the retrieval of benthic reflectance will still suffer from the same problems associated with passive remote sensing such as removal of surface reflectance and correcting benthic signals for attenuation within the water column. An additional source of uncertainty associated with the approach is knowledge of the illumination intensity associated with individual caustics. A random surface wave field will result in lenslets of different focal lengths that produce caustics of different intensity when projected onto a bottom at any given depth. Knowledge of illumination intensity is critical for the accurate retrieval of reflectance.

11.1.4 Multispectral imaging, detection, and active reflectance (MiDAR)

In addition to detector design and implementation, light sources are also an important aspect of determining benthic reflectance. The use of submerged lamps in place of solar illumination and lasers used in LiDAR are examples of artificial light sources that collectively define active measurement systems. Multispectral Imaging, Detection, and Active Reflectance Instrument (MiDAR) is a spectral imaging approach that uses structured lighting from modulated LEDs to illuminate an environment of interest (Chirayath, 2018; Chirayath & Li 2019). When combined with a high sensitivity panchromatic detector array, the structured lighting can be used to generate multispectral images with well-controlled illumination. Such a system deployed below water can be used in combination with non-proximal approaches to construct imagery of benthic reflectance. Above water, the approach can be used day or night as an active fluid lensing imager to construct detailed benthic images at depths that potentially exceed traditional passive remote sensing approaches.

11.2 Remotely Operated and Autonomous Surveying Platforms

The development of new sensing technologies for measuring benthic reflectance addresses only part of the overall problem. The other necessary capability is the means of optimally deploying and positioning the sensors in order to yield the desired data. Investments in new sensing platforms over the past several decades have resulted in compact, robust systems that operate semi-autonomously on pre-determined survey instructions. An example is a platform that follows a survey route defined by GPS waypoints at a defined speed and, in the case of a sub-surface platform, range of platform depths and/or distances from the bottom. Initially, these systems were developed for surveying water column properties, e.g., temperature, salinity, and chlorophyll a concentration, in deep water. However, more recently, attention has focused on more dynamic and shallow coastal environments that are difficult to access using traditional survey methods.

Underwater hyperspectral imagers have been deployed on different types of platforms, including ROVs, AUVs, and Autonomous Surface Vehicles (ASVs). ROV operations are controlled in real-time by an above-water operator through an attached communications cable. Video cameras and platform orientation data indicate to the operator how best to position the radiometric sensors relative to an intended target. AUV operations tend to be used in deeper water and typically follow the seafloor bathymetry at a user defined standoff distance to limit the effects of signal attenuation within the intervening water. Benthic reflectance maps collected in this way have been used to characterize and monitor natural benthic cover and to identify human made objects of interest (Johnsen et al. 2013, 2020; Liu et al. 2020; Sørensen et al. 2020). Details regarding image correction due to platform pitch, roll, yaw, speed, and geoposition are outlined in Johnsen et al. (2013, 2016), Ludvigsen et al. (2014), Sørensen et al. (2020), Ludvigsen and Johnsen (2025)

Most recently, autonomous sensing and surveying of benthic reflectance has been conducted in shallow water environments with radiometers, in combination with a variety of ancillary environmental sensors, deployed on surface platforms (Figure 11.3). Ackleson et al. (2017) used an instrumented, self-navigating kayak towing a

radiometer buoy to survey shallow coral reefs in Kane'ohe Bay, Hawai'i in support of high-altitude hyperspectral remote sensing operations (Figure 11.4). The system recorded hyperspectral downwelling irradiance above the water surface, upwelling radiance measured just below the water surface, water depth, side-scan sonar imagery of the bottom, and high-definition photography to document benthic cover. The data were used to estimate ρ_b using the non-proximal techniques (ref: Equation, Section) using measurements of adjacent deep-water reflectance (r_{od}) and diffuse attenuation (K_d). Mogstad et al. (2019) used a Sea-Otter ASV (Martim Robotics, Trondheim, Norway) equipped with an Ecotone UHI to map shallow benthic habitats along the coast of Norway.

Another approach deploys above-water radiometers and a unique *in situ* profiling sensor package on a small ASV catamaran, LimnoVIS (Plattner et al. 2022). Remote sensing reflectance (R_{rs}) from the optically shallow water is computed using established protocols regarding measurement geometry relative to the sun location (Mueller et al. 2003). Following the successful Kane'ohe Bay surveys, Ackleson (2021) designed a new autonomous surveyor capable of providing, in addition to hyperspectral radiometry for non-proximal determinations of ρ_b, more complete descriptions of the shallow water environment including side-scan sonar for acoustical benthic mapping, water temperature, salinity, and optical properties, and vertical current profile. The platform design is essentially an instrumented outrigger system that can be attached to any recreational kayak and powered with standard 12 V marine batteries. The outrigger provides enhanced platform stability and the outrigger arms provide room to attach additional sensors such as an underwater imaging LiDAR.

For deep water applications, as noted in Chapter 10, underwater hyperspectral imagery has been performed down to 4200 m depth providing photomosaics of seafloor using ROVs (Dumke et al. 2018a,b). Recent UHI-surveys, using AUVs with self-propelled robotic arms or “snake robots” have been used from the surface down to -2000 m (Ludvigsen and Johnsen 2025, Sture et al. 2019). Figure 11.3 presents some examples of these new platforms (Fig. 11.3).

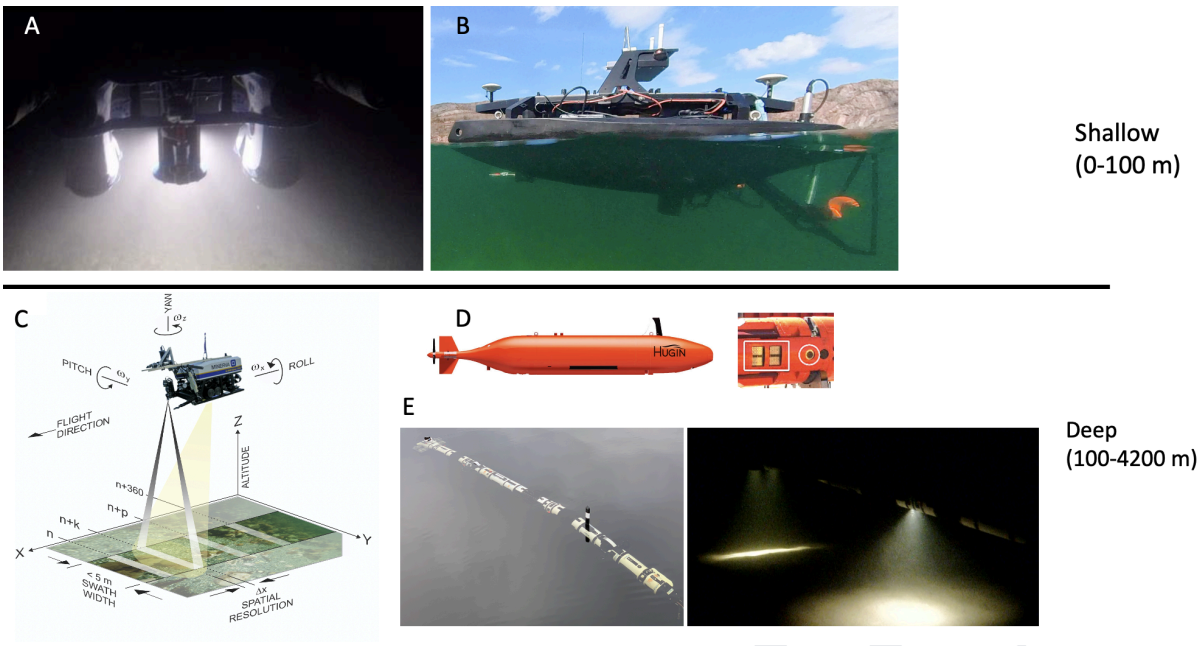

Figure 11.3 Overview of UHI-carrying mobile platforms for use in shallow or deep waters. A) Small battery-powered mini-ROV (BluEye)-UHI system (depth range 0-500 m) with total weight of 35 kg deployed from shore by 2 persons. Picture from mapping of brown-, green- and red macroalgae (1-5 m depth) survey during the Polar Night (Summers et al 2022). B) An ASV (Otter, Maritime Robotics, 65 kg) mapping seafloor habitats from 1-5 m depth (Mogstad et al. 2019). C) Mid size observation ROV (Sperre, 250 kg, depth rating 700 m) using dynamic position system (DP, acoustic communication vessel-ROV) providing <10 cm position accuracy. This ROV-UHI system requires a vessel with DP system, deck space for 15 m^2 ROV-container (including pilot room) and 4 persons (2 pilots, winch and umbilical handler and instrument person). See details in Johnsen et al. 2013, 2016, Ludvigsen et al. 2014 and Mogstad et al. 2022. Larger ROV-UHI systems have been used to map minerals at 4200 m depth (Dumke et al. 2018a,b). D) HUGIN 3000 AUV (5.5 m long, 1400 kg, Kongsberg Maritime) with UHI (depth rating 3000 m) and SeaLED lamps (Imenco 300, 4x130 W) used for mineral mapping at 2400 m depth at mid-Atlantic Ridge, detailed in Sture et al. (2017). E) an AUV with self-propelled robotic arms “snake robot” from Eelume equipped with UHI at surface (left) and at 250 m depth (right) identifying and mapping grenades using UHI with illumination for image slit (narrow light beam) and RGB camera using wide illumination in October 2024 (unpublished).

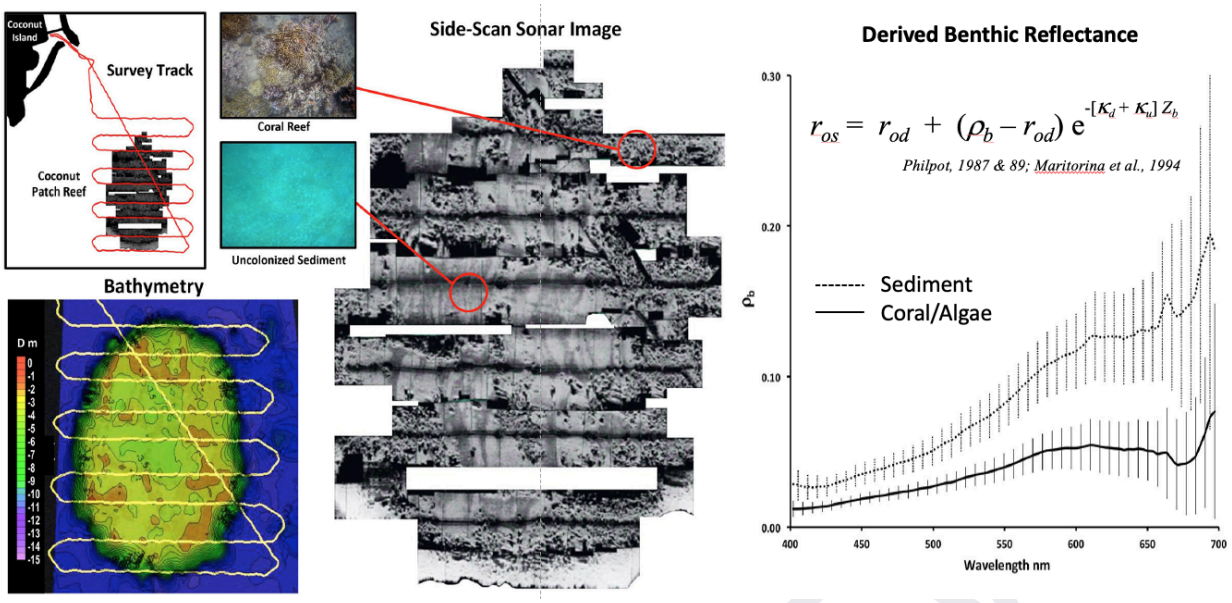

Figure 11.4 Autonomous survey of a small patch reef in Kaneohe Bay using a modified kayak equipped with a side-scan sonar and towing a radiometer buoy (Ackleson et al. 2017). Benthic reflectance was computed using non-proximal methods.

Abbreviations & Definitions

AUV	Autonomous Underwater Vehicle
ASV	Autonomous Surface Vehicle
$a_n(\lambda)$	Albedo of substrate n at wavelength λ
a(λ)	Absorption coefficient of a water body at wavelength λ
$b_{b(\lambda)}$	Backscattering coefficient of a water body at wavelength λ
B	Bottom boundary of an aquatic ecosystem as defined by user and/or the field of view of the instrumentation
Benthos	Flora and fauna found on the bottom boundary, or in the bottom sediments, of an aquatic ecosystem
Benthic	Of, relating to, or occurring at the bottom boundary of an aquatic ecosystem
BFT	Benthic Functional Type refers to a benthic community defined by its component set of organisms and substrates
BRDF	Bidirectional Reflectance Distribution Function
C	Concentrations of water constituent
CDOM	Chromophoric Dissolved Organic Matter
D	Distance between a sensor's optical lens and the target
DEM	Digital elevation model
DSM	Deep sea mining
f_n	Product of the areal fraction of substrate n within an pixel and its relative amplitude compared to the albedo in a spectral database
FOV	Field of View
FTIR	Fourier transform infrared spectroscopy
GFP	Green fluorescent protein
h	Height above benthos (m)
HSI	Hyperspectral imaging / imager
IOP	Inherent Optical Properties
IFOV	Instantaneous Field of View
K_d	Attenuation coefficient for downwelling irradiance
k_{uB}	Attenuation coefficient for upwelling irradiance from the bottom
k_{uW}	Attenuation coefficient for upwelling irradiance from the water layer
LED	Light-emitting diode
LiDAR	Light Detection and Ranging
MiDAR	Multispectral Imaging, Detection, and Active Reflectance Instrument
NAP	Non-algal particles
NIR	Near infrared
R_B	Irradiance Reflectance of the benthic target
RGB	Red green blue
Rrs	Remote Sensing Reflectance
ROV	Remotely Operated Vehicle
SF	Sampling footprint
SAS	Synthetic Aperture Sonar
SAV	Submerged aquatic vegetation
SNR	Signal-to-Noise Ratio

TSM	Total Suspended Matter
UCH	Underwater cultural heritage (site)
UHI	Underwater Hyperspectral Imaging
UV	Ultraviolet spectrum
VIS	Visible light
VSF	Volume Scattering Function
z_B	Depth of bottom (bathymetry) (m)
	Depth in water of measurement (m)

References

Aarrestad, S. (2014). Use of Underwater Hyperspectral Imagery for geological characterization of seabed. NTNU MSc thesis, 185 pp.

Aas, E. (1987). Two-stream irradiance model for deep waters. Appl. Opt., 1987, 26, 2095-2101.

Abbott, I.A. and Hollenberg, G.J. (1976) Marine Algae of California. Stanford University Press.

Ackleson, S. G. 2021. Robotic Surveyors for Shallow Coastal Environments. Oceanography, doi: 10.5670/oceanog.2021.supp02.xx.

Ackleson , S., Klemas. V. (1986). Two-flow simulation of the natural light field within a canopy of submerged aquatic plants. Applied Optics 25: 1129–1136, doi:10.1364/AO.25.001129

Ackleson, S. G., J. P. Smith, L. M. Rodriguez, W. J. Moses, and B. J. Russell. 2017. Autonomous coral reef survey in support of remote sensing. Front. Mar. Sci. 4:325, doi: 10.3389/fmars.2017.00325.

Adams, M. S., Scarpace, F. L., Scherz, J. P., and Woelkerling, W. J. (1977). Assessment of Aquatic Environments by Remote Sensing. IES Report 84. Environmental Monitoring and Data Acquisition Group. Institute for Environmental Studies. University of Wisconsin-Madison.

Adams, J.B., Smith, M.O., Johnson, P.E. (1986) Spectral mixture modeling: A new analysis of rock and soil types at the Viking Lander 1 site. Journal of Geophysical Research 91(B8):8098-8112.

Albert, A. and Mobley, C. (2003). An analytical model for subsurface irradiance and remote sensing reflectance in deep and shallow case-2 waters. Opt. Express 2003, 11, 2873-2890.

Al-Janabi, B., Kruse, I., Graiff, A., Winde, V., Lenz, M., and Wahl, M.(2016) Buffering and amplifying interactions among OAW (Ocean Acidification and Warming) and nutrient enrichment on early life-stage Fucus vesiculosus L. (Phaeophyceae) and their carry over effects to hypoxia impact, PLoS ONE, 11, e0152948, https://doi.org/10.1371/journal.pone.0152948,

Andersson, I. (2017). Bio-optical diversity on cold water coral habitats. NTNU, Trondheim, Norway. MSc thesis, 84 pp.

Andréfouët, S., Hochberg, E. J., Payri, C., Atkinson, M. J., Muller-Karger, F. E., & Ripley, H. (2003a). Multi-scale remote sensing of microbial mats in an atoll environment. International Journal of Remote Sensing, 24(13), 2661-2682.

Andréfouët, S., P. Kramer, D. Torres-Pulliza, and others. (2003b). Multi-site evaluation of IKONOS data for classification of tropical coral reef environments. Remote Sensing of Environment 88: 128–143.

Andréfouët, S., Payri, C., Hochberg, E. J., Che, L. M., & Atkinson, M. J. (2003c). Airborne hyperspectral detection of microbial mat pigmentation in Rangiroa atoll (French Polynesia). Limnology and Oceanography, 48(1part2), 426-430.

Arabi, B., Mhd.S. Salama, D. van der Wal, J. Pitarch and W. Verhoef (2020). The impact of sea bottom effects on the retrieval of water constituent concentrations from MERIS and OLCI images in shallow tidal waters supported by radiative transfer modeling, Remote Sensing of Environment, 237.

Armstrong, R. A. (1993) Remote sensing of submerged vegetation canopies for biomass estimation. International Journal of Remote Sensing 14: 621–627.

Ball, D. W. (2006). Field guide to spectroscopy (Vol. 8). Bellingham, Washington: Spie Press.

Bajjouk Touria, Jauzein Cecile, Drumetz Lucas, Dalla Mura Mauro, Duval Audrey, Dubois Stanislas (2020). Hyperspectral and Lidar: Complementary Tools to Identify Benthic Features and Assess the Ecological Status of Sabellaria alveolata Reefs . Frontiers In Marine Science , 7, 575218 (16p.) https://doi.org/10.3389/fmars.2020.575218

Baranoski, G.V.G. (2006). Modeling the interaction of infrared radiation (750 to 2500 nm) with bifacial and unifacial plant leaves. Remote Sens. Environ. 2006, 100, 335–347.

Barnes, B. B., R. Garcia, C. Hu, and Z. Lee. (2018) Multi-band spectral matching inversion algorithm to derive water column properties in optically shallow waters: An optimization of parameterization. Remote Sensing of Environment 204: 424–438.

Barrett, J. and Anderson, J.M. (1980) 'The P-700-chlorophyl a-protein complex and two major light-harvesting complexes of Acrocarpia paniculata and other brown seaweeds', BBA - Bioenergetics, 590(3), pp. 309–323. Available at: https://doi.org/10.1016/0005-2728(80)90202-9.

Bastidas C, Benzie JAH, Uthicke S, Fabricius KE (2001) Genetic differentiation among populations of a broadcast spawning soft coral, Sinularia flexibilis, on the Great Barrier Reef. Mar Biol 138:517-525

Bell, T.W., Cavanaugh, K.C. and Siegel, D.A. (2015) 'Remote monitoring of giant kelp biomass and physiological condition: An evaluation of the potential for the Hyperspectral Infrared Imager (HyspIRI) mission', Remote Sensing of Environment, 167, pp. 218–228. Available at: https://doi.org/10.1016/j.rse.2015.05.003.

Bell, T.W., Cavanaugh, Ky.C., Saccomanno, V.R., Cavanaugh, Ka.C., Houskeeper, H.F., Eddy, N., Schuetzenmeister, F., Rindlaub, N., Gleason, M. (2023), Kelpwatch: A new visualization and analysis tool to explore kelp canopy dynamics reveals variable response to and recovery from marine heatwaves, PLOS ONE, 18, e0271477.

Bellec, V., Thorsnes, T., & Bøe, R. (2014). Mapping of bioclastic sediments - data, methods and confidence. Trondheim: Geological Survey of Norway. Rapport.nr. 2014.006.

Ben-Yosef DZ, Benayahu Y (1999) The gorgonian coral Acabaria biseralis: life history of a successful colonizer of artificial substrata. Mar Biol 135:473-481

Berner T (1990) Coral-reef algae. In: Dubinsky Z (ed) Ecosystems of the World 25: Coral Reefs. Elsevier, Amsterdam, pp253-264

Besterman, A.F., K.J. McGlathery, M.A. Reidenbach, P.L. Wiberg, and M.L. Pace. Predicting benthic macroalgal abundance in shallow coastal lagoons from geomorphology and hydrologic flow patterns. Limnol. Oceanogr., 66:123-140, doi: 10.1002/ino.11592.

Bidigare RR, Ondrusek ME, Morrow JH, Kiefer DA (1990) In vivo absorption properties of algal pigments. Ocean Optics X 1302:290-302

Birchenough, S. N. R., Phillip Williamson, and Carol Mary Turley. (2017) "Future of the sea: ocean acidification." Review of ocean acidification. Foresight Future of the Sea Project, Government Office Science.

Birchenough, S.N.R., Reiss, H., Degraer, S., Mieszkowska, N., Borja, ´A., Buhl-Mortensen, L., Braeckman, U., Craeymeersch, J., De Mesel, I., Kerckhof, F., Kr¨oncke, I., Parra, S., Rabaut, M., Schr¨oder, A., Van Colen, C., Van Hoey, G., Vincx, M., W¨atjen, K., (2015). Climate change and marine benthos: a review of existing research and future directions in the North Atlantic. Wiley Interdisciplinary Reviews: Climate Change 6, 203–223.

Boggs, S. J. (2010). Principles of Sedimentology and Stratigraphy. (4th international ed.). Upper Saddle River, Pearson Prentice Hall.

Bohren, C.F. (1987). Multiple scattering of light and some of its observable consequences. American Journal of Physics 55, 524-533.

Borrego-Acevedo, R., C. M. Roelfsema, S. R. Phinn and A. R. Grinham (2014). "Predicting Distribution of Microphytobenthos Abundance on a Reef Platform by Combining in Situ Underwater Spectrometry and Pigment Analysis." Remote Sensing Letters, https://doi.org/10.1080/2150704X.2014.922723

Botha, E.H., Brando, V.E., Anstee, J.M., Dekker, A.G.& Sagar, S. (2013) Increased spectral resolution enhances coral detection under varying water conditions, Remote Sensing of Environment 131: pp 247–261 http://dx.doi.org/10.1016/j.rse.2012.12.021

Brando, V.E., Anstee, J.M., Wettle, Dekker, A.G., Phinn, S.R., and Roelfsema, C. (2009). A Physics Based Retrieval and Quality Assessment of Bathymetry from Suboptimal Hyperspectral Data. Remote Sens. Environ. 113: 755-770, 10.1016/j.rse.2008.12.003

Bricaud, A, Morel, A, Babin, M., Allali, K. and Claustre, H. (1998). Variations of light absorption by suspended particles with the chlorophyll-a a concentration in oceanic (Case 1) waters: Analysis and implications for bio-optical models. J. Geophy. Res. 1998, 103, 31033–31044.

Briese, C., M. Pfennigbauer, H. Lehner, A. Ullrich, W. Wagner, and N. Pfeifer. 2012. Radiometric calibration of multi-wavelength airborne laser scanning data. ISPRS Ann. Photogramm. Remote Sens. Spat. Inf. Sci, vol. 1, pp. 335–340.

Briese, C., M. Pfennigbauer, A. Ullrich, and M. Doneus. 2013. Multi-wavelength airborne laser scanning for archaeological prospection. Int. Arch. Photogramm. Remote Sens. Spat. Inf. Sci, vol. 40, pp. 119–124.

Brocke, H., Holtrop, T., Kandukuri, R., Rigot, G., Lesage, A.-L., Oehlmann, N., den Haan, J. (2024). Closing the data gap – Automated seafloor health maps to accelerate nature-based solutions. The International Hydrographic Review, 30(1), pp. 136-142. https://doi.org/10.58440/ihr-30-1-c03

Buddemeier R, Smith SV (1999) Coral adaptation and acclimatization: a most ingenious paradox. Am Zool 39:1-9
Buhl-Mortensen, L., Hodnesdal, H., & Thorsnes, T. (Eds.) (2010). Til bunns i Barentshavet og havområdene utenfor Lofoten–ny kunnskap fra MAREANO for økosystembasert forvaltning. Trondheim: Norges geologiske undersøkelse.
Bukata, R. P., Jerome, J. H., Kondratyev, K. Y., Pozdnyakov, D. V., 1995. Optical Properties and Remote Sensing of Inland and Coastal Waters. CRC Press, Boca Raton – New York – London – Tokyo.
Bush A, Sollmann R, Wilting A, Bohmann K, Cole B, Balzter H, Martius C, Zlinszky A, Calvignac-Spencer S, Cobbold CA, Dawson TP. (2017) Connecting Earth observation to high-throughput biodiversity data. Nature ecology & evolution. 2017 Jun 22;1(7):0176.
Casal, G., Kutser, T., Domínguez-Gómez, J.A., Sánchez-Carnero, N., Freire, J. (2011a). Mapping benthic macroalgal communities in the coastal zone using CHRIS-PROBA mode 2 images. Estuarine, Coastal and Shelf Science, 94 (3): 281-290 https://doi.org/10.1016/j.ecss.2011.07.008
Casal, G., Sánchez-Carnero, Domínguez-Gómez, Kuster, T., Freire, J. (2012). Assessment of AHS (Airborne Hyperspectral Scanner) sensor to map macroalgal communities on the Ría de Vigo and Ría de Aldán coast (NW Spain). Marine Biology, 159: 1997-2013.
Casal, G., Sánchez-Carnero, N., Sánchez-rodríguez, E., Freire, J. (2011b). Remote sensing with SPOT-4 for mapping kelp forests in turbid waters on the south European Atlantic shelf. Estuarine, Coastal and Shelf Science, 91: 371-378. https://doi.org/10.1016/j.ecss.2010.10.024
Casal. G., Kutser, T., Domínguez-Gómez, J.A., Sánchez-Carnero, N., Freire, J. (2013). Assessing of the hyperspectral sensor CASI-2 for macroalgal discrimination on the Ría de Vigo coast (NW Spain) using field spectroscopy and modelled spectral libraries. Continental Shelf Research, 55: 129-140 https://doi.org/10.1016/j.csr.2013.01.010
Castagna, A., L. Amadei Martínez, M. Bogorad, and others. 2022. Optical and biogeochemical properties of Belgian inland and coastal waters. Earth System Science Data Discussions 2022: 1–39.
Cavanaugh, K. C., Reed, D. C., Bell, T. W., Castorani, M. C., & Beas-Luna, R. (2019). Spatial variability in the resistance and resilience of giant kelp in southern and Baja California to a multiyear heatwave. Frontiers in Marine Science, 6, 413.https://doi.org/10.3389/fmars.2019.00413.
Cavanaugh, K. C., D. A. Siegel, B. P. Kinlan, and D. C. Reed. (2010) Scaling giant kelp field measurements to regional scales using satellite observations. Marine Ecology Progress Series 403: 13–27.
Chai, F., K.S. Johnson, H. Claustre, X. Xing, Y. Wang, E. Boss, S. Riser, K. Fennel, O. Schofield, and A. Sutton. 2020. Monitoring ocean biogeochemistry with autonomous platforms. Nat. Rev. Earth Environ., 1:315–326, doi: 10.1038/s43017-020-0053-y.
Chapman, M.G., T.J. Tolhurst, R.J. Murphy, and A.J. Underwood. 2010. Complex and inconsistent patterns of variation in benthos, micro-algae, and sediment over multiple spatial scales. Mar. Ecol. Prog. Ser., 398:33-47, doi: 10.3354/meps08328.
Chen, P., C. Jamet, Z.Z. Zhang, Y. He, Z. Mao, D. Pan, T. Wang, and D. Yuan. 2021. Vertical distribution of subsurface phytoplankton layer in South China Sea using airborne lidar. Rem. Sens. Environ., 263:112567, doi: 10.1016/j.rse.2021.112567.
Chirayath, V. 2018. System and Method for Imaging Underwater Environments Using Fluid Lensing. United States Patent and Trade Office, 62/634,803, 2018. [Online]. Available: https://patents.google.com/patent/US10041833B1/en.
Chirayath, V. and A. Li. 2019. Next-Generation Optical Sensing Technologies for Exploring Ocean Worlds—NASA FluidCam, MiDAR, and NeMO-Net. Front Mar Sci, vol. 6, no. September, 2019, doi: 10.3389/fmars.2019.00521.
Chirayath, V. and R. Instrella, “Fluid lensing and machine learning for centimeter-resolution airborne assessment of coral reefs in American Samoa,” Remote Sens Environ, vol. 235, no. September 2018, p. 111475, 2019, doi: 10.1016/j.rse.2019.111475.
Chirayath, V. “Airborne Fluid Lensing for Precision Reef Mapping--New Results from Guam’s Priority Coral Reefs,” in Hyperspectral Imaging and Sounding of the Environment, 2021, pp. HTu2C--1.

Cochrane S, Ekehaug S, Pettersen R, Refit E, Hansen I, Aas L. Detection of deposited drill cuttings on the sea floor-A comparison between underwater hyperspectral imagery and the human eye. Marine pollution bulletin. 2019; 145:67–80. https://doi.org/10.1016/j.marpolbul.2019.04.031 PMID: 31590836 JTECH-D-19-0139.1

Coddington, O. M., E. C. Richard, D. Harber, and others. 2023. Version 2 of the TSIS-1 Hybrid Solar Reference Spectrum and Extension to the Full Spectrum. Earth and Space Science 10: e2022EA002637. doi:10.1029/2022EA002637

Collin, A., P. Archambault, and B. Long. 2011. Predicting species diversity of benthic communities within turbid nearshore using full waveform bathymetric LiDAR and machine learners. PloS One 6(6): e21265, doi: 10.1371/journal.pone.0021265.

Colombo-Pallotta, M.F., García-Mendoza, E. and Ladah, L.B. (2006) 'Photosynthetic Performance, Light Absorption, and Pigment Composition of Macrocystis Pyrifera (laminariales, Phaeophyceae) Blades from Different Depths', Journal of Phycology, 42(6), pp. 1225–1234. Available at: https://doi.org/10.1111/j.1529-8817.2006.00287.x.

Conger C, Fletcher C, Hochberg E, Frazer N, Rooney J (2009) Remote sensing of sand distribution patterns across an insular shelf: Oahu, Hawaii. Marine Geology 267:175-190

Connell JH (1997) Disturbance and recovery of coral assemblages. Coral Reefs 16:S101-S113

Costa, B.M., T.A. Battista, and S.J. Pittman. (2009). Comparative evaluation of airborne LiDAR and ship-based multibeam SoNAR bathymetry and intensity for mapping coral reef ecosystems. Rem. Sen. Environ. 113 (5): 1082–1100, doi: 10.1007/s12237-019-00652-9.

Costello, M. J., McCrea, M., Freiwald, A., Lundälv, T., Jonsson, L., Bett, B. J., et al. (2005). "Role of Cold-Water Lophelia pertusa Coral Reefs as Fish Habitat in the NE Atlantic," in Cold-Water Corals and Ecosystems. Eds. A. Freiwald and J. M. Roberts (Berlin: Springer), 771–805.

Cózar, A., Echevarría, F., González-Gordillo, J.I., Irigoien, X., Úbeda, B., Hernández-León, S., Palma, Á.T., Navarro, S., García-de-Lomas, J. and Ruiz, A. (2014) Plastic debris in the open ocean. Proceedings of the National Academy of Sciences. 2014;111(28):10239-10244.

Cummings, M., and R. Zimmerman. (2003). Light harvesting and the package effect in Thalassia testudinum Koenig and Zostera marina L.: Optical constraints on photoacclimation. Aquat. Bot. 75: 261-274.

Davies, J. S., Guillaumont, B., Tempera, F., Vertino, A., Beuck, L., Ólafsdóttir, S. H., et al. (2017). A New Classification Scheme of European Cold-Water Coral Habitats: Implications for Ecosystem-Based Management of the Deep Sea. Deep Sea Res. II 145, 102–109. doi: 10.1016/j.dsr2.2017.04.014

Dekker, A.G. (2021) Aquatic Spectral Library Phase II, Commissioned by Geoscience Australia-Digital Earth Australia; SatDek Pty Ltd, Sutton, NSW, Australia: pp 28. For further information see Australian National Spectral Database (NSD) service: https://cmi.ga.gov.au/data-products/dea/643/australian-national-spectral-database

Dekker, A. G., Anstee, J. M., and Brando, V. E. (2005) Retrospective seagrass change detection in a shallow coastal tidal Australian lake, Rem. Sens. Environm. Vol. 97 (4), pp. 415-433.

Dekker, A.G., Clementson, L.A., Wettle, M., Cherukuru, N., Botha, H. and Oubelkheir, K. (2022) Bio-Optical Measurements Indicative of Biogeochemical Transformations of Ocean Waters by Coral Reefs"; Special Issue Advances in Remote Sensing and Mapping for Integrated Studies of Reef Ecosystems in Oceania (Great Barrier Reef and Beyond), Remote Sens. 2022, 14(12), 2892; https://doi.org/10.3390/rs14122892

Dekker, A.G., Phinn, S.R., Anstee, J.M., Bissett, P. Brando ,V.E., Casey, B. Fearns, P., Hedley, J., Klonowski, W., Lee, Z.P., Lynch, M., Lyons, M., Mobley, C. and Roelfsema, C. (2011). Intercomparison of shallow water bathymetry, hydro-optics and benthos mapping techniques in Australian and Caribbean coastal environments; Limnology & Oceanography Methods. 9: 396-425. | DOI: 10.4319/lom.2011.9.396

Di Franco, S., Salzano, R., Boldrini, E., Salvatori, R. (2022). Increasing the interoperability of snow/ice hyperspectral observations. Computers & Geosciences, 162:105076.

Dierssen, H. M. (2010) Benthic ecology from space: optics and net primary production in seagrass and benthic algae across the Great Bahama Bank. Mar. Ecol. Progress Ser. 411: 1–15. doi:10.3354/meps08665.

Dierssen, H. M., S. G. Ackleson, K. E. Joyce, E. L. Hestir, A. Castagna, S. Lavender, and M. A. McManus. (2021) Living up to the hype of hyperspectral aquatic remote sensing: science, resources and outlook. Frontiers in Environmental Science 9.

Dierssen, H. M., K. J. Bostrom, A. Chlus, K. Hammerstrom, D. R. Thompson, and Z. Lee. (2019) Pushing the limits of seagrass remote sensing in the turbid waters of Elkhorn Slough, California. Remote Sensing 11: 1664.
Dierssen, H. M., Gierach, M., Guild, L. S., Mannino, A., Salisbury, J., Schollaert Uz, S., ... & Werdell, P. J. (2023). Synergies between NASA's hyperspectral aquatic missions PACE, GLIMR, and SBG: Opportunities for new science and applications. Journal of Geophysical Research: Biogeosciences, 128(10), e2023JG007574.
Dierssen, H. M., R. C. Zimmerman, and D. J. Burdige. (2009). Optics and remote sensing of Bahamian carbonate sediment whitings and potential relationship to wind-driven Langmuir circulation. Biogeosciences 6: 487–500.
Dierssen, H. M., R. C. Zimmerman, L. A. Drake, and D. Burdige. (2010) Benthic ecology from space: optics and net primary production in seagrass and benthic algae across the Great Bahama Bank. Marine Ecology Progress Series 411: 1–15.
Dierssen, H. M., R. C. Zimmerman, R. A. Leathers, T. V. Downes, and C. O. Davis. (2003) Ocean colour remote sensing of seagrass and bathymetry in the Bahamas Banks by high-resolution airborne imagery. Limnology & Oceanography 48: 444–455. doi:10.4319/lo.2003.48.1_part_2.0444
Done, T. J. (1982). "Patterns in the distribution of coral communities across the central Great Barrier Reef." Coral Reefs 1(2): 95-107.
Dörnhöfer, K.; Göritz, A.; Gege, P.; Pflug, B.; Oppelt, N. (2016) Water constituents and water depth retrieval from Setinel-2A – a first evaluation in an oligotrophic lake. Remote Sensing 2016/7/941, doi:10.3390/rs811094
Douay, F.; Verpoorter, C.; Duong, G.; Spilmont, N.; Gevaert, F. (2022) New Hyperspectral Procedure to Discriminate Intertidal Macroalgae. Remote Sens. 14, 346. DOI: 10.3390/rs14020346
Dove SG, Takabayashi M, Hoegh-Guldberg O (1995) Isolation and partial characterization of the pink and blue pigments of Pocilloporid and Acroporid corals. Biol Bull 189:288-297
Dove SG, Hoegh-Guldberg O, Ranganathan S (2001) Major colour patterns of reef-building corals are due to a family of GFP-like proteins. Coral Reefs 19:197-204
Drake, L., F. Dobbs, and R. Zimmerman. (2003) Effects of epiphyte load on optical properties and photosynthetic potential of the seagrasses Thalassia testudinum Koenig and Zostera marina L. Limnol. Oceanogr. 48: 456-463.
Duarte, C.M. (2017) Reviews and synthesis: Hidden forests, the role of vegetated coastal habitats in the ocean carbon budget. Biogeosci. 14: 301-310. DOI: 10.5194/bg-14-301-2017
Dubrovinskaya, F. Dalgleish, B. Ouyang and P. Casari, (2018) "Underwater LiDAR Signal Processing for Enhanced Detection and Localization of Marine Life," 2018 OCEANS - MTS/IEEE Kobe Techno-Oceans (OTO), 2018, pp. 1-8, doi:10.1109/OCEANSKOBE.2018.8559113.
Dumke I, Ludvigsen M, Ellefmo S, Søreide F, Johnsen G, Murton BJ (2019). Underwater hyperspectral imaging using a stationary platform in the Trans-Atlantic geotraverse hydrothermal field. Transactions on Geoscience Remote Sens, IEEE (online publ 24 Dec 2018). 57:2947-2962. DOI: 10.1109/TGRS.2018.2878923.
Dumke, I., Nornes, S.M., Purser, A., Marcon, Y., Ludvigsen, M., Ellefmo, S.L., Johnsen, G. and Søreide, F. (2018a). First hyperspectral imaging survey of the deep seafloor: high-resolution mapping of manganese nodules. Remote Sensing of Environment. 209:19-30. https://doi.org/10.1016/j.rse.2018.02.024
Dumke, I., Purser, A., Marcon, Y., Nornes, S.M., Johnsen, G., Ludvigsen, M. and Søreide, F. (2018b). Underwater hyperspectral imaging as an in situ taxonomic tool for deep-sea megafauna. Scientific Reports. 8:12860 | DOI:10.1038/s41598-018-31261-4.
Egger, M., Sulu-Gambari, F. and Lebreton, L. (2020). First evidence of plastic fallout from the North Pacific Garbage Patch. Scientific reports. 10(1):7495.
Elde, A., Pettersen, Bruheim, P., Järnegren, J., Johnsen, G. (2012). Pigmentation and Spectral Absorbance Signatures in Deep-Water Corals from the Trondheimsfjord, Norway.Mar. Drugs, 10-1400-1411; doi:10.3390/md10061400
Ellefmo, S., Ardelan, M., Granum Carson, S., Helmons, R. L. J., & Sævik, S. (2024). Interdisciplinary Approach to Deep-Sea Mining - With an Emphasis on the Water Column. In R. Sharma (Ed.), Deep-Sea Mining and the Water Column: Advances, Monitoring and Related Issues (pp. 41-64). Springer. https://doi.org/10.1007/978-3-031-59060-3_2
Ellis, J. and D.C. Schneider. 2008. Spatial and benthic scaling in benthic ecology. J. Exp. Mar. Bio. Ecolog., 366:92-98, doi: 10.1016/j.jembe.2008.07.012.

Emerson, S. and Hedges J. (2004) Sediment diagenesis and benthic flux. In H.D. Holland, K.K. Turekiann (Eds), Ocean. Mar. Geochemistry, 6 (pp. 293-319). Elsevier-Pergamon. Oxford.
Enríquez S, Merino M, Iglesias-Prieto R (2002) Variations in the photosynthetic performance along the leaves of the tropical seagrass Thalassia testudinum. Mar Biol In press
Fabricius KE (1997) Soft coral abundance on the central Great Barrier Reef: effects of Acanthaster planci, space availability, and aspects of the physical environment. Coral Reefs 16:159-167
Fabricius KE, De'ath G, McCook L, Turak E, Williams DM. (2005). Changes in algal, coral and fish assemblages along water quality gradients on the inshore Great Barrier Reef. Marine pollution bulletin. 51(1-4):384-98.)
Faltynkova, A., Johnsen, G., & Wagner, M. (2021). Hyperspectral imaging as an emerging tool to analyze microplastics: A systematic review and recommendations for future development. Microplastics and Nanoplastics, 1(1), 1-19.
Fogarty, M. C., M. R. Fewings, A. C. Paget, and H. M. Dierssen. 2018. The Influence of a Sandy Substrate, Seagrass, or Highly Turbid Water on Albedo and Surface Heat Flux. JGR Oceans 123: 53–73. doi:10.1002/2017JC013378
Foglini F, Grande V, Marchese F, Bracchi VA, Prampolini M, Angeletti L, et al. Application of hyperspectral imaging to underwater habitat mapping, Southern Adriatic Sea. Sensors. 2019; 19(10). https://doi.org/10.3390/s19102261 PMID: 31100805
Fong P, Paul VJ (2011) Coral reef algae. In: Dubinsky Z, Stambler N (eds) Coral Reefs: An Ecosystem in Transition. Springer, Dordrecht, The Netherlands, pp241-272
Fosså, J. H., Lindberg, B., Christensen, O., Lundälv, T., Svellingen, I., Mortensen, P. B. and Alvsvåg, J. (2005). Mapping of Lophelia reefs in Norway: experiences and survey methods. In A. Freiwald & J. M. Roberts (Eds.), Cold-water Corals and Ecosystems. (pp. 359-391). Berlin Heidelberg: Springer-Verlag.
Fournier, G., J.-P. Ardouin, and M. Levesque. (2018). Modeling Sea Bottom Hyperspectral Reflectance. Applied Sciences 8: 2680.
Frouin RJ, Franz BA, Ibrahim A, Knobelspiesse K, Ahmad Z, Cairns B, Chowdhary J, Dierssen HM, Tan J, Dubovik O, Huang X, Davis AB, Kalashnikova O, Thompson DR, Remer LA, Boss E, Coddington O, Deschamps P-Y, Gao B-C, Gross L, Hasekamp O, Omar A, Pelletier B, Ramon D, Steinmetz F and Zhai P-W (2019) Atmospheric Correction of Satellite Ocean-Color Imagery During the PACE Era. Front. Earth Sci. 7:145. doi: 10.3389/feart.2019.00145
Fyfe, S. K. (2003) Spatial and temporal variation in spectral reflectance: Are seagrass species spectrally distinct?, Limnol. Oceanogr., 48(1, part 2), 2003, 464–479.
Fujii T, Raffaelli D. (2008) Sea-level rise, expected environmental changes, and responses of intertidal benthic macrofauna in the Humber estuary, UK. Mar Ecol Prog Ser, 371: 23–35
Gao, B. C., M. J. Montes, Z. Ahmad, and C. O. Davis. 2000. Atmospheric correction algorithm for hyperspectral remote sensing of ocean colour from space. Applied Optics 39: 887–896.
Garaba, S. P., and H. M. Dierssen. (2018) An airborne remote sensing case study of synthetic hydrocarbon detection using short wave infrared absorption features identified from marine-harvested macro-and microplastics. Remote Sensing of Environment 205: 224–235.
Garcia, R. A., Z. Lee, B. B. Barnes, C. Hu, H. M. Dierssen, and E. J. Hochberg. (2020). Benthic classification and IOP retrievals in shallow water environments using MERIS imagery. Remote Sensing of Environment 249: 112015.
Garcia, R. A., L. I. W. McKinna, J. D. Hedley, and P. R. C. S. Fearns. (2014). Improving the optimization solution for a semi‐analytical shallow water inversion model in the presence of spectrally correlated noise. Limnology & Ocean Methods 12: 651–669. doi:10.4319/lom.2014.12.651
Gege, P. (2017). Radiative transfer theory for inland waters. In: Mishra D.R., Ogashawara I., Gitelson A.A. (Eds.), Bio-Optical Modelling and Remote Sensing of Inland Waters Elsevier, 27-69. http://dx.doi.org/10.1016/B978-0-12-804644-9.00002-1
Gege, Peter and König, Marcel and Oppelt, Natascha (2019): Reflectance measurements (Ocean Optics STS-VIS) of bare ice and melt ponds on Arctic sea ice acquired during POLARSTERN cruise PS106/1. PANGAEA, https://doi.org/10.1594/PANGAEA.908074,
Gendall, L; Schroeder, S; Wills, P; Hessing-Lewis, M.; Costa. M. (2023). A Multi-Satellite Mapping Framework for Floating Kelp. Remote Sensing. 15(5), 1276.
Gernez, P, D Stramski, M Darecki. 2011. Vertical changes in the probability distribution of downward irradiance within the near‐surface ocean under sunny conditions. Journal of Geophysical Research: Oceans, 116 (C7): C00H07 2011

Giardino, C., Candiani, G., Bresciani, M., Lee, Z., Gagliano, S., & Pepe, M. (2012). BOMBER: A tool for estimating water quality and bottom properties from remote sensing images. Computers & Geosciences, 45, 313-318. https://doi.org/10.1016/j.cageo.2011.11.022

Gilerson, A. A., Stepinski, J., Ibrahim, A. I., You, Y., Sullivan, J. M., Twardowski, M. S., ... & Kattawar, G. W. (2013). Benthic effects on the polarization of light in shallow waters. Applied optics, 52(36), 8685-8705.

Glasby, G.P. (2000). Manganese: predominant role of nodules and crusts, In: Schulz H. D and Zabe M (eds.). Marine Geochemistry. Springer, Berlin, 335–372.

Glynn PW (1990) Feeding ecology of coral-reef macroconsumers. In: Dubinsky Z (ed) Ecosystems of the World 25: Coral Reefs. Elsevier, Amsterdam, pp365-400

Goodman, J.A. (2008). Hyperspectral remote sensing of coral reefs: deriving bathymetry, aquatic optical properties and a benthic spectral unmixing classification using AVIRIS data in the Hawaiian Islands. Doctoral dissertation, University of California, Davis.

Goodman, J.A., Purkis, S.J. and Phinn, S.R., (2013) Coral reef remote sensing. A guide for mapping, monitoring and management. 436p, 4. Preisendorfer. R.W. (1961). Application of radiative transfer theory to light measurements in the sea. Union Geod Geophys Inst Monogr 10:11–30

Gordon, H.R., Wang, M., (1994) Retrieval of water-leaving radiance and aerosol optical thickness over the oceans with SeaWiFS: a preliminary algorithm. Appl. Opt. 33 (3), 443–452.

Graham, M.H., Vásquez, J.A. and Buschmann, A.H. (2007) 'GLOBAL ECOLOGY OF THE GIANT KELP MACROCYSTIS: FROM ECOTYPES TO ECOSYSTEMS', Oceanography and Marine Biology: An Annual Review, 45, pp. 39–88.

Graiff, A., & Karsten, U. (2021). Antioxidative properties of Baltic Sea keystone macroalgae (Fucus vesiculosus, Phaeophyceae) under ocean warming and acidification in a seasonally varying environment. Biology, 10(12), 1330.

Grall, J., & Chauvaud, L. (2002). Marine eutrophication and benthos: the need for new approaches and concepts. Global Change Biology, 8(9), 813-830.

Guenther, G.C., M.W.Brooks, and P.E. LaRocque. 2000. New capabilities of the "SHOALS" airborne Lidar Bathymeter. Rem. Sems. Environ., 73:247-255, doi:,10.1016/S0034-4257(00)00099-7.

Guinotte JM, Orr J, Cairns S, Freiwald A, Morgan L, George R. (2006) Will human-induced changes in seawater chemistry alter the distribution of deep-sea scleractinian corals? Front Ecol Environ, 4: 141–146.

Hale, G.M. and M.R. Querry (1973). Optical Constants of Water in the 200-nm to 200-μm Wavelength Region, Applied Optics, 12(3).

Halpern B, Selkoe K, Micheli F, Kappel C. (2007) Evaluating and ranking the vulnerability of global marine ecosystems to anthropogenic threats. Conserv Biol, 21:1301–1315.

Hamylton, S. M. (2017). Mapping coral reef environments: A review of historical methods, recent advances and future opportunities. Progress in Physical Geography, 41(6), 803-833

Hedley, J. (2008) A three-dimensional radiative transfer model for shallow water environments. Optics Express 16:21887-21902

Hedley, J., Enríquez, S. (2010) Optical properties of canopies of the tropical seagrass Thalassia testudinum estimated by a three-dimensional radiative transfer model. Limnology and Oceanography 55:1537-1550. doi: 10.4319/lo.2010.55.4.1537

Hedley, J.D., Mirhakak, M., Wentworth, A., Dierssen, H.M. (2018) Influence of three-dimensional coral structures on hyperspectral benthic reflectance and water-leaving Reflectance. Applied Sciences: 8, 2688. doi:10.3390/app8122688

Hedley, J.D., C.D. Mobley, (2021) HYDROLIGHT 6.0 ECOLIGHT 6.0 Technical documentation. Numerical Optics Ltd., Tiverton, UK.

Hedley, J. D., and P. J. Mumby. (2002) Biological and remote sensing perspectives of pigmentation in coral reef organisms. Advances in Marine Biology 43: 277–317.

Hedley, J.D., Mumby, P.J., Joyce, K.E., Phinn. S. (2004). Spectral unmixing of coral reef benthos under ideal conditions. Coral Reefs 23:60–73. doi:10.1007/s00338-003-0354-x

Hedley, J.D., Roelfsema, C.M., Chollett, I., Harborne, A.R., Heron, S.F., Weeks, S., Skirving, W.J., Strong, A.E., Eakin, C.M., Christensen, T.R.L., Ticzon, V., Bejarano, S. and Mumby, P.J. (2016a). Remote sensing of coral reefs for monitoring and management: a review. Remote Sens. 8: 118, DOI: 10.3390/rs8020118

Hedley, J. D., C. M. Roelfsema, S. R. Phinn, and P. J. Mumby. (2012) Environmental and sensor limitations in optical remote sensing of coral reefs: implications for monitoring and sensor design. Remote Sensing 4: 271–302.

Hedley, J., B. Russell, K. Randolph, and H. Dierssen. (2016b). A physics-based method for the remote sensing of seagrasses. Remote Sensing of Environment 174: 134–147.
Hedley, J. D., B. J. Russell, K. Randolph, M. A. Perez-Castro, R. M. Vasquez-Elizondo, S. Enriquez, and H. M. Dierssen. (2017). Remote sensing of seagrass leaf area index and species: The capability of a model inversion method assessed by sensitivity analysis and hyperspectral data of Florida Bay. Frontiers in Marine Science 4: 362.
Held, P.; Schneider von Deimling, J. (2019) New Feature Classes for Acoustic Habitat Mapping—A Multibeam Echosounder Point Cloud Analysis for Mapping Submerged Aquatic Vegetation (SAV). Geosciences 2019, 9, 235. https://doi.org/10.3390/geosciences9050235
Hestir, E., and I. Dronova. (2023) Remote sensing of primary producers in the Bay–Delta. San Francisco Estuary and Watershed Science 20.
Hiddink, J.G., Burrows, M.T., García Molinos, J., (2015) Temperature tracking by North Sea benthic invertebrates in response to climate change. Glob. Change Biol. 21, 117e129.
Hieronymi, M., Bi, S., Müller, D., Schütt, E. M., Behr, D., Brockmann, C., ... & Vanhellemont, Q. (2023). Ocean colour atmospheric correction methods in view of usability for different optical water types. Frontiers in Marine Science, 10, 1129876.
Hill, V. J., Zimmerman, R. C., Bissett, W. P., Dierssen, H., & Kohler, D. D. (2014). Evaluating light availability, seagrass biomass, and productivity using hyperspectral airborne remote sensing in Saint Joseph's Bay, Florida. Estuaries and coasts, 37(6), 1467-1489.
Hill, V. J., R. C. Zimmerman, P. Bissett, D. Kohler, B. Schaeffer, M. Coffer, J. Li, and K. A. Islam. (2023) Impact of Atmospheric Correction on Classification and Quantification of Seagrass Density from WorldView-2 Imagery. Remote Sensing 15: 4715.
Hochberg EJ, Atkinson MJ (2003) Capabilities of remote sensors to classify coral, algae and sand as pure and mixed spectra. Remote Sens Environ 85:174-189 doi: 10.1016/S0034-4257(02)00201-8.
Hochberg, E. J., S. Andréfouët, and M. R. Tyler. (2003a) Sea surface correction of high spatial resolution Ikonos images to improve bottom mapping in near-shore environments. Geoscience and Remote Sensing, IEEE Transactions on 41: 1724–1729.
Hochberg EJ, Atkinson MJ, Andréfouët S (2003b) Spectral reflectance of coral reef bottom-types worldwide and implications for coral reef remote sensing. Remote Sens Environ 85:159-173
Hochberg EJ, Atkinson MJ, Apprill A, Andréfouët S (2004) Spectral reflectance of coral. Coral Reefs 23:84-95
Hochberg, E. J., Ducret, H., & Dierssen, H. M. (2025). Revised empirical models for estimating coral pigment concentrations from optical reflectance spectra. Applied Optics, 64(35), 10603-10610.
Hovland, M., & Mortensen, P. B. (1999). Norske korallrev og prosesser i havbunnen. Bergen: Grieg (In Norwegian).
Hubas, C., Jesus, B., Passarelli, C., & Jeanthon, C. (2011). Tools providing new insight into coastal anoxygenic purple bacterial mats: review and perspectives. Research in Microbiology, 162(9), 858-868.
Hueni, A., Chisholm, L.A., Ong, C., Malthus, T.J., Wyatt, M., Trim, SA., Schaepman, M.E. (2020). The SPECCHIO Spectral Information System_IEEE Journal of Selected Topics in Applied Earth Observations and Remote Sensing, 13:5789-5799.
Huot, M., F. Dalgleish, E. Rehm, M. Piché, and P. Archambault. 2022. Underwater multispectral laser serial imager for spectral differentiation of macroalgae and coral substrates. Rem. Sens., 14:3105, doi: 10.3390/rs14133105.
Jacobs, P., J. Pitarch, J. C. Kromkamp, and C. J. M. Philippart (2021), Assessing biomass and primary production of microphytobenthos in depositional coastal systems using spectral information, PLOS ONE, 16(7), e0246012, doi: 10.1371/journal.pone.0246012.
Jerlov, N. G., (1976). Marine Optics, second ed. Elsevier, Amsterdam – Oxford – New York.
Johnsen, G., Ludvigsen, M., Sørensen, A. and Aas LM. (2016). The use of underwater hyperspectral imaging deployed on remotely operated vehicle – methods and applications. IFAC papersOnLine. Volume 49(23):476-481.
Johnsen, G., Mogstad, A. A., Berge, J. and Cohen, J.H. (2020) Operative habitat mapping and monitoring in the Polar Night, pp 277-306. In: Berge, J., Johnsen, G. and Cohen, J. (eds) POLAR NIGHT Marine Ecology – Life and light in the dead of the night. Springer, 380 pp.
Johnsen, G., Volent, Z., Dierssen, H., Pettersen, R., Ardelan, M. V., Søreide, F., Fearns, P., Ludvigsen, M. and Moline, M. (2013). Underwater hyperspectral imagery to create

biogeochemical maps of seafloor properties. In “Subsea optics and imaging”, [Eds] Watson, J. and Zielinski, O. Chapter 20, 508-535. Woodhead Publishing Ltd., Cambridge, UK, 608 pp.
Joyce, K. E., & Phinn, S. R. (2010). Bi-directional reflectance of corals. International Journal of Remote Sensing, 23(2), 389–394. https://doi.org/10.1080/01431160110079420
Joyce K.E., Roelfsema C.M. , Atkinson M.J. ,Cochrane K., Goodman J.A., Hochberg E.J., Marshall J., Palandro D. (2002) Collaborative Coral Reef Remote Sensing Workshop Summary: Heron Island, In: Proceedings of the 11th Australasian Remote Sensing and Photogrammetry Conference, Brisbane, 2-6 September, CD-Rom, Causal Publications.
Kashani, A.G., M.J. Olsen, C. E. Parrish, and N. Wilson. 2015. A review of LiDAR radiometric processing: from ad hoc intensity correction to rigorous radiometric correction. Sensors, 15, 28099-28128, doi: 10.3390/s151128099.
Kench P (2011) Sediment dynamics. In: Hopley D (ed) Encyclopedia of Modern Coral Reefs: Structure, Form and Process. Springer, Dordrecht, The Netherlands, pp994-1005
Kinsey DW (1985) Metabolism, calcification and carbon production I: Systems level studies. Fifth International Coral Reef Congress 4:505-526
Kirk JTO (2011) Light and Photosynthesis in Aquatic Environments, Third Edition. Cambridge University Press, Cambridge
Klemas, V. (2012) Remote Sensing of Algal Blooms: An Overview with Case Studies. J. Coast. Res. 2012, 28, 34–43.
Klonowski, W. M., P. R. Fearns, and M. J. Lynch. (2007) Retrieving key benthic cover types and bathymetry from hyperspectral imagery. Journal of Applied Remote Sensing 1: 011505.
Klumpp DW, McKinnon AD (1989) Temporal and spatial patterns in primary production of a coral-reef epilithic algal community. J Exp Mar Biol Ecol 131:1-22
Knipling, E.B. (1970) ‘Physical and physiological basis for the reflectance of visible and near-infrared radiation from vegetation’, Remote Sensing of Environment, 1(3), pp. 155–159. Available at: https://doi.org/10.1016/S0034-4257(70)80021-9.
Kröncke, I., Reiss, H., Eggleton, J.D., Aldridge, J., Bergman, M.J.N., Cochrane, S., Craeymeersch, J.A., Degraer, S., Desroy, N., Dewarumez, J.-M., Duineveld, G.C.A., Essink, K., Hillewaert, H., Lavaleye, M.S.S., Moll, A., Nehring, S., Newell, R., Oug, E., Pohlmann, T., Rachor, E., Robertson, M., Rumohr, H., Schratzberger, M., Smith, R., Vanden Berghe, E., van Dalfsen, J., van Hoey, G., Vincx, M., Willems, W., Rees, H.L., 2011. Changes in North Sea macrofauna communities and species distribution between 1986 and 2000. Estuar. Coast. Shelf Sci. 94, 1e15.
Kuhwald, K., Schneider v Deimling, J., Schubert, P, Oppelt, N. (2022). How can Sentinel‐2 contribute to seagrass mapping in shallow, turbid Baltic Sea waters? Remote Sens. Ecol. Conserv., 8(3): 328-346. DOI: 10.1002/rse2.246
Kutser, T., Dekker, A.G., Skirving, W (2003) Modelling spectral discrimination of Great Barrier Reef benthic communities by remote sensing instruments. Limnology and Oceanography 48: 497-510
Kutser, T., Hedley, J., Giardino, C., Roelfsema, C., Brando, V.E. (2020). Remote sensing of shallow waters – a 50 years retrospective and future directions. Remote Sens. Environ. 240: 11161, DOI: 10.1016/j.rse.2019.111619
Kutser, T. and D.L.B. Jupp (2006) On the possibility of mapping living corals to the species level based on their optical signatures. Estuarine, Coastal and Shelf Science, 69: 607-614.
Kutser, T., I. Miller, D.L.B. Jupp (2006) Mapping coral reef benthic substrates using hyperspectral space-borne images and spectral libraries. Estuarine Coastal and Shelf Science, 70: 449-460
La Barre, S. (2014) Marine biodiversity and chemodiversity - the treasure troves of the future. Oscar Grillo. Biodiversity - The Dynamic Balance of the Planet, InTech, pp.1-26, 2014, ISBN 978-953-51- 1315-7. Hal-00982766
Laugié, M., Michel, J., Pohl, A., Poli, E., & Borgomano, J. (2019). Global distribution of modern shallow-water marine carbonate factories: a spatial model based on environmental parameters. Scientific Reports, 9(1), 16432. https://doi.org/10.1038/s41598-019-52821-2.
Lebreton, L.C., Van Der Zwet, J., Damsteeg, J-W., Slat, B., Andrady, A. and Reisser, J. (2017). River plastic emissions to the world’s oceans. Nature communications. 8(1):15611.
Lecours, V., R. Devillers, D.C. Schneider, V.L. Lucieer, C.J. Brown, and E.N. Edinger. 2015. Spatial scale and geographic context in benthic habitat mapping: review and future directions. Mar. Ecol. Prog. Ser., 535:259-284, doi: 10.3354/meps11378.

Lee, Z. and Carder, K.L. (2002). Effect of spectral band numbers on the retrieval of water column and bottom properties from ocean colour data. Appl. Opt., AO 41: 2191–2201, DOI: 10.1364/AO.4.00219
Lee, Z., K. L. Carder, C. D. Mobley, R. G. Steward, and J. S. Patch. (1998) Hyperspectral remote sensing for shallow waters. I. A semianalytical model. Applied optics 37: 6329–6338.
Lee, Z., K. L. Carder, C. D. Mobley, R. G. Steward, and J. S. Patch. (1999) Hyperspectral Remote Sensing for Shallow Waters. 2. Deriving Bottom Depths and Water Properties by Optimization. Appl. Optics 38: 3831–3843.
Lee, Z., Shang, S., Hu, C., Du, K., Weidemann, A., Hou, W., ... & Lin, G. (2015). Secchi disk depth: A new theory and mechanistic model for underwater visibility. Remote sensing of environment, 169, 139-149.
Léger-Dailge R., Noissette F., Bélanger S., Cusson M., Nozais, C. 2022. Photoacclimation and light thresholds for cold temperate seagrasses. Frontiers in Plant Science, 13:805065. doi: 10.3389/fpls.2022.805065
Leiper, I., Phinn, S., & Dekker, A. G. (2011). Spectral reflectance of coral reef benthos and substrate assemblages on Heron Reef, Australia. International Journal of Remote Sensing, 33(12), 3946–3965. https://doi.org/10.1080/01431161.2011.637675
Lesser, M. P. and C. D. Mobley (2007) Bathymetry, water optical properties, and benthic classification of coral reefs using hyperspectral remote sensing imagery. Coral Reefs, 26: 819-829 DOI 10.1007/s00338-007-0271-5
Letard, M.; Collin, A.; Corpetti, T.; Lague, D.; Pastol, Y.; Ekelund, A. Classification of Land-Water Continuum Habitats Using Exclusively Airborne Topobathymetric Lidar Green Waveforms and Infrared Intensity Point Clouds. Remote Sens. 2022, 14, 341. https://doi.org/10.3390/rs14020341.
Letnes PA, Hansen IM, Aas LMS, Eide I, Pettersen R, Tassara L, et al. Underwater hyperspectral classification of deep sea corals exposed to 2-methylnaphthalene. PloS one. 2019; 14(2):e0209960. https://doi.org/10.1371/journal.pone.0209960 PMID: 30811426
Levin L, Ekau W, Gooday A, Jorissen F, Middelburg J, Naqvi S, Neira C, Rabalais N, Zhang J. (2009) Effects of natural and human-induced hypoxia on coastal benthos. Biogeosciences, 6:2063–2098
Liefmann, S., Järnegren, J., Johnsen, G. and Murray, F. (2018). Eco-physiological responses of cold-water soft corals to anthropogenic sedimentation and particle shape. Journal of Experimental Marine Biology and Ecology. 504: 61-71. https://doi.org/10.1016/j.jembe.2018.02.009
Lim, A., Bronner, M., Johansen, S. E., and Dumais, M. A. (2019). Hydrothermal activity at the ultraslow-spreading Mohns ridge: new insights from near seafloor magnetics. Geochem. Geophys. Geosyst. 20, 5691–5709. doi: 10.1029/2019GC008439
Littler MM, Littler DS (2011) Algae, Turf. In: Hopley D (ed) Encyclopedia of Modern Coral Reefs: Structure, Form and Process. Springer, Dordrecht, The Netherlands, pp38-39
Liu, Z., Y. Zhang, X. Yu, and C. Yuan. 2016. Unmanned surface vehicles: An overview of developments and challenges. Ann. Rev. Control, 41:71-93, doi: 10.1016/j.arcontrol.2016.04.018.
Liu, R. et al. “Detection of Chlorophyll a and CDOM Absorption Coefficient with a Dual-Wavelength Oceanic Lidar: Wavelength Optimization Method,” Remote Sensing , vol. 12, no. 18. 2020. doi: 10.3390/rs12183021.
Lohrenz, S.E., Weidemann, A.D. and Merritt, T. (2003). Phytoplankton spectral absorption as influenced by community size structure and pigment composition. Journal of Plankton Research, 2003, 25 (1), 35-61.
Louchard, E. M., R. P. Reid, and C. F. Stephens. (2000). Classification of sediment types and estimation of water depth using spectral libraries. Office of Naval Research.
Lubin, D., W. Li, P. Dustan, C. H. Mazel, and K. Stamnes. 2001. Spectral Signatures of Coral Reefs: Features from Space. Remote Sensing of Environment 75: 127–137. doi:10.1016/S0034-4257(00)00161-9
Ludvigsen, M., and Johnsen, G. (2025). Observing systems and technology. In The Barents Sea System. *Gateway to the changing Arctic*. Reigstad M, Sundfjord A, Johnsen G (eds). Fagbokforlaget, 340-390.
Ludvigsen, M., Aasly, K., Ellefmo, S. L., Hilário, A., Ramirez-Llodra, E., Søreide, F. X., et al. (2016). MarMine Cruise Report-ArcticMid-Ocean Ridge. Trondheim, NO: NTNU

Ludvigsen, M., Sortland, B., Johnsen, G. and Singh, H., 2007. Applications of geo-referenced underwater photo mosaics in marine biology and archaeology. Oceanography. 20:74-83.
Ludvigsen, M. Johnsen, G., Sørensen, A.J., Lågstad, P.A. and Ødegård, Ø. (2014). Scientific Operations Combining ROV and AUV in the Trondheim Fjord. Marine Technology Society journal. 48:59-71.
Lukyanov KA, Fradkov AF, Gurskaya NG, Matz MV, Labas YA, Savitsky AP, Markelov ML, Zaraisky AG, Zhao X, Fang Y, Tan W, Lukyanov SA (2000) Natural animal colouration can be determined by a nonfluorescent green fluorescent protein homolog. J Biol Chem 275:25,879-825,882
Lyons, M. B., Murray, N. J., Kennedy, E. V., Kovacs, E. M., Castro-Sanguino, C., Phinn, S. R., ... & Roelfsema, C. M. (2024). New global area estimates for coral reefs from high-resolution mapping. Cell Reports Sustainability, 1(2).
Lyzenga, D. R. (1978). Passive remote sensing techniques for mapping water depth and bottom features. Applied Optics 17, 379–383.Mobley, C. D. 1994. Light and water: Radiative transfer in natural waters, Academic Press.
Lyzenga D.R., Malinas N.P., Tanis F.J. (2006). Multispectral bathymetry using a simple physically based algorithm. IEEE Transactions on Geoscience and Remote Sensing. 2006 Jul 24;44(8):2251-9.
Løvås, H.S., Mogstad, A.A., Sørensen, A.J. and Johnsen, G. (2022). A methodology for consistent georegistration in underwater hyperspectral imaging. IEEE Journal of Oceanographic Engineering, DOI: 10.1109/JOE.2021.3108229148.
Mac Arthur, A., C. J. MacLellan, and T. Malthus. 2012. The fields of view and directional response functions of two field spectroradiometers. IEEE transactions on geoscience and remote sensing 50: 3892–3907.
Macreadie et al. (2019). The future of Blue Carbon science. Nat Comm. 10, 3998.
Maffione, R.A. (2000). Deep problems in optically shallow waters. Backscatter 11 (3): 28–31.
Malthus, T.J. (2017). Bio-optical modeling and remote sensing of aquatic macrophytes. In: D.R. Mishra, I. Ogashawara and A.A. Gitelson (Eds.) Bio-optical modeling and remote sensing of inland waters. Amsterdam: 263–308.
Maritorena, S., A. Morel, and B. Gentili. 1994. Diffuse reflectance of oceanic shallow waters: Influence of water depth and bottom albedo. Limnology and Oceanography 39: 1689–1703.
Mazel CH, Lesser MP, Gorbunov MY, Barry TM, Farrel JH, Wyman KD, Falkowski PG (2003) Green-fluorescent proteins in Caribbean corals. Limnol Oceanogr 48:402-411
McClelland, James W., and I. Valiela. (1998) "Changes in food web structure under the influence of increased anthropogenic nitrogen inputs to estuaries." Marine Ecology Progress Series 168: 259-271.
McKinna, L. I. W., P. R. C. Fearns, S. J. Weeks, P. J. Werdell, M. Reichstetter, B. A. Franz, D. M. Shea, and G. C. Feldman. (2015) A semianalytical ocean colour inversion algorithm with explicit water column depth and substrate reflectance parameterization. JGR Oceans 120: 1741–1770. doi:10.1002/2014jc010224
McKinna, L. I., and P. J. Werdell. (2018) Approach for identifying optically shallow pixels when processing ocean-colour imagery. Optics express 26: A915–A928.
Mcleod, E.; Chmura, G; Bouillon, S.; Salm, R.; Björk, M.; Duarte, C. (2011): A blueprint for blue carbon: Toward an improved understanding of the role of vegetated coastal habitats in sequestering CO2. Front. Ecol. Environ. 9. DOI: 10.1890/110004.
McPherson, M. L., V. J. Hill, R. C. Zimmerman, and H. M. Dierssen. (2011) The optical properties of Greater Florida Bay: Implications for seagrass abundance. Estuaries and Coasts 1–11.
Meier, H. E. M., Hordoir, R., Andersson, H. C., Dieterich, C., Eilola, K., Gustafsson, B. G., ... & Schimanke, S. (2012). Modeling the combined impact of changing climate and changing nutrient loads on the Baltic Sea environment in an ensemble of transient simulations for 1961–2099. Climate Dynamics, 39(9), 2421-2441.
Miller, I., Forster, B. C., Laffan, S. W., & Brander, R. W. (2016). Bidirectional reflectance of coral growth-forms. International Journal of Remote Sensing, 37(7), 1553–1567. https://doi.org/10.1080/01431161.2016.1154220
Miller KA, Thompson KF, Johnston P and Santillo D (2018) An Overview of Seabed Mining Including the Current State of Development, Environmental Impacts, and Knowledge Gaps. Front. Mar. Sci. 4:418. doi: 10.3389/fmars.2017.00418

Mobley, C. D. (1999). Estimation of the remote sensing reflectance from above-surface measurements. Applied Optics 38: 7442–7455.
Mobley, C., Boss, E., Roesler, C., (2023). Radiative Transfer Theory. In: Ocean Optics Web Book.https://www.oceanopticsbook.info/view/radiative-transfer-theory/the-srte-heuristic-development. Accessed August 7, 2023.
Mobley, C. D., Gentili, B., Gordon, H. R., Jin, Z., Kattawar, G. W., Morel, A., Reinersman, P., Stamnes, K.,Stavn, R. H., (1993). Comparison of numerical models for computing underwater light fields. Appl. Opt. 32, 7484-7504.
Mobley, C.D., Sundman, L.K. (2003a) Effects of optically shallow bottoms on upwelling radiances: Inhomogeneous and sloping bottoms. Limnology and Oceanography 48(1, part 2):329-336.
Mobley, C.D., Zhang, H., Voss, K.J. (2003b) Effects of optically shallow bottoms on upwelling radiances: Bidirectional reflectance distribution function effects. Limnology and Oceanography 48(1, part 2):337-345.
Mobley, C.D., Sundman, L.K., Davis, C.O., Bowles, J.H., Downes, T.V., Leathers, R.A., Montes, M.J., Bissett, W.P., Kohler, D.D.R., Reid, R.P., Louchard, E.M. and Gleason, A. (2005). Interpretation of hyperspectral remote-sensing imagery by spectrum matching and look-up tables. Appl. Opt., AO 44: 3576–3592. DOI: 10.1364/AO.44.003576
Mogstad, A.A. (2021). Underwater Hyperspectral Imaging as a Tool for Benthic Habitat Mapping. Ph.D. Thesis. Norwegian University of Science and Technology (NTNU). Trondheim, Norway.
Mogstad, A.A. and Johnsen, G. (2017). Spectral characteristics of coralline algae: a multi-instrumental approach, with emphasis on underwater hyperspectral imaging. Appl. Opt. 56, 9957-9975. https://doi.org/10.1364/AO.56.009957
Mogstad, A., Johnsen, G. and Ludvigsen, M. (2019). Shallow-water habitat mapping using underwater hyperspectral imaging from an unmanned surface vehicle: a pilot study. Remote Sens. 11: 685. doi:10.3390/rs11060685.
Mogstad, A.A., Løvås, H.S., Sture, Ø., Johnsen, G. And Ludvigsen, M. (2022). Remote sensing of the Tautra Ridge: an overview of the world's shallowest cold-water coral reefs. Front. Mar. Sci. 9:848888. doi: 10.3389/fmars.2022.848888
Mogstad, A. A., Ødegård, Ø., Nornes, S. M., Ludvigsen, M., Johnsen, G., Sørensen, A. J., and Berge, J. (2020). Mapping the historical shipwreck Figaro in the high arctic using underwater sensor-carrying robots. Remote Sensing, 12(6), 997.
Mollica, N.R., Guo, W.; Cohen, A.L., Solow, A.R. (2018). Ocean acidification affects coral growth by reducing skeletal density. PNAS, 115 (8): 1754-1759, DOI: 10.1073/pnas.1712806115
Montes-Herrera, J. C., Cimoli, E., Cummings, V. J., D'Archino, R., Nelson, W. A., Lucieer, A., & Lucieer, V. (2024). Quantifying pigment content in crustose coralline algae using hyperspectral imaging: A case study with Tethysphytum antarcticum (Ross Sea, Antarctica). Journal of Phycology.
Mora-Soto, A., Capsey, A., Friedlander, A. M., Palacios, M., Brewin, P. E., Golding, N., ... & Macias-Fauria, M. (2021). One of the least disturbed marine coastal ecosystems on Earth: Spatial and temporal persistence of Darwin's sub-Antarctic giant kelp forests. Journal of Biogeography, 48(10), 2562-2577.
Morawetz K, Thoms S, Kutschan B. Formation of brine channels in sea ice. Eur Phys J E Soft Matter. 2017 Mar;40(3):25. doi: 10.1140/epje/i2017-11512-x. Epub 2017 Mar 3. PMID: 28255919.
Morel, A., 2001. Bio-optical models, in: Thorpe, S.A., Turekian, K.K. (Eds.), Encyclopedia of Ocean Sciences. Academic press, pp. 317-326. http://dx.doi.org/10.1006/rwos.2001.0407.
Morel, A. and Bricaud, A. (1981). Theoretical results concerning light absorption in a discrete medium, and application to specific absorption of phytoplankton. Deep Sea Res. 1981, 28, 1375–1393.
Mortensen, P. B., Hovland, M. T., Fosså, J. H., and Furevik, D. M. (2001). Distribution, Abundance and Size of Lophelia pertusa Coral Reefs in Mid- Norway in Relation to Seabed Characteristics. J. Mar. Biol. Assoc. UK 81, 581–597. doi: 10.1017/S002531540100426X
Mueller, J.L., D.K. Clark, V.S. Kuwahara, G. Lazin, S.W. Brown, G.S. Fargion, M.A. Yarbrough, et al. 2003. Ocean Optics Protocols for Satellite Ocean Color Sensor Validation, Revision 4, Volume VI: Special Topics in Ocean Optics Protocols and Appendices. NASA/TM—2003–211621/Rev4–Vol.VI, doi: 10.25607/OBP-66.
Muller-Karger, F. E., Hestir, E., Ade, C., Turpie, K., Roberts, D. A., Siegel, D., ... & Jetz, W. (2018). Satellite sensor requirements for monitoring essential biodiversity variables of coastal ecosystems. Ecological applications, 28(3), 749-760. doi: 10.1002/eap.1682

Murphy, R.J., Underwood, A.J., Pinkerton, M.H. and Range, P., 2005. Field spectrometry: new methods to investigate epilithic micro-algae on rocky shores. Journal of Experimental Marine Biology and Ecology, 325(1), pp.111-124.
Nakajima, R., Tsuchiya, M., Yabuki, A., Masuda, S., Kitahashi, T., Nagano, Y., Ikuta, T., Isobe, N., Nakata, H. and Ritchie, H. (2021). Massive occurrence of benthic plastic debris at the abyssal seafloor beneath the Kuroshio Extension, the North West Pacific. Marine Pollut. Bull. 166:112188.
Neale, P. J., Smyth, R. L. (2018). Are warmer waters, brighter waters? An examination of the irradiance environment of lakes and oceans in a changing climate. In D. P. Hader & K. Gao (Eds.), Aquatic Ecosystems in a Changing Climate (pp. 89–115). USA: CRC.
Neale, P.J., Williamson, C.E., Banaszak, A.T. et al. (2023). The response of aquatic ecosystems to the interactive effects of stratospheric ozone depletion, UV radiation, and climate change. Photochem Photobiol Sci 22, 1093–1127. DOI: 10.1007/s43630-023-00370-z
Nelson, J.R., J.E. Eckman, C.Y. Robertson, R.L.Marinelli, and R.A. Jahnke. 1999. Cont. Self Res., 19:477-505, doi: 10.1016/S0278-4343(98)00092-2.
Nevstad, M. B. (2022). Use of different imaging systems for ROV-based mapping of complex benthic habitats. MSc thesis, NTNU, 73 pp
Nicodemus, F.E., Richmond, J.C., Hsia, J.J., Ginsberg, I.W. and Limperis, T. (1977). Geometrical considerations and nomenclature for reflectance. National Bureau of standards, 52 pp.
Nicolaus, M., Gerland, S., Hudson, S. R., Hanson, S., Haapala, J., and Perovich, D. K (2010) Seasonality of spectral albedo and transmittance as observed in the Arctic Transpolar Drift in 2007, J. Geophys. Res., 115, C11011, https://doi.org/10.1029/2009JC006074
Olmedo-Masat, O. M., Raffo, M. P., Rodríguez-Pérez, D., Arijón, M., & Sánchez-Carnero, N. (2020). How far can we classify macroalgae remotely? An example using a new spectral library of species from the south west atlantic (argentine patagonia). Remote Sensing, 12(23), 3870. https://doi.org/10.3390/rs12233870.
Olsen, Y. S., Potouroglou, M., Garcias-Bonet, N., & Duarte, C. M. (2015). Warming reduces pathogen pressure on a climate-vulnerable seagrass species. Estuaries and Coasts, 38(2), 659-667.
Ortiz, J., Bozec, YM., Wolff, N. et al. (2014) Global disparity in the ecological benefits of reducing carbon emissions for coral reefs. Nature Clim Change 4, 1090–1094. https://doi.org/10.1038/nclimate2439
Ødegård, Ø., Mogstad, A.A., Johnsen, G., Sørensen, A. J. and Ludvigsen, M. (2018). Underwater hyperspectral imaging: a new tool for marine archaeology. Appl. Opt. 57: 3214-3223.
Ødegård, Ø., Sørensen, A. J., Hansen, R. E. And Ludvigsen, M. (2016). A new method for underwater archaeological surveying using sensors and unmanned platforms. IFAC-PapersOnLine, 49(23), 486-493.
Park, J., Lee, H., Asselman, J., Janssen, C., Depuydt, S., De Saeger, J., … Han, T. (2024). Harnessing the power of tidal flat diatoms to combat climate change. Critical Reviews in Environmental Science and Technology, 54(19), 1395–1416. https://doi.org/10.1080/10643389.2024.2315004
Parmesan, C., Yohe, G., (2003). A globally coherent fingerprint of climate change impacts across natural systems. Nature 421, 37e42.
Perovich, D. K.: The optical properties of sea ice, US Army Cold Regions Research and Engineering Laboratory (CRREL) Report 96-1, Hanover, NH, USA, available at: www.dtic.mil/cgi-bin/GetTRDoc?AD=ADA310586
Perry, R. A., J. M. Vaudrey, and H. M. Dierssen. 2018. Long range transport and carbon and nitrogen dynamics of floating seagrass wracks in Greater Florida Bay. Estuarine, Coastal and Shelf Science 209: 7–17.
Pettersen R, Johnsen G, Bruheim P, Andreassen T (2013) Development of hyperspectral imaging as a bio- optical taxonomic tool for pigmented marine organisms. Org Divers Ecol, DOI 10.1007/s13127-013-0163-1
Petzold, T. J. (1972). Volume scattering functions for selected ocean waters. Tech. Rep. SIO 72–78, Scripps Institution of Oceanography, San Diego, Calif., 79 pp.
Philpot, W. D. (1987). Radiative transfer in stratified waters: a single-scattering approximation for irradiance. Applied Optics, 26(19), 4123-4132.
Phinn, S., Roelfsema, C., Kovacs, E., Canto, R., Lyons, M., Saunders, M. and Maxwell, P., (2018) Mapping, monitoring and modelling seagrass using remote sensing techniques. In

Seagrasses of Australia: Structure, ecology and conservation (pp. 445-487). Cham: Springer International Publishing.
Pilla, R. M., Williamson, C. E., Zhang, J., Smyth, R. L., Lenters, J. D., Brentrup, J. A., Knoll, L. B., & Fisher, T. J. (2018). Browning-related decreases in water transparency lead to long-term increases in surface water temperature and thermal stratification in two small lakes. Journal of Geophysical Research: Biogeosciences, 123(5), 1651–1665. DOI: 10.1029/2017jg004321
Pizarro O, Friedman A, Bryson M, Williams SB, Madin J. A simple, fast, and repeatable survey method for underwater visual 3D benthic mapping and monitoring. Ecol Evol. 2017;7:1770–1782. https://doi.org/10.1002/ece3.2701
Plattner, S., P. Gege, and T. Schwarzmaier. 2022. LimnoVIS–A robotic surface vehicle for spectral measurements in inland waters. Ocean OpticsXXV Conference, QuyNhon, Vietnam.
Polashenski, C., Perovich, D., and Courville, Z. (2012) The mechanisms of sea ice melt pond formation and evolution, J. Geophys. Res., 117, C01001, https://doi.org/10.1029/2011JC007231
Poloczanska, E.S., Burrows, M.T., Brown, C.J., García Molinos, J., Halpern, B.S., Hoegh-Guldberg, O., Kappel, C.V., Moore, P.J., Richardson, A.J., Schoeman, D.S., Sydeman, W.J., (2016). Responses of marine organisms to climate change across oceans. Frontiers in Marine Science 3, 62.
Preisendorfer. R.W. (1961). Application of radiative transfer theory to light measurements in the sea. Union Geod Geophys Inst Monogr 10:11–30
Rahul. S. (2022). Perspectives on Deep-Sea Mining Sustainability, Technology, Environmental Policy and Management. DOI: 10.1007/978-3-030-87982-2, ISBN: 978-3-030-87981-5, Springer Nature Switzerland
Ramirez-Llodra ,E., Hilario, A., Paulsen, E., Costa, C.V., Bakken, T., Johnsen, G. and Rapp, H.T. (2020). Benthic Communities on the Mohn's Treasure Mound: Implications for Management of Seabed Mining in the Arctic Mid-Ocean Ridge. Front. Mar. Sci. 7:490. doi: 10.3389/fmars.2020.00490
Ramey, P.A., J.P. Grassle, J.F. Grassle, and R.F. Petrecca. Small-scale, patchy distributions of infauna in hydrodynamically mobile continental shelf sands: do ripple crests and troughs support different communities? Cont. Shelf Res., 29:222-2233, doi: 10.1016/j.csr.2009.08.020.
Rasaiah, B.A., Jones, S.D., Bellman, C., Malthus, T.J., Hueni, A., (2015a). Assessing field spectroscopy metadata quality. Remote Sens., 7:4499–4526.
Raven, J. (2018). Blue carbon: past, present and future with emphasis on macroalgae. Biol. Lett. 14: 20180336, DOI: 10.1098/rsbl.2018.0336
Reusch, T. B. H., Dierking, J., Andersson, H. C., Bonsdorff, E., Carstensen, J., Casini, M., Czajkowski, M., Hasler, B., Hinsby, K., Hyytiainen, K., Johannesson, K., Jomaa, S., Jormalainen, V., Kuosa, H., Kurland, S., Laikre, L., MacKenzie, B. R., Margonski, P., Melzner, F., Oesterwind, D., Ojaveer, H., Refsgaard, J. C., Sandström, A., Schwarz, G., Tonderski, K., Winder, M., and Zandersen, M (2018) The Baltic Sea as a time machine for the future coastal ocean, Science Advances, 4, eaar8195, https://doi.org/10.1126/sciadv.aar8195
Roberts, J. M., Wheeler, A. J. and Freiwald, A. (2006). Reefs of the Deep: The Biology and Geology of Cold-Water Coral Ecosystems. Science, 312(5773), 543-547.
Roelfsema, C.M., S.R. Phinn and W.C. Dennison (2003) Spatial Distribution of Benthic Microalgae on Coral Reefs Determined by Remote Sensing. Coral Reefs https://doi.org/10.1007/s00338-002-0242-9
Rousset, G., De Boissieu, F., Menkes, C.E., Lefèvre, J., Frouin, R., Rodier, M., Ridoux, V., Laran, S., Bonnet, S. and Dupouy, C., (2018). Remote sensing of Trichodesmium spp. mats in the western tropical South Pacific. Biogeosciences, 15(16), pp.5203-5219.
Roy DP, Li J, Zhang HK, Yan L, Huang H, Li Z.(2017). Examination of Sentinel-2A multi-spectral instrument (MSI) reflectance anisotropy and the suitability of a general method to normalize MSI reflectance to nadir BRDF adjusted reflectance. Remote Sens Environ 2017; 199: 25–38.
Russell, B. J., and H. M. Dierssen. (2015). Use of hyperspectral imagery to assess cryptic colour matching in Sargassum associated crabs. PLoS One 10: e0136260.
Russell, B. J., and H. M. Dierssen. (2023). Underwater spectral reflectance measurements: the reflectance standard submersion factor and its impact on derived target reflectance. Applied Optics 62: 6299–6306.

Russell, B. J., H. M. Dierssen, T. C. LaJeunesse, K. D. Hoadley, M. E. Warner, D. W. Kemp, and T. G. Bateman. (2016). Spectral reflectance of Palauan reef-building coral with different symbionts in response to elevated temperature. Remote Sensing 8: 164.
Ryan, J. P., S. B. Johnson, A. Sherman, K. Rajan, F. Py, H. Thomas, J.B.J. Harvey, L. Bird, J. D. Paduan, and R. C. Vrljenhoek. 2010. Mobile autonomous process sampling within coastal ocean observing systems. Limnol. Oceanogr. Meth., 8:394-402, doi: 10.4319/lom.2010.8.394.
Sahla, M., Tolvanen, H., Ruuskanen, A., and Kurvinen, L.: Assessing long term change of Fucus spp. communities in the northern Baltic Sea using monitoring data and spatial modeling, Estuar. Coast. Shelf S., 245, 107023, https://doi.org/10.1016/j.ecss.2020.107023, 2020
Sakshaug, E. and Sneli, J. A. (2000). Trondheimsfjorden (Trondheim: Tapir Academic Press).
Salih A, Larkum A, Cox G, Kühl M, Hoegh-Guldberg O (2000) Fluorescent pigments in corals are photoprotective. Nature 408:850-853
Salvatore, M. R., Borges, S. R., Barrett, J. E., Sokol, E. R., Stanish, L. F., Power, S. N., & Morin, P. (2020). Remote characterization of photosynthetic communities in the Fryxell basin of Taylor Valley, Antarctica. Antarctic Science, 32(4), 255-270.
Sand‐Jensen, K., Riis, T., Vestergaard, O., & Larsen, S. E. (2000). Macrophyte decline in Danish lakes and streams over the past 100 years. Journal of Ecology, 88(6), 1030-1040.
Sandmeier, S.R. (2000). Acquisition of Bidirectional Reflectance Factor Data with Field Goniometers, Remote Sensing of Environment, 73(3). http://dx.doi.org/10.1016/s0034-4257(00)00102-4.
Sandulli, R., Ingels, J., Zeppilli, D., Kvassnes, A., Sweetman, A.K., Mincks, S.H:, Mienis, F., Wei, C-L. (2021). Extreme benthic communities in the age of global change. Editorial to the special issue Front. Mar. Sci. 7:609648. doi: 10.3389/fmars.2020.609648
Schaepman-Strub, G., Schaepman, M. E., Painter, T. H., Dangel, S., & Martonchik, J. V. (2006). Reflectance quantities in optical remote sensing—Definitions and case studies. Remote sensing of environment, 103(1), 27-42.
Schütt, Eike M., Florian Uhl, Philipp R. Schubert, Thorsten B.H. Reusch, Natascha Oppelt, (2025) Mapping subtidal seagrass in the turbid Baltic Sea: Rethinking satellite sensor selection using a sensor-agnostic pipeline,Science of Remote Sensing, Volume 11, 100243, ISSN 2666-0172, https://doi.org/10.1016/j.srs.2025.100243.
Shaffer, G.P. and C.P. Onuf. 1985. Reducing the error in estimating annual production of benthic microflora: hourly to monthly rates, patchiness in space and time. Mar. Ecol. Prog. Ser., 26:221-231.
Schroeder, S.B.; Boyer, L.; Juanes, F.; Costa, M. (2020) Spatial and Temporal Trends of Nearshore Kelp Beds on the West Coast of British Columbia, Canada using Satellite Remote Sensing. Remote Sensing in Ecology and Conservation. doi: 10.1002/rse2.142
Schroeder, S. B., Dupont, C., Boyer, L., Juanes, F., & Costa, M. (2019). Passive remote sensing technology for mapping bull kelp (Nereocystis luetkeana): A review of techniques and regional case study. Global Ecology and Conservation, 19, e00683.
Schubert, P.R., Hukriede, W., Karez, R. & Reusch, T.B.H. (2015). Mapping and modeling eelgrass Zostera marina distribution in the western Baltic Sea. Marine Ecol. Progr. Ser. 522: 79– 95.
Scrivner, E., Palacios, S.L., Chlus, A., Vanhellemont, Q., Turner, J., Giardino, C., Castagna, A., Russell, B. and Dierssen, H. (2023). Discriminating Benthic Green Macroalgae From Seagrass Using Novel PRISMA Hyperspectral Satellite Imagery. Manuscript in preparation.
Singh, H., Armstrong, R., Gilbes, F. et al. (2004). Imaging Coral I: Imaging Coral Habitats with the SeaBED AUV. Subsurface Sensing Technologies and Applications 5, 25–42). https://doi.org/10.1023/B:SSTA.0000018445.25977.f3
Sorte, C.J.B., Williams, S.L., Carlton, J.T., (2010). Marine range shifts and species introductions: comparative spread rates and community impacts. Global Ecol. Biogeogr. 19, 303–316
Smith, R. 1969. An underwater spectral irradiance collector. J. Mar. Res. 27: 341-351.
Stephens, F.C., Louchard E.M., Reid, R.P., Maffione, R.A (2003) Effects of microalgal communities on reflectance spectra of carbonate sediments in subtidal optically shallow marine environments. Limnology and Oceanography, 48: 535-546.
Stenseth, N. C., Payne, M. R., Bonsdorff, E., Dankel, D. J., Durant, J. M., Anderson, L. G., Armstrong, C. W., Blenckner, T., Brakstad, A., Dupont, S., Eikeset, A. M., Goksøyr, A., Jónsson, S., Kuparinen, A., Vage, K., Österblom, H., and Paasche, O.: Attuning to a changing ocean, P. Natl. Acad. Sci. USA, 117, 20363– 20371, https://doi.org/10.1073/pnas.1915352117, 2020
Stoddart DR (1969) Ecology and morphology of recent coral reefs. Biol Rev Camb Philos Soc 44:433-498

Stoughton, M. A.. (2009) "A Bio-Optical Model for Syringodium filiforme Canopies". Master of Science (MS), Thesis, Ocean & Earth Sciences, Old Dominion University, DOI: 10.25777/txqp-3t51 https://digitalcommons.odu.edu/oeas_etds/302
Strahler B, Muller AHJ, Lucht W, Schaaf C, Tsang T, Gao F et al. (1999). MODIS BRDF/albedo product: algorithm theoretical basis document version 5.0. MODIS documentation; 23.4: 42–47
Stumpf, Richard P., Kristine Holderied, et Mark Sinclair (2003). Determination of Water Depth with High-Resolution Satellite Imagery over Variable Bottom Types. Limnology and Oceanography 48, no 1part2 (2003): 547 56. https://doi.org/10.4319/lo.2003.48.1_part_2.0547.
Sture, Ø., Snook, B. and Ludvigsen, M. (2019). Obtaining hyperspectral signatures for seafloor massive sulphide exploration. Minerals. 9: 694; doi:10.3390/min9110694
Summers, N., Johnsen, G., Mogstad, A., Løvås, H., Fragoso, G. and Berge, J. (2022). Underwater Hyperspectral Imaging of Arctic Macroalgal Habitats during the Polar Night Using a Novel Mini-ROV-UHI Portable System. Remote Sens. 14, 1325. https://doi.org/10.3390/rs14061325
Sweetman, A. K., Smith, C. R., Shulse, C. N., Maillot, B., Lindh, M., Church, M. J., ... & Gooday, A. J. (2019). Key role of bacteria in the short-term cycling of carbon at the abyssal seafloor in a low particulate organic carbon flux region of the eastern Pacific Ocean. Limnology and Oceanography, 64(2), 694-713.
Sørensen, A. J., M. Ludvigsen, P. Norgren, Ø. Ødegård, F. Cottier (2020). Sensor-Carrying Platforms. In: Marine Ecology – Life and Light in the Dead of Night, J. Berge, G. Johnsen, J. H. Cohen, Advances in Polar Ecology, Springer, Bremen, Germany, pp. 241-275. ISBN 978-3-030-33207-5, https://doi.org/10.1007/978-3-030-33208-2
Tait, L. W., Thoral, F., Pinkerton, M. H., Thomsen, M. S., & Schiel, D. R. (2021). Loss of giant kelp, Macrocystis pyrifera, driven by marine heatwaves and exacerbated by poor water clarity in New Zealand. Frontiers in Marine Science, 8, 721087. https://doi.org/10.3389/fmars.2021.721087.
Talsky, G. (1994). Derivative Spectrophotometry. doi:10.1002/3527601570
Timmer, B., Reshitnyk, L. Y., Hessing-Lewis, M., Juanes, F., & Costa, M. (2022). Comparing the use of red-edge and near-infrared wavelength ranges for detecting submerged kelp canopy. Remote Sensing, 14(9), 2241. https://doi.org/10.3390/rs14092241.
Thoen, H. H. (2014). Colour Vision in Mantis Shrimps: Understanding One of the Most Complex Visual Systems in the World. PhD Thesis, University of Queensland, Australia, 156 pp.
Trégarot, E., D'Olivo, J.P., Botelho, A.Z., Cabrito, A., Cardoso, G.O., Casal, G., Cornet, C.C., Cragg, S.M., Degia, A.K., Frediksen, S., Furlan, E., Heiss, G., Kersting, D.K., Maréchal, J.P., Meesters, E., O'Leary, B., Pérez, G., Seijo-Núñez, C., Simide, R., van der Geest, M., de Juan, S. (2024). Effects of climate change on marine coastal ecosystems-A review to guide research and management. Biological Conservation, 289, 110394.
Thompson, D. R., Hochberg, E. J., Asner, G. P., Green, R. O., Knapp, D. E., Gao, B. C., ... & Fick, R. (2017). Airborne mapping of benthic reflectance spectra with Bayesian linear mixtures. Remote sensing of Environment, 200, 18-30.
Thompson, D. R., B.-C. Gao, R. O. Green, D. A. Roberts, P. E. Dennison, and S. R. Lundeen. (2015) Atmospheric correction for global mapping spectroscopy: ATREM advances for the HyspIRI preparatory campaign. Remote Sensing of Environment 167: 64–77. doi:10.1016/j.rse.2015.02.010
Thompson, D, R., Natraj, Vijay, Green, Robert O., Helmlinger, Mark C., Gao, Bo-Cai, & Eastwood, Michael L. (2018). Optimal estimation for imaging spectrometer atmospheric correction. Remote Sensing of Environment 216, 355-373.
Thuiller, W., (2004). Patterns and uncertainties of species' range shifts under climate change. Glob. Change Biol. 10, 2020e2027.
Torres-Pulliza, D., Dornelas, M.A., Pizarro, O. et al. (2020). A geometric basis for surface habitat complexity and biodiversity. Nat Ecol Evol 4, 1495–1501 (2020). https://doi.org/10.1038/s41559-020-1281-8
Uhl, F.; Oppelt, N.; Bartsch, I. (2013). Spectral mixture of intertidal marine macroalgae around the island of Helgoland (Germany, North Sea). Aquatic Botany 111, pp. 112-124, dx.doi.org//10.1016/j.aquabot.2013.06.001.
Uhl, F.; Bartsch, I.; Oppelt, N. (2016). Submerged kelp detection with hyperspectral data. Remote Sensing, special issue on Coastal Remote Sensing 8/487; doi:10.3390/rs8060487

Uhl, F.; Græsdal Rasmussen, T.; Oppelt, N. (2022) Classification Ensembles for Beach Cast and Drifting Vegetation Mapping with Sentinel-2 and PlanetScope. Geosciences, 12, 15. DOI: 10.3390/geosciences12010015
Vahtmäe, E., T. Kutser, G. Martin, J. Kotta (2006) Feasibility of hyperspectral remote sensing for mapping benthic macroalgal cover in turbid coastal waters. Remote Sensing of Environment, 101: 342-351.
Vahtmäe, E., Paavel, P., Kutser, T. (2020). How much benthic information can be retrieved with hyperspectral sensor from the optically complex coastal waters? J. Appl. Remote Sens. 14(1): 016504, DOI: 10.1117/1.JRS.14.016504
Vahtmäe, E., Kotta, J., Orav-Kotta, H., Kotta, I., Pärnoja, M., Kutser, T. (2017) Predicting macroalgal pigments (chlorophyll a, chlorophyll b, chlorophyll a+b, carotenoids) in various environmental conditions using high-resolution hyperspectral spectroradiometers. International Journal of Remote Sensing, doi: 10.1080/01431161.2017.1399481.
Valiela, I., McClelland, J., Hauxwell, J., Behr, P. J., Hersh, D., & Foreman, K. (1997). Macroalgal blooms in shallow estuaries: controls and ecophysiological and ecosystem consequences. Limnology and oceanography, 42(5part2), 1105-1118.
Van Lancker, V., Van Heteren, S., Leth, J., Kupschus, S., Coggan, R., Mason, C., Monteys, X., Scott, G., & Hardy, D. (2012). Standardisation and harmonisation in seabed habitat mapping: role and added value of geological data and information. Part A: Sediment characterization. British Geological Survey.
Van Sebille, E., Wilcox, C., Lebreton, L., Maximenko, N., Hardesty, B.D., Van Franeker, J.A., Eriksen, M., Siegel, D., Galgani, F. and Law, K.L. (2015). A global inventory of small floating plastic debris. Environmental Research Letters. 10(12):124006.
Vanhellemont, Q. (2020) Sensitivity analysis of the dark spectrum fitting atmospheric correction for metre-and decametre-scale satellite imagery using autonomous hyperspectral radiometry. Optics Express 28: 29948–29965.
Vidal, C., & Pasquini, C. (2021). A comprehensive and fast microplastics identification based on near-infrared hyperspectral imaging (HSI-NIR) and chemometrics. Environ. Pollut., 285, 117251.
Viitasalo, M., and E. Bonsdorff. (2022) "Global climate change and the Baltic Sea ecosystem: direct and indirect effects on species, communities and ecosystem functioning." Earth System Dynamics 13.2: 711-747.
Voss, K.J. and Zhang, H. (2006). Bidirectional reflectance of dry and submerged Labsphere Spectralon plaque. Appl. Opt. 45, 7924-7927.
Voss, K. J., A. Chapin, M. Monti, and H. Zhang. (2000). Instrument to measure the bidirectional reflectance distribution function of surfaces. Applied Optics 39: 6197-6206.
Voss, K., C. Mobley, L. Sundman, J. Ivey, and C. Mazel. (2003). The spectral upwelling radiance distribution in optically shallow waters. Limnol. Oceanogr. 48: 364-373.
Wilson, N., C.E. Parrish, T. Battista, C.W. Wright, B. Costa, R.K.Slocom, J.A. Dijkstra, and M.T. Tyler. 2022. Mapping seafloor relative reflectance and assessing coral reef morphology with EAARL-B topobathymetric Lidar waveforms. Estuar. Coasts, 45:923-937, doi: 10.1007/s12237-019-00652-9.
Wang, C.-K. and W. D. Philpot. 2007. Using airborne bathymetric lidar to detect bottom type variation in shallow waters. Remote Sensing of Environment, vol. 106, no. 1, pp. 123–135, 2007, doi: https://doi.org/10.1016/j.rse.2006.08.003.
Watanabe F, Nakamura K, Samarakoon L, Mabuchi Y, Ishibashi A (1993) A procedure for estimating and monitoring red soil spread on coral reefs of Okinawa using multitemporal Landsat TM data. Proc 1993 Int Geoscience Remote Sens Symp 2:696-699
Waycott, M., Duarte, C., Carruther, T.J., Orth, R.J., Dennison, W.C., Olyarnike, S., Calladine, A., Fourqurean, J.W., Heck, K. L. Hughes, R.A:, Kendrick, G.A., Kenworthy, J., Short, F.T., Williams, S.L.(2009). Accelerating loss of seagrasses across the globe threatens coastal ecosystems. PNAS 106(30): 12377-12381, doi.10.1073.pnas.0905620106
Weinert, M., Mathis, M., Kröncke, I., Pohlmann, T., & Reiss, H. (2021). Climate change effects on marine protected areas: Projected decline of benthic species in the North Sea. Marine Environmental Research, 163, 105230.
Wettle, M., Brando, V. E., Dekker, A.G. (2004) A methodology for retrieval of environmental noise equivalent spectra applied to four Hyperion scenes of the same tropical coral reef. Rem. Sens. Environm. (93): p 188 – 197.

Wicaksono, P., M.A. Fauzan, I. Salivian, W. Kumara, R.N. Yogyantoro, W. Lazuardi, and Z. Zhafarina. 2019. Analysis of reflectance spectra of tropical seagrass species and their value for mapping using multispectral satellite images. Int. J. Rem. Sen., 40(23): 8955-8978, doi: 10.1080/01431161.2019.1624866.

Williams, S. B., Pizarro, O. R., Jakuba, M. V., Johnson, C. R., Barrett, N. S., Babcock, R. C., Friedman, A. (2012). Monitoring of benthic reference sites: Using an autonomous underwater vehicle. IEEE Robotics and Automation Magazine, 19(1), 73–84

Woolway, R. I., & Merchant, C. J. (2019). Worldwide alteration of lake mixing regimes in response to climate change. Nature Geoscience, 12(4), 271-276.

WoRMS Editorial Board (2016). World Register of Marine Species. Available from http://www.marinespecies.org at VLIZ. Accessed [YYYY-MM-DD]. doi:10.14284/170

Yao, W., Morganti, T. M., Wu, J., Borchers, M., Anschütz, A., Bednarz, L.-K., et al. (2025): Exploring site-specific carbon dioxide removal options with storage or sequestration in the marine environment – the 10 Mt CO2 yr-1 removal challenge for Germany. Earth's Future (13), e2024EF004902. https://doi.org/10.1029/2024EF004902

Zhang, H., and K. J. Voss. 2006. Bidirectional reflectance of dry and submerged labsphere spectralon plaque. Applied optics 45: 7924-7927.

Zhang, H., K.J. Voss, R.P. Reid, and E.M. Louchard. (2003) Bidirectional reflectance measurements of sediments in the vicinity of Lee Stocking Island, Bahamas. Limnol. Oceanogr., 48(1, part 2): 380-389, doi: 10.4319/lo.2003.48.1_part_2.0380.

Zhou, Y., Y. Chen, H. Zhao, C. Jamet, D. Dionisi, M. Chami, P. Di Girolamo, et al. (2022). Shipborne oceanic high-spectral-resolution lidar for accurate estimation of seawater depth-resolved optical properties. Light Sci. App., 11:261, doi: 10.1038/s41377-022-00951-0.

Zhou, G., Niu, C., Xu, W.,Yang, W., Wang, J., Zhao, H. (2015) Canopy modeling of aquatic vegetation: A radiative transfer approach. Remote Sensing of Environment: 163: 186-205, doi:10.1016/j.rse.2015.03.015.

Zibordi, G., Holben, B., Mélin, F., D'Alimonte, D., Berthon, J. F., Slutsker, I., & Giles, D. (2010). AERONET-OC: an overview. Canadian Journal of Remote Sensing, 36(5), 488-497.

Zimmerman, R. (2003a). Radiative transfer in seagrass canopies. Limnol. Oceanogr. 48: 568–585.

Zimmerman, R.C. (2003b). A biooptical model of irradiance distribution and photosynthesis in seagrass canopies. Limnology and Oceanography 48(1, part 2): 568-585. doi: 10.4319/lo.2003.48.1_part_2.0568

Zwada, D.G., G.A. Piniak, and C.J. Heam. 2010. Topographic complexity and roughness of a tropical benthic seascape. Geophy. Res. Let., 37:L14604, doi: 10.1029/2010GL043789.